Univerzita Karlova

Přírodovědecká fakulta

Studijní program: Biochemie
Studijní obor: Biochemie

Tomáš Knedlík

Glutamátkarboxypeptidasa II jako cíl farmaceutického zásahu a molekulární adresa pro léčbu nádorových onemocnění

Glutamate Carboxypeptidase II as a Drug Target and a Molecular Address for Cancer Treatment

Disertační práce

Doc. RNDr. Jan Konvalinka, CSc.

Praha, 2017

Charles University

Faculty of Science

Study program: Biochemistry
Branch of study: Biochemistry

Tomáš Knedlík

Glutamate Carboxypeptidase II as a Drug Target and a Molecular Address for Cancer
Treatment

Glutamátkarboxypeptidasa II jako cíl farmaceutického zásahu a molekulární adresa pro léčbu
nádorových onemocnění

Dissertation thesis

Jan Konvalinka, Ph.D.

Prague, 2017

Prohlašuji, že jsem tuto disertační práci vypracoval samostatně pod vedením školitele doc. RNDr. Jana Konvalinky, CSc., a všechny použité prameny jsem řádně citoval. Tato práce ani její podstatná část nebyla předložena k získání jiného nebo stejného akademického titulu.

V Praze, dne 9. 9. 2017　　　　　　　　　　..

Acknowledgement

ABSTRACT

Glutamate carboxypeptidase II (GCPII), also known as prostate-specific membrane antigen (PSMA), is a membrane metallopeptidase overexpressed on most prostate cancer cells. Additionally, GCPII also attracted neurologists' attention because it cleaves neurotransmitter *N*-acetyl-L-aspartyl-L-glutamate (NAAG). Since NAAG exhibits neuroprotective effects, GCPII may participate in a number of brain disorders, which were shown to be ameliorated by GCPII selective inhibitors. Therefore, GCPII has become a promising target for imaging and prostate cancer targeted therapy as well as therapy of neuronal disorders.

Globally, prostate cancer represents the second most prevalent cancer in men. With the age, most men will develop prostate cancer. However, prostate tumors are life threatening only if they escape from the prostate itself and start to spread to other tissues. Therefore, considerable efforts have been made to discover tumors earlier at more curable stages as well as to target aggressive metastatic cancers that have already invaded other tissues and become resistant to the standard treatment. Since patients undergoing a conventional therapy (a combination of chemotherapy and surgery) suffer from severe side effects, more effective ways of treatment are being searched for. Novel approaches include selective targeting of tumor antigens overexpressed on tumor cells. GCPII represents such a target that may be used either for imaging of advanced cancers or as an address for prostate-targeted drug delivery.

The studies presented in the thesis focused on GCPII as a potential diagnostic and therapeutic target as well as development of novel molecular tools for studying physiological and pathological role of GCPII in various tissues. Therefore, we evaluated GCPII potential to become a serum marker of prostate cancer and determined its concentration in the blood plasma among healthy population. Since the development and testing of novel therapeutics and methods require a model organism, we characterized mouse GCPII as mice represent most widely used model animals. Finally, we developed polymer conjugates decorated with GCPII inhibitors that might become a tool for an active drug delivery to cells expressing GCPII. These conjugates might also serve as antibody mimetics enabling selective targeting of desired proteins, their isolation and visualization *in vitro* and *in vivo*. Therefore, this novel chemical-biological tool, called iBodies, also has the application outside of the area of GCPII.

Abstrakt

Glutamátkarboxypeptidasa II (GCPII), známá také jako membránový antigen specifický pro prostatu (PSMA), je membránová metalopeptidasa, jež je exprimovaná na buňkách karcinomu prostaty. GCPII si dále získala pozornost neurologů, neboť v mozku štěpí neurotransmiter *N*-acetyl-L-aspartyl-L-glutamát (NAAG). Touto aktivitou se GCPII může podílet na řadě mozkových poruch, jelikož NAAG vykazuje neuroprotektivní účinky. GCPII se proto stala prostředkem pro zobrazování a možnou cílenou léčbu nádorů prostaty stejně jako pro léčbu mozkových poruch.

Nádory prostaty celosvětově představují druhé nejčastější mužské nádorové onemocnění. U většiny mužů, dříve či později, dochází k vytvoření určité formy nádoru prostaty. Nádory prostaty jsou ovšem život ohrožující pouze při opuštění samotné prostaty a rozšíření do jiných tkání. Z tohoto důvodu bylo enormní úsilí vloženo do dřívější detekce nádorů v lépe léčitelných stupních, stejně jako do cílení na agresivní metastatické nádory resistentní na standardní léčbu. Pacienti procházející konvenční terapií (kombinace chemoterapie a chirurgického zákroku) trpí poměrně závažnými vedlejšími účinky – proto jsou hledány účinnější způsoby léčby zahrnující selektivní směrování na nádorové antigeny, jež jsou mnohonásobně více produkovány nádorovými buňkami. GCPII představuje tento cíl, jenž by mohl být použit buď pro detekci pokročilých stupňů nádorů či jako molekulární adresa pro cílené doručování léčiv přímo do nádorové tkáně.

Studie uvedené v této práci se zaměřují na GCPII jako potenciální diagnostický a terapeutický cíl a dále na vývoj nových molekulárních nástrojů pro studium fyziologické i patologické role GCPII. Z těchto důvodů jsme zhodnotili potenciál GCPII stát se sérovým markerem nádorů prostaty a určili její koncentraci v krvi zdravé populace. Vzhledem k tomu, že vývoj nových terapeutik a léčebných metod vyžaduje modelové organismy, charakterizovali jsme myší GCPII, jelikož myši představují nejčastěji používaná pokusná zvířata. Nakonec jsme vyvinuli polymerní konjugáty nesoucí inhibitory GCPII, které by se mohly stát nástroji pro aktivní transport léčiv do buněk exprimujících GCPII. Tyto konjugáty mohou ovšem sloužit i jako mimetika protilátek umožňující selektivní cílení zvolených proteinů, jejich izolaci a vizualizaci *in vitro* a *in vivo*. Tento nový chemicko-biologický nástroj, nazvaný iBodies, má tak uplatnění i mimo oblast nádorového antigenu GCPII.

TABLE OF CONTENTS

1. Introduction

The *Introduction* is divided into several sections. The first one describes the protein of interest – glutamate carboxypeptidase II (GCPII) – bringing the most important pieces of information regarding GCPII enzyme activity, structure and its close homologs. The second section deals with GCPII and its implication in human health disorders. The third part summarizes diagnostic and therapeutic approaches based on GCPII. Finally, the last section is not focused primarily on GCPII, however, it introduces a world of polymer conjugates to readers and their use in targeted drug delivery.

1.1. GCPII – the protein of interest

1.1.1. Discovery and name(s)

Glutamate carboxypeptidase II (GCPII; **EC 3.4.17.21**) is a membrane metallopeptidase that has been a target of research interest over the past three decades. At the beginning, the protein was studied in three various scientific fields, which led to different names of the protein: ***prostate-specific membrane antigen*** (***PSMA***) in urology [1], ***N-acetylated-alpha-linked acidic dipeptidase*** (***NAALADase***) in neurology [2] and ***folate hydrolase*** in dietology [3]. In 1987, GCPII was first described in the rat nervous system as an enzyme capable of cleaving the most abundant brain peptide neurotransmitter *N*-acetyl-L-aspartyl-L-glutamate (NAAG); therefore, neuroscientists termed the protein NAALADase, or less often NAAG peptidase [2]. In the same year, GCPII was recognized as the antigen of monoclonal antibody 7E11.C5 specifically immunostaining prostate epithelium, which was the reason why the protein was called PSMA [1]. Several years later, it was shown that above-mentioned names represent the same protein, which also possesses the same enzyme activity as folate hydrolase located on the jejunal brush border [3-6]. Today, in spite of the recommendation of the International Union for Biochemistry and Molecular Biology for the use of name "GCPII", PSMA remains the most common name used throughout the literature.

1.1.2. GCPII structure

GCPII is a homodimeric type II transmembrane glycoprotein [7]. Each monomer consists of 750 amino acids that form a short N-terminal cytoplasmic tail (19 amino acids), a

transmembrane domain (24 amino acids), and an extensive C-terminal ectodomain (707 amino acids) responsible for catalytic activity of GCPII [8, 9]. The polypeptide chain is heavily glycosylated; oligosaccharides account for approximately 20% of the GCPII molecular weight (approximately 100 kDa) [10]. Appropriate GCPII glycosylation was shown to be indispensable for the proper folding and activity of the enzyme [11]; therefore, it has been impossible to prepare GCPII using bacterial and yeast expression systems [12]. That was one of the reasons why the first GCPII X-ray structures were published as late as in 2005 and 2006 by two independent groups [8, 9]. To date (October 2017; search for "glutamate carboxypeptidase II, Q04609"), 63 crystal structures of GCPII/GCPII mutants with various ligands have been determined and stored at the Protein Data Bank, the vast majority of them with resolution under 2.0 Å. All structures were resolved for the GCPII ectodomain (amino acids 44-750); the short intracellular part is presumed not to adapt any stable conformation.

The large extracellular part of GCPII consists of three domains (Fig. 1; p. 10): the apical (amino acids 117-351), the C-terminal (amino acids 591-750), and the protease-like domain (amino acids 57-116 and 352-590) [8, 9]. The active site is formed by amino acids residues originating from all three domains [9, 13, 14]. As already mentioned, GCPII bears also oligosaccharide chains that contribute to its solubility and stability [15, 16]; GCPII primary sequence contains 10 potential N-glycosylation sites. Oligosaccharide chains are usually rather flexible and, therefore, their precise roles in protein structure stabilization cannot be precisely determined. However, there is a noteworthy exception: Asn638 glycosylation, which was described to interact with an amino acid side chain of the other monomer and is indispensable for GCPII activity [11].

Besides amino acids and oligosaccharides, there are also four ions [9]: two zinc ions in the active site playing a crucial role in the enzyme catalysis [17]; a calcium cation and a chloride anion are probably involved in the stabilization of the GCPII structure and substrate specificity, respectively (Fig. 1; p. 10) [9, 18, 19].
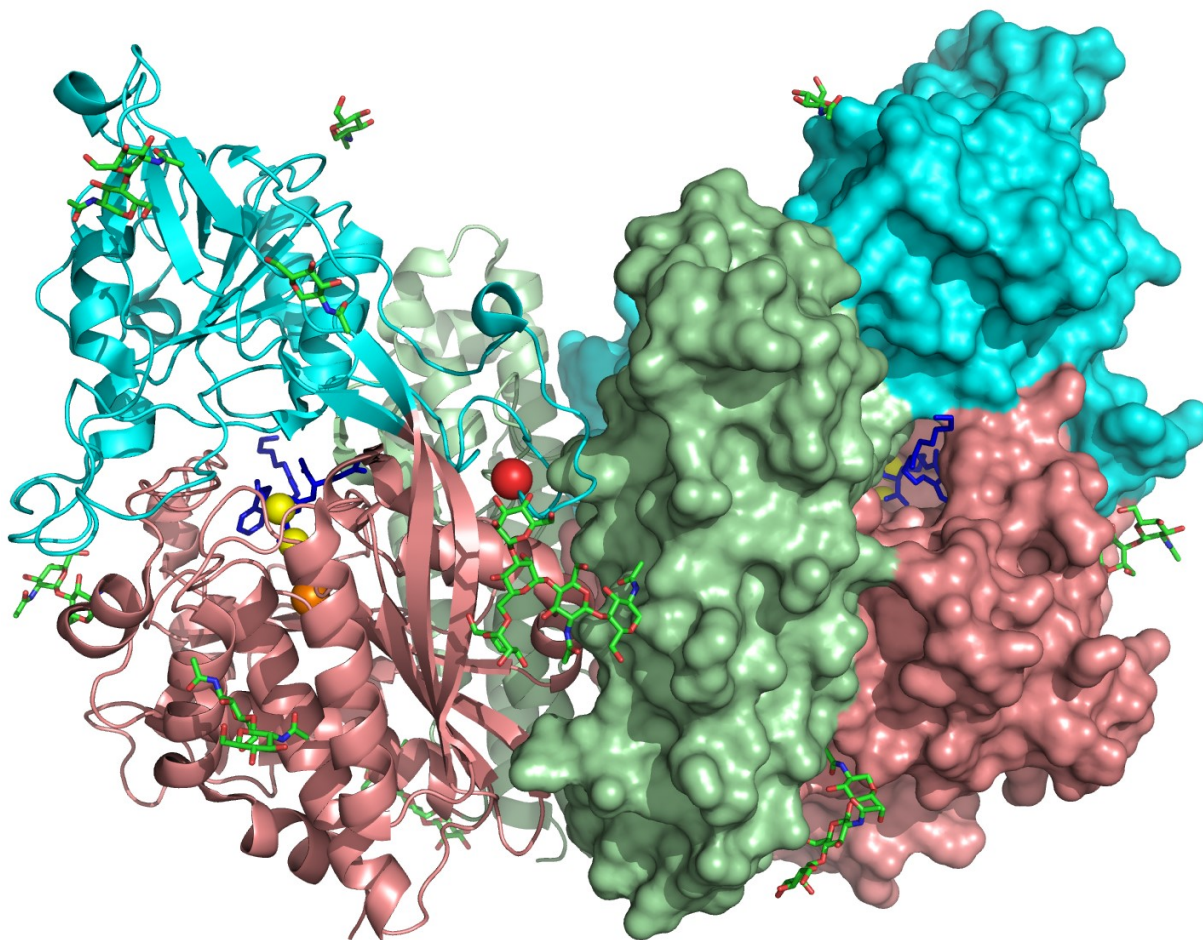
Fig. 1: Crystal structure of a GCPII ectodomain in a complex with a urea-based inhibitor.

GCPII is a transmembrane homodimer with short cytoplasmic and transmembrane domains (not shown) and a large extracellular part (monomers are depicted in the cartoon and surface representation). The ectodomain is divided into three separate domains: the apical (cyan), the C-terminal (green) and the protease-like (pink). All three domains form a tunnel leading towards the GCPII active site. The colored spheres (yellow, red and orange) represent active site zinc, calcium and chloride ions. GCPII is heavily glycosylated; the oligosaccharide chains are shown as sticks. The active site bound urea-based inhibitor (containing biotin attached via a polyethylene glycol linker) is shown as blue sticks; the inhibitor is visible to stick out of a GCPII active site tunnel. Structure PDB code: 4NGP [20].

1.1.3. GCPII tissue distribution

GCPII is quite widely distributed among human tissues and is not exclusively restricted to the prostate, as its alternative name (i.e. prostate-specific membrane antigen, PSMA) may suggest. GCPII is highly expressed in several human tissues: the nervous system (astrocytes and Schwann cells), prostate (acinar epithelium), small intestine (jejunal-brush border), kidney (proximal tubules) and liver [21-26]. Importantly, GCPII expression in

prostate carcinoma is approximately 10-fold higher than in the normal prostate [22, 26, 27]. Thanks to this unique expression, GCPII represents an important target for prostate cancer imaging and therapy (see Chapter 1.4.2. "GCPII as a target in prostate cancer").

Interestingly, GCPII was also detected on endothelial cells in the tumor-associated neovasculature [28-31] but not in the normal blood vessels. GCPII was shown to be expressed in the neovasculature of breast, renal, lung, gastric and colorectal carcinoma and malignant melanoma [28-30]. Since solid tumors require blood vessels for their survival and growth, the tumor neovasculature represents a promising target for anticancer therapy (so called "anti-vascular tumor therapy") [32]. Indeed, proof-of-concept experiments employing anti-GCPII antibody J591 were performed, assessing GCPII as a potential neovascular target for therapy and imaging of solid tumors [33, 34].

Since GCPII is overexpressed in prostate carcinoma, researchers were motivated to detect GCPII protein in the human blood (serum/plasma) to serve as a diagnostic serum marker, similarly to the current prostate cancer screening test assaying prostate specific antigen (PSA) in the men's blood [35]. The previous publications on the GCPII presence in the blood are slightly conflicting, reporting that GCPII blood concentrations range between 1 and 800 ng/ml [36-42]. Naturally, if GCPII were found in the blood in such high levels, serious problems would arise for imaging/therapeutic agents targeting GCPII in the brain or prostate. In addition, the potential for blood GCPII levels to serve as a useful cancer prognostic marker has not been definitely answered.

1.2. GCPII FUNCTIONS

1.2.1. GCPII enzyme activity

GCPII belongs to the MH clan (family M28) of metallopeptidases; all of them are cocatalytic zinc peptidases containing two zinc ions coordinated by five amino acid residues in their active sites [43]. The MH clan peptidases use a water molecule as a nucleophile, which is bound in the active site by the zinc ions and five residues [43]. A proton shuttle residue is inevitable for the catalysis (Glu424 in GCPII) and its mutation leads towards the loss of the enzyme activity [17].

GCPII was shown to have a strong preference for dipeptides with a glutamate moiety in the P1' position [2, 12]. The observation led to a design of a canonical GCPII inhibitor scaffold that usually involves a glutamate moiety to fit into the glutamate-binding subsite.

There are two endogenous substrates of GCPII in the human body – NAAG in the brain (NAALADase activity; Fig. 2a) [2] and poly-gamma-glutamylated folates in the small intestine (folate hydrolase activity; Fig. 2b) [3, 5]. Both peptidase activities release glutamates from the particular substrate, which has subsequent significant physiological effects in the particular tissue.
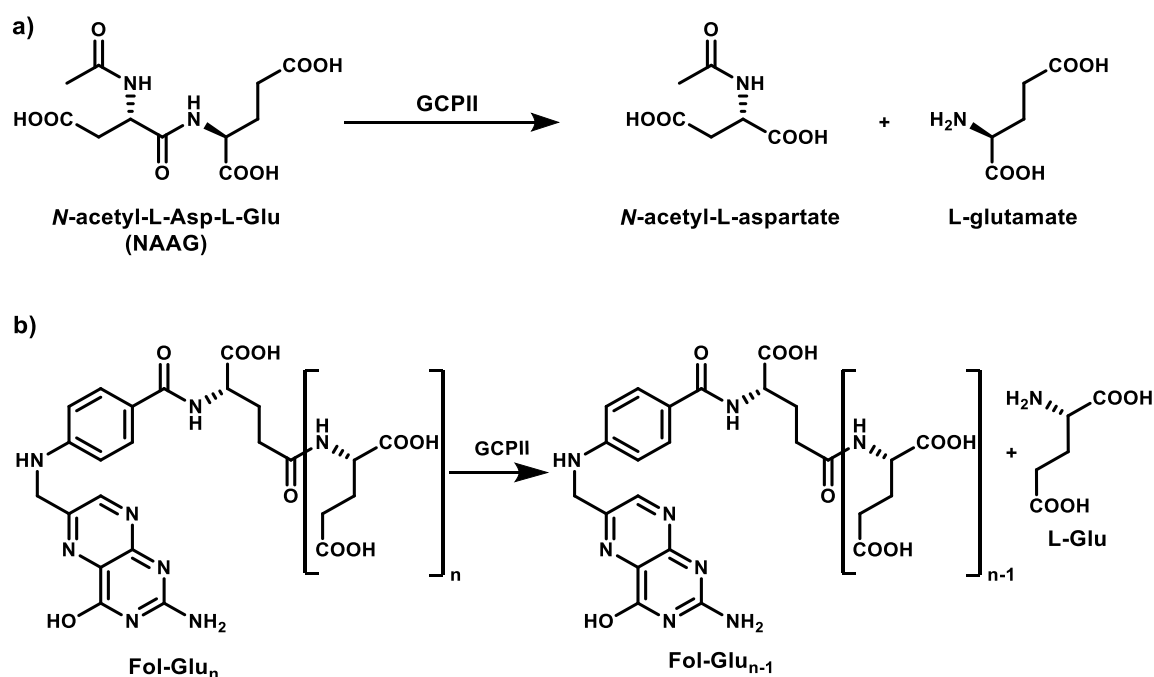
Fig. 2: Physiological enzyme functions of GCPII.

GCPII possesses two physiological functions (in the brain and jejunum) that include releasing terminal glutamates from its endogenous substrates. a) GCPII hydrolyzes the most abundant peptide neurotransmitter *N*-acetyl-L-aspartyl-L-glutamate (NAAG) in the human brain. Free glutamate, a product of the hydrolysis, has strong excitatory effects and its high concentration causes excitatory neurotoxicity. b) In the jejunal brush border, GCPII cleaves off terminal glutamates from poly-gamma-glutamylated folates, thus enabling folate to be transported across the intestinal mucosa into the blood.

In the human central nervous system, GCPII is responsible for hydrolyzing NAAG into *N*-acetyl-L-aspartate and free L-glutamate (Fig. 2a) [2, 44]. NAAG is one of the most prevalent neurotransmitters in the human brain [45, 46]. It specifically binds and activates metabotropic glutamate receptors [47], which leads to neuroprotective effects [48, 49]. In

sharp contrast to NAAG, free glutamate, the most abundant and major excitatory neurotransmitter in the brain, is often the cause of excitatory neurotoxicity [50].

In the human jejunum, GCPII was identified as a folate hydrolase [3-5], the enzyme that cleaves off terminal glutamates from dietary poly-gamma-glutamylated folates (Fig. 2b; p. 12) [5], which cannot be transported across the intestinal mucosa. Thus, after the removal of the glutamate residues, the folate molecules can be transported from the intestine to the blood.

1.2.2. GCPII inhibitors

Inhibition of GCPII enzyme activity in the brain leads to neuroprotection (described in more detail in the chapter 1.4.1. "GCPII in neurological disorders"), therefore, selective GCPII inhibitors have represented an important branch of the GCPII-focused research. Moreover, inhibitors can also be used as "homing devices" for GCPII-based imaging of prostate cancer [51-53]. Therefore, over the past 20 years, a high number of GCPII inhibitors with different chemical scaffolds have been presented; virtually all GCPII inhibitors were originally derived from NAAG (Fig. 3; p. 14).

Naturally, general metallopeptidase inhibitors that act as chelators of divalent metal cations, such as EDTA, EGTA or 1,10-phenanthroline, completely abolish GCPII enzyme activity [2]. For the same reason, GCPII is also inhibited by polyvalent anions, e.g. phosphate or sulfate [2].

GCPII contains two active-site zinc ions and the GCPII pharmacophore (S1') pocket exhibits a strong preference for glutamate and glutamate-like moieties [9, 12]. Therefore, it is not surprising that the majority of GCPII potent and specific inhibitors have a general structure consisting of a zinc-binding group and a glutamate moiety interacting with amino acid residues in the S1' pocket site of GCPII (Fig. 3; p. 14). Based on the zinc-binding group, GCPII inhibitors are classified into three major categories: phosphorus-containing compounds (e.g. phosphonates and phosphinates), ureas, and thiols (Fig. 3; p. 14).
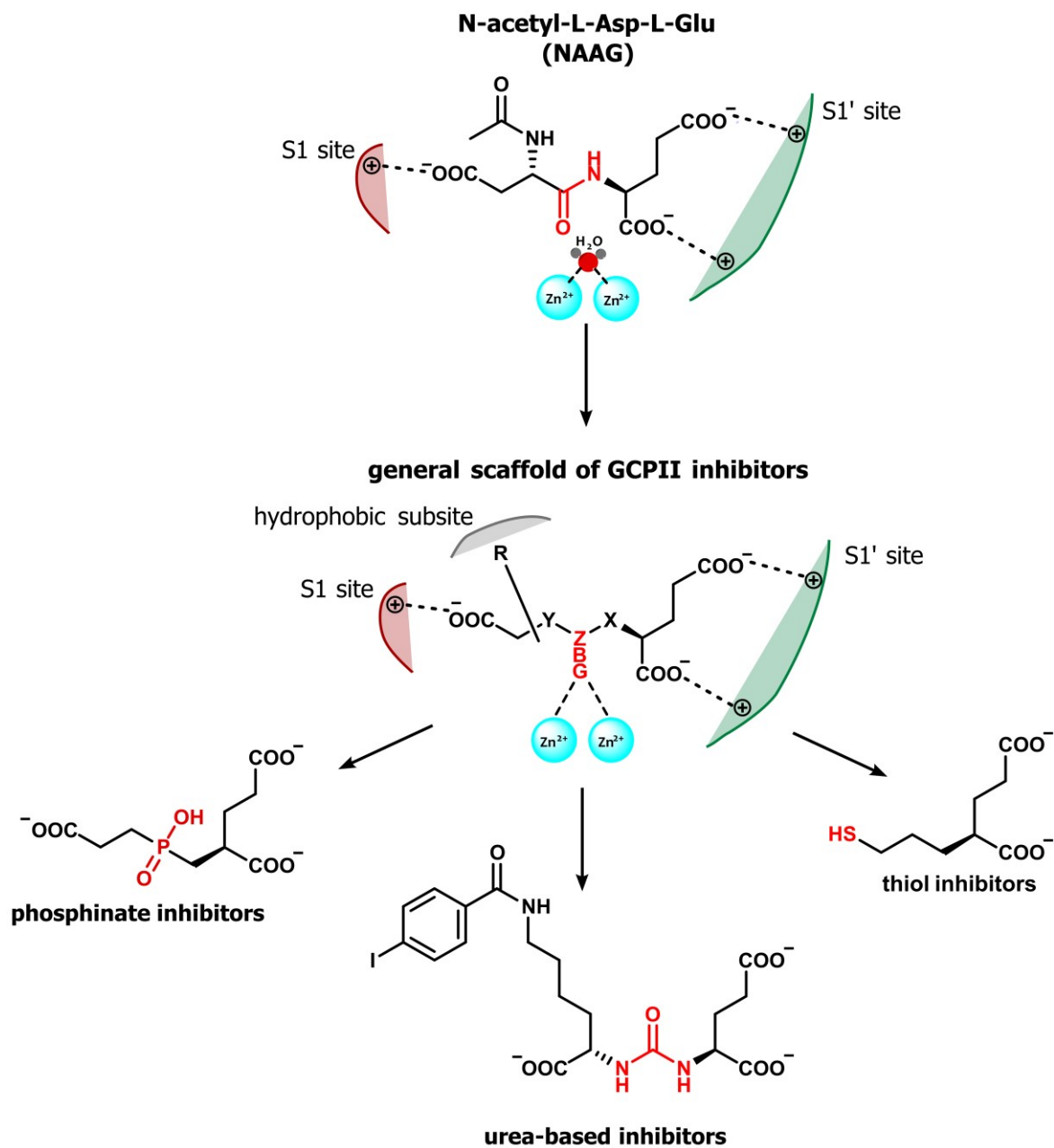
Fig. 3: General design of GCPII inhibitors.

Design of GCPII inhibitors is based on the structure of neurotransmitter NAAG, an endogenous GCPII substrate in the brain. The GCPII inhibitors contain a zinc-binding group (ZBG) that chelates the catalytic zinc ions in the active site. The ZBG is attached to the glutamate moiety at its 2-position (*via* linker X); glutamate is tightly bound by the residues in the S1' site. An additional carboxyl group at the P1 position (connected *via* linker Y) is bound by the hydrophilic subsite S1. Finally, some inhibitors (often used for fluorescent/SPECT/PET visualization) contain bulky side chain R branching from the linker Y. GCPII inhibitors are classified according to the type of the ZBG into three major groups: phosphonate-/phosphinate-based, urea-based and thiol-based compounds. Inspired by [54].

1.2.2.1. Phosphorus-containing GCPII inhibitors

Phosphorus-containing inhibitors represent the first generation of GCPII inhibitors and they were the core contributors in understanding of physiological functions of GCPII [55]. Mechanistically, the tetrahedral phosphorus group mimics a (tetrahedral) transition state of the cleaved peptide bond [14]. A major discovery was made in 1996 when a phosphonate-based GCPII inhibitor 2-(phosphonomethyl)pentanedioic acid (2-PMPA) was introduced [55], soon becoming the gold standard of all GCPII inhibitors in terms of their potency and selectivity for GCPII (Fig. 4a).
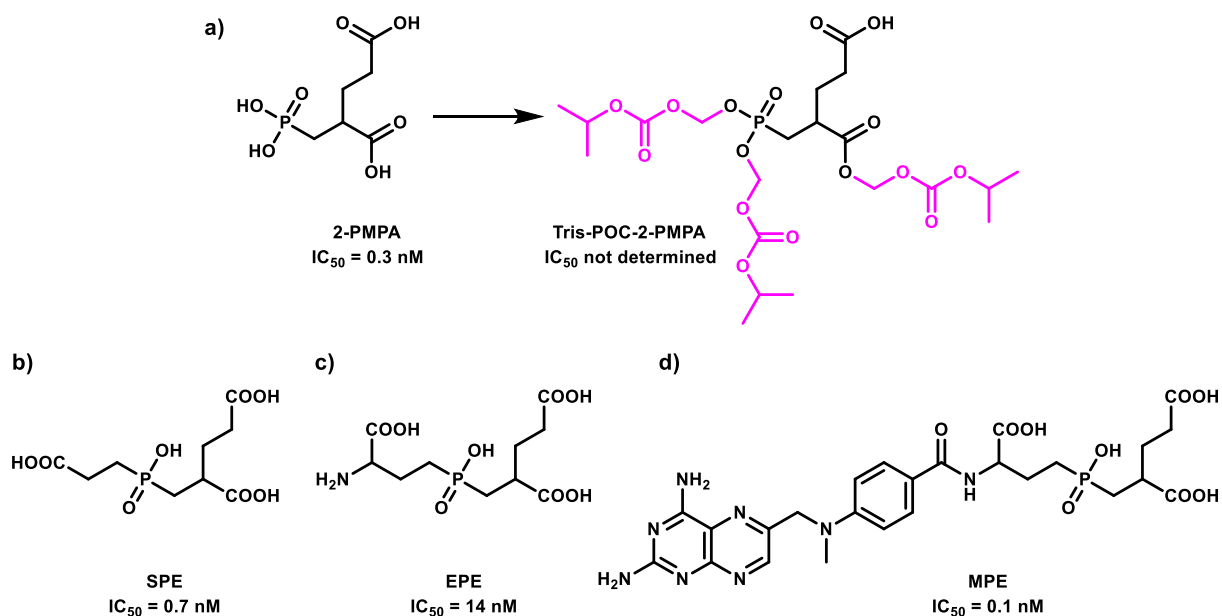
Fig. 4: Phosphorus-containing GCPII inhibitors.

Phosphonate- and phosphinate-based compounds represent one of the most potent and frequently used classes of GCPII inhibitors. a) 2-(phosphonomethyl)pentanedioic acid (2-PMPA) is the canonical phosphonate inhibitor of GCPII [55]. 2-PMPA is highly potent and selective for GCPII; however, it has low oral availability. Therefore, a prodrug of 2-PMPA with phosphonate and α-carboxylate covered with hydrophobic isopropyloxycarbonyloxymethyl (POC) was prepared (Tris-POC-2-PMPA) and showed excellent oral bioavailability [56]. b, c, d) A series of phosphinate GCPII inhibitors (SPE, EPE, MPE) [18]. Interestingly, binding of MPE leads to the rearrangement of two arginine residues in the S1 site, which results in 100-fold more potent inhibition of GCPII by MPE compared to EPE [18].

Besides 2-PMPA and other phosphonates, a number of phosphinate GCPII inhibitors were described, including compounds such as SPE, EPE, and MPE (Fig. 4b,c,d) [18]; nevertheless, they have never fulfilled their potential to be used as therapeutic agents, mainly due to their lack of oral bioavailability, and the research took different direction, especially

towards urea-based inhibitors [57]. Therefore, it was rather surprising when orally available prodrugs of 2-PMPA were published in 2016 (Fig. 4a; p. 15) [56]. The authors achieved oral availability by preparing prodrugs that liberate the active species upon hydrolysis *in situ*. This approach might lead to the design and development of other orally available phosphonate-based GCPII-specific inhibitors.

1.2.2.2. Urea-based GCPII inhibitors

Urea-based GCPII inhibitors were developed in the early 2000s [58, 59] and now represent the most widely used group of selective GCPII inhibitors (Fig. 5; p.17). The inhibitors usually contain a glutamate residue to bind to the S1'pocket of the enzyme; the ureido group mimics a planar peptide bond of the cleaved substrate [54]. The major advantage of the urea-based inhibitors is the modularity of their structure (especially in the P1 position) and their relative simple synthesis and subsequent modification of the basic scaffold, usually based on (*S*)-Lys-C(O)-(*S*)-Glu (Fig. 5a; p. 17) [60]. Therefore, a large number of various urea-based inhibitors (conjugated with radionuclides, fluorophores, or toxins) were synthetized and successfully used in experimental imaging and therapy of prostate cancer [51, 61-63]. [^{125}I]DCIBzL, containing a phenyl ring binding to the hydrophobic pocket in the S1 site, represents a prime example of such compounds and one of the most potent GCPII inhibitors (Fig. 5b; p. 17) [60]. On the other hand, the treatment of neurological diseases with a urea-based class of GCPII inhibitors is rather improbable due to their poor pharmacokinetic profile, as was demonstrated by ZJ-43 (Fig. 5c; p. 17), which was one of the most extensively used urea-based inhibitors in mice models [64-67].
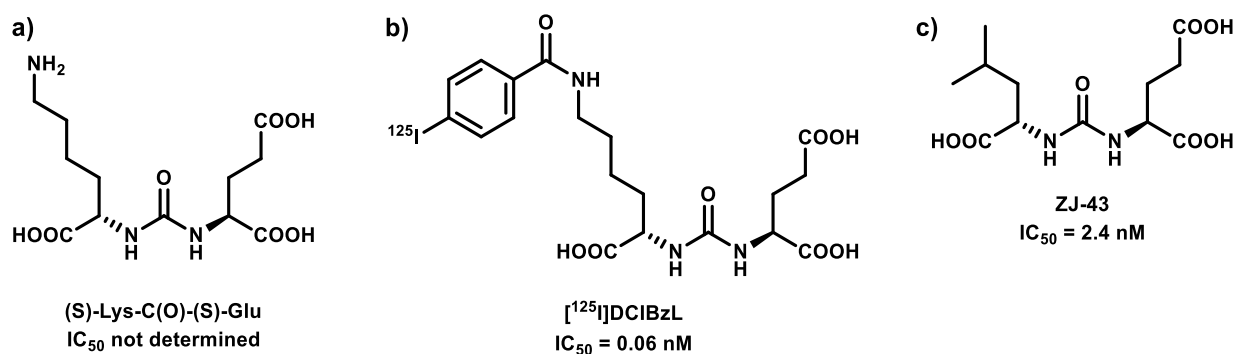
Fig. 5: Urea-based GCPII inhibitors.

Urea-based GCPII inhibitors have become the most widely used GCPII inhibitors, especially due to their modularity, easy synthesis and potency. a) (*S*)-Lys-C(O)-(*S*)-Glu offers an useful scaffold for the development of imaging agents containing fluorescent or radiolabeled group attached *via* the ε-amino group of the lysine residue [60, 68]. b) [^{125}I]DCIBzL represents a low-molecular-weight agent targeted against GCPII for single-photon emission computed tomography (SPECT) [60]. c) ZJ-43 has been used in numerous GCPII inhibition *in vivo* experiments [64-67].

1.2.2.3. Thiol-based and other inhibitors

The unique feature of thiol-based GCPII inhibitors is their oral bioavailability; in fact, they were developed as a response to the already mentioned unsuitable pharmacokinetic profile and high polarity of phosphorus-based GCPII inhibitors. Therefore, in 2003, a potent thiol-based GCPII inhibitor, 2-(3-mercaptopropyl)pentanedioic acid (2-MPPA), was described (Fig. 6a; p. 18). 2-MPPA was shown to be orally available in rats [69] and, importantly, efficacious in several animal models of diseases after their oral administration, including neuropathic pain [69], diabetic neuropathy [70], or familial amyotrophic lateral sclerosis [71]. Later, 2-MPPA was tested in phase I clinical trials [72], but its further development was stopped due to its toxicity in animals. Generally, the thiol-based compounds are not ideal drugs, since the thiol group is quite susceptible to oxidation.

Phosphoramidate GCPII inhibitors containing P1 carboxylate and hydrophobic benzoyl moiety were shown to pseudoirreversibly inhibit GCPII (Fig. 6b; p. 18) [73].

Hydroxamate compounds represent another alternative zinc-binding group [74, 75]. Recently, hydroxamic acid-based inhibitors possessing nanomolar affinity for human GCPII were discovered; they exhibit a unique binding mode in which the glutarate-like moiety occupies the entrance funnel and not the S1' pocket (Fig. 6c; p. 18) [74].
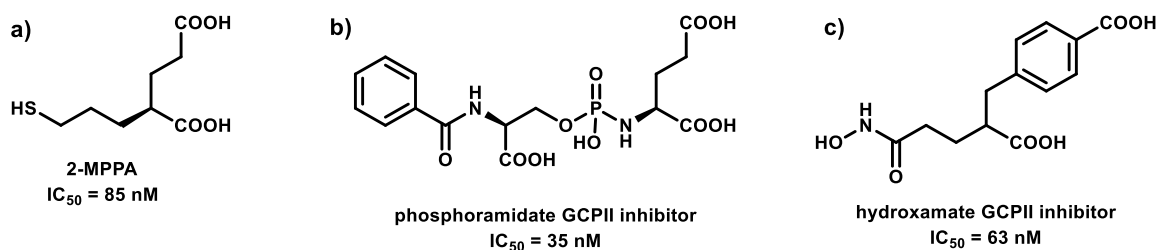
Fig. 6: Thiol, phosphoramidate and hydroxamate GCPII inhibitors.

a) 2-(3-mercaptopropyl)pentanedioic acid (2-MPPA) was shown to be orally bioavailable in animal models and underwent phase I clinical trials; however, its further development was stopped due to the adverse effects in animals [69, 72]. b) An example of a phosphoramidate GCPII inhibitor pseudoirreversibly inhibiting GCPII [73]. c) A hydroxamate GCPII inhibitor with a glutarate-like moiety exhibits nanomolar affinity for GCPII and a novel binding mode to the GCPII active site [74].

1.2.3. Potential non-enzyme functions of GCPII

Since its discovery, GCPII has been thoroughly studied as an enzyme – its enzyme activities, inhibition profile and substrate specificity have been described in a large detail in numerous studies. Therefore, the physiological roles, where GCPII works as an enzyme, have been at least partially understood. Nonetheless, GCPII may play also other, non-enzyme functions, as it is suggested by several features possessed by GCPII, which are commonly associated with cell receptors and transporters.

Interestingly, GCPII shares 60% sequence similarity with transferrin receptor (TfR) that is often considered an archetype of an internalizing receptor. TfR binds iron-loaded transferrin, which in turn induces internalization of the TfR-transferrin complex into the cell. As already mentioned, GCPII is a noncovalent transmembrane homodimer located on a cell membrane. Formation of a homodimer is the dominant feature of many membrane receptors [76]. Homodimerization is often induced by binding of a specific ligand, which usually results in a cellular response [77]. Besides sequence similarity, GCPII and TfR share also similar overall fold and domain organization. Therefore, it was not surprising when GCPII was shown to undergo both constitutive and antibody-induced internalization [78, 79]. After endocytosis from the plasma membrane, GCPII is transported back to the cell surface via recycling endosomal compartment [80], analogously as TfR. These observations, together with a mysterious GCPII role in the prostate and prostate cancer, led to the hypothesis that GCPII might work as a membrane receptor and triggered a search for a (yet) unidentified putative ligand of GCPII.

18

Besides its potential receptor function, GCPII was reported be involved in a number of other processes. GCPII was described to regulate angiogenesis by modulating integrin signal transduction [81] and by producing pro-angiogenic peptides (generated by GCPII-catalyzed laminin proteolysis) [82, 83]. Furthermore, GCPII was described to promote cell proliferation by activation of the NF-κB pathway [84] and to be associated with the anaphase-promoting complex [85]. However, none of those hypotheses has been supported or confirmed by other groups and further studies are needed to validate these GCPII potential non-enzyme functions.

1.3. GCPII HOMOLOGS

Apart from (human) GCPII, there are several other proteins that are related to GCPII (protein homologs; reviewed in [86]). The homologs may be found within one species (paralogs), where they can play identical, similar or completely different roles, depending on a degree of similarity and their tissue expression. Secondly, the corresponding proteins found in the different species are called orthologs, usually with the very same function, (e.g. human, mouse, rat, and pig GCPII).

In the human body, several GCPII homologs are found – their overall structure is closely related (type II glycosylated homodimers), however, their functions are not well understood and might be distinct from those of GCPII. The closest homolog PSMAL contains an approximately 300 amino acid long N-terminal deletion and thus is probably proteolytically inactive. Glutamate carboxypeptidase III (GCPIII), another close homolog, is the only one with preserved NAAG-hydrolyzing activity [87, 88]. More distant GCPII homologs NAALADase L (a different protein from PSMAL) and NAALADase L2 do not preserve any of GCPII enzyme activities [89-91]. NAALADase L has been recently shown to be a human ileal aminopeptidase (HILAP) rather than a neural carboxypeptidase [91].

Since GCPIII is the best-studied GCPII homolog and mouse GCPII represents an important model protein, they are introduced in more detail below.

1.3.1.1. Glutamate carboxypeptidase III

Glutamate carboxypeptidase III (GCPIII; also known as NAALADase II) shares 67% amino acid identity with GCPII [87, 89, 92]. GCPIII was shown to be present in the brain of GCPII mice knockouts, which preserved ability to hydrolyze NAAG in spite of the lack of

GCPII; therefore, GCPIII was suggested to compensate the missing GCPII activity [93]. On the other hand, its pH dependence and substrate specificity as well as mRNA expression profile (found in the testis, ovary, spleen, and brain) are somewhat different from GCPII [87]. Physiological role of GCPIII remained elusive until 2011 when it was identified as β-citryl-L-glutamate (BCG) hydrolase from the mouse testes [94]. GCPII was shown to be responsible for the hydrolysis of BCG [94], a compound also found in high concentration in the developing brain [95]. In spite of the fact that the physiological function of BCG (and GCPIII as well) is still unknown, BCG was suggested to be involved in brain development, spermatogenesis and regulation of iron and copper concentrations [96-98]. Therefore, GCPIII, as an enzyme degrading BCG, might regulate concentration of BCG and thus play an important role in the above-mentioned functions.

1.3.1.2. Mouse glutamate carboxypeptidase II

Nowadays, mouse GCPII represents the most important ortholog since the majority of preclinical experiments is performed using mice models.

Mouse GCPII shares 91% amino acid similarity with human GCPII and thus, not surprisingly, preserves both enzyme activities of its human counterpart: it hydrolyzes both endogenous substrates of the human enzyme: NAAG and pteroyl-poly-glutamates [99]. All key amino acids that participate in substrate binding and hydrolysis are preserved in mouse GCPII, therefore, the mouse GCPII active site is presumed to be identical (or at least highly similar) with human GCPII. However, until now, no crystal structure of mouse GCPII has been published. In stark contrast to the tissue distribution of human GCPII, mouse GCPII is not expressed in the mouse prostate but is found in high amounts in the mouse kidney and brain [99].

Over the past 15 years, several studies using GCPII mouse knockouts have been conducted to shed light on the role of GCPII [93, 100, 101]. However, their results were not consistent – one group described early embryonic death of the knockouts [100], while other two reported normal development to adulthood (noting that mice lacking GCPII are less susceptible to traumatic and ischemic brain injury) [93, 101].

1.4. GCPII AS A THERAPEUTIC TARGET

1.4.1. GCPII in neurological disorders

As it was already mentioned in the previous sections, GCPII is expressed in the central nervous system cleaving there NAAG, a neurotransmitter exhibiting neuroprotective effects. Thanks to the NAAG inactivation, GCPII may participate in glutamate-mediated neurotoxicity and its inhibition was shown to be neuroprotective in animal models [102]. Therefore, researchers are developing orally available GCPII inhibitors to increase NAAG, decrease glutamate and thus provide neuroprotection.

1.4.1.1. NAAG: a major peptide neurotransmitter

NAAG was discovered in the mammalian brain (horse, bovine and human) in the mid-1960s by three independent groups [46, 103, 104]. Slightly surprisingly at that time, NAAG concentrations in the central nervous system were found to be low millimolar [105] – thus being the most abundant peptide neurotransmitter and one of the most prevalent neurotransmitters in general. Using immunohistochemistry, NAAG was shown to be broadly distributed throughout the central nervous system with 10-fold concentration variations across different brain areas [106-108].

NAAG is synthetized enzymatically by NAAG synthetase in a ribosome independent manner [106, 109, 110]. As other neurotransmitters, NAAG is stored in the synaptic vesicles of neurons [111] and is released following synaptic activation in a calcium dependent, depolarization-induced manner [112-114]. After its release, NAAG activates cAMP-negatively coupled group II metabotropic glutamate (mGlu) receptors, particularly mGlu receptors type 3 (mGluR3; Fig. 7; p. 22) [47, 115, 116]. Under basal conditions, NAAG, as an agonist of presynaptic mGluR3, inhibits the (further) release of cotransmitters, e.g. glutamate [48, 117]. At the same time, NAAG also activates mGluR3 expressed on the glial cells (astrocytes and oligodendrocytes) – stimulation of glial mGluR3 leads towards the release of neuroprotective trophic factors such as transforming growth factor β (TGF-β) (Fig. 7; p. 22) [118]. Importantly, mGluR3 antagonists, such as LY341495, minimize or completely abolish the effects of the GCPII inhibitors [64, 66].
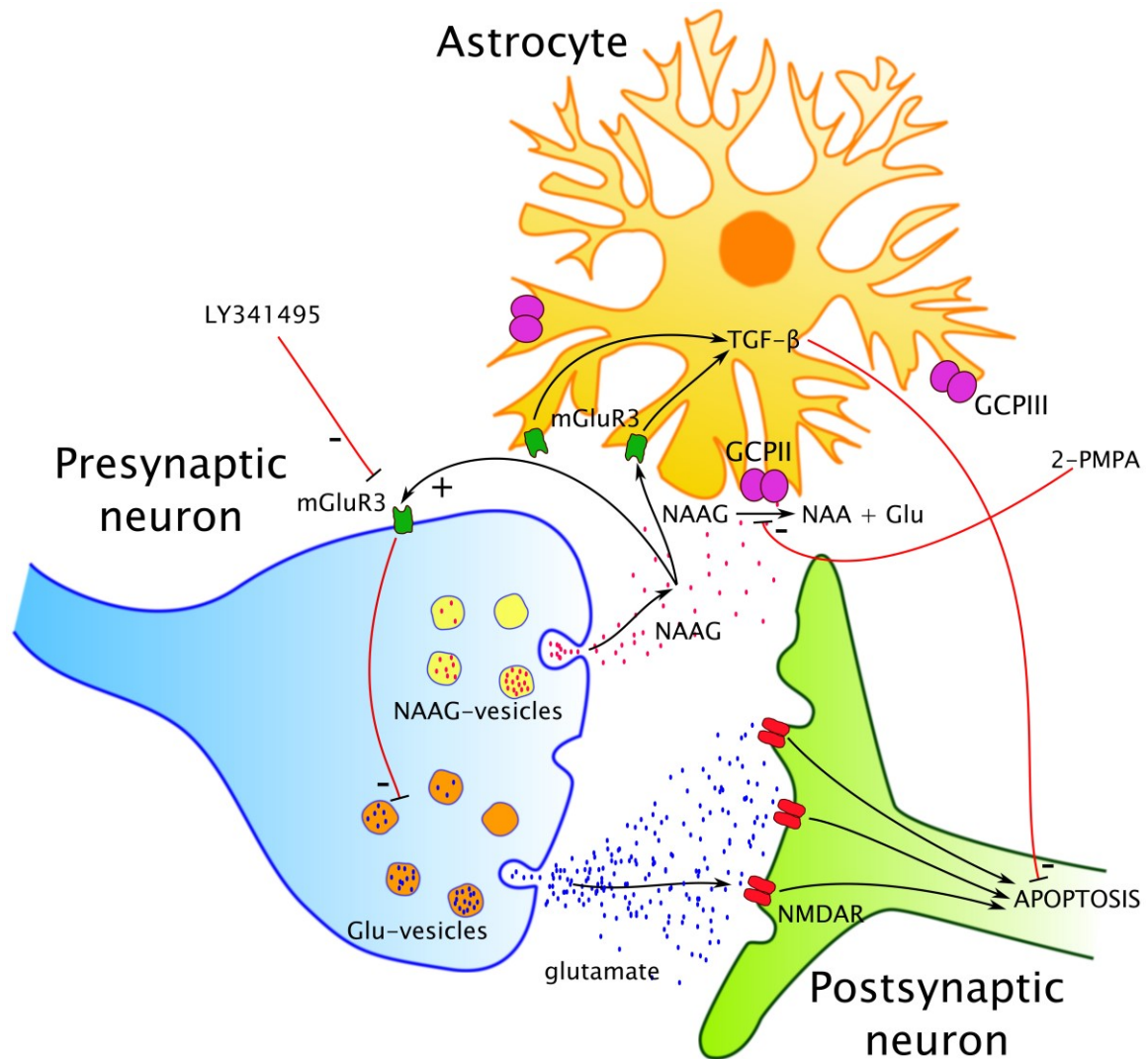
Fig. 7: Proposed functions of NAAG, glutamate and GCPII on the synaptic endings.

Neurotransmitters NAAG and glutamate are released into the synaptic cleft from a presynaptic neuron. Glutamate activates *N*-methyl-D-aspartate receptors (NMDAR), which leads to apoptosis under pathological conditions associated with excessive glutamate levels. NAAG activates metabotropic glutamate 3 receptors (mGluR3) on presynaptic neurons (resulting in the decrease of released glutamate) and on astrocytes (leading to the secretion of neuroprotective factors, such as TGF-β). GCPII (and possibly GCPIII) hydrolyzes NAAG into *N*-acetyl-L-aspartyl (NAA) and glutamate and, consequently, abolishes protective effects of NAAG. Selective inhibition of GCPII increases intact NAAG levels and subsequently mGluR3 activation, which results in neuroprotective processes. On the contrary, the beneficial effects of NAAG could be blocked by mGluR3 antagonists (e.g. LY341495). Inspired by [119].

1.4.1.2. GCPII as a NAAG peptidase

High concentrations of glutamate released from neurons are associated with several pathological conditions including ischemia/stroke, traumatic brain injury or inflammatory and

neuropathic pain. Excess glutamate overactivates *N*-methyl-D-aspartate receptors (NMDAR), which triggers a cascade of processes leading to apoptosis (Fig. 7; p. 22) (reviewed in [50]).

Once NAAG is released into the synaptic cleft, it is hydrolyzed by GCPII (and possibly also by GCPIII) localized at plasma membrane of astrocytes and Schwann cells [120, 121]. Therefore, the NAAG-hydrolyzing activity of GCPII further increases the concentration of synaptic glutamate and, more importantly, prevents NAAG from its neuroprotective activation of both presynaptic and glial mGluR3 (Fig. 7; p. 22).

Therefore, inhibition of the NAAG-hydrolyzing activity in the brain using selective GCPII inhibitors seems to help in two ways: by increasing amounts of neuroprotective NAAG and, naturally, by decreasing concentration of glutamate as a reaction product. Uncleaved NAAG can then activate presynaptic mGluR3 (reducing further glutamate release) and glial mGluR3 (releasing TGF-β) (Fig. 7; p. 22).

1.4.1.3. GCPII inhibitors as therapeutic agents

A number of *in vivo* studies have evaluated therapeutic potential of selective GCPII inhibitors for various neurological disorders; most studies focused on brain injury and pain perception (reviewed in [51, 119]). Importantly, GCPII inhibitors seem not to influence normal glutamate functions but rather pathological excessive glutamate signaling [102], which is in contrast with other strategies modulating glutamatergic neurotransmission, such as NMDAR antagonists [122].

Administration of 2-PMPA (the selective and potent GCPII inhibitor) reduced neuron cell death and protected against ischemic brain injury in rat model of a stroke [102, 123]. Similarly, ZJ-43 inhibitor reduced neuronal and astrocyte damage following traumatic brain injury in rats [124]. The GCPII inhibitors were also employed to reduce inflammatory and neuropathic pain in rat models, exhibiting analgesic effects [64, 125, 126]. Chronic glutamate toxicity may also be associated with the pathogenesis of amyotrophic lateral sclerosis (ALS) [127]. GCPII inhibitors protected motor neuron from death in both *in vitro* cell culture experiments and transgenic mouse models of ALS [71]. Furthermore, oral administration of the inhibitors delayed the onset of the disease and slowed its progression in the mice models [71].

Above-mentioned data suggest that GCPII inhibition in the nervous system offers an undoubted therapeutical potential. However, all the studies were performed using either polar inhibitors not crossing the blood-brain barrier (2-PMPA, ZJ-43) or containing potentially metabolically unstable sulfur (2-MPPA). Therefore, there is a need for a novel generation of less polar GCPII inhibitors that retain the potency and selectivity of 2-PMPA. As described in the section (1.2.2.1. "Phosphorus-containing GCPII inhibitors"), employing a POC prodrugs of 2-PMPA might represent a promising strategy in the future development of GCPII inhibitors [56].

1.4.2. GCPII as a target in prostate cancer

1.4.2.1. Prostate cancer

Prostate cancer is the second leading cause of cancer death in men in the USA, killing roughly 30,000 men a year [128]. It is also the most commonly diagnosed cancer (approximately 200,000 new cases a year); most of men will eventually develop prostate cancer if they live long enough. On the other hand, many men will die from unrelated causes since most prostate cancers are slowly growing and not aggressive.

A considerable effort has been made to detect prostate cancer earlier at more treatable stages and before it becomes life threatening. Screening for prostate specific antigen (PSA), a protein produced by the prostate and found in the blood when prostate cancer is present, used to be a promising approach to diagnose the disease [35, 129]. However, today the test is considered controversial since high blood levels of PSA are often not associated with prostate cancer and, therefore, the screening leads to many false positive results [130, 131]. Naturally, there is a need for additional biomarkers that would either replace or supplement the PSA test – the ideal marker would only be produced by the prostate cancer and associated with its aggressive and high-grade stages.

There are several types of prostate cancer treatment. Currently, conservative approach is often considered for low-risk prostate cancer – monitoring the tumor over time and launching further and more invasive treatment only if the disease progresses. Localized prostate cancer is most commonly treated by radical prostatectomy (removal of the prostate) and radiotherapy. Once the cancer has escaped from the prostate itself and spread (usually) to the bones and lymph nodes, the disease is much less treatable and the outlook is poor. The

treatment involves chemical castration – administration of drugs suppressing male hormones; however, the advanced metastasized prostate cancer is currently considered incurable (reviewed in [132]).

1.4.2.2. GCPII in the prostate

GCPII is strongly expressed on the secretory acinar surface of prostate glandular cells [1, 22, 25, 42]. GCPII expression was shown to increase with increasing cancer grades (Fig. 8), reaching highest expression levels in androgen-resistant prostate cancer [24]. Despite its strong expression, the GCPII function in the prostate (if any) has not been revealed yet. GCPII enzyme activity was postulated to increase folate uptake and subsequently proliferation of prostate cancer cells [133, 134]; nevertheless, the hypothesis has been confirmed by neither other group nor experiments. Thus, the physiological role of GCPII in prostate cancer remains unknown. Anyway, GCPII, strongly expressed on prostate cancer epithelial cells, represents a tempting target for both prostate cancer imaging and therapy.

a) b) c)
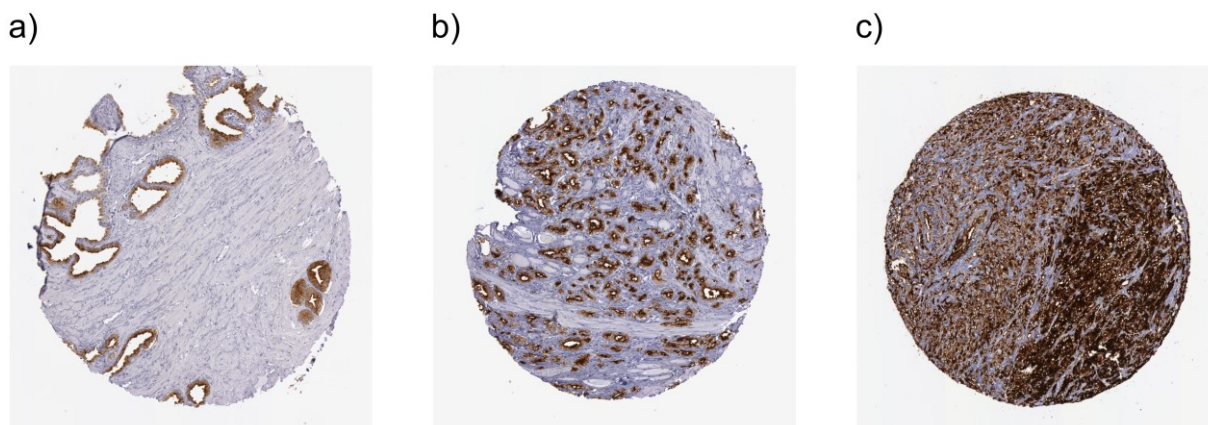
Fig. 8: Immunohistochemistry analysis of GCPII expression in the prostate and prostate cancer.
GCPII expression in the prostate tissues was analyzed using CAB001451 antibody. a) Male, age 64 (prostate cancer not diagnosed). b) Male, age 53 (adenocarcinoma, medium grade). c) Male, age 68 (adenocarcinoma, high grade). Images were obtained from the Human Protein Atlas, entry "FOLH1" (http://www.proteinatlas.org/ENSG00000086205-FOLH1/tissue).

1.4.2.3. GCPII-based prostate cancer imaging

Molecular imaging enables non-invasive detection and visualization of molecular and cellular processes in living organisms. There is a variety of techniques to be used, such as positron emission tomography (PET), single photon emission computed tomography (SPECT), magnetic resonance imaging (MRI), computed tomography (CT) and fluorescence

imaging (usually near-infrared). Imaging has become an indispensable tool in both life sciences and medicine (reviewed in [135, 136]). Agents targeting GCPII (both for imaging and therapy) fall into two major categories: anti-GCPII antibodies and low-molecular-weight GCPII inhibitors.

Currently, the only imaging agent approved by the U.S. Food and Drug Administration (FDA) for GCPII-based prostate cancer imaging is the ^{111}In-labeled monoclonal antibody 7E11 [137, 138]. The conjugate known as ^{111}In-capromab pendetide or ProstaScint™ has been used to detect and localize prostate cancer metastases spread to soft tissues outside the prostate as well as recurrent prostate cancer after radical prostatectomy [139, 140]. However, the negative properties of the 7E11 antibody (recognizing the intracellular GCPII epitope), non-specific tissue uptake (e.g. liver, kidney) and inherent limitations of SPECT lead towards difficult interpretations of the results [141, 142].

There were high expectations with second-generation antibody J591 that binds the external portion of GCPII and thus visualizes GCPII on viable cells [28, 31, 143]. J591 was humanized and radiolabeled with ^{111}In, ^{99m}Tc or [89]Zr for imaging and ^{90}Y or ^{177}Lu for therapy [144-146]. Indeed, [89]Zr-J591 detected bone lesions that were not identified by conventional imaging [147] and ^{177}Lu-J591 exhibited higher target-to-background signals compared with [111]In-7E11 [148].

Since antibodies suffer from the poor pharmacokinetics, usually requiring several days to clear from non-specifically bound tissues (approximately 1 week), researchers have been developing low-molecular-weight inhibitors to address and overcome this drawback. Small molecules are bound by tumor GCPII and rapidly removed from the circulation by the renal filtration. Research on urea-based inhibitors radiolabeled with ^{18}F, ^{68}Ga or ^{64}Cu for PET (or ^{177}Lu for therapy) has become one of the most dynamically developing branches of GCPII-focused studies [61, 149]. Currently, ^{68}Ga-PSMA-11 (or ^{68}Ga-PSMA-11-HBED-CC) represents the most promising PET tracer that has already demonstrated high potential for detection of recurrent prostate cancer and metastases (Fig. 9a; p. 27) [150-152]. Another PET agent, named ^{18}F-DCFPyL, with lower positron emission energy, offers higher image resolution and might identify small prostate lesions with higher fidelity than ^{68}Ga-PSMA-11 (Fig. 9b,c; p. 27) [153, 154].
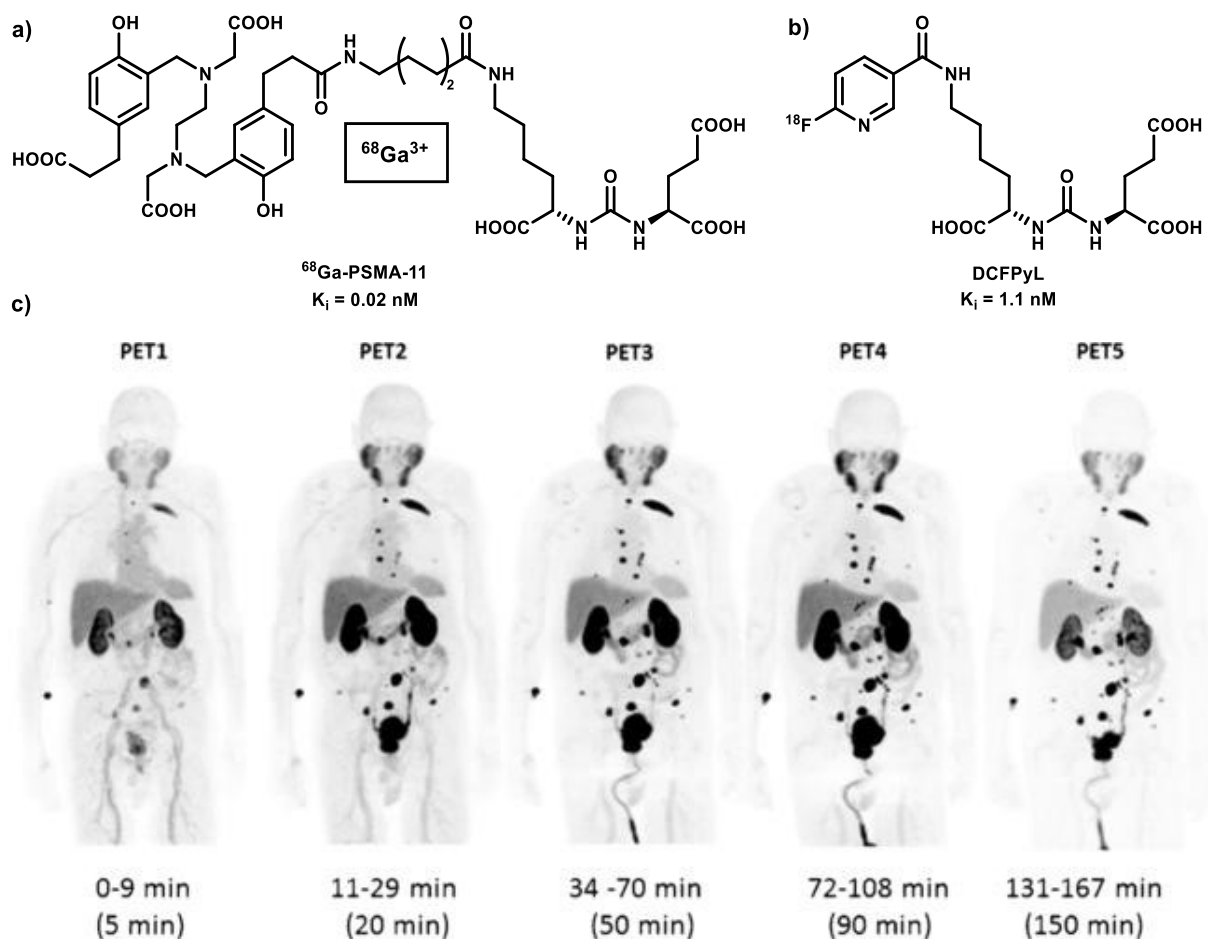
Fig. 9: GCPII-targeted PET imaging agents.

a) Radiometal-labeled agent ^{68}Ga-PSMA-11; its structure consists of a urea-based GCPII inhibitor, linker and metal chelator. The linker allows the inhibitor to reach the GCPII active site while keeping the bulky "reporting part" outside of GCPII [61]. Radionuclide ^{68}Ga does not require an on-site cyclotron and has a shorter half-life in comparison with ^{18}F (68 min vs. 110 min). b) Radiolabeled agent [^{18}F]DCFPyL [149]. c) PET image sequence of a prostate cancer patient acquired by [^{18}F]DCFPyL that demonstrated presence of metastatic lesions in multiple bones and lymph nodes (black spots). Adapted from [154].

1.4.2.4. Prostate cancer therapy based on GCPII targeting

Successful *in vivo* GCPII targeting is an important prerequisite for prostate cancer therapy using GCPII as a target. Although the biology and function of GCPII in prostate cancer remain to be explained, GCPII, strongly expressed on prostate cell membranes and internalizing, is an excellent target for the treatment of prostate cancer. Similarly to imaging, there is a number of approaches including the use of (radiolabeled) antibodies, antibody-drug conjugates (ADCs), small-molecules (radiolabeled or conjugated with toxins) and others.

27

Not surprisingly, the first GCPII-targeted "therapeutic" agent was 7E11 antibody, radiolabeled with ^{90}Y instead of ^{111}In (used in ProstaScint™); however, its use was associated with hematologic toxicity [155, 156]. The toxicity and inability of 7E11 antibody to bind viable tumor cells led to second-generation radiolabeled antibody ^{177}Lu-J591 [144] that was tested in several phase I and II trials [148, 157, 158]. The phase II study in men with metastatic castration-resistant prostate cancer (mCRPC) demonstrated excellent targeting of ^{177}Lu-J591 and a dose-dependent PSA decline; a single dose of ^{177}Lu-J591 was well tolerated with reversible myelosuppression [148].

Besides radioimmunotherapy, the monoclonal antibodies (namely J591) might serve as homing devices for the delivery of cytotoxic molecules and toxins (i.e. ADCs). Deimmunized J591 was conjugated to maytansinoid 1 (DM-1), an extremely potent cytotoxic drug [159]; the phase 1/2 trial showed limited activity in mCRPC patients and neurotoxicity caused by disulfide linker lability and rapid deconjugation of DM-1 [160]. Additionally, a conjugate of anti-GCPII antibody and monomethyl auristatin E (MMAE) was developed [161, 162] that later underwent a phase II trial, exhibiting low toxicity and a PSA response $\geq$ 50% in 33% of the mCRPC patients [163]. Other GCPII-targeted ADCs involve conjugates of J591 and ricin A-chain [164] or anti-GCPII single-chain antibody fragment (scFv) D7 and the toxic domain of Pseudomonas exotoxin A (PE40) [165]; the latter exhibited a significant growth inhibition of a GCPII-positive tumor xenograft in mice [166].

As for small molecules, recently prepared ^{177}Lu-PSMA-617 is a promising therapeutic agent for the treatment of mCRPC [167], which has been intensively studied and evaluated during the last two years [168-170]. Two recent German retrospective multicenter studies investigating ^{177}Lu-PSMA-617 radioligand therapy (145 and 59 mCRPC patients) showed favorable safety and efficacy of the radioconjugate (a PSA decline $\geq$ 50% occurred in 45% and 53% of the patients, respectively) [170, 171]. In February 2017, the first U.S. multicenter phase II trial of ^{177}Lu-PSMA-617 targeted radioligand therapy received FDA clearance [172] (ClinicalTrials.gov Identifier: NCT03042312), demonstrating a great potential of ^{177}Lu-PSMA-617 for its future therapeutic use.

The use of small molecules is not limited to radioconjugates. Theranostic conjugate of a GCPII inhibitor, cytotoxic drug (DM-1) and PET imaging probe was used for GCPII *in vivo*

visualization in tumor xenografts in mice and selective toxicity towards GCPII-expressing cells [173]. Furthermore, GCPII inhibitors have also been used as targeting moieties in a number of various nanoparticles targeting GCPII, designed for imaging, therapy or theranostics [174-176].

1.4.3. GCPII as a target for treatment of inflammatory bowel disease

In contrast to the established connection between GCPII and treatment of brain disorders and prostate cancer, the potential of GCPII for therapy of inflammatory bowel disease (IBD) has been discovered rather recently. GCPII enzyme activity was shown to be increased in IBD patients and murine models of IBD [177]. Interestingly, daily administration of 2-PMPA dramatically ameliorated murine IBD symptoms and substantially reduced disease severity [177, 178]; however, the mechanism of 2-PMPA action has not been determined. Nevertheless, the results suggest that GCPII inhibition may represent a novel IBD therapy, but further extensive research must be conducted to enlighten the role of GCPII in IBD.

1.5. HPMA COPOLYMER CONJUGATES

N-(2-hydroxypropyl)methacrylamide (HPMA) copolymer conjugates are multivalent macromolecules that have been widely used as drug delivery carriers or imaging agents (reviewed in [179-181]). The HPMA copolymers trace their roots to Prague in the 1960s when Jindřich Kopeček started to work on water-soluble and biocompatible polymers based on *N*-substituted methacrylamides [182-184]. The first use of HPMA copolymers was as blood plasma expanders [185]. Slightly later, the HPMA copolymers were suggested to be used as polymeric drug carriers [186].

HPMA copolymers could be prepared to contain a number of reactive groups, such as thiazolidine-2-thione, randomly distributed along the polymer chain (Fig. 10; p. 30) [187]. These functional groups enable easy modification of the copolymer backbone with various molecules, e.g. enzyme inhibitors for selective targeting, fluorophores and radionuclides for visualization and drugs for cytotoxic effects [181, 187-190].

Since the detailed description of HPMA copolymer conjugates is beyond the scope of the thesis, the interested readers can find more pieces of information in a recent review by

Ulbrich *et al.* [180] or in reviews by the fathers of HPMA polymers – Kopeček *et al.* [179] and Duncan *et al.* [191].
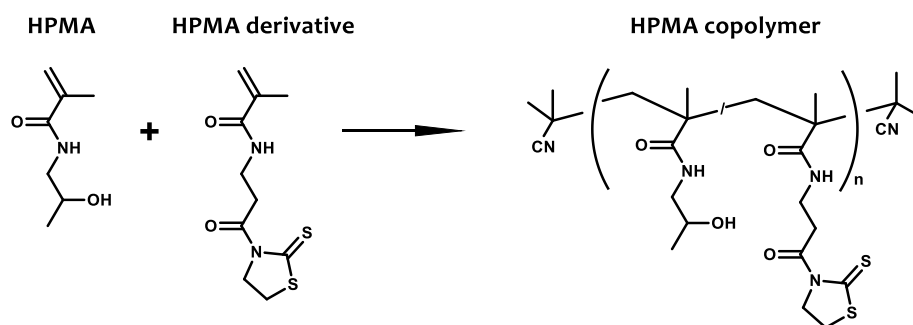
Fig. 10: Synthesis of HPMA copolymers.

Preparation of HPMA copolymers by reversible addition-fragmentation chain transfer (RAFT) copolymerization of two monomer units: *N*-(2-hydroxypropyl)methacrylamide (HPMA) and 3-(3-methacrylamido-propanoyl)thiazolidine-2-thione (Ma-ß-Ala-TT). Ma-ß-Ala-TT contains thiazolidine-2-thione group that is reactive towards primary amino groups [187]. Therefore, by aminolysis of the reactive group, HPMA copolymers can be easily decorated with a number of various molecules.

1.5.1. HPMA copolymer-drug conjugates

Traditional cancer treatment has involved the use of non-specific cytotoxic molecules that inhibited mitosis and thus affecting preferentially the rapidly dividing cancer cells. However, modern "targeted therapy" aims to target only the tumor cells, not harming the healthy tissues. To achieve accumulation of the cytotoxic drugs in a tumor, a selective delivery system is required. Antibody-drug conjugates represent a highly effective and one of the best examples of selective anti-cancer (bio)molecules.

HPMA copolymer-drug conjugates offer an alternative approach for "targeted" drug delivery to tumor cells. In contrast to "active" targeting by selective antibodies, HPMA copolymer conjugates rely on the "passive" accumulation in tumors via the enhanced-permeability and retention (EPR) effect (described in more detail in the next chapter) [192-194]. When compared to low-molecular-weight drugs, the advantage of polymer-conjugated drugs is (besides their accumulation in the tumor via EPR effect) their improved pharmacokinetics (increased circulation times in the bloodstream) and "solubilization" of usually hydrophobic molecules by their conjugation to the water-soluble polymers [195, 196].

After endocytosis into a cancer cell, the conjugates enter a lysosomal compartment; therefore, the drugs must be connected to an HPMA backbone via a cleavable linker.

A disulfide group (undergoing reduction) [197, 198], pH-sensitive bonds (unstable in low lysosomal pH) [199] and tetrapeptide Gly-Phe-Leu-Gly sequence (cleavable by lysosomal cathepsin B) [200] are examples of such linkers. A doxorubicin, an anthracycline molecule intercalating DNA and interfering with its function, is an archetypal drug used for delivery by HPMA conjugates [201]. The HPMA copolymer–doxorubicin conjugates PK1 and PK2 (Fig. 11) underwent phase I and phase II clinical trials and showed antitumor activity against breast, lung [202, 203] and hepatocellular carcinoma [204], respectively. A large number of other polymer-drug conjugates were prepared, containing various drugs, linkers or even targeting ligands. Incorporation of targeting ligands selective for cancer cells, such as oligosaccharides (conjugate PK2) [204], peptides [205] or fragments of antibodies [206, 207], enables also active targeting via cancer cell surface proteins.
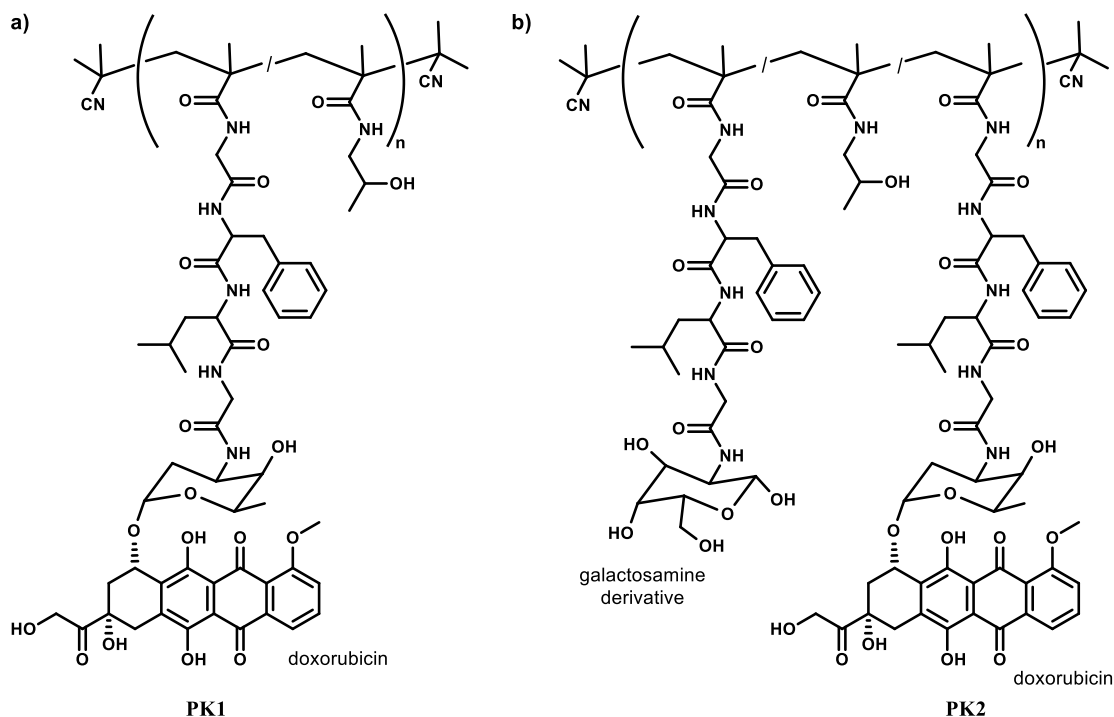
Fig. 11: HPMA copolymer-doxorubicin conjugates PK1 and PK2.

a) Conjugate PK1 contains doxorubicin attached by Gly-Phe-Leu-Gly tetrapeptide linker that is cleaved by cathepsin B present in the lysosomes. PK1 delivery to solid tumor depends solely on its passive accumulation via the enhanced-permeability and retention (EPR) effect [202, 203]. b) Conjugate PK2 bears besides doxorubicin a galactosamine derivative that binds a specific receptor on hepatocytes [204].

1.5.2. Enhanced-permeability and retention (EPR) effect

The enhanced-permeability and retention (EPR) effect is a phenomenon by which macromolecules accumulate in solid tumors more than in normal tissues [208, 209]. The EPR effect is attributed especially to two factors: defective tumor vasculature and impaired lymphatic drainage. Since rapidly growing (solid) tumor cells become dependent on the blood supply, they must promote the production of new blood vessels in order to be supplied with oxygen and nutrients and grow quickly [210]. This process, called tumor angiogenesis, results in the formation of abnormal imperfect neovasculature that contains poorly aligned endothelial cells with fenestrations [211]. Due to the leaking vessels, molecules can escape from the vessels and begin accumulate in the solid tumor. At the same time, malfunctioning lymphatic drainage cannot properly remove accumulated molecules; this process is highly dependent on the size of the molecules – the larger the molecules (and their surface charge), the more efficient accumulation in solid tumors [208]. Taken all above-mentioned facts into account, the EPR effect is the major mechanism by which macromolecular polymer-drug conjugates exhibit their therapeutic effects on solid tumors [193].

The EPR effect represents "passive targeting" of tumor agents, which is in contrast to active (i.e. selective) targeting usually accomplished by a specific interaction between a cell surface protein and a targeting agent.

1.5.3. HPMA copolymer conjugates targeting GCPII

Kopeček's group published two studies on HPMA conjugates targeting GCPII. In the first publication, they conjugated anti-GCPII antibody (serving thus as a targeting moiety) to an HPMA copolymer and analyzed subcellular trafficking of the obtained conjugate [212]. The binding affinity of the conjugated antibody was not compromised by the attachment to the copolymer; interestingly, the conjugate was rapidly internalized into the cells and subsequently transported to late endosomes [212]. The second study describes HPMA-docetaxel conjugates decorated with GCPII inhibitors for GCPII-targeted drug delivery [190]. They observed no difference between the GCPII-targeted and non-targeted conjugate in *in vitro* cytotoxicity assay (probably due to the deconjugation of docetaxel from the conjugate); nonetheless, the GCPII-targeted conjugate exhibited stronger *in vivo* antitumor activity in nude mice bearing prostate C4-2 cancer xenografts [190].

Recently, hyperbranched polyethylene glycol polymer conjugate loaded with doxorubicin and featuring urea-based GCPII inhibitors on its periphery was described [213]. Tumor regression study in mice demonstrated 90% reduction in tumor volume while free doxorubicin reduced the tumor volume only by 30% and caused considerable toxicity to the mice [213].

2. RESULTS

2.1. AIMS OF THE THESIS

1. To develop a method for the detection and quantitation of GCPII in the human blood. To verify if other enzymes contribute to GCPII activity. To analyze the origin and function of GCPII in the blood and determine if GCPII levels in the blood correlate with age, sex or, eventually, prostate cancer stage.

2. To prepare and characterize mouse GCPII regarding its enzyme activity, inhibition profile, substrate specificity and, importantly, tissue distribution in mice. To compare the results with human GCPII and elucidate if mouse is a suitable animal model for GCPII-based therapies.

3. To design and develop polymer-based antibody mimetics capable of GCPII targeting in common biochemical methods. To prepare these antibody mimetics for other enzymes and proteins and verify their universal and versatile applicability.

2.2. Publications

Publications included in the thesis

I. Knedlik T, Navratil V, Vik V, Pacik D, Sacha P, Konvalinka J: **Detection and quantitation of glutamate carboxypeptidase II in human blood.** *Prostate 2014*, 74(7):768-780.

II. Knedlik T, Vorlova B, Navratil V, Tykvart J, Sedlak F, Vaculin S, Franek M, Sacha P, Konvalinka J: **Mouse glutamate carboxypeptidase II (GCPII) has a similar enzyme activity and inhibition profile but a different tissue distribution to human GCPII.** *FEBS Open Bio 2017,* 7(9):1362-1378.

III. Sacha P, Knedlik T, Schimer J, Tykvart J, Parolek J, Navratil V, Dvorakova P, Sedlak F, Ulbrich K, Strohalm J, Majer P, Subr V, Konvalinka J: **iBodies: Modular Synthetic Antibody Mimetics Based on Hydrophilic Polymers Decorated with Functional Moieties.** *Angew Chem Int Ed Engl 2016*, 55(7):2356-2360.

Publications not included in the thesis

I. Dvorakova P, Busek P, Knedlik T, Schimer J, Etrych T, Kostka L, Stollinova Sromova L, Subr V, Sacha P, Sedo A, Konvalinka J: **Inhibitor-Decorated Polymer Conjugates Targeting Fibroblast Activation Protein.** *J Med Chem 2017*, accepted.

II. Tykvart J, Sacha P, Barinka C, Knedlik T, Starkova J, Lubkowski J, Konvalinka J: **Efficient and versatile one-step affinity purification of in vivo biotinylated proteins: expression, characterization and structure analysis of recombinant human glutamate carboxypeptidase II.** *Protein Expr Purif 2012*, 82(1):106-115.

III. Navratil V, Schimer J, Tykvart J, Knedlik T, Vik V, Majer P, Konvalinka J, Sacha P: **DNA-linked Inhibitor Antibody Assay (DIANA) for sensitive and selective enzyme detection and inhibitor screening.** *Nucleic Acids Res 2017*, 45(2):e10.

2.2.1. Paper I: Detection and quantitation of glutamate carboxypeptidase II in the human blood

Motivation of the study

Glutamate carboxypeptidase II, better known as prostate-specific membrane antigen (PSMA) among urologists, is strongly expressed in the human prostate and, interestingly, approximately 10-fold overexpressed in prostate cancer. Even though its role in the prostate and prostate cancer progression (if any) is not known, GCPII's potential to become a diagnostic and/or therapeutic target was recognized 20 years ago. An [111]indium-antibody conjugate raised against GCPII, trade name ProstaScint™, became the first (and unfortunately also the last) detection agent to image GCPII expression and thus the extent of prostate cancer, which was approved by the FDA.

GCPII presence was also analyzed in the human blood. GCPII was detected in the human blood by several groups, however, the results were inconsistent and GCPII levels in the blood differed significantly. Besides GCPII, another metallopeptidase (plasma glutamate carboxypeptidase, PGCP) was identified in the blood plasma and reported to possess NAAG-hydrolyzing activity.

To make the situation clear, we decided to determine GCPII concentration in human blood via its NAAG-hydrolyzing activity. Furthermore, we were interested if GCPII levels in the blood vary among healthy volunteers.

Summary

We shed light upon conflicting reports on the presence of GCPII in the human blood. We also analyzed if another protease, plasma glutamate carboxypeptidase, may contribute to the NAAG-hydrolyzing activity of GCPII.

First, we cloned two PGCP constructs (containing an Avi-tag placed at its either C-terminus, or N-terminus), expressed them in insect cells and purified them via affinity chromatography. We then verified that the proteins are properly folded and enzymatically active – both constructs cleaved a cognate substrate of PGCP (L-seryl-L-methionine). In contrast with the previous report, neither of the constructs cleaved NAAG, the endogenous substrate of GCPII.

Having proved that PGCP does not contribute to the enzyme activity of GCPII, we used a NAAG-hydrolyzing assay for detection and subsequent quantitation of GCPII in the human blood plasma. We analyzed three blood plasma samples from healthy individuals and detected NAAG-hydrolyzing activity in all of them (Fig. 12a). The activity was sensitive to 2-PMPA and other selective GCPII inhibitors, suggesting that GCPII is solely responsible for the activity (Fig. 12a). Furthermore, we confirmed presence of GCPII in the blood plasma by immunoprecipitation of GCPII from the diluted blood plasma using biotinylated monoclonal antibody raised against native GCPII (Fig. 12b).
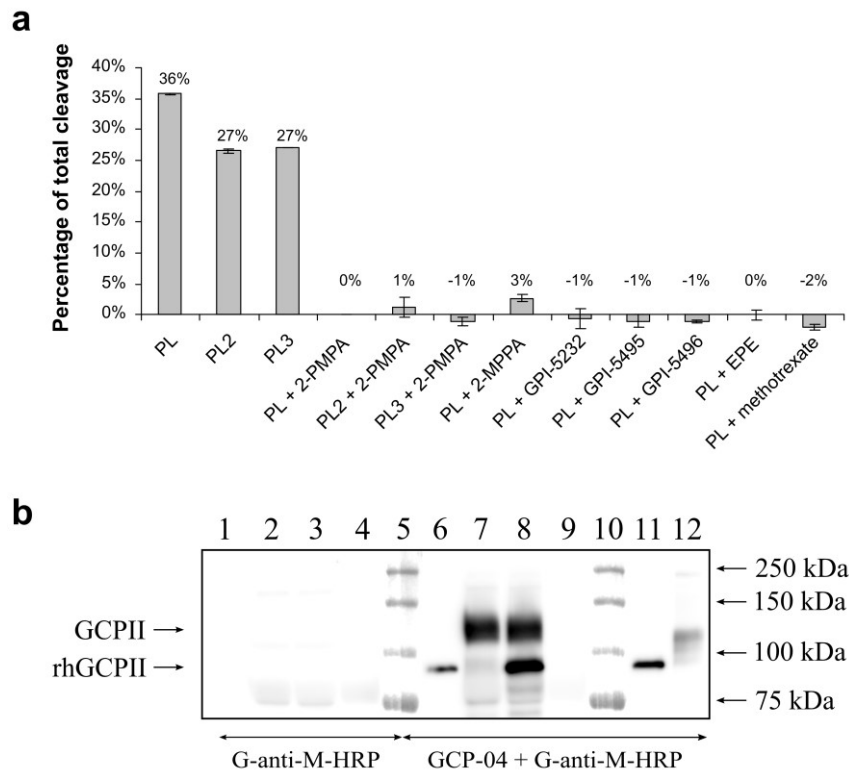
Fig. 12: GCPII was detected in the blood plasma.

GCPII was detected and isolated from the blood plasma. a) NAAG-hydrolyzing activity, which is GCPII-specific, was detected in three volunteers' heparin blood plasma samples (PL, PL2 and PL3). The activity was inhibited by a panel of selective GCPII inhibitors. b) GCPII was immunoprecipitated (IP) from the human blood plasma using biotinylated GCPII-specific antibody 2G7 (lane 7). As a positive control, the plasma sample was spiked with recombinant human GCPII (rhGCPII). As a negative control, blank streptavidin agarose was used. GCPII on the western blot was visualized with anti-GCPII monoclonal antibody GCP-04, followed by horseradish peroxidase-conjugated goat anti-mouse IgG secondary antibody (G-anti-M-HRP). A half of the membrane was probed with G-anti-M-HRP to visualize the nonspecific signal caused by the secondary antibody. (1,6) rhGCPII standard, 1 ng; (2,7) Elution from IP; (3,8) Elution from IP-positive control; (4,9) Elution from IP-negative control; (5,10) All blue standard (Bio-Rad); (11) rhGCPII standard, 2 ng; (12) lymph node carcinoma of the prostate (LNCaP) cell lysate, 1.5 μg total protein. Twenty-five microliters of the elution fraction sample was loaded to each lane.

Finally, we collected blood plasma samples from healthy individuals and determined GCPII concentration in their blood (Tab. 1). The GCPII levels ranged between 1.3 and 17.2 ng/ml; slightly surprisingly, we detected GCPII also in the female samples, which suggests a non-prostatic origin of GCPII. The geometrical mean of the GCPII levels in the blood plasma was 3.2 ng/ml; for men only: 3.7 ng/ml; and female only: 2.0 ng/ml. We observed no correlation between GCPII concentration and the age of the volunteers.

Tab. 1: GCPII levels in the blood plasma of healthy volunteers.

Using GCPII-specific radioenzymatic assay, GCPII concentration in the heparin blood plasma of healthy volunteers was determined. The samples were measured in duplicates in three separate experiments and the results are mean ± standard deviation. Recombinant extracellular GCPII was used as a standard of NAAG-hydrolyzing activity. No correlation between GCPII levels and the age or sex was observed.

	Age (years)	GCPII in plasma (ng/ml)
female 1	22	1.4 ± 0.3
female 2	31	1.3 ± 0.3
female 3	43	1.9 ± 0.3
female 4	46	4.3 ± 0.3
male 1	20	3.7 ± 0.6
male 2	22	4.0 ± 0.6
male 3	24	2.3 ± 0.4
male 4	25	5.7 ± 0.8
male 5	26	1.8 ± 0.3
male 6	26	1.4 ± 0.3
male 7	27	1.3 ± 0.3
male 8	27	3.4 ± 0.7
male 9	28	4.6 ± 0.7
male 10	28	1.5 ± 0.3
male 11	33	3.2 ± 0.5
male 12	34	17.2 ± 5.0
male 13	45	2.4 ± 0.6
male 14	50	3.0 ± 0.4
male 15	52	9.9 ± 1.0

My contribution

In this paper, I conducted all the experiments presented. I prepared two constructs of human plasma glutamate carboxypeptidase, expressed them in insect cells, purified and tested them for their enzyme activity. I also showed the presence of glutamate carboxypeptidase II in the human blood plasma and quantified its levels among volunteers not diagnosed with prostate cancer. I also wrote a draft of the manuscript.

2.2.2. Paper II: Biochemical characterization and tissue distribution of mouse glutamate carboxypeptidase II

Motivation of the study

Glutamate carboxypeptidase II, which is overexpressed on prostate carcinoma cells and also implicated in glutamate excitotoxicity in the brain, became an interesting diagnostic marker of prostate cancer and a possible therapeutic target both for prostate cancer and neuronal disorders connected with increased levels of glutamate in the central nervous system.

For the development and subsequent testing of novel therapeutics, it is necessary to have a suitable animal model. Mice represent usually the most promising candidates while rats and pigs are the second choice. Several years ago, a study comparing human, rat and pig GCPII was performed in our laboratory [21]; however, the mouse ortholog was not included although mice are the most widely used animals in the GCPII-focused research.

Mouse GCPII is highly similar to its human counterpart (91% of amino acid similarity). Mouse GCPII was shown to possess both enzyme activities of human GCPII: NAAG-hydrolyzing activity in the brain and folate hydrolase activity in the small intestine. On the other hand, its absence in the mouse prostate is in marked contrast to the tissue distribution of human GCPII. Therefore, we set to perform a thorough study assessing mouse GCPII enzyme activity and tissue distribution, which had been needed.

Summary

In this paper, we prepared recombinant mouse GCPII and compared it in detail with the human ortholog. We focused particularly on the expression pattern of mouse GCPII since this is a highly relevant aspect for the development of new anticancer and neuroprotective therapies based on GCPII.

First, we characterized the enzyme activity of mouse and human GCPII using both endogenous substrates: NAAG (brain) and pteroyl-di-L-glutamate (small intestine). We observed no striking differences between the compared enzymes – mouse GCPII possessed lower catalytic efficiency but similar substrate preferences compared to the human enzyme. We also analyzed the inhibition profile of both enzymes using a panel of ten common GCPII inhibitors, showing comparable inhibition constants for the majority of inhibitors.

Finally, we focused on the GCPII distribution in mouse tissues. We collected tissue samples from six mice (3 females and 3 males) and determined GCPII expression levels using two independent assays (western blotting and GCPII activity assay) (Fig. 13).
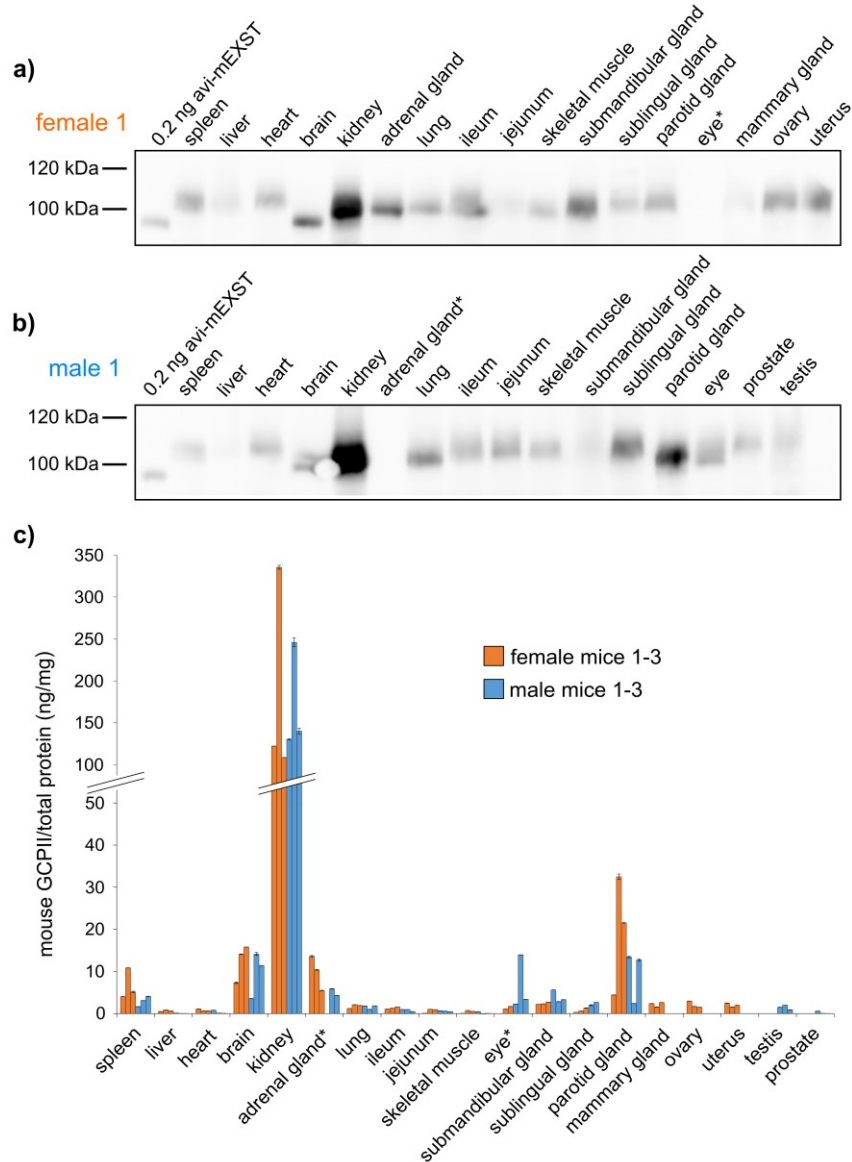
Fig. 13: Expression profile of GCPII in mice.

a, b) Western blot analysis of the GCPII distribution in mouse female and male tissues, respectively. GCPII was visualized by monoclonal antibody GCP-04, followed by HRP-conjugated goat anti-mouse IgG secondary antibody. Recombinant mouse extracellular GCPII was used as a standard (avi-mGCPII) and 50 µg of total protein was loaded. c) Expression profile of GCPII in mice tissues determined by quantification of GCPII-specific NAAG-hydrolyzing activity by radioenzymatic assay using [³H]NAAG as a substrate and avi-mGCPII as a standard. Each tissue sample was measured in duplicate using 1-50 µg total protein in the reaction; the assay was performed with the same tissue samples used in the western blot analysis. The asterisk (*) represents the missing sample (female 1 eye, male 1 adrenal gland).

We detected highest GCPII expression levels in the mouse kidney, brain and salivary glands. We did not detect GCPII in the mouse prostate, which is in agreement with previous studies (Fig. 13; p. 41).

Taken together, our results show that there are no significant differences in enzyme activities of both proteins. Thus, mouse GCPII is a proper substitute for human GCPII in the development of novel inhibitors. Nevertheless, the different expression pattern must be considered when using mice as an animal model for the development of targeted anticancer drug delivery approaches.

My contribution

I expressed and purified recombinant mouse glutamate carboxypeptidase II (GCPII). I performed the majority of the experiments, including analysis of GCPII enzyme activity, inhibition profile and distribution of the GCPII protein in mouse tissues. I also wrote a draft of the manuscript.

2.2.3. Paper III: iBodies: modular synthetic antibody mimetics based on hydrophilic polymers decorated with functional moieties

Motivation of the study

Monoclonal antibodies caused a revolution in biochemistry and now represent indispensable tools for biomedicine and therapy. As for GCPII, there is a number of antibodies available, however, their use might suffer from several disadvantages, such as difficulty of chemical modification and limited stability. For other proteins, it may be even impossible to prepare antibodies with sufficient binding potency and selectivity towards the target.

Apart from antibodies, selective enzyme inhibitors may be another choice for targeting a protein of interest. In the field of GCPII, there are several groups of potent and selective inhibitors, which are already used as low-molecular-weight molecules for GCPII imaging both *in vitro* and *in vivo*. Almost every laboratory studying a particular enzyme owns a number of more or less potent and selective inhibitors.

Therefore, we combined these two approaches together and developed synthetic antibody mimetics, which we called iBodies. The iBodies are based on water-soluble *N*-(2-hydroxypropyl)methacrylamide (HPMA) copolymer decorated with three low-molecular-weight ligands: a targeting ligand (usually an enzyme inhibitor), an imaging probe and an affinity anchor (Fig. 14; p. 44). The ligands ensure selective targeting of a protein of interest, visualization of the conjugate and enable its isolation.

Our initial goal was to develop a novel biochemical tool to study GCPII physiological functions; however, during the development we realized that we had in our hands a universal platform that could be "easily" adapted virtually for all proteins, for which a targeting ligand is known.

Summary

In this study, we developed novel polymer-based antibody mimetics, using enzyme inhibitors as targeting ligands (Fig. 14; p. 44). We chose glutamate carboxypeptidase II (GCPII) as a model protein and our primary target.
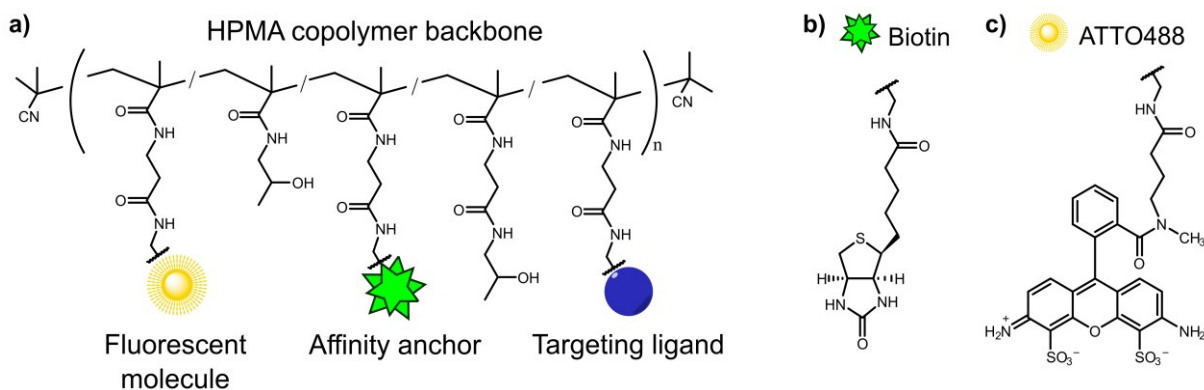
Fig. 14: Schematic structure of iBodies.

The iBodies are polymer-based antibody mimetics. a) The iBodies consist of an *N*-(2-hydroxypropyl)methacrylamide (HPMA) copolymer, which is substituted with various small molecules for distinct functions: an imaging probe, affinity anchor and targeting ligand (e.g. selective enzyme inhibitors); b) affinity anchor biotin; c) fluorescent molecule ATTO488.

A previously described selective GCPII inhibitor was conjugated to an HPMA copolymer, serving as a targeting ligand and enabling selective recognition of GCPII (Fig. 15a; p. 45). Besides the inhibitor molecules, ATTO488 (functioning as an imaging probe) and biotin (for isolation/immobilization of the conjugate) were attached to the copolymer backbone. The obtained conjugate, an anti-GCPII iBody, was then tested in a number of biochemical applications to evaluate its properties and applicability.

The binding of the conjugate to GCPII was analyzed using GCPII enzyme activity inhibition assay and further by surface plasmon resonance, which revealed remarkably low dissociation constant of the interaction (Fig. 15b; p. 45). Therefore, we proceeded to *in vitro* methods such as "immunoprecipitation" (isolation of GCPII from cell lysates and the blood serum; Fig. 15c; p. 45) and sandwich ELISA (reaching limit of detection as low as 1 pg GCPII; Fig. 15d; p. 45). Having succeeded, we also verified the suitability of the iBody as a tool for the selective GCPII visualization on GCPII positive cells using flow cytometry (Fig. 15e; p. 45) and confocal microscopy (Fig. 15f; p. 45). All above-mentioned methods showed that anti-GCPII iBody is an excellent substitute for anti-GCPII antibodies in common biochemical applications.
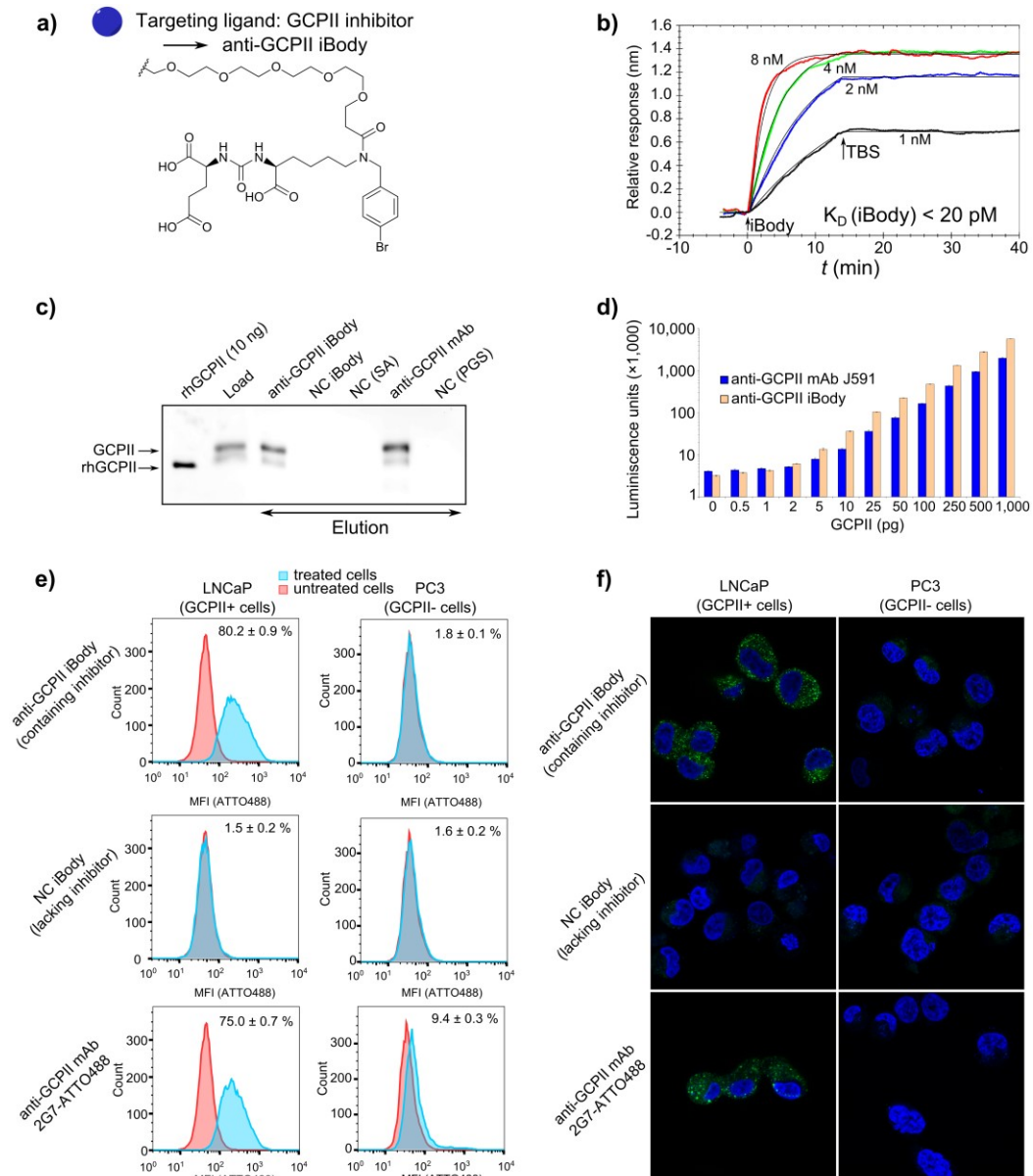
Fig. 15: Applications of anti-GCPII iBody in biochemical methods.

a) Selective GCPII inhibitor used as an iBody ligand. b) Surface plasmon resonance (SPR) analysis of the interaction between (immobilized) GCPII and anti-GCPII iBody. c) Western blot analysis of GCPII "immunoprecipitation" from lymph node carcinoma of the prostate (LNCaP) cell lysate using anti-GCPII iBody or monoclonal antibody (mAb) J591. As negative controls, iBody lacking the selective GCPII inhibitor (NC iBody) and blank streptavidin agarose (NC(SA)) or blank protein G sepharose (NC(PGS)) were used. As a standard, recombinant extracellular GCPII was used (rhGCPII). d) Sandwich ELISA using GCPII-specific mAb 2G7 as a capture antibody and either anti-GCPII iBody or biotinylated mAb J591 as a detecting agent. e) Flow cytometry of cells expressing and not expressing GCPII (LNCaP and PC-3, respectively). Cells were incubated with either anti-GCPII iBody or anti-GCPII mAb 2G7 labeled with ATTO488 (2G7-ATTO488) to compare iBody staining and antibody staining. As a negative control, iBody lacking the selective GCPII inhibitor was used (NC iBody). f) Confocal microscopy analysis of LNCaP and PC-3 cells, incubated with anti-GCPII iBody, mAb 2G7-ATTO488 or NC iBody.

45

Furthermore, we showed universality of the approach by developing of iBodies targeting other enzymes: HIV-1 protease (using a selective HIV-1 protease inhibitor based on commercially available inhibitor ritonavir) and a group of enzymes (using a class-selective inhibitor of all aspartic proteases – pepstatin A). To demonstrate that iBodies can be created towards virtually any target, for which a ligand is known, we prepared iBodies targeting His-tagged proteins, using Ni^{2+}/Co^{2+}-loaded nitrilotriacetic acid (NTA) derivative.

Altogether, iBodies represent a modular and versatile biochemical tool that can be used as a non-animal-based, chemically stable and easily modifiable antibody mimetic suitable for use in a number of biochemical applications.

My contribution

In this complex paper, I was responsible for the biochemical part of the project. I conducted the majority of the experiments that evaluated applicability and functionality of the prepared conjugates in biochemical methods. I tested all conjugates in a number of applications ranging from enzyme inhibition assay and surface plasmon resonance to cell culture experiments using flow cytometry and confocal microscopy. Besides, I also supervised undergraduate students, who significantly contributed to the paper. I also wrote a draft of the manuscript.

3. Discussion and conclusions

GCPII has become a potential diagnostic and therapeutic target in two distinct areas, as reviewed in the Introduction chapter. First, researchers are trying to develop orally available GCPII inhibitors to block GCPII (undesirable) NAAG-hydrolyzing activity in the brain during neuropathological conditions associated with glutamate-mediated excitotoxicity. Second, due to its high and relatively specific expression on the surface of prostate carcinoma cells, GCPII represents an ideal molecule to be targeted in order to image and/or treat prostate cancer.

A considerable progress in the field of GCPII targeting has been done within the last 10 years, concerning mainly highly potent and selective GCPII monoclonal antibodies and small inhibitors. On the other hand, there are still challenging questions that remain to be answered. Is there a putative GCPII (protein) ligand? Does GCPII function as a receptor transporting the unknown ligand into the cells? What is the physiological role (if any) of GCPII in the prostate? Are the increased levels of GCPII in prostate cancer the cause or the consequence of the malignant transition? Why is GCPII expressed in the neovasculature of most solid tumors? An answer to any of the above-mentioned issues will represent a milestone and probably also a turning point in the GCPII-related research.

Sadly, this thesis has not shed light upon any of these questions. Nevertheless, we provided important information regarding GCPII presence in the human blood. Previous papers reported conflicting findings, high blood concentrations of GCPII and most importantly the correlation between GCPII levels and prostate cancer stage. If there was such a correlation, GCPII could be "easily" used for screening for prostate cancer (and its stage). Similarly, prostate-specific antigen (PSA) blood test used to be used for that purpose. However, in 2011 the United States Preventive Services Task Force (USPSTF) recommended against PSA screening in healthy population – the risks outweighed the potential benefits since the correlation was not strong enough. Furthermore, the reported high GCPII blood levels would have led to problems with all GCPII-targeting agents for imaging and therapy since they would have been bound by GCPII already in the blood, rendering these diagnostic or therapeutic tools useless. These considerations motivated us to carry out a study assessing GCPII presence (and concentration) in the human blood. Using two unrelated methods (enzyme activity and immunoprecipitation followed by western blotting and mass

spectrometry), we confirmed GCPII presence in the human blood plasma. In sharp contrast to previous findings, we detected much lower GCPII concentrations – nanograms per milliliter instead of hundreds of nanograms per milliliter. Importantly, we also detected GCPII in the women's blood plasma, thus suggesting that GCPII originates from a non-prostatic source. Moreover, GCPII blood levels did not show any significant variations between healthy men and women. While working on the project, we developed methodology and collected samples from prostate cancer patients in order to perform a follow-up study to resolve the possible link between GCPII blood levels and a prostate cancer stage.

In 2008, our group published a study on animal homologs of human GCPII comparing their enzyme activity, inhibition properties and tissue distribution. However, mouse GCPII was not included in the comparison, in spite of being by far the most commonly used animal in the GCPII-oriented preclinical trials. Several pieces of information regarding mouse GCPII tissue expression had been collected over the years from different papers; nonetheless, the detailed and systematic characterization remained lacking. Therefore, we performed such a study, carefully comparing both enzyme activity properties (including inhibition profile and substrate specificity) and GCPII distribution in the mouse tissues (analyzed by quantitative PCR, western blotting, enzyme activity and immunohistochemistry). Since mice are widely used as preclinical models in the development of novel low-molecular-weight inhibitors as well as imaging and therapeutic agents, potential differences in either enzyme activity or tissue expression might be highly relevant. We discovered that mouse GCPII approximates well human GCPII, which was rather expectable, taking into account their high sequence similarity. Contrastingly, we observed differences in their tissue expression, especially no GCPII expression in the mouse prostate and high expression in the mouse kidney and salivary glands. Our results should provide the researchers with sufficient information to design their experiments in a proper way and to avoid potential complications stemming from a distinct GCPII expression profile.

Finally, we set out to develop novel antibody mimetics (called iBodies) that could be used to study GCPII (and not only GCPII) physiological functions. Traditionally, monoclonal antibodies capable of highly selective targeting of the desired protein have been used for this purpose. In spite of their tremendous success, antibodies might suffer from various problems; therefore, scientists developed antibody mimetics – molecules structurally different from

antibodies and binding their targets. Affibodies, designed ankyrin repeat proteins (DARPins) and aptamers represent prime examples of such molecules. Our efforts were inspired by *N*-(2-hydroxypropyl)methacrylamide (HPMA) copolymer conjugates used for targeted drug delivery to solid tumors via the enhanced-permeability and retention (EPR) effect rather than via active and selective targeting. Since our laboratory has a strong background in the design and structure-activity relationship studies of GCPII inhibitors, we used low-molecular-weight GCPII inhibitors as targeting molecules and conjugated them to an HPMA copolymer. We developed an HPMA conjugate that selectively binds GCPII (having the K_i of 3 pM) and evaluated its properties in several commonly used *in vitro* and cell culture applications. The extremely low inhibition constant is probably the result of the synergy of multiple targeting ligands bound to a single molecule of a carrier, leading to the tighter binding to the target. Besides the conjugate "raised" against GCPII, we also developed analogous conjugates targeting other clinically relevant proteins, demonstrating the versatility of the approach – having replaced one inhibitor with another, we switched the selectivity of the whole conjugate. For GCPII, a number of successive conjugates have been developed, varying in their size, number of inhibitors, or types of additional ligands attached. We hope that this battery of tools will help with elucidation of some of the GCPII mysterious questions mentioned at the beginning of the Discussion.

To conclude, we confirmed GCPII presence in the human blood plasma and showed that its levels do not vary significantly among healthy males and females. Additionally, the project constitutes a basis for a follow-up study elucidating a potential correlation between GCPII levels in the blood and prostate cancer stage. Secondly, we performed the detailed biochemical characterization of mouse GCPII that is enzymatically rather similar to its human counterpart; however, these two proteins differ in their tissue distribution. Lastly, we developed polymer conjugates decorated with GCPII inhibitors for future selective drug delivery to cells expressing GCPII. Additionally, these conjugates also serve as antibody mimetics enabling selective targeting of desired proteins *in vitro* and *in vivo*. Therefore, this novel class of antibody mimetics, called iBodies, represents a versatile chemical-biological tool that also has the application outside of the area of GCPII.

4. References

1. Horoszewicz JS, Kawinski E and Murphy GP. Monoclonal antibodies to a new antigenic marker in epithelial prostatic cells and serum of prostatic cancer patients. *Anticancer Res.* 1987**, 7**:927-935.

2. Robinson MB, Blakely RD, Couto R and Coyle JT. Hydrolysis of the brain dipeptide N-acetyl-L-aspartyl-L-glutamate. Identification and characterization of a novel N-acetylated alpha-linked acidic dipeptidase activity from rat brain. *J. Biol. Chem.* 1987**, 262**:14498-14506.

3. Pinto JT, Suffoletto BP, Berzin TM, Qiao CH, Lin S, Tong WP, May F, Mukherjee B and Heston WD. Prostate-specific membrane antigen: a novel folate hydrolase in human prostatic carcinoma cells. *Clin. Cancer Res.* 1996**, 2**:1445-1451.

4. Halsted CH, Ling EH, Luthi-Carter R, Villanueva JA, Gardner JM and Coyle JT. Folylpoly-gamma-glutamate carboxypeptidase from pig jejunum - Molecular characterization and relation to glutamate carboxypeptidase II. *J. Biol. Chem.* 1998**, 273**:20417-20424.

5. Chandler CJ, Wang TT and Halsted CH. Pteroylpolyglutamate hydrolase from human jejunal brush borders. Purification and characterization. *J. Biol. Chem.* 1986**, 261**:928-933.

6. Carter RE, Feldman AR and Coyle JT. Prostate-specific membrane antigen is a hydrolase with substrate and pharmacologic characteristics of a neuropeptidase. *Proc. Natl. Acad. Sci. U. S. A.* 1996**, 93**:749-753.

7. Israeli RS, Powell CT, Fair WR and Heston WD. Molecular cloning of a complementary DNA encoding a prostate-specific membrane antigen. *Cancer Res.* 1993**, 53**:227-230.

8. Davis MI, Bennett MJ, Thomas LM and Bjorkman PJ. Crystal structure of prostate-specific membrane antigen, a tumor marker and peptidase. *Proc. Natl. Acad. Sci. U. S. A.* 2005**, 102**:5981-5986.

9. Mesters JR, Barinka C, Li W, Tsukamoto T, Majer P, Slusher BS, Konvalinka J and Hilgenfeld R. Structure of glutamate carboxypeptidase II, a drug target in neuronal damage and prostate cancer. *EMBO J.* 2006**, 25**:1375-1384.

10. Holmes EH, Greene TG, Tino WT, Boynton AL, Aldape HC, Misrock SL and Murphy GP. Analysis of glycosylation of prostate-specific membrane antigen derived from LNCaP cells, prostatic carcinoma tumors, and serum from prostate cancer patients. *Prostate* 1996:25-29.

11. Barinka C, Sacha P, Sklenar J, Man P, Bezouska K, Slusher BS and Konvalinka J. Identification of the N-glycosylation sites on glutamate carboxypeptidase II necessary for proteolytic activity. *Protein Sci.* 2004**, 13**:1627-1635.

12. Barinka C, Rinnova M, Sacha P, Rojas C, Majer P, Slusher BS and Konvalinka J. Substrate specificity, inhibition and enzymological analysis of recombinant human glutamate carboxypeptidase II. *J. Neurochem.* 2002**, 80**:477-487.

13. Mlcochova P, Plechanovova A, Barinka C, Mahadevan D, Saldanha JW, Rulisek L and Konvalinka J. Mapping of the active site of glutamate carboxypeptidase II by site-directed mutagenesis. *FEBS J.* 2007**, 274**:4731-4741.

14. Barinka C, Rovenska M, Mlcochova P, Hlouchova K, Plechanovova A, Majer P, Tsukamoto T, Slusher BS, Konvalinka J and Lubkowski J. Structural insight into the

pharmacophore pocket of human glutamate carboxypeptidase II. *J. Med. Chem.* 2007**, 50**:3267-3273.

15.   Ghosh A and Heston WD. Effect of carbohydrate moieties on the folate hydrolysis activity of the prostate specific membrane antigen. *Prostate* 2003**, 57**:140-151.

16.   Christiansen JJ, Rajasekaran SA, Inge L, Cheng L, Anilkumar G, Bander NH and Rajasekaran AK. N-glycosylation and microtubule integrity are involved in apical targeting of prostate-specific membrane antigen: implications for immunotherapy. *Mol. Cancer Ther.* 2005**, 4**:704-714.

17.   Klusak V, Barinka C, Plechanovova A, Mlcochova P, Konvalinka J, Rulisek L and Lubkowski J. Reaction mechanism of glutamate carboxypeptidase II revealed by mutagenesis, X-ray crystallography, and computational methods. *Biochemistry* 2009**, 48**:4126-4138.

18.   Barinka C, Hlouchova K, Rovenska M, Majer P, Dauter M, Hin N, Ko YS, Tsukamoto T, Slusher BS, Konvalinka J and Lubkowski J. Structural basis of interactions between human glutamate carboxypeptidase II and its substrate analogs. *J. Mol. Biol.* 2008**, 376**:1438-1450.

19.   Barinka C, Starkova J, Konvalinka J and Lubkowski J. A high-resolution structure of ligand-free human glutamate carboxypeptidase II. *Acta Crystallogr. Sect. F Struct. Biol. Cryst. Commun.* 2007**, 63**:150-153.

20.   Tykvart J, Schimer J, Barinkova J, Pachl P, Postova-Slavetinska L, Majer P, Konvalinka J and Sacha P. Rational design of urea-based glutamate carboxypeptidase II (GCPII) inhibitors as versatile tools for specific drug targeting and delivery. *Bioorg. Med. Chem.* 2014**, 22**:4099-4108.

21.   Rovenska M, Hlouchova K, Sacha P, Mlcochova P, Horak V, Zamecnik J, Barinka C and Konvalinka J. Tissue expression and enzymologic characterization of human prostate specific membrane antigen and its rat and pig orthologs. *Prostate* 2008**, 68**:171-182.

22.   Kinoshita Y, Kuratsukuri K, Landas S, Imaida K, Rovito PM, Jr., Wang CY and Haas GP. Expression of prostate-specific membrane antigen in normal and malignant human tissues. *World J. Surg.* 2006**, 30**:628-636.

23.   Berger UV, Luthi-Carter R, Passani LA, Elkabes S, Black I, Konradi C and Coyle JT. Glutamate carboxypeptidase II is expressed by astrocytes in the adult rat nervous system. *J. Comp. Neurol.* 1999**, 415**:52-64.

24.   Bostwick DG, Pacelli A, Blute M, Roche P and Murphy GP. Prostate specific membrane antigen expression in prostatic intraepithelial neoplasia and adenocarcinoma: a study of 184 cases. *Cancer* 1998**, 82**:2256-2261.

25.   Silver DA, Pellicer I, Fair WR, Heston WD and Cordon-Cardo C. Prostate-specific membrane antigen expression in normal and malignant human tissues. *Clin. Cancer Res.* 1997**, 3**:81-85.

26.   Mhawech-Fauceglia P, Zhang S, Terracciano L, Sauter G, Chadhuri A, Herrmann FR and Penetrante R. Prostate-specific membrane antigen (PSMA) protein expression in normal and neoplastic tissues and its sensitivity and specificity in prostate adenocarcinoma: an immunohistochemical study using mutiple tumour tissue microarray technique. *Histopathology* 2007**, 50**:472-483.

27. Lapidus RG, Tiffany CW, Isaacs JT and Slusher BS. Prostate-specific membrane antigen (PSMA) enzyme activity is elevated in prostate cancer cells. *Prostate* 2000**, 45**:350-354.

28. Chang SS, Reuter VE, Heston WDW, Bander NH, Grauer LS and Gaudin PB. Five different anti-prostate-specific membrane antigen (PSMA) antibodies confirm PSMA expression in tumor-associated neovasculature. *Cancer Res.* 1999**, 59**:3192-3198.

29. Chang SS, O'Keefe DS, Bacich DJ, Reuter VE, Heston WDW and Gaudin PB. Prostate-specific membrane antigen is produced in tumor-associated neovasculature. *Clin. Cancer Res.* 1999**, 5**:2674-2681.

30. Haffner MC, Kronberger IE, Ross JS, Sheehan CE, Zitt M, Muhlmann G, Ofner D, Zelger B, Ensinger C, Yang XJ, Geley S, Margreiter R and Bander NH. Prostate-specific membrane antigen expression in the neovasculature of gastric and colorectal cancers. *Hum. Pathol.* 2009**, 40**:1754-1761.

31. Liu H, Moy P, Kim S, Xia Y, Rajasekaran A, Navarro V, Knudsen B and Bander NH. Monoclonal antibodies to the extracellular domain of prostate-specific membrane antigen also react with tumor vascular endothelium. *Cancer Res.* 1997**, 57**:3629-3634.

32. Eichhorn ME, Strieth S and Dellian M. Anti-vascular tumor therapy: recent advances, pitfalls and clinical perspectives. *Drug Resist. Updat.* 2004**, 7**:125-138.

33. Milowsky MI, Nanus DM, Kostakoglu L, Sheehan CE, Vallabhajosula S, Goldsmith SJ, Ross JS and Bander NH. Vascular targeted therapy with anti-prostate-specific membrane antigen monoclonal antibody J591 in advanced solid tumors. *J. Clin. Oncol.* 2007**, 25**:540-547.

34. Pandit-Taskar N, O'Donoghue JA, Divgi CR, Wills EA, Schwartz L, Gonen M, Smith-Jones P, Bander NH, Scher HI, Larson SM and Morris MJ. Indium 111-labeled J591 anti-PSMA antibody for vascular targeted imaging in progressive solid tumors. *EJNMMI Res.* 2015**, 5**:28.

35. Catalona WJ, Richie JP, Ahmann FR, Hudson MA, Scardino PT, Flanigan RC, deKernion JB, Ratliff TL, Kavoussi LR, Dalkin BL and et al. Comparison of digital rectal examination and serum prostate specific antigen in the early detection of prostate cancer: results of a multicenter clinical trial of 6,630 men. *J. Urol.* 1994**, 151**:1283-1290.

36. Xiao Z, Adam BL, Cazares LH, Clements MA, Davis JW, Schellhammer PF, Dalmasso EA and Wright GL, Jr. Quantitation of serum prostate-specific membrane antigen by a novel protein biochip immunoassay discriminates benign from malignant prostate disease. *Cancer Res.* 2001**, 61**:6029-6033.

37. Beckett ML, Cazares LH, Vlahou A, Schellhammer PF and Wright GL. Prostate-specific membrane antigen levels in sera from healthy men and patients with benign prostate hyperplasia or prostate cancer. *Clin. Cancer Res.* 1999**, 5**:4034-4040.

38. Murphy GP, Kenny GM, Ragde H, Wolfert RL, Boynton AL, Holmes EH, Misrock SL, Bartsch G, Klocker H, Pointner J, Reissigl A, McLeod DG, Douglas T, Morgan T and Gilbaugh J. Measurement of serum prostate-specific membrane antigen, a new prognostic marker for prostate cancer. *Urology* 1998**, 51**:89-97.

39. Murphy GP, Maguire RT, Rogers B, Partin AW, Nelp WB, Troychak MJ, Ragde H, Kenny GM, Barren RJ, 3rd, Bowes VA, Gregorakis AK, Holmes EH and Boynton AL. Comparison of serum PSMA, PSA levels with results of Cytogen-356 ProstaScint scanning in prostatic cancer patients. *Prostate* 1997**, 33**:281-285.

40.   Murphy GP, Tino WT, Holmes EH, Boynton AL, Erickson SJ, Bowes VA, Barren RJ, Tjoa BA, Misrock SL, Ragde H and Kenny GM. Measurement of prostate-specific membrane antigen in the serum with a new antibody. *Prostate* 1996, **28**:266-271.

41.   Rochon YP, Horoszewicz JS, Boynton AL, Holmes EH, Barren RJ, 3rd, Erickson SJ, Kenny GM and Murphy GP. Western blot assay for prostate-specific membrane antigen in serum of prostate cancer patients. *Prostate* 1994, **25**:219-223.

42.   Troyer JK, Beckett ML and Wright GL. Detection and Characterization of the Prostate-Specific Membrane Antigen (Pmsa) in Tissue-Extracts and Body-Fluids. *Int. J. Cancer* 1995, **62**:552-558.

43.   Barrett AJ, Rawlings ND, Salvesen G and Woessner JF. Handbook of Proteolytic Enzymes Introduction. *Handbook of Proteolytic Enzymes, Vols 1 and 2, 3rd Edition* 2013:I-Iv.

44.   Slusher BS, Robinson MB, Tsai G, Simmons ML, Richards SS and Coyle JT. Rat brain N-acetylated alpha-linked acidic dipeptidase activity. Purification and immunologic characterization. *J. Biol. Chem.* 1990, **265**:21297-21301.

45.   Curatolo A, D'Arcangelo P, Lino A and Brancati A. [Brain concentration of glutamic, aspartic, N-acetylaspartic and N-acetylaspartyl-glutamic acids in rats chronically treated with aspartic and N-acetylaspartic acids]. *Boll. Soc. Ital. Biol. Sper.* 1965, **41**:588-590.

46.   Miyamoto E, Kakimoto Y and Sano I. Identification of N-acetyl-alpha-aspartylglutamic acid in the bovine brain. *J. Neurochem.* 1966, **13**:999-1003.

47.   Wroblewska B, Wroblewski JT, Pshenichkin S, Surin A, Sullivan SE and Neale JH. N-acetylaspartylglutamate selectively activates mGluR3 receptors in transfected cells. *J. Neurochem.* 1997, **69**:174-181.

48.   Zhao J, Ramadan E, Cappiello M, Wroblewska B, Bzdega T and Neale JH. NAAG inhibits KCl-induced [(3)H]-GABA release via mGluR3, cAMP, PKA and L-type calcium conductance. *Eur. J. Neurosci.* 2001, **13**:340-346.

49.   Bruno V, Wroblewska B, Wroblewski JT, Fiore L and Nicoletti F. Neuroprotective activity of N-acetylaspartylglutamate in cultured cortical cells. *Neuroscience* 1998, **85**:751-757.

50.   Doble A. The role of excitotoxicity in neurodegenerative disease: Implications for therapy. *Pharmacol. Ther.* 1999, **81**:163-221.

51.   Zhou J, Neale JH, Pomper MG and Kozikowski AP. NAAG peptidase inhibitors and their potential for diagnosis and therapy. *Nat. Rev. Drug Discov.* 2005, **4**:1015-1026.

52.   Rowe SP, Gorin MA, Allaf ME, Pienta KJ, Tran PT, Pomper MG, Ross AE and Cho SY. PET imaging of prostate-specific membrane antigen in prostate cancer: current state of the art and future challenges. *Prostate Cancer Prostatic Dis.* 2016, **19**:223-230.

53.   Kiess AP, Banerjee SR, Mease RC, Rowe SP, Rao A, Foss CA, Chen Y, Yang X, Cho SY, Nimmagadda S and Pomper MG. Prostate-specific membrane antigen as a target for cancer imaging and therapy. *Q. J. Nucl. Med. Mol. Imaging* 2015, **59**:241-268.

54.   Ferraris DV, Shukla K and Tsukamoto T. Structure-activity relationships of glutamate carboxypeptidase II (GCPII) inhibitors. *Curr. Med. Chem.* 2012, **19**:1282-1294.

55.   Jackson PF, Cole DC, Slusher BS, Stetz SL, Ross LE, Donzanti BA and Trainor DA. Design, synthesis, and biological activity of a potent inhibitor of the neuropeptidase N-acetylated alpha-linked acidic dipeptidase. *J. Med. Chem.* 1996, **39**:619-622.

56. Majer P, Jancarik A, Krecmerova M, Tichy T, Tenora L, Wozniak K, Wu Y, Pommier E, Ferraris D, Rais R and Slusher BS. Discovery of Orally Available Prodrugs of the Glutamate Carboxypeptidase II (GCPII) Inhibitor 2-Phosphonomethylpentanedioic Acid (2-PMPA). *J. Med. Chem.* 2016, **59**:2810-2819.

57. Vornov JJ, Hollinger KR, Jackson PF, Wozniak KM, Farah MH, Majer P, Rais R and Slusher BS. Still NAAG'ing After All These Years: The Continuing Pursuit of GCPII Inhibitors. *Adv. Pharmacol.* 2016, **76**:215-255.

58. Kozikowski AP, Nan F, Conti P, Zhang J, Ramadan E, Bzdega T, Wroblewska B, Neale JH, Pshenichkin S and Wroblewski JT. Design of remarkably simple, yet potent urea-based inhibitors of glutamate carboxypeptidase II (NAALADase). *J. Med. Chem.* 2001, **44**:298-301.

59. Kozikowski AP, Zhang J, Nan F, Petukhov PA, Grajkowska E, Wroblewski JT, Yamamoto T, Bzdega T, Wroblewska B and Neale JH. Synthesis of urea-based inhibitors as active site probes of glutamate carboxypeptidase II: efficacy as analgesic agents. *J. Med. Chem.* 2004, **47**:1729-1738.

60. Chen Y, Foss CA, Byun Y, Nimmagadda S, Pullambhatla M, Fox JJ, Castanares M, Lupold SE, Babich JW, Mease RC and Pomper MG. Radiohalogenated prostate-specific membrane antigen (PSMA)-based ureas as imaging agents for prostate cancer. *J. Med. Chem.* 2008, **51**:7933-7943.

61. Eder M, Schafer M, Bauder-Wust U, Hull WE, Wangler C, Mier W, Haberkorn U and Eisenhut M. 68Ga-complex lipophilicity and the targeting property of a urea-based PSMA inhibitor for PET imaging. *Bioconjug. Chem.* 2012, **23**:688-697.

62. Foss CA, Mease RC, Fan H, Wang Y, Ravert HT, Dannals RF, Olszewski RT, Heston WD, Kozikowski AP and Pomper MG. Radiolabeled small-molecule ligands for prostate-specific membrane antigen: in vivo imaging in experimental models of prostate cancer. *Clin. Cancer Res.* 2005, **11**:4022-4028.

63. Chen Y, Dhara S, Banerjee SR, Byun Y, Pullambhatla M, Mease RC and Pomper MG. A low molecular weight PSMA-based fluorescent imaging agent for cancer. *Biochem. Biophys. Res. Commun.* 2009, **390**:624-629.

64. Yamamoto T, Hirasawa S, Wroblewska B, Grajkowska E, Zhou J, Kozikowski A, Wroblewski J and Neale JH. Antinociceptive effects of N-acetylaspartylglutamate (NAAG) peptidase inhibitors ZJ-11, ZJ-17 and ZJ-43 in the rat formalin test and in the rat neuropathic pain model. *Eur. J. Neurosci.* 2004, **20**:483-494.

65. Yamamoto T, Saito O, Aoe T, Bartolozzi A, Sarva J, Zhou J, Kozikowski A, Wroblewska B, Bzdega T and Neale JH. Local administration of N-acetylaspartylglutamate (NAAG) peptidase inhibitors is analgesic in peripheral pain in rats. *Eur. J. Neurosci.* 2007, **25**:147-158.

66. Olszewski RT, Bukhari N, Zhou J, Kozikowski AP, Wroblewski JT, Shamimi-Noori S, Wroblewska B, Bzdega T, Vicini S, Barton FB and Neale JH. NAAG peptidase inhibition reduces locomotor activity and some stereotypes in the PCP model of schizophrenia via group II mGluR. *J. Neurochem.* 2004, **89**:876-885.

67. Feng JF, Van KC, Gurkoff GG, Kopriva C, Olszewski RT, Song M, Sun S, Xu M, Neale JH, Yuen PW, Lowe DA, Zhou J and Lyeth BG. Post-injury administration of NAAG peptidase inhibitor prodrug, PGI-02776, in experimental TBI. *Brain Res.* 2011, **1395**:62-73.

68. Maresca KP, Hillier SM, Femia FJ, Keith D, Barone C, Joyal JL, Zimmerman CN, Kozikowski AP, Barrett JA, Eckelman WC and Babich JW. A series of halogenated heterodimeric inhibitors of prostate specific membrane antigen (PSMA) as radiolabeled probes for targeting prostate cancer. *J. Med. Chem.* 2009**, 52**:347-357.

69. Majer P, Jackson PF, Delahanty G, Grella BS, Ko YS, Li W, Liu Q, Maclin KM, Polakova J, Shaffer KA, Stoermer D, Vitharana D, Wang EY, Zakrzewski A, Rojas C, Slusher BS, Wozniak KM, Burak E, Limsakun T and Tsukamoto T. Synthesis and biological evaluation of thiol-based inhibitors of glutamate carboxypeptidase II: discovery of an orally active GCP II inhibitor. *J. Med. Chem.* 2003**, 46**:1989-1996.

70. Zhang W, Murakawa Y, Wozniak KM, Slusher B and Sima AA. The preventive and therapeutic effects of GCPII (NAALADase) inhibition on painful and sensory diabetic neuropathy. *J. Neurol. Sci.* 2006**, 247**:217-223.

71. Ghadge GD, Slusher BS, Bodner A, Canto MD, Wozniak K, Thomas AG, Rojas C, Tsukamoto T, Majer P, Miller RJ, Monti AL and Roos RP. Glutamate carboxypeptidase II inhibition protects motor neurons from death in familial amyotrophic lateral sclerosis models. *Proc. Natl. Acad. Sci. U. S. A.* 2003**, 100**:9554-9559.

72. van der Post JP, de Visser SJ, de Kam ML, Woelfler M, Hilt DC, Vornov J, Burak ES, Bortey E, Slusher BS, Limsakun T, Cohen AF and van Gerven JM. The central nervous system effects, pharmacokinetics and safety of the NAALADase-inhibitor GPI 5693. *Br. J. Clin. Pharmacol.* 2005**, 60**:128-136.

73. Liu T, Toriyabe Y, Kazak M and Berkman CE. Pseudoirreversible inhibition of prostate-specific membrane antigen by phosphoramidate peptidomimetics. *Biochemistry* 2008**, 47**:12658-12660.

74. Novakova Z, Wozniak K, Jancarik A, Rais R, Wu Y, Pavlicek J, Ferraris D, Havlinova B, Ptacek J, Vavra J, Hin N, Rojas C, Majer P, Slusher BS, Tsukamoto T and Barinka C. Unprecedented Binding Mode of Hydroxamate-Based Inhibitors of Glutamate Carboxypeptidase II: Structural Characterization and Biological Activity. *J. Med. Chem.* 2016**, 59**:4539-4550.

75. Stoermer D, Liu Q, Hall MR, Flanary JM, Thomas AG, Rojas C, Slusher BS and Tsukamoto T. Synthesis and biological evaluation of hydroxamate-Based inhibitors of glutamate carboxypeptidase II. *Bioorg. Med. Chem. Lett.* 2003**, 13**:2097-2100.

76. Heldin CH. Dimerization of cell surface receptors in signal transduction. *Cell* 1995**, 80**:213-223.

77. Schlessinger J. Ligand-induced, receptor-mediated dimerization and activation of EGF receptor. *Cell* 2002**, 110**:669-672.

78. Rajasekaran SA, Anilkumar G, Oshima E, Bowie JU, Liu H, Heston W, Bander NH and Rajasekaran AK. A novel cytoplasmic tail MXXXL motif mediates the internalization of prostate-specific membrane antigen. *Mol. Biol. Cell* 2003**, 14**:4835-4845.

79. Liu H, Rajasekaran AK, Moy P, Xia Y, Kim S, Navarro V, Rahmati R and Bander NH. Constitutive and antibody-induced internalization of prostate-specific membrane antigen. *Cancer Res.* 1998**, 58**:4055-4060.

80. Anilkumar G, Rajasekaran SA, Wang S, Hankinson O, Bander NH and Rajasekaran AK. Prostate-specific membrane antigen association with filamin A modulates its internalization and NAALADase activity. *Cancer Res.* 2003**, 63**:2645-2648.

81. Conway RE, Petrovic N, Li Z, Heston W, Wu D and Shapiro LH. Prostate-specific membrane antigen regulates angiogenesis by modulating integrin signal transduction. *Mol. Cell. Biol.* 2006**, 26**:5310-5324.

82. Conway RE, Joiner K, Patterson A, Bourgeois D, Rampp R, Hannah BC, McReynolds S, Elder JM, Gilfilen H and Shapiro LH. Prostate specific membrane antigen produces pro-angiogenic laminin peptides downstream of matrix metalloprotease-2. *Angiogenesis* 2013**, 16**:847-860.

83. Conway RE, Rojas C, Alt J, Novakova Z, Richardson SM, Rodrick TC, Fuentes JL, Richardson NH, Attalla J, Stewart S, Fahmy B, Barinka C, Ghosh M, Shapiro LH and Slusher BS. Prostate-specific membrane antigen (PSMA)-mediated laminin proteolysis generates a pro-angiogenic peptide. *Angiogenesis* 2016**, 19**:487-500.

84. Colombatti M, Grasso S, Porzia A, Fracasso G, Scupoli MT, Cingarlini S, Poffe O, Naim HY, Heine M, Tridente G, Mainiero F and Ramarli D. The prostate specific membrane antigen regulates the expression of IL-6 and CCL5 in prostate tumour cells by activating the MAPK pathways. *PLoS One* 2009**, 4**:e4608.

85. Rajasekaran SA, Christiansen JJ, Schmid I, Oshima E, Ryazantsev S, Sakamoto K, Weinstein J, Rao NP and Rajasekaran AK. Prostate-specific membrane antigen associates with anaphase-promoting complex and induces chromosomal instability. *Mol. Cancer Ther.* 2008**, 7**:2142-2151.

86. Hlouchova K, Navratil V, Tykvart J, Sacha P and Konvalinka J. GCPII variants, paralogs and orthologs. *Curr. Med. Chem.* 2012**, 19**:1316-1322.

87. Hlouchova K, Barinka C, Klusak V, Sacha P, Mlcochova P, Majer P, Rulisek L and Konvalinka J. Biochemical characterization of human glutamate carboxypeptidase III. *J. Neurochem.* 2007**, 101**:682-696.

88. Hlouchova K, Barinka C, Konvalinka J and Lubkowski J. Structural insight into the evolutionary and pharmacologic homology of glutamate carboxypeptidases II and III. *FEBS J.* 2009**, 276**:4448-4462.

89. Pangalos MN, Neefs JM, Somers M, Verhasselt P, Bekkers M, van der Helm L, Fraiponts E, Ashton D and Gordon RD. Isolation and expression of novel human glutamate carboxypeptidases with N-acetylated alpha-linked acidic dipeptidase and dipeptidyl peptidase IV activity. *J. Biol. Chem.* 1999**, 274**:8470-8483.

90. Tonkin ET, Smith M, Eichhorn P, Jones S, Imamwerdi B, Lindsay S, Jackson M, Wang TJ, Ireland M, Burn J, Krantz ID, Carr P and Strachan T. A giant novel gene undergoing extensive alternative splicing is severed by a Cornelia de Lange-associated translocation breakpoint at 3q26.3. *Hum. Genet.* 2004**, 115**:139-148.

91. Tykvart J, Barinka C, Svoboda M, Navratil V, Soucek R, Hubalek M, Hradilek M, Sacha P, Lubkowski J and Konvalinka J. Structural and biochemical characterization of a novel aminopeptidase from human intestine. *J. Biol. Chem.* 2015**, 290**:11321-11336.

92. Bzdega T, Crowe SL, Ramadan ER, Sciarretta KH, Olszewski RT, Ojeifo OA, Rafalski VA, Wroblewska B and Neale JH. The cloning and characterization of a second brain enzyme with NAAG peptidase activity. *J. Neurochem.* 2004**, 89**:627-635.

93. Bacich DJ, Ramadan E, O'Keefe DS, Bukhari N, Wegorzewska I, Ojeifo O, Olszewski R, Wrenn CC, Bzdega T, Wroblewska B, Heston WD and Neale JH. Deletion of the glutamate carboxypeptidase II gene in mice reveals a second enzyme activity that hydrolyzes N-acetylaspartylglutamate. *J. Neurochem.* 2002**, 83**:20-29.

94. Collard F, Vertommen D, Constantinescu S, Buts L and Van Schaftingen E. Molecular identification of beta-citrylglutamate hydrolase as glutamate carboxypeptidase 3. *J. Biol. Chem.* 2011**, 286**:38220-38230.

95. Miyake M, Kakimoto Y and Sorimachi M. Isolation and identification of beta-citryl-L-glutamic acid from newborn rat brain. *Biochim. Biophys. Acta* 1978**, 544**:656-666.

96. Narahara M, Tachibana K, Adachi S, Iwasa A, Yukii A, Hamada-Kanazawa M, Kawai Y and Miyake M. Immunocytochemical localization of beta-citryl-L-glutamate in primary neuronal cells and in the differentiation of P19 mouse embryonal carcinoma cells into neuronal cells. *Biol. Pharm. Bull.* 2000**, 23**:1287-1292.

97. Miyake M, Kume S and Kakimoto Y. Correlation of the level of beta-citryl-L-glutamic acid with spermatogenesis in rat testes. *Biochim. Biophys. Acta* 1982**, 719**:495-500.

98. Narahara M, Hamada-Kanazawa M, Kouda M, Odani A and Miyake M. Superoxide scavenging and xanthine oxidase inhibiting activities of copper-beta-citryl-L-glutamate complex. *Biol. Pharm. Bull.* 2010**, 33**:1938-1943.

99. Bacich DJ, Pinto JT, Tong WP and Heston WD. Cloning, expression, genomic localization, and enzymatic activities of the mouse homolog of prostate-specific membrane antigen/NAALADase/folate hydrolase. *Mamm. Genome* 2001**, 12**:117-123.

100. Tsai G, Dunham KS, Drager U, Grier A, Anderson C, Collura J and Coyle JT. Early embryonic death of glutamate carboxypeptidase II (NAALADase) homozygous mutants. *Synapse* 2003**, 50**:285-292.

101. Gao Y, Xu SY, Cui ZW, Zhang MK, Lin YY, Cai L, Wang ZG, Luo XG, Zheng Y, Wang Y, Luo QZ, Jiang JY, Neale JH and Zhong CL. Mice lacking glutamate carboxypeptidase II develop normally, but are less susceptible to traumatic brain injury. *J. Neurochem.* 2015**, 134**:340-353.

102. Slusher BS, Vornov JJ, Thomas AG, Hurn PD, Harukuni I, Bhardwaj A, Traystman RJ, Robinson MB, Britton P, Lu XC, Tortella FC, Wozniak KM, Yudkoff M, Potter BM and Jackson PF. Selective inhibition of NAALADase, which converts NAAG to glutamate, reduces ischemic brain injury. *Nat. Med.* 1999**, 5**:1396-1402.

103. Curatolo A, D AP, Lino A and Brancati A. Distribution of N-Acetyl-Aspartic and N-Acetyl-Aspartyl-Glutamic Acids in Nervous Tissue. *J. Neurochem.* 1965**, 12**:339-342.

104. Auditore JV, Olson EJ and Wade L. Isolation, purification, and probable structural configuration of N-acetyl aspartyl glutamate in human brain. *Arch. Biochem. Biophys.* 1966**, 114**:452-458.

105. Miyamoto E and Tsujio T. Determination of N-acetyl-alpha-aspartyl-glutamic acid in the nervous tissue of mammals. *J. Neurochem.* 1967**, 14**:899-903.

106. Cangro CB, Namboodiri MA, Sklar LA, Corigliano-Murphy A and Neale JH. Immunohistochemistry and biosynthesis of N-acetylaspartylglutamate in spinal sensory ganglia. *J. Neurochem.* 1987**, 49**:1579-1588.

107. Anderson KJ, Monaghan DT, Cangro CB, Namboodiri MA, Neale JH and Cotman CW. Localization of N-acetylaspartylglutamate-like immunoreactivity in selected areas of the rat brain. *Neurosci. Lett.* 1986**, 72**:14-20.

108. Koller KJ, Zaczek R and Coyle JT. N-acetyl-aspartyl-glutamate: regional levels in rat brain and the effects of brain lesions as determined by a new HPLC method. *J. Neurochem.* 1984**, 43**:1136-1142.

109. Gehl LM, Saab OH, Bzdega T, Wroblewska B and Neale JH. Biosynthesis of NAAG by an enzyme-mediated process in rat central nervous system neurons and glia. *J. Neurochem.* 2004**, 90**:989-997.

110. Collard F, Stroobant V, Lamosa P, Kapanda CN, Lambert DM, Muccioli GG, Poupaert JH, Opperdoes F and Van Schaftingen E. Molecular identification of N-acetylaspartylglutamate synthase and beta-citrylglutamate synthase. *J. Biol. Chem.* 2010**, 285**:29826-29833.

111. Williamson LC and Neale JH. Ultrastructural localization of N-acetylaspartylglutamate in synaptic vesicles of retinal neurons. *Brain. Res.* 1988**, 456**:375-381.

112. Pittaluga A, Barbeito L, Serval V, Godeheu G, Artaud F, Glowinski J and Cheramy A. Depolarization-evoked release of N-acetyl-L-aspartyl-L-glutamate from rat brain synaptosomes. *Eur. J. Pharmacol.* 1988**, 158**:263-266.

113. Zollinger M, Amsler U, Do KQ, Streit P and Cuenod M. Release of N-acetylaspartylglutamate on depolarization of rat brain slices. *J. Neurochem.* 1988**, 51**:1919-1923.

114. Tsai G, Forloni G, Robinson MB, Stauch BL and Coyle JT. Calcium-dependent evoked release of N-[3H]acetylaspartylglutamate from the optic pathway. *J. Neurochem.* 1988**, 51**:1956-1959.

115. Schweitzer C, Kratzeisen C, Adam G, Lundstrom K, Malherbe P, Ohresser S, Stadler H, Wichmann J, Woltering T and Mutel V. Characterization of [(3)H]-LY354740 binding to rat mGlu2 and mGlu3 receptors expressed in CHO cells using semliki forest virus vectors. *Neuropharmacology* 2000**, 39**:1700-1706.

116. Wroblewska B, Wroblewski JT, Saab OH and Neale JH. N-acetylaspartylglutamate inhibits forskolin-stimulated cyclic AMP levels via a metabotropic glutamate receptor in cultured cerebellar granule cells. *J. Neurochem.* 1993**, 61**:943-948.

117. Sanabria ER, Wozniak KM, Slusher BS and Keller A. GCP II (NAALADase) inhibition suppresses mossy fiber-CA3 synaptic neurotransmission by a presynaptic mechanism. *J. Neurophysiol.* 2004**, 91**:182-193.

118. Thomas AG, Olkowski JL and Slusher BS. Neuroprotection afforded by NAAG and NAALADase inhibition requires glial cells and metabotropic glutamate receptor activation. *Eur. J. Pharmacol.* 2001**, 426**:35-38.

119. Neale JH, Olszewski RT, Gehl LM, Wroblewska B and Bzdega T. The neurotransmitter N-acetylaspartylglutamate in models of pain, ALS, diabetic neuropathy, CNS injury and schizophrenia. *Trends Pharmacol. Sci.* 2005**, 26**:477-484.

120. Sacha P, Zamecnik J, Barinka C, Hlouchova K, Vicha A, Mlcochova P, Hilgert I, Eckschlager T and Konvalinka J. Expression of glutamate carboxypeptidase II in human brain. *Neuroscience* 2007**, 144**:1361-1372.

121. Berger UV, Carter RE, McKee M and Coyle JT. N-acetylated alpha-linked acidic dipeptidase is expressed by non-myelinating Schwann cells in the peripheral nervous system. *J. Neurocytol.* 1995**, 24**:99-109.

122. Parsons CG, Danysz W and Quack G. Glutamate in CNS disorders as a target for drug development: an update. *Drug News Perspect.* 1998**, 11**:523-569.

123. Tortella FC, Lin Y, Ved H, Slusher BS and Dave JR. Neuroprotection produced by the NAALADase inhibitor 2-PMPA in rat cerebellar neurons. *Eur. J. Pharmacol.* 2000**, 402**:31-37.

124. Zhong C, Zhao X, Sarva J, Kozikowski A, Neale JH and Lyeth BG. NAAG peptidase inhibitor reduces acute neuronal degeneration and astrocyte damage following lateral fluid percussion TBI in rats. *J. Neurotrauma* 2005, **22**:266-276.

125. Yamamoto T, Nozaki-Taguchi N, Sakashita Y and Inagaki T. Inhibition of spinal N-acetylated-alpha-linked acidic dipeptidase produces an antinociceptive effect in the rat formalin test. *Neuroscience* 2001, **102**:473-479.

126. Carpenter KJ, Sen S, Matthews EA, Flatters SL, Wozniak KM, Slusher BS and Dickenson AH. Effects of GCP-II inhibition on responses of dorsal horn neurones after inflammation and neuropathy: an electrophysiological study in the rat. *Neuropeptides* 2003, **37**:298-306.

127. Zarei S, Carr K, Reiley L, Diaz K, Guerra O, Altamirano PF, Pagani W, Lodin D, Orozco G and Chinea A. A comprehensive review of amyotrophic lateral sclerosis. *Surg. Neurol. Int.* 2015, **6**:171.

128. Siegel RL, Miller KD and Jemal A. Cancer statistics, 2016. *CA Cancer J. Clin.* 2016, **66**:7-30.

129. Kuriyama M, Wang MC, Papsidero LD, Killian CS, Shimano T, Valenzuela L, Nishiura T, Murphy GP and Chu TM. Quantitation of prostate-specific antigen in serum by a sensitive enzyme immunoassay. *Cancer Res.* 1980, **40**:4658-4662.

130. Hayes JH and Barry MJ. Screening for prostate cancer with the prostate-specific antigen test: a review of current evidence. *JAMA* 2014, **311**:1143-1149.

131. Sohn E. Screening: Diagnostic dilemma. *Nature* 2015, **528**:S120-122.

132. Attard G, Parker C, Eeles RA, Schroder F, Tomlins SA, Tannock I, Drake CG and de Bono JS. Prostate cancer. *Lancet* 2016, **387**:70-82.

133. Yao V and Bacich DJ. Prostate specific membrane antigen (PSMA) expression gives prostate cancer cells a growth advantage in a physiologically relevant folate environment in vitro. *Prostate* 2006, **66**:867-875.

134. Yao V, Berkman CE, Choi JK, O'Keefe DS and Bacich DJ. Expression of Prostate-Specific Membrane Antigen (PSMA), Increases Cell Folate Uptake and Proliferation and Suggests a Novel Role for PSMA in the Uptake of the Non-Polyglutamated Folate, Folic Acid. *Prostate* 2010, **70**:305-316.

135. Fass L. Imaging and cancer: a review. *Mol. Oncol.* 2008, **2**:115-152.

136. Weissleder R and Pittet MJ. Imaging in the era of molecular oncology. *Nature* 2008, **452**:580-589.

137. Kahn D, Williams RD, Seldin DW, Libertino JA, Hirschhorn M, Dreicer R, Weiner GJ, Bushnell D and Gulfo J. Radioimmunoscintigraphy with 111indium labeled CYT-356 for the detection of occult prostate cancer recurrence. *J. Urol.* 1994, **152**:1490-1495.

138. Haseman MK, Reed NL and Rosenthal SA. Monoclonal antibody imaging of occult prostate cancer in patients with elevated prostate-specific antigen. Positron emission tomography and biopsy correlation. *Clin. Nucl. Med.* 1996, **21**:704-713.

139. Petronis JD, Regan F and Lin K. Indium-111 capromab pendetide (ProstaScint) imaging to detect recurrent and metastatic prostate cancer. *Clin. Nucl. Med.* 1998, **23**:672-677.

140. Kahn D, Williams RD, Manyak MJ, Haseman MK, Seldin DW, Libertino JA and Maguire RT. 111Indium-capromab pendetide in the evaluation of patients with

residual or recurrent prostate cancer after radical prostatectomy. The ProstaScint Study Group. *J. Urol.* 1998**, 159**:2041-2046; discussion 2046-2047.

141. Troyer JK, Beckett ML and Wright GL, Jr. Location of prostate-specific membrane antigen in the LNCaP prostate carcinoma cell line. *Prostate* 1997**, 30**:232-242.

142. Taneja SS. ProstaScint(R) Scan: Contemporary Use in Clinical Practice. *Rev. Urol.* 2004**, 6 Suppl 10**:S19-28.

143. Smith-Jones PM, Vallabhajosula S, Navarro V, Bastidas D, Goldsmith SJ and Bander NH. Radiolabeled monoclonal antibodies specific to the extracellular domain of prostate-specific membrane antigen: preclinical studies in nude mice bearing LNCaP human prostate tumor. *J. Nucl. Med.* 2003**, 44**:610-617.

144. Bander NH, Trabulsi EJ, Kostakoglu L, Yao D, Vallabhajosula S, Smith-Jones P, Joyce MA, Milowsky M, Nanus DM and Goldsmith SJ. Targeting metastatic prostate cancer with radiolabeled monoclonal antibody J591 to the extracellular domain of prostate specific membrane antigen. *J. Urol.* 2003**, 170**:1717-1721.

145. Osborne JR, Green DA, Spratt DE, Lyashchenko S, Fareedy SB, Robinson BD, Beattie BJ, Jain M, Lewis JS, Christos P, Larson SM, Bander NH and Scherr DS. A prospective pilot study of (89)Zr-J591/prostate specific membrane antigen positron emission tomography in men with localized prostate cancer undergoing radical prostatectomy. *J. Urol.* 2014**, 191**:1439-1445.

146. Vallabhajosula S, Kuji I, Hamacher KA, Konishi S, Kostakoglu L, Kothari PA, Milowski MI, Nanus DM, Bander NH and Goldsmith SJ. Pharmacokinetics and biodistribution of 111In- and 177Lu-labeled J591 antibody specific for prostate-specific membrane antigen: prediction of 90Y-J591 radiation dosimetry based on 111In or 177Lu? *J. Nucl. Med.* 2005**, 46**:634-641.

147. Pandit-Taskar N, O'Donoghue JA, Durack JC, Lyashchenko SK, Cheal SM, Beylergil V, Lefkowitz RA, Carrasquillo JA, Martinez DF, Fung AM, Solomon SB, Gonen M, Heller G, Loda M, Nanus DM, Tagawa ST, Feldman JL, Osborne JR, Lewis JS, Reuter VE, Weber WA, Bander NH, Scher HI, Larson SM and Morris MJ. A Phase I/II Study for Analytic Validation of 89Zr-J591 ImmunoPET as a Molecular Imaging Agent for Metastatic Prostate Cancer. *Clin. Cancer Res.* 2015**, 21**:5277-5285.

148. Tagawa ST, Milowsky MI, Morris M, Vallabhajosula S, Christos P, Akhtar NH, Osborne J, Goldsmith SJ, Larson S, Taskar NP, Scher HI, Bander NH and Nanus DM. Phase II study of Lutetium-177-labeled anti-prostate-specific membrane antigen monoclonal antibody J591 for metastatic castration-resistant prostate cancer. *Clin. Cancer Res.* 2013**, 19**:5182-5191.

149. Chen Y, Pullambhatla M, Foss CA, Byun Y, Nimmagadda S, Senthamizhchelvan S, Sgouros G, Mease RC and Pomper MG. 2-(3-{1-Carboxy-5-[(6-[18F]fluoro-pyridine-3-carbonyl)-amino]-pentyl}-ureido)-pen tanedioic acid, [18F]DCFPyL, a PSMA-based PET imaging agent for prostate cancer. *Clin. Cancer Res.* 2011**, 17**:7645-7653.

150. Afshar-Oromieh A, Avtzi E, Giesel FL, Holland-Letz T, Linhart HG, Eder M, Eisenhut M, Boxler S, Hadaschik BA, Kratochwil C, Weichert W, Kopka K, Debus J and Haberkorn U. The diagnostic value of PET/CT imaging with the (68)Ga-labelled PSMA ligand HBED-CC in the diagnosis of recurrent prostate cancer. *Eur. J. Nucl. Med. Mol. Imaging* 2015**, 42**:197-209.

151. Afshar-Oromieh A, Zechmann CM, Malcher A, Eder M, Eisenhut M, Linhart HG, Holland-Letz T, Hadaschik BA, Giesel FL, Debus J and Haberkorn U. Comparison of

PET imaging with a (68)Ga-labelled PSMA ligand and (18)F-choline-based PET/CT for the diagnosis of recurrent prostate cancer. *Eur. J. Nucl. Med. Mol. Imaging* 2014, **41**:11-20.

152. Afshar-Oromieh A, Malcher A, Eder M, Eisenhut M, Linhart HG, Hadaschik BA, Holland-Letz T, Giesel FL, Kratochwil C, Haufe S, Haberkorn U and Zechmann CM. PET imaging with a [68Ga]gallium-labelled PSMA ligand for the diagnosis of prostate cancer: biodistribution in humans and first evaluation of tumour lesions. *Eur. J. Nucl. Med. Mol. Imaging* 2013, **40**:486-495.

153. Dietlein M, Kobe C, Kuhnert G, Stockter S, Fischer T, Schomacker K, Schmidt M, Dietlein F, Zlatopolskiy BD, Krapf P, Richarz R, Neubauer S, Drzezga A and Neumaier B. Comparison of [(18)F]DCFPyL and [(68)Ga]Ga-PSMA-HBED-CC for PSMA-PET Imaging in Patients with Relapsed Prostate Cancer. *Mol. Imaging Biol.* 2015, **17**:575-584.

154. Szabo Z, Mena E, Rowe SP, Plyku D, Nidal R, Eisenberger MA, Antonarakis ES, Fan H, Dannals RF, Chen Y, Mease RC, Vranesic M, Bhatnagar A, Sgouros G, Cho SY and Pomper MG. Initial Evaluation of [(18)F]DCFPyL for Prostate-Specific Membrane Antigen (PSMA)-Targeted PET Imaging of Prostate Cancer. *Mol. Imaging Biol.* 2015, **17**:565-574.

155. Deb N, Goris M, Trisler K, Fowler S, Saal J, Ning S, Becker M, Marquez C and Knox S. Treatment of hormone-refractory prostate cancer with 90Y-CYT-356 monoclonal antibody. *Clin. Cancer Res.* 1996, **2**:1289-1297.

156. Kahn D, Austin JC, Maguire RT, Miller SJ, Gerstbrein J and Williams RD. A phase II study of [90Y] yttrium-capromab pendetide in the treatment of men with prostate cancer recurrence following radical prostatectomy. *Cancer Biother. Radiopharm.* 1999, **14**:99-111.

157. Bander NH, Milowsky MI, Nanus DM, Kostakoglu L, Vallabhajosula S and Goldsmith SJ. Phase I trial of 177lutetium-labeled J591, a monoclonal antibody to prostate-specific membrane antigen, in patients with androgen-independent prostate cancer. *J. Clin. Oncol.* 2005, **23**:4591-4601.

158. Tagawa ST, Beltran H, Vallabhajosula S, Goldsmith SJ, Osborne J, Matulich D, Petrillo K, Parmar S, Nanus DM and Bander NH. Anti-prostate-specific membrane antigen-based radioimmunotherapy for prostate cancer. *Cancer* 2010, **116**:1075-1083.

159. Henry MD, Wen S, Silva MD, Chandra S, Milton M and Worland PJ. A prostate-specific membrane antigen-targeted monoclonal antibody-chemotherapeutic conjugate designed for the treatment of prostate cancer. *Cancer Res.* 2004, **64**:7995-8001.

160. Milowsky MI, Galsky MD, Morris MJ, Crona DJ, George DJ, Dreicer R, Tse K, Petruck J, Webb IJ, Bander NH, Nanus DM and Scher HI. Phase 1/2 multiple ascending dose trial of the prostate-specific membrane antigen-targeted antibody drug conjugate MLN2704 in metastatic castration-resistant prostate cancer. *Urol. Oncol.* 2016, **34**:530 e515-530 e521.

161. Ma D, Hopf CE, Malewicz AD, Donovan GP, Senter PD, Goeckeler WF, Maddon PJ and Olson WC. Potent antitumor activity of an auristatin-conjugated, fully human monoclonal antibody to prostate-specific membrane antigen. *Clin. Cancer Res.* 2006, **12**:2591-2596.

162. DiPippo VA, Olson WC, Nguyen HM, Brown LG, Vessella RL and Corey E. Efficacy studies of an antibody-drug conjugate PSMA-ADC in patient-derived prostate cancer xenografts. *Prostate* 2015**, 75**:303-313.

163. An Open-label Extension Study of PSMA ADC 2301 in mCRPC (September 28, 2017). https://clinicaltrials.gov/ct2/show/record/NCT02020135?sect=X01256

164. Fracasso G, Bellisola G, Cingarlini S, Castelletti D, Prayer-Galetti T, Pagano F, Tridente G and Colombatti M. Anti-tumor effects of toxins targeted to the prostate specific membrane antigen. *Prostate* 2002**, 53**:9-23.

165. Wolf P, Gierschner D, Buhler P, Wetterauer U and Elsasser-Beile U. A recombinant PSMA-specific single-chain immunotoxin has potent and selective toxicity against prostate cancer cells. *Cancer Immunol. Immunother.* 2006**, 55**:1367-1373.

166. Wolf P, Alt K, Wetterauer D, Buhler P, Gierschner D, Katzenwadel A, Wetterauer U and Elsasser-Beile U. Preclinical evaluation of a recombinant anti-prostate specific membrane antigen single-chain immunotoxin against prostate cancer. *J. Immunother.* 2010**, 33**:262-271.

167. Benesova M, Schafer M, Bauder-Wust U, Afshar-Oromieh A, Kratochwil C, Mier W, Haberkorn U, Kopka K and Eder M. Preclinical Evaluation of a Tailor-Made DOTA-Conjugated PSMA Inhibitor with Optimized Linker Moiety for Imaging and Endoradiotherapy of Prostate Cancer. *J. Nucl. Med.* 2015**, 56**:914-920.

168. Kratochwil C, Giesel FL, Stefanova M, Benesova M, Bronzel M, Afshar-Oromieh A, Mier W, Eder M, Kopka K and Haberkorn U. PSMA-Targeted Radionuclide Therapy of Metastatic Castration-Resistant Prostate Cancer with 177Lu-Labeled PSMA-617. *J. Nucl. Med.* 2016**, 57**:1170-1176.

169. Baum RP, Kulkarni HR, Schuchardt C, Singh A, Wirtz M, Wiessalla S, Schottelius M, Mueller D, Klette I and Wester HJ. 177Lu-Labeled Prostate-Specific Membrane Antigen Radioligand Therapy of Metastatic Castration-Resistant Prostate Cancer: Safety and Efficacy. *J. Nucl. Med.* 2016**, 57**:1006-1013.

170. Rahbar K, Ahmadzadehfar H, Kratochwil C, Haberkorn U, Schafers M, Essler M, Baum RP, Kulkarni HR, Schmidt M, Drzezga A, Bartenstein P, Pfestroff A, Luster M, Lutzen U, Marx M, Prasad V, Brenner W, Heinzel A, Mottaghy FM, Ruf J, Meyer PT, Heuschkel M, Eveslage M, Bogemann M, Fendler WP and Krause BJ. German Multicenter Study Investigating 177Lu-PSMA-617 Radioligand Therapy in Advanced Prostate Cancer Patients. *J. Nucl. Med.* 2017**, 58**:85-90.

171. Brauer A, Grubert LS, Roll W, Schrader AJ, Schafers M, Bogemann M and Rahbar K. 177Lu-PSMA-617 radioligand therapy and outcome in patients with metastasized castration-resistant prostate cancer. *Eur. J. Nucl. Med. Mol. Imaging* 2017**, 44**:1663-1670.

172. Lutetium-177 (Lu177) Prostate-Specific Antigen (PSMA)-Directed EndoRadiotherapy (September 28, 2017). https://clinicaltrials.gov/ct2/show/record/NCT03042312

173. Kumar A, Mastren T, Wang B, Hsieh JT, Hao G and Sun X. Design of a Small-Molecule Drug Conjugate for Prostate Cancer Targeted Theranostics. *Bioconjug. Chem.* 2016**, 27**:1681-1689.

174. Chen Z, Penet MF, Nimmagadda S, Li C, Banerjee SR, Winnard PT, Jr., Artemov D, Glunde K, Pomper MG and Bhujwalla ZM. PSMA-targeted theranostic nanoplex for prostate cancer therapy. *ACS Nano* 2012**, 6**:7752-7762.

175. Banerjee SR, Foss CA, Horhota A, Pullambhatla M, McDonnell K, Zale S and Pomper MG. 111In- and IRDye800CW-Labeled PLA-PEG Nanoparticle for Imaging Prostate-Specific Membrane Antigen-Expressing Tissues. *Biomacromolecules* 2017, **18**:201-209.

176. Chen Y, Chatterjee S, Lisok A, Minn I, Pullambhatla M, Wharram B, Wang Y, Jin J, Bhujwalla ZM, Nimmagadda S, Mease RC and Pomper MG. A PSMA-targeted theranostic agent for photodynamic therapy. *J. Photochem. Photobiol. B* 2017, **167**:111-116.

177. Rais R, Jiang W, Zhai H, Wozniak KM, Stathis M, Hollinger KR, Thomas AG, Rojas C, Vornov JJ, Marohn M, Li X and Slusher BS. FOLH1/GCPII is elevated in IBD patients, and its inhibition ameliorates murine IBD abnormalities. *JCI Insight* 2016, **1**.

178. Date AA, Rais R, Babu T, Ortiz J, Kanvinde P, Thomas AG, Zimmermann SC, Gadiano AJ, Halpert G, Slusher BS and Ensign LM. Local enema treatment to inhibit FOLH1/GCPII as a novel therapy for inflammatory bowel disease. *J. Control. Release* 2017.

179. Kopecek J and Kopeckova P. HPMA copolymers: origins, early developments, present, and future. *Adv. Drug Deliv. Rev.* 2010, **62**:122-149.

180. Ulbrich K, Hola K, Subr V, Bakandritsos A, Tucek J and Zboril R. Targeted drug delivery with polymers and magnetic nanoparticles: covalent and noncovalent approaches, release control, and clinical studies. *Chem. Rev.* 2016, **116**:5338-5431.

181. Ulbrich K and Subr V. Structural and chemical aspects of HPMA copolymers as drug carriers. *Adv. Drug Deliv. Rev.* 2010, **62**:150-166.

182. Kopecek J. Soluble biomedical polymers. *Polim. Med.* 1977, **7**:191-221.

183. Voldrich Z, Tomanek Z, Vacik J and Kopecek J. Long-term experience with poly(glycol monomethacrylate) gel in plastic operations of the nose. *J. Biomed. Mater. Res.* 1975, **9**:675-685.

184. Sprincl L, Kopecek J, Vacik J and Lim D. Biological tolerance of poly(N-substituted methacrylamides). *J. Biomed. Mater. Res.* 1971, **5**:197-205.

185. Sprincl L, Exner J, Sterba O and Kopecek J. New types of synthetic infusion solutions. III. Elimination and retention of poly-[N-(2-hydroxypropyl)methacrylamide] in a test organism. *J. Biomed. Mater. Res.* 1976, **10**:953-963.

186. Obereigner B, Buresova M, Vrana A and Kopecek J. Preparation of Polymerizable Derivatives of N-(4-Aminobenzenesulfonyl)-N'-Butylurea. *J. Polym. Sci., Polym. Symp.* 1979:41-52.

187. Subr V and Ulbrich K. Synthesis and properties of new N-(2-hydroxypropyl)-methacrylamide copolymers containing thiazolidine-2-thione reactive groups. *React. Funct. Polym.* 2006, **66**:1525-1538.

188. Subr V, Sivak L, Koziolova E, Braunova A, Pechar M, Strohalm J, Kabesova M, Rihova B, Ulbrich K and Kovar M. Synthesis of Poly[N-(2-hydroxypropyl)methacrylamide] Conjugates of Inhibitors of the ABC Transporter That Overcome Multidrug Resistance in Doxorubicin-Resistant P388 Cells in Vitro. *Biomacromolecules* 2014, **15**:3030-3043.

189. Ulbrich K, Subr V, Strohalm J, Plocova D, Jelinkova M and Rihova B. Polymeric drugs based on conjugates of synthetic and natural macromolecules I. Synthesis and physico-chemical characterisation. *J. Control. Release* 2000, **64**:63-79.

190. Peng ZH, Sima M, Salama ME, Kopeckova P and Kopecek J. Spacer length impacts the efficacy of targeted docetaxel conjugates in prostate-specific membrane antigen expressing prostate cancer. *J. Drug Target.* 2013**, 21**:968-980.

191. Duncan R and Vicent MJ. Do HPMA copolymer conjugates have a future as clinically useful nanomedicines? A critical overview of current status and future opportunities. *Adv. Drug Deliv. Rev.* 2010**, 62**:272-282.

192. Shiah JG, Dvorak M, Kopeckova P, Sun Y, Peterson CM and Kopecek J. Biodistribution and antitumour efficacy of long-circulating N-(2-hydroxypropyl)methacrylamide copolymer-doxorubicin conjugates in nude mice. *Eur. J. Cancer* 2001**, 37**:131-139.

193. Noguchi Y, Wu J, Duncan R, Strohalm J, Ulbrich K, Akaike T and Maeda H. Early phase tumor accumulation of macromolecules: a great difference in clearance rate between tumor and normal tissues. *Jpn. J. Cancer Res.* 1998**, 89**:307-314.

194. Seymour LW, Miyamoto Y, Maeda H, Brereton M, Strohalm J, Ulbrich K and Duncan R. Influence of molecular weight on passive tumour accumulation of a soluble macromolecular drug carrier. *Eur. J. Cancer* 1995**, 31A**:766-770.

195. Seymour LW, Duncan R, Strohalm J and Kopecek J. Effect of molecular weight (Mw) of N-(2-hydroxypropyl)methacrylamide copolymers on body distribution and rate of excretion after subcutaneous, intraperitoneal, and intravenous administration to rats. *J. Biomed. Mater. Res.* 1987**, 21**:1341-1358.

196. Van S, Das SK, Wang XH, Feng ZL, Jin Y, Hou Z, Chen F, Pham A, Jiang N, Howell SB and Yu L. Synthesis, characterization, and biological evaluation of poly(L-gamma-glutamyl-glutamine)-paclitaxel nanoconjugate. *Int. J. Nanomedicine* 2010**, 5**:825-837.

197. Saito G, Swanson JA and Lee KD. Drug delivery strategy utilizing conjugation via reversible disulfide linkages: role and site of cellular reducing activities. *Adv. Drug Deliv. Rev.* 2003**, 55**:199-215.

198. Etrych T, Chytil P, Mrkvan T, Sirova M, Rihova B and Ulbrich K. Conjugates of doxorubicin with graft HPMA copolymers for passive tumor targeting. *J. Control. Release* 2008**, 132**:184-192.

199. Kratz F, Beyer U and Schutte MT. Drug-polymer conjugates containing acid-cleavable bonds. *Crit. Rev. Ther. Drug Carrier Syst.* 1999**, 16**:245-288.

200. Rihova B, Strohalm J, Plocova D, Subr V, Srogl J, Jelinkova M, Sirova M and Ulbrich K. Cytotoxic and cytostatic effects of anti-Thy 1.2 targeted doxorubicin and cyclosporin A. *J. Control. Release* 1996**, 40**:303-319.

201. Tacar O, Sriamornsak P and Dass CR. Doxorubicin: an update on anticancer molecular action, toxicity and novel drug delivery systems. *J. Pharm. Pharmacol.* 2013**, 65**:157-170.

202. Vasey PA, Kaye SB, Morrison R, Twelves C, Wilson P, Duncan R, Thomson AH, Murray LS, Hilditch TE, Murray T, Burtles S, Fraier D, Frigerio E and Cassidy J. Phase I clinical and pharmacokinetic study of PK1 [N-(2-hydroxypropyl)methacrylamide copolymer doxorubicin]: first member of a new class of chemotherapeutic agents-drug-polymer conjugates. Cancer Research Campaign Phase I/II Committee. *Clin. Cancer Res.* 1999**, 5**:83-94.

203. Seymour LW, Ferry DR, Kerr DJ, Rea D, Whitlock M, Poyner R, Boivin C, Hesslewood S, Twelves C, Blackie R, Schatzlein A, Jodrell D, Bissett D, Calvert H, Lind M, Robbins A, Burtles S, Duncan R and Cassidy J. Phase II studies of polymer-

doxorubicin (PK1, FCE28068) in the treatment of breast, lung and colorectal cancer. *Int. J. Oncol.* 2009**, 34**:1629-1636.

204. Seymour LW, Ferry DR, Anderson D, Hesslewood S, Julyan PJ, Poyner R, Doran J, Young AM, Burtles S, Kerr DJ and Cancer Research Campaign Phase IIICTc. Hepatic drug targeting: phase I evaluation of polymer-bound doxorubicin. *J. Clin. Oncol.* 2002**, 20**:1668-1676.

205. Mitra A, Nan A, Papadimitriou JC, Ghandehari H and Line BR. Polymer-peptide conjugates for angiogenesis targeted tumor radiotherapy. *Nucl. Med. Biol.* 2006**, 33**:43-52.

206. Lu ZR, Kopeckova P and Kopecek J. Polymerizable Fab' antibody fragments for targeting of anticancer drugs. *Nat. Biotechnol.* 1999**, 17**:1101-1104.

207. Johnson RN, Kopeckova P and Kopecek J. Biological activity of anti-CD20 multivalent HPMA copolymer-Fab' conjugates. *Biomacromolecules* 2012**, 13**:727-735.

208. Maeda H, Wu J, Sawa T, Matsumura Y and Hori K. Tumor vascular permeability and the EPR effect in macromolecular therapeutics: a review. *J. Control. Release* 2000**, 65**:271-284.

209. Matsumura Y and Maeda H. A new concept for macromolecular therapeutics in cancer chemotherapy: mechanism of tumoritropic accumulation of proteins and the antitumor agent smancs. *Cancer Res.* 1986**, 46**:6387-6392.

210. Folkman J. Tumor angiogenesis: therapeutic implications. *N. Engl. J. Med.* 1971**, 285**:1182-1186.

211. Nishida N, Yano H, Nishida T, Kamura T and Kojiro M. Angiogenesis in cancer. *Vasc. Health Risk Manag.* 2006**, 2**:213-219.

212. Liu J, Kopeckova P, Buhler P, Wolf P, Pan H, Bauer H, Elsasser-Beile U and Kopecek J. Biorecognition and subcellular trafficking of HPMA copolymer-anti-PSMA antibody conjugates by prostate cancer cells. *Mol. Pharm.* 2009**, 6**:959-970.

213. Pearce AK, Simpson JD, Fletcher NL, Houston ZH, Fuchs AV, Russell PJ, Whittaker AK and Thurecht KJ. Localised delivery of doxorubicin to prostate cancer cells through a PSMA-targeted hyperbranched polymer theranostic. *Biomaterials* 2017**, 141**:330-339.

5. Abbreviations

2-MPPA	2-(3-Mercaptopropyl)pentanedioic Acid
2-PMPA	2-(Phosphonomethyl)pentanedioic Acid
ADC	Antibody Drug Conjugate
ALS	Amyotrophic Lateral Sclerosis
BCG	β-Citryl-L-Glutamate
cAMP	Cyclic Adenosine Monophosphate
CT	Computed Tomography
DARPin	Designed Ankyrin Repeat Protein
DM-1	Maytansinoid 1
ELISA	Enzyme-Linked Immunosorbent Assay
EPR	Enhanced-Permeability and Retention (Effect)
FDA	Food and Drug Administration
FOLH	Folate Hydrolase
GCPII	Glutamate Carboxypeptidase II
GCPIII	Glutamate Carboxypeptidase III
HILAP	Human Ileal Aminopeptidase
HPMA	N-(2-hydroxypropyl)methacrylamide
HRP	Horseradish Peroxidase
IHC	Immunohistochemistry
LNCaP	Lymph Node Carcinoma of the Prostate
mAb	Monoclonal Antibody
mCRPC	Metastatic Castration-Resistant Prostate Cancer
mGluR	Metabotropic Glutamate Receptor

MMAE	Monomethyl Auristatin E
MRI	Magnetic Resonance Imaging
NAAG	*N*-Acetyl-L-Aspartyl-L-Glutamate
NAALADase	*N*-Acetylated Alpha-Linked Acidic Dipeptidase
NAALADase II	*N*-Acetylated Alpha-Linked Acidic Dipeptidase II
NAALADase L	Acetylated Alpha-Linked Acidic Dipeptidase-Like
NF-κB	Nuclear Factor κB
NMDA	*N*-Methyl-D-Aspartate
NTA	Nitrilotriacetic Acid
PET	Positron Emission Tomography
PGCP	Plasma Glutamate Carboxypeptidase
POC	Isopropyloxycarbonyloxymethyl
PSA	Prostate Specific Antigen
PSMA	Prostate Specific Membrane Antigen
PSMAL	Prostate Specific Membrane Antigen-Like
RAFT	Reversible Addition-Fragmentation Chain Transfer
rhGCPII	Recombinant Human GCPII
scFv	Single-Chain Variable Fragment
SPECT	Single-Photon Emission Computed Tomography
SPR	Surface Plasmon Resonance
TfR	Transferrin Receptor
TGF-β	Tumor Growth Factor β
USPSTF	United States Preventive Services Task Force
ZBG	Zinc-Binding Group

6. Figures and tables

7. Appendix: Reprints of the publications described in the thesis

The following section contains reprints of three publications.

Paper I:

Knedlik T, Navratil V, Vik V, Pacik D, Sacha P, Konvalinka J: Detection and quantitation of glutamate carboxypeptidase II in human blood. *Prostate* 2014, **74**(7):768-780.

Paper II:

Knedlik T, Vorlova B, Navratil V, Tykvart J, Sedlak F, Vaculin S, Franek M, Sacha P, Konvalinka J: Mouse glutamate carboxypeptidase II (GCPII) has a similar enzyme activity and inhibition profile but a different tissue distribution to human GCPII. *FEBS Open Bio* 2017, **7**(9):1362-1378.

Paper III:

Sacha P, Knedlik T, Schimer J, Tykvart J, Parolek J, Navratil V, Dvorakova P, Sedlak F, Ulbrich K, Strohalm J, Majer P, Subr V, Konvalinka J: iBodies: Modular Synthetic Antibody Mimetics Based on Hydrophilic Polymers Decorated with Functional Moieties. *Angew Chem Int Ed Engl* 2016, **55**(7):2356-2360.

7.1. Paper I

Tomáš Knedlík, Václav Navrátil, Viktor Vik, Dalibor Pacík, Pavel Šácha

and Jan Konvalinka

Detection and quantitation of glutamate carboxypeptidase II in human blood.

Prostate 2014, **74**(7):768-780.

Detection and Quantitation of Glutamate Carboxypeptidase II in Human Blood

Tomáš Knedlík,[1,2] Václav Navrátil,[1,2] Viktor Vik,[3] Dalibor Pacík,[4] Pavel Šácha,[1,2] and Jan Konvalinka[1,2]*

[1]Gilead Sciences and IOCB Research Centre, Institute of Organic Chemistry and Biochemistry, Academy of Sciences of the Czech Republic, Prague, Czech Republic
[2]Department of Biochemistry, Faculty of Science, Charles University in Prague, Prague, Czech Republic
[3]Department of Urology, Thomayer Hospital in Prague, Prague, Czech Republic
[4]Department of Urology, Medical School Masaryk University, University Hospital Brno, Brno, Czech Republic

BACKGROUND. Glutamate carboxypeptidase II (GCPII) is a transmembrane enzyme that cleaves N-acetyl-L-aspartyl-L-glutamate (NAAG) in the brain. GCPII is highly expressed in the prostate and prostate cancer and might be associated with prostate cancer progression. Another exopeptidase, plasma glutamate carboxypeptidase (PGCP), was reported to be similar to GCPII and to share its NAAG-hydrolyzing activity.
METHODS. We performed a radioenzymatic assay with [^{3}H]NAAG as a substrate to detect and quantify the enzymatic activity of GCPII in plasma. Using a specific antibody raised against native GCPII (2G7), we immunoprecipitated GCPII from human plasma. We also cloned two PGCP constructs, expressed them in insect cells, and tested them for their NAAG-hydrolyzing activity.
RESULTS. We detected GCPII protein in human plasma and found that its concentration ranges between 1.3 and 17.2 ng/ml in volunteers not diagnosed with prostate cancer. Recombinant PGCP was enzymatically active but exhibited no NAAG-hydrolyzing activity.
CONCLUSION. GCPII is present in human blood, and its concentration within a healthy population varies. Recombinant PGCP does not hydrolyze NAAG, suggesting that GCPII alone is responsible for the NAAG-hydrolyzing activity observed in human blood. The potential correlation between GCPII serum levels and the disease status of prostate cancer patients will be further investigated. *Prostate 74:768–780, 2014.* © 2014 Wiley Periodicals, Inc.

KEY WORDS: glutamate carboxypeptidase II; prostate-specific membrane antigen; serum marker; prostate cancer; plasma glutamate carboxypeptidase

INTRODUCTION

Prostate cancer is the most prevalent type of cancer and one of the leading causes of death among men in the United States and Western Europe. An estimated 233,000 men will be diagnosed with prostate cancer in the United States in 2014, and 29,000 men will die of the disease [1].

Glutamate carboxypeptidase II (GCPII), also known as prostate-specific membrane antigen (PSMA), N-acetylated-alpha-linked acidic dipeptidase (NAALA-Dase) or folate hydrolase, is a transmembrane metallopeptidase with a short cytoplasmic tail and a large extracellular domain [2–4]. In humans, GCPII is expressed predominantly in the prostate and in lower amounts in several other tissues, such as brain, kidney, and small intestine [5–8]. GCPII possesses two known

enzymatic activities: (1) in the central nervous system, it hydrolyzes the abundant peptidic neurotransmitter N-acetyl-L-aspartyl-L-glutamate (NAAG) into N-acetyl-L-aspartate and free L-glutamate, thus participating in glutamate excitotoxicity [4]; (2) in the small intestine, GCPII cleaves glutamates from poly-gamma-glutamylated folates, enabling folate to be transported across the intestinal mucosa [9]. Although GCPII is highly expressed on prostate epithelial cells, the physiological role of the protein in this tissue has not yet been elucidated. Several hypotheses have been suggested; however, so far none of them has been widely accepted by the scientific community [10–14].

Interestingly, GCPII expression in prostate cancer seems to be 10-fold higher than in benign prostate tissue [15]. Although the function of GCPII in the prostate is still unclear, the protein's potential as a diagnostic and/or therapeutic target was identified many years ago [16]. As a transmembrane protein that undergoes internalization, GCPII seems to be an ideal target for monoclonal antibody or inhibitor-based imaging or therapy [17–19]. An ^{111}In-labeled antibody raised against GCPII (trade name ProstaScint[20]) currently is used in the first diagnostic scan detecting GCPII expression in prostate cancer. This conjugate is used clinically for imaging prostate cancer and its metastatic invasion into other tissues [20]. However, ProstaScint[20] can bind only damaged or dead cells, since the antibody recognizes an internal epitope of GCPII [21]. In the past 10 years, scientists have been working on second generation antibodies that recognize the extracellular portion of GCPII, enabling visualization of viable cells [22,23]. These antibodies, coupled with either a radionuclide or a toxic agent, would specifically bind to prostate cancer cells expressing large quantities of GCPII and, following internalization, would cause damage to the cancer cells [24,25] (reviewed in Ref. [26]).

GCPII's potential as a diagnostic and/or prognostic marker motivated efforts to identify the enzyme in human plasma, either as a secreted or shedded species. Although GCPII has been well-studied as a membrane target, its role as a potential serum marker is less clear. GCPII was first found in human serum in a series of works using Western blot analysis, a semi-quantitative method providing results as relative band intensities [27–29]. Wright's group was first unable to detect GCPII in serum using Western blot [30], but they subsequently showed GCPII to be present in serum [31]. Later, Xiao et al. developed a SELDI quantitative immunoassay using ProteinChip mass spectrometry. In contrast to the Western blot results, this approach led to quantitation of serum GCPII in concentrations in the range of hundreds of nanograms per milliliter [32].

The current prostate cancer screening test is based on quantitation of prostate specific antigen (PSA) in a man's blood [33]. PSA levels are elevated in men with prostate cancer. However, benign prostate hyperplasia and some other factors, such as age, race, or prostate infection, also may lead to elevated PSA levels [34]. Consequently, the Centers for Disease Control and Prevention (CDC) and the U.S. Preventive Services Task Force (USPSTF) have recommended against PSA-based screening for men who do not have symptoms of prostate cancer [35]. Measuring the level of GCPII in blood might be an alternative to the PSA-based screening test. Different levels of GCPII in blood also may correlate with prostate cancer stage, as GCPII expression increases in high-grade cancers and metastatic disease. On the other hand, high concentrations of GCPII in blood, if confirmed, might pose a serious problem for drug delivery targeting GCPII on the prostate epithelium.

It is important to note that another metallopeptidase homologous to GCPII, called plasma glutamate carboxypeptidase (PGCP), also has been reported to be present in human blood [36]. PGCP is secreted into blood plasma and has been reported to possess both NAAG-hydrolyzing and SerMet-hydrolyzing activity [36,37]. Due to its potential NAAG-hydrolyzing activity, PGCP might interfere with the detection of GCPII in enzyme-based assays. The function of PGCP is unknown, but it has been suggested to play a role in hydrolysis of circulating peptides and proteins [36].

In this work, we set out to resolve the conflicting reports concerning GCPII's presence in the blood and its potential to serve as a marker for prostate cancer prognosis. We also analyze the potential GCPII-like activity of PGCP, which might interfere with GCPII-based assay.

MATERIALS AND METHODS

Radioenzymatic Determination of NAAG-Hydrolyzing Activity in Human Plasma

The radioenzymatic assay was performed as previously described [4,38,39], with minor modifications. Plasma samples were diluted 10- to 100-fold with 20 mM Tris–HCl, 150 mM NaCl, 0.1% Tween 20, pH 7.4, (and inhibitor solution, if used) to a final volume of 90 μl. Reactions were first incubated for 5 min at 37°C and then started by adding 10 μl of 1 μM NAAG (containing 50 nM tritium-labeled NAAG, labeled at the terminal glutamate moiety; Perkin-Elmer), and incubated at 37°C for 18 hr. The reactions were stopped with 100 μl of ice-cold 200 mM KH_2PO_4, 2 mM 2-mercaptoethanol, pH 7.4. The released glutamate was then separated from the unreacted substrate using ion exchange AG1-X8 resin (Bio-Rad). The radioactivity of

the sample was quantified by liquid scintillation using the Rotiszint ECO Plus scintillation cocktail (Roth) on a Tri-Carb Liquid Scintillation Counter (Perkin-Elmer). The samples were measured in duplicates or triplicates.

Preparation, Purification, and Biotinylation of the GCPII-Specific Antibody 2G7

The novel mouse monoclonal antibody 2G7, which binds an extracellular epitope in native (i.e., enzymatically active) GCPII, was prepared in the laboratory of Vaclav Horejsi (Institute of Molecular Genetics, Academy of Sciences of the Czech Republic, Prague, Czech Republic). Mice (F1 hybrids of BALB/c and B10.A strains) were immunized with recombinant extracellular GCPII (amino acids 44–750) as previously described [40].

The antibody 2G7 was purified from 800 ml of hybridoma-conditioned medium that was concentrated to 10 ml using a LabScale TFF System (with Pellicon® XL 50 Cassette, Biomax 100, MWCO 100 kDa; Millipore). The concentrated medium was mixed in a 3:1 ratio with 4 M NaCl, 2 M glycine, pH 8.5, and the equilibrated concentrated medium was loaded onto a HiTrap™ FF Protein A Sepharose column (1 ml column volume; GE Healthcare Life Sciences) connected to an AKTA PRIME machine. The column was then washed with 50 ml of 1 M NaCl, 0.5 M glycine, pH 8.5. Bound antibodies were eluted with 100 mM sodium citrate, pH 5.0, and elution fractions were immediately neutralized with 1 M HEPES, pH 8.0 (mixed in a 5:1 ratio). The elution fractions were mixed and dialyzed against PBS using Slide-A-Lyzer® MINI Dialysis Units (10 kDa MWCO; Thermo Scientific).

The purified antibody was biotinylated using EZ-Link Sulfo-NHS-LC-Biotin (Thermo Fisher Scientific, Inc.) according to the manufacturer's instructions. Briefly, 1.2 ml of purified 2G7 antibody in PBS (concentration 0.4 mg/ml) was mixed with 24 µl of 10 mM Sulfo-NHS-LC-Biotin, resulting in a 75-fold molar excess of the biotinylation reagent. The reaction was incubated on ice for 12 hr, then stopped by dialysis against 20 mM Tris–HCl, 150 mM NaCl, pH 7.4, using Slide-A-Lyzer® MINI Dialysis Units (10 kDa MWCO; Thermo Scientific).

Immunoprecipitation of GCPII from Human Plasma

GCPII was immunoprecipitated with biotinylated 2G7. First, 10 µg of biotinylated 2G7 was diluted into 1 ml of 20 mM Tris–HCl, 150 mM NaCl, 0.1% Tween-20, pH 7.4 (TBST buffer). The antibody solution was mixed with 50 µl of Streptavidin Sepharose (GE Healthcare Life Sciences) and incubated for 2 hr at 6°C. Afterwards, the resin with bound 2G7 was washed

twice with 1 ml TBST. A citrate plasma sample (600 µl) was diluted 20-fold with TBST, mixed with the resin with bound 2G7 and incubated for 18 hr at 6°C. The resin was then washed three times with 1 ml TBST. Proteins were eluted from the Streptavidin Sepharose by adding 50 µl reducing SDS sample buffer and heating to 100°C for 10 min.

Blood Plasma Sample Preparation

Blood plasma samples were provided by healthy volunteers at Thomayer Hospital in Prague, with agreement of the local ethical commission. Blood was withdrawn into Vacuette® tubes (Greiner Bio-One) containing either sodium citrate (# 456323) or lithium heparin (# 456083) and placed in the refrigerator. Within 8 hr, tubes were centrifuged at 2,000g for 10 min with minimal deceleration, and blood plasma was transferred into a microtube. Samples were stored at −20°C until analysis.

Measurements of blood PSA levels were carried out according to standard procedure at Thomayer Hospital in Prague using the ARCHITECT Total PSA Reagent Kit (Abbott Diagnostics).

SDS-PAGE and Western Blotting

Protein samples were resolved by reducing sodium dodecyl sulfate polyacrylamide gel electrophoresis (SDS-PAGE). Gels were either silver-stained, stained with colloidal Coomassie G-250 (blue silver) for mass-spectrometry analysis, or electroblotted onto a PVDF membrane.

After blotting, the membrane was blocked with Blocker™ Casein solution (Thermo Scientific) at room temperature for 1 hr. To visualize GCPII, the blots were incubated with the primary antibody GCP-04 (described in Ref. [41]) for 12 hr at 4°C (diluted in Blocker™ Casein, 360 ng/ml), washed three times with PBS containing 0.05% Tween 20 (PBST buffer), and incubated with goat anti-mouse antibody conjugated with horseradish peroxidase (Thermo Scientific; diluted in Blocker™ Casein, 32 ng/ml).

The blots were then washed three times with PBST to remove unbound antibodies and developed with SuperSignal West Femto Chemiluminescent Substrate (Thermo Scientific). Chemiluminiscence was captured with a ChemiDoc-It™ 600 Imaging System (UVP).

Cloning of PGCP Constructs

The pFastBacPGCP plasmid, containing DNA encoding the full-length PGCP sequence (amino acids 1–472), was a kind gift from Dr. Dolenc (Department of Biochemistry and Molecular and Structural Biology, J. Stefan Institute, Ljubljana, Slovenia). To remove the

*Bgl*II restriction site inside the PGCP sequence, we used site-directed mutagenesis with the following two primers: 5′-gcactctcacttattaaggatcttgggctgcg-3′ and 5′-cgcagcccaagatccttaataagtgagagtgc-3′. The mutagenesis was carried out according to the manufacturer's protocol (QuikChange™ Site-Directed Mutagenesis, Stratagene). Then, the mutated pFastBacPGCP plasmid was used for preparation of two PGCP constructs.

The first construct, aviPGCP, contains a peptide sequence corresponding to the biotin ligase substrate (Avi-tag; [42]) and tobacco-etch virus protease (TEV; [43]) cleavage sequence at the N-terminus of mature PGCP (amino acids 45–472). The sequence corresponding to the mature PGCP chain was amplified by standard PCR with the following primers: 5′-aaaagatctgatgttgctaaagcaatcatc-3′ and 5′-aaactcgagcctaggacctaggcag-3′ (restriction sites introduced into the sequence are underlined). The primers introduced a *Bgl*II site at the 5′ end and an *Xho*I site at the 3′ end of the sequence. The resulting DNA fragment was cleaved with *Bgl*II and *Xho*I and ligated into pMT/BiP/AviTEV/rhGCPII plasmid [39] cleaved with the same endonucleases.

The second construct, ProPGCPavi, contains the propeptide part and the mature chain of PGCP (amino acids 21–44 and 45–472, respectively), followed by a DNA sequence corresponding to the AviTag™ sequence (GeneCopoeia, Inc.) at the C-terminus. The DNA sequence encoding PGCP with propeptide was amplified using primers 5′-aaaagatctaaagctatatgcaagaatg-3′ and 5′- aaatgatcatctccgcttcctccggacctaggcagcattt-3′. Two restriction sites (underlined) were introduced into the sequence: *Bgl*II at the 5′ end and *Bcl*I at the 3′ end of the sequence. The amplicon was cleaved with *Bgl*II and *Bcl*I and inserted into plasmid pTRE-Tight/NaalL2_1-124spacAvi cleaved with *Bgl*II (Šácha et al., manuscript in preparation). This ligation led to introduction of a stop codon between the PGCP and Avi-tag sequence; therefore, mutagenesis was performed to remove the stop-codon sequence using primers 5′-ggaggaagcggaggaagatctggcctgaacg-3′ and 5′-cgttcaggccagatcttcctccgcttcctcc-3′. The mutagenesis was carried out according to the manufacturer's protocol (QuikChange™ Site-Directed Mutagenesis, Stratagene). Finally, the C-terminally Avi-tagged ProPGCP sequence in pTRE-Tight vector was cleaved with *Bgl*II and *Xho*I and inserted into pMT/BiP/V5-HisA (Invitrogen).

The correct sequences of both resulting plasmids were verified by DNA sequencing.

Preparation of Stable *Drosophila* S2 Cell Lines Expressing aviPGCP and ProPGCPavi

Previously prepared *Drosophila* S2 cells expressing BirA biotin-protein ligase localized in ER were used for preparation of stable aviPGCP and ProPGCPavi transfectants [39]. BirA ensures specific in vivo biotinylation of the expressed protein at its Avi-tag sequence. The cells were transfected using Calcium Phosphate Transfection Kit (Invitrogen) with 9 µg of either pMT/BiP/aviPGCP or pMT/BiP/ProPGCPavi together with 0.5 µg of pCoBlast (Invitrogen), analogously as previously described [38]. The transfected cells were cultivated in the presence of both blasticidin (5 µg/ml, Invitrogen) and hygromycin B (300 µg/ml, Invitrogen).

Approximately 2×10^6 stably transfected cells were transferred into a 35 mm Petri dish supplemented with 2 ml SF900II medium (Invitrogen). The following day, protein expression was induced by adding $CuSO_4$ (Sigma) to a final concentration of 1 mM. After 3 days, cells were harvested by centrifugation, and the medium was frozen until use.

Large-Scale Expression of ProPGCPavi and aviPGCP in *Drosophila* S2 Cells

The protocol for large-scale expression of PGCP constructs was identical to that described previously [40]. The final volume of cell suspension was 100 ml for aviPGCP and 500 ml for ProPGCPavi.

Purification of PGCP Constructs

Purification of PGCP constructs was performed as previously described [39]. Briefly, cell medium containing secreted biotinylated ProPGCPavi (500 ml) or aviPGCP (100 ml) was centrifuged at 3,400g for 45 min. Then, it was concentrated 10-fold using a LabScale TFF System (Millipore) with a Pellicon® XL 50 Cassette, Biomax 100 (ProPGCPavi purification) or 20-fold using a Vivaspin-6 centrifugal concentrator with a 10 kDa MWCO membrane (aviPGCP purification). The concentrated medium was centrifuged again at 3,400g for 20 min and equilibrated with 300 mM Tris–HCl, 450 mM NaCl, pH 7.2 (in a 2:1 ratio). The equilibrated concentrated ProPGCPavi medium was then mixed with 1 ml (or 200 µl for aviPGCP purification) of Streptavidin Mutein Matrix (Roche) and incubated with gentle shaking at 6°C for 15 hr. Afterwards, the resin was washed with 50 column volumes of 100 mM Tris–HCl, 150 mM NaCl, pH 7.2. Bound biotinylated proteins were eluted with 5 ml of 100 mM Tris–HCl, 150 mM NaCl, 2 mM D-biotin, pH 7.2, in five consecutive elution fractions (after the first elution fraction, the resin was incubated with elution buffer for 1 hr). After regeneration of the resin, the flow-through fraction was again mixed with the resin, and the purification procedure was repeated.

74

HPLC Determination of SerMet-Hydrolyzing Activity

Purified enzyme (30 ng), inhibitor solution (if used), and buffer solution (either 100 mM sodium acetate, 15 mM zinc acetate, pH 5.5, or 100 mM Tris–HCl, 1 mM zinc acetate, pH 7.5) were mixed in a final volume of 45 μl. Then, 5 μl of 10 mM L-seryl-L-methionine (Bachem) was added, and reactions were incubated at 37°C for 1 hr. Reactions were stopped by adding 125 μl of 200 mM sodium borate, pH 10. Reaction products were detected and quantified according to a previously described method using o-phthalaldehyde (OPA) derivatization [44] and analyzed on an Agilent 1200 Series system using an AccQ-Tag Ultra column (2.1 × 100 mm; Waters).

Protein Identification in Blood Plasma by Liquid Chromatography/Mass Spectrometry Analysis (LC–MS/MS)

Blood plasma samples were resolved by SDS gel electrophoresis and the gel was stained with colloidal Coomassie G-250. The gel was cut to pieces and the proteins in gel were destained, reduced by dithiothreitol, alkylated by iodacetamide and digested by trypsin. The peptides were extracted and dissolved in 0.1% formic acid. Samples were analyzed on UltiMate 3000 RSLCnano system (Dionex) coupled to a TripleTOF 5600 mass spectrometer with a NanoSpray III source (AB Sciex). The peptides were separated on Acclaim PepMap100 analytical column (3 μm, 15 cm × 75 μm ID, Thermo Scientific) using gradient from 5% to 30% over 55 min. MS mass range was set to 350–1,250 m/z, up to 25 ion candidates per cycle was allowed to be fragmented. In MS/MS mode the instrument acquired fragmentation spectra within m/z range from 100 to 1,600. Protein Pilot 4.0 (AB Sciex) was used for protein identification against *Homo Sapiens* Database (UniProt—SwissProt and TrEMBL, November 18, 2013).

RESULTS

NAAG-Hydrolyzing Activity in Human Plasma Can Be Blocked by GCPII Inhibitors

Three citrate plasma samples obtained from three different individuals (denominated PL, PL2, and PL3) were tested for their NAAG-hydrolyzing activity using radioenzymatic assay with tritium-labeled NAAG. Prior to the assay, plasma samples were dialyzed against 50 mM Tris–HCl, 25 mM NaCl, pH 7.4.

We observed NAAG-hydrolyzing activity in all three plasma samples (Fig. 1A). This activity was

The Prostate

sensitive to the GCPII-specific inhibitor 2-(phosphonomethyl)pentanedioic acid (2-PMPA, final concentration 500 nM) and was also inhibited by a collection of other specific GCPII inhibitors, including 2-(3-mercaptopropyl)pentanedioic acid (2-MPPA, 100 μM), 2-[(pentafluorophenylmethyl)hydroxyphosphinyl]methyl-pentanedioic acid (GPI-5232, 500 μM; GPI-5495, 200 μM; GPI-5496, 1 mM), (2S,3'S)-{[(3'-amino-3'-carboxy-propyl)-hydroxyphosphinoyl]methyl}-pentanedioic acid (EPE, 1 mM), and methotrexate (1 mM). Inhibitors GPI-5232, GPI-5495, and GPI-5496 are stereoisomers. The plasma samples PL2 and PL3 were tested only with 2-PMPA (Fig. 1A).

The diluted plasma samples exhibited a linear dependence of substrate conversion on added plasma volume. More concentrated samples (non-diluted or less than 10-fold dilution) reached a conversion plateau (Fig. 1B), presumably due to matrix effects. Therefore, 10- to 100-fold dilution of plasma samples (the linear area of the curve) was used for GCPII quantification in plasma. Standards of recombinant extracellular GCPII (rhGCPII; prepared as described in Ref. [40]) exhibited linear dependence of substrate conversion on rhGCPII amount in the region between 0 and 50 pg rhGCPII (Fig. 1C).

GCPII Can Be Immunoprecipitated from Plasma and Detected by Mass Spectrometry

To verify that GCPII is in fact present in human blood, we immunoprecipitated GCPII from human citrate plasma with biotinylated antibody 2G7 coupled to Streptavidin Sepharose resin. The presence of GCPII in plasma was confirmed by Western blot analysis of the elution fractions with GCPII-specific antibody GCP-04 (Fig. 2) and eventually by mass spectrometry, which detected peptides covering 34% of the GCPII sequence (data not shown).

As a positive control, the diluted plasma sample was spiked with recombinant extracellular GCPII (rhGCPII; prepared as described in Ref. [40]) to a final concentration of 850 pg/ml (Fig. 2, lanes 3 and 8). As a negative control, no 2G7 antibody was bound to the Streptavidin Sepharose resin mixed with the diluted plasma sample (Fig. 2, lanes 4 and 9). The diffuse appearance of the GCPII bands suggests GCPII is heterogenously glycosylated, in contrast to uniform high-mannose glycosylation of rhGCPII standard expressed in insect cells (Fig. 2).

Interestingly, we were unable to immunoprecipitate GCPII with non-biotinylated antibodies raised against native GCPII (including J591) that were bound to Protein G Sepharose rather than Streptavidin Sepharose (data not shown).
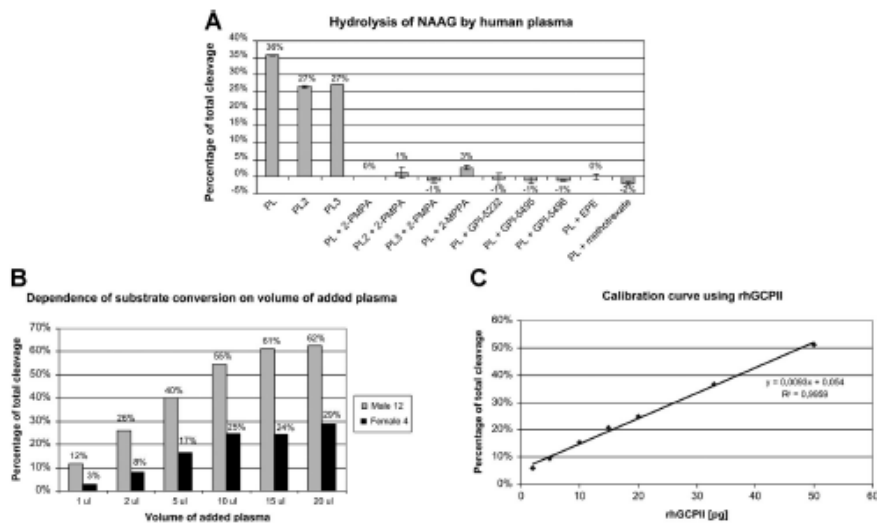
Fig. I. NAAG-hydrolyzing activity in human plasma and its inhibition by a set of specific GCPII inhibitors. **Panel A**: NAAG-hydrolyzing activity of three different human plasma samples (PL, PL2, PL3) was analyzed using radioenzymatic assay with [^{3}H]NAAG. To probe GCPII inhibition, a panel of GCPII inhibitors was used: 2-PMPA (500 nM), 2-MPPA (100 μM), GPI-5232 (500 μM), GPI-5495 (200 μM), GPI-5496 (1 mM), EPE (1 mM), and methotrexate (1 mM). The activities were measured in duplicate; values are presented as the mean ± standard deviation. Ten microliters of plasma was loaded in each reaction. **Panel B**: Two plasma samples (male #12 and female #4, see Table I) of different GCPII concentration were chosen to illustrate the dependence of substrate conversion on the volume of added plasma. When more than 10 μl of undiluted plasma was added, substrate conversion reached its plateau. **Panel C**: Calibration curve of cleaved [^{3}H]NAAG by recombinant extracellular GCPII (rhGCPII). The analyzed plasma samples were diluted to fit into the linear region of the calibration curve (0–50 pg rhGCPII).

Low Concentrations of GCPII are Present in the Plasma of Healthy Individuals

We set out to analyze the distribution of GCPII concentration in the blood of healthy individuals. Blood samples were collected from volunteers not diagnosed with prostate cancer, including four females. All individuals' PSA levels fell below 2.5 ng/ml (Table I), and therefore they can be considered healthy and without considerable risk of prostate cancer [45]. The GCPII concentration was determined in these samples using radioenzymatic assay with [^{3}H]NAAG as a substrate. Purified recombinant extracellular GCPII (0.01–1 ng/ml; prepared as described in Ref. [40]) was used as a standard. Plasma samples were diluted 10- to 100-fold, which was necessary to fit into the range of the standards. To verify that GCPII is the proteolytic agent, patients' plasma samples were inhibited with 500 nM 2-PMPA. The addition of the GCPII-specific inhibitor led to complete loss of the activity in all tested samples. The GCPII concentration in plasma ranged between 1.3 and 17.2 ng/ml. Since the values for the GCPII amount in the blood are always positive, they should

follow log-normal distribution. Therefore, geometrical mean and non-symmetrical standard deviations are used and reach the following values (see Table I): 3.2 ng/ml (+3.3; −1.6 ng/ml); for men only: 3.7 ng/ml (+3.8; −1.9 ng/ml); all female samples fell under 5 ng/ml: 2.0 ng/ml (+1.4; −0.8 ng/ml).

The GCPII concentration in plasma did not correlate with the age of the volunteers (Pearson's correlation coefficient: 0.28; P-value: 0.31). The Pearson's correlation analysis revealed no correlation between GCPII and PSA plasma concentrations (Pearson's correlation coefficient: 0.08; P-value: 0.81).

Purified Recombinant PGCP Constructs are Enzymatically Active but do not Possess NAAG-Hydrolyzing Activity

We prepared two PGCP constructs to elucidate whether and to what extent PGCP contributes to NAAG-hydrolyzing activity in human plasma.

Endogenous PGCP contains a signal peptide, pro-peptide, and mature chain. We replaced the endogenous signal peptide with the BiP signal sequence and

76
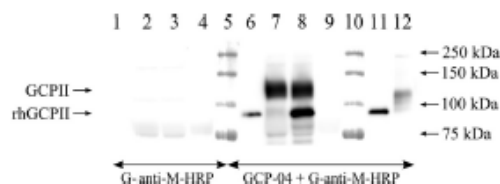
Fig. 2. Immunoprecipitation of GCPII from human plasma. GCPII was immunoprecipitated from 600 μl citrate plasma with biotinylated antibody 2G7 bound to Streptavidin Sepharose. As a negative control, an experiment without antibody 2G7 was performed. As a positive control, diluted plasma sample was spiked with recombinant extracellular GCPII (rhGCPII), lacking its endogenous intracellular and transmembrane parts. The Western blot was performed with the antibody GCP-04 (described in Ref. [41]), recognizing denatured GCPII, followed by HRP-conjugated goat anti-mouse IgG secondary antibody (G-anti-M-HRP; Thermo Scientific). A half of the membrane was probed with G-anti-M-HRP only to visualise the non-specific signal caused by the secondary antibody. The arrows indicate the position of immunoprecipitated GCPII (lanes 7 and 8), rhGCPII in the spiked sample (lane 8), or rhGCPII used as a standard (lanes 6 and 11). (1,6) rhGCPII standard, 1 ng; (2,7) Elution from IP; (3,8) Elution from IP-positive control; (4,9) Elution from IP-negative control; (5,10) All blue standards (Bio-Rad); (11) rhGCPII standard, 2 ng; (12) LNCaP lysate, 1.5 μg total protein. Twenty-five microliters of the elution fraction sample was loaded to each lane.

placed an Avi-tag at the N-terminus or C-terminus. The propeptide part was preserved only in the C-terminally tagged construct, allowing it to remain free for further molecular processing and activation of PGCP (Fig. 3A,C).

Conditioned media from cultures of *Drosophila* S2 cells stably transfected with ProPGCPavi or aviPGCP were concentrated, and Avi-tagged PGCP constructs were purified by affinity chromatography using Streptavidin Mutein Matrix. The purification yield was 3.3 mg of ProPGCPavi (purified from 500 ml of cell-conditioned medium) and 0.22 mg of aviPGCP (purified from 100 ml of cell-conditioned medium). The purity of the proteins was determined by SDS-PAGE (Fig. 3B,D).

The availability of sufficient amounts of recombinant purified PGCP (ProPGCPavi and aviPGCP) enabled determination of PGCP's enzymatic activities. To verify that we obtained properly folded and active PGCP constructs, we determined their proteolytic activity using a cognate substrate of PGCP, the dipeptide L-seryl-L-methionine (SerMet) [37,46]. The determinations were performed in two different buffers: in 100 mM Tris–HCl, 1 mM ZnCl$_2$, pH 7.5 (according to Gingras et al. [36]), and in 100 mM sodium acetate, pH 5.5, including 15 mM zinc acetate (according to Zajc et al. [37]).

TABLE I. GCPII Concentrations in Plasma of Healthy Individuals

|	Age (years)	GCPII in plasma (ng/ml)	PSA in plasma (ng/ml)
Female 1	22	1.4 ± 0.3	0.004
Female 2	31	1.3 ± 0.3	N/D
Female 3	43	1.9 ± 0.3	N/D
Female 4	46	4.3 ± 0.3	N/D
Male 1	20	3.7 ± 0.6	0.79
Male 2	22	4.0 ± 0.6	0.41
Male 3	24	2.3 ± 0.4	0.83
Male 4	25	5.7 ± 0.8	2.11
Male 5	26	1.8 ± 0.3	N/D
Male 6	26	1.4 ± 0.3	N/D
Male 7	27	1.3 ± 0.3	0.56
Male 8	27	3.4 ± 0.7	0.95
Male 9	28	4.6 ± 0.7	0.47
Male 10	28	1.5 ± 0.3	0.57
Male 11	33	3.2 ± 0.5	0.90
Male 12	34	17.2 ± 5.0	0.49
Male 13	45	2.4 ± 0.6	0.85
Male 14	50	3.0 ± 0.4	0.62
Male 15	52	9.9 ± 1.0	1.63

Radioenzymatic assay with [³H]NAAG was used to determined GCPII concentrations in heparin-treated plasma samples withdrawn from 19 healthy volunteers. The samples were measured in duplicate using different volumes (2.5 and 5 μl, or 5 and 10 μl) of added plasma in three separate experiments; values are presented as the mean ± standard deviation. PSA concentrations were determined at Thomayer Hospital in Prague. Recombinant extracellular GCPII (0.01–1 ng/ml) was used to construct a calibration curve of NAAG-hydrolyzing activity.

Both ProPGCPavi and aviPGCP possessed SerMet-hydrolyzing activity (Fig. 4A). The enzymes hydrolyzed SerMet in both buffers; however, they exhibited higher activity in the acetate buffer. The activity was sensitive to 25 mM EDTA but completely insensitive to 500 nM 2-PMPA, a GCPII-specific inhibitor (Fig. 4A).

Using a very sensitive radioenzymatic assay for quantification of NAAG-hydrolyzing activity, we did not observe any cleavage of NAAG, even when using 5 μg of ProPGCPavi or 3.3 μg of aviPGCP in a single reaction. For comparison, 5 pg of recombinant GCPII showed significant activity (Fig. 4B).

DISCUSSION

GCPII was identified as a potential target for imaging and therapy of prostate cancer 15 years ago [47,48]. However, the precise physiological role of the enzyme in the prostate and prostate cancer remains unknown. Although GCPII is considered a prostate cancer marker, there currently are no methods available that monitor GCPII levels to predict prostate
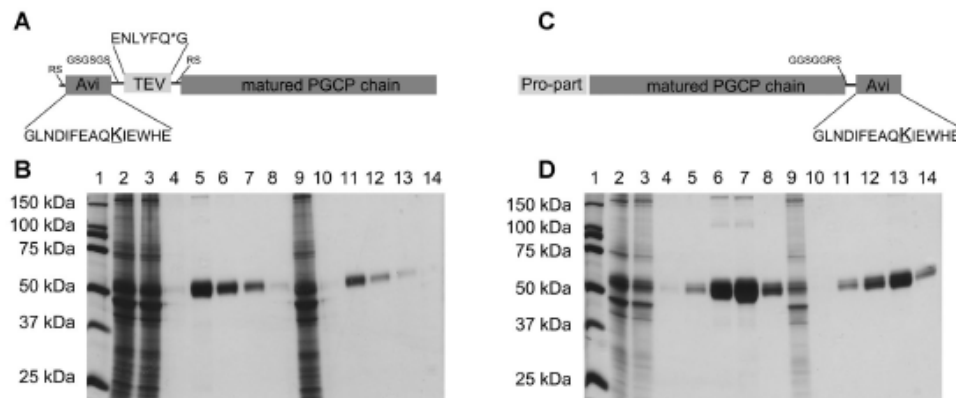
Fig. 3. Recombinant PGCP constructs and their purification. **Panels A,C**: Schematic representation of aviPGCP and ProPGCPavi, respectively. Avi—sequence of l5 amino acids recognized by biotin-protein ligase and biotinylated on the ε-amino group of the lysine residue (underlined); TEV—sequence of 7 amino acids specifically recognized by TEV protease (cleavage site is marked with an asterisk); Pro-part—endogenous propeptide sequence of PGCP. Spacer sequence and amino acids introduced during cloning are depicted in a smaller font size. Created according to Ref. [39]. **Panels B,D**: Analysis of purification of aviPGCP and ProPGCPavi, respectively. Proteins were expressed in *Drosophila* S2 cells, and equilibrated concentrated medium was mixed with Streptavidin Mutein Matrix and incubated overnight at 4°C. The resin with bound biotinylated proteins was separated on a gravity-flow column. The column was washed with Tris buffer, and proteins were eluted with an excess of biotin. Fractions from purification were separated by SDS-PAGE and analyzed by silver-staining. (I) All blue standards (Bio-Rad), recombinant extracellular GCPII (90 kDa); (2) Load; (3) Flow-through; (4) Wash; (5–8) Elutions I–4; (9) Flow-through; (I0) Wash; (II–I4) Elutions I–4. Purification of each protein was performed in two rounds; the first round is represented by lanes 3–8, the second by lanes 9–14. A half microliter of load, flow-through, and E2 and 5 μl of wash, EI, E3, and E4 were loaded onto the gel.

cancer progress. Quantitation of GCPII potentially present in human plasma might be a useful tool for predicting prostate cancer development and prognosis.

Moreover, cancer imaging using antibodies, inhibitors, and other structures, as well as specific drug delivery targeting GCPII, has made remarkable progress in recent years [18,25,49]. Attenuation of GCPII activity might also play an important role in the treatment of neurological disorders associated with excess glutamate [50]. The potential presence of GCPII in blood may compromise these approaches due to non-specific interaction of the ligands with the soluble enzyme circulating in the blood. However, in 2012 Denmeade et al. [51] described a PSMA prodrug that was not hydrolyzed upon prolonged incubation in human plasma. This observation suggests that GCPII concentration in plasma is low and does not suffice to significant hydrolysis of tested prodrugs.

After detecting NAAG-hydrolyzing activity in human blood plasma, we tested the possibility of inhibiting this activity with GCPII-specific inhibitors. We found out that the activity could be inhibited with all inhibitors tested, suggesting the presence of GCPII or its close homolog GCPIII (Fig. 1A). The activity was dependent upon the volume of added plasma but reached a plateau in larger volumes of added sample (Fig. 1B). This is probably caused by matrix effects, a phenomenon often observed when complex matrices such as blood samples are used.

Furthermore, we performed experiments to confirm the presence of GCPII in plasma. In our hands, Western blots yielded irreproducible results due to the very high background caused by the high protein concentrations in plasma samples. Therefore, we used immunoprecipitation for partial purification of the target antigen from a plasma sample. Using a biotinylated mouse monoclonal antibody raised against native GCPII (2G7), we were able to immunoprecipitate GCPII from human plasma samples (Fig. 2). The specificity of the GCPII detection was assured by two additional steps: after the immunoprecipitation, the elution fraction was analyzed with a second previously described anti-GCPII antibody GCP-04 and by mass spectrometry (a direct method of identification). Although the Western blot analysis of immunoprecipitated GCPII was not used for GCPII quantification in the blood, the quantity of immunoprecipitated GCPII roughly corresponded to that predicted by radioenzymatic assay. Mass spectrometry detected 18 different peptides covering 34% of the full-length GCPII sequence. One peptide corresponds to the first 16 amino

78
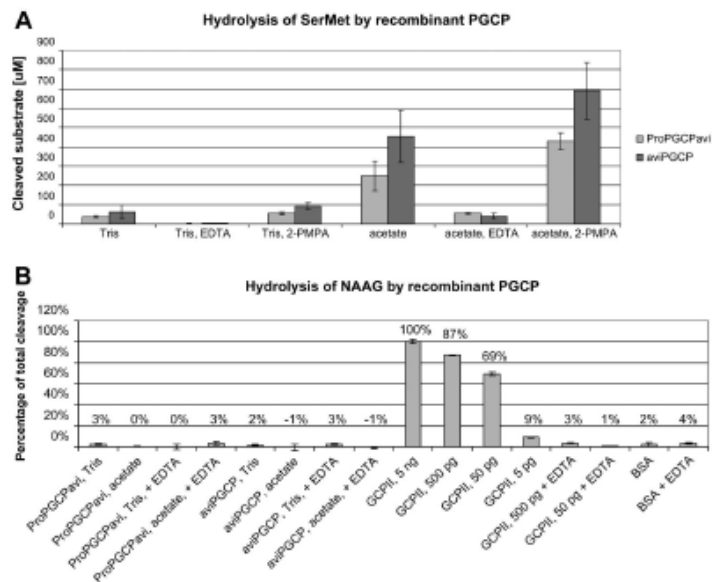
Fig. 4. Analysis of enzymatic activities of PGCP constructs. **Panel A**: SerMet-hydrolyzing activity of PGCP constructs was measured using an HPLC-based method with o-phthalaldehyde (OPA) derivatization. Measurements were performed in two different buffers: 100 mM Tris–HCl, 1 mM ZnCl₂, pH 7.5 (according to Gingras et al. [36]) and 100 mM sodium acetate, pH 5.5, including 15 mM zinc acetate (according to Zajc et al. [37]). The amount of ProPGCPavi and aviPGCP in the reaction was 30 ng. The activity of PGCP constructs was inhibited by 25 mM EDTA but not by 500 nM 2-PMPA. **Panel B**: The NAAG-hydrolyzing activity of PGCP constructs was determined using radioenzymatic assay with [³H]NAAG. The assay was performed in two different buffers: 100 mM Tris–HCl, pH 7.5, 1 mM ZnCl₂ (according to Gingras et al. [36]) and 100 mM sodium acetate, pH 5.5, including 15 mM zinc acetate (according to Zajc et al. [37]). The amounts of ProPGCPavi and aviPGCP used in the reactions were 5 μg and 3.3 μg, respectively. As the SerMet-hydrolyzing activity of PGCP constructs was inhibited with 25 mM EDTA, the same EDTA concentration was tested in this experimental setup as well. Recombinant GCPII (5 ng to 5 pg) was used as a positive control; GCPII activity was measured in 50 mM Tris–HCl, 150 mM NaCl, pH 7.4, 0.1% Tween-20 (TBST). BSA (5 μg) in TBST served as a negative control.

acids of the intracellular part of GCPII (MWNLLHETDSAVATAR), whereas all other peptides correspond to the extracellular domain of GCPII.

The source of the GCPII that we observed in plasma remains unclear. GCPII, as a transmembrane protein, may be partly shed from the cell surface by the action of an unknown protease, or it could be secreted into plasma in the form of a soluble protein lacking the intracellular and transmembrane regions. Several GCPII splice variants have been described; however, none of them is a secreted protein [52–54]. Lastly, GCPII could stem from an extraprostatic source, which could explain the activity in female plasma samples. We analyzed the immunoprecipitated GCPII by Western blot with the antibody GCP-04, which recognizes denatured GCPII. As shown in Figure 2, GCPII migrated at a molecular weight of about 120 kDa, corresponding to full-length, heavily glycosylated GCPII, rather than to a truncated form of the enzyme.

Importantly, we were not able to immunoprecipitate GCPII from plasma with unmodified antibodies including J591 (i.e., not biotinylated or not covalently bound to resin). This might have been caused by high concentrations of endogenous antibodies that blocked binding sites on Protein G Sepharose.

To identify how GCPII concentration in plasma varies within a healthy men and women of various ages, we took blood samples from 19 volunteers and determined GCPII concentrations in the samples using radioenzymatic assay. The GCPII concentration was in the range of 1.3–17.2 ng/ml; geometrical mean and non-symmetrical deviations were 3.2 ng/ml (+3.3; −1.6 ng/ml); for males: 3.7 ng/ml (+3.8; −1.9 ng/ml); for females: 2.0 ng/ml (+1.4; −0.8 ng/ml). We did not observe a correlation between GCPII concentration and the age of volunteers. The Pearson's correlation analysis showed no correlation between GCPII and PSA concentrations in plasma. It would be interesting

79

to analyze GCPII concentrations in the blood of prostate cancer patients to determine whether there is a correlation between the level of GCPII and prostate cancer stage.

Our quantitation of GCPII in plasma was based on a radioenzymatic assay making use of ability of GCPII to hydrolyze NAAG. This marks the first time that GCPII concentration in plasma has been determined by its enzymatic activity. Previously, GCPII was detected using antibody-based approaches, such as Western blot and SELDI immunoassay [27–32]. Using Western blot, GCPII was detected in the serum of normal men, men with benign prostate hyperplasia (BPH), and prostate cancer patients. The correlation between GCPII concentration and prostate cancer progress remains unclear. Some groups have revealed prognostic correlations in advanced prostate cancer [28], whereas others do not consider GCPII a good serum marker [31]. In the SELDI ProteinChip immunoassay study, significant differences were observed in the mean GCPII concentration between groups of men aged <50, aged >50, with BPH and with prostate cancer; nonetheless, GCPII concentration range was wide and overlapping in all groups [32]. They determined the concentration of GCPII in blood of normal males between 106.4 and 611.5 ng/ml, significantly higher than shown by our work [32]. Both studies showed GCPII concentration in blood of healthy males to be higher than the concentration of PSA.

The NAAG-hydrolyzing activity was inhibited with EDTA, a metallopeptidase inhibitor, as well as with other inhibitors specific to GCPII (Fig. 1A). On the other hand, the activity was not affected by "cOmplete Protease Inhibitor Cocktail, EDTA-free" (Roche; data not shown) suggesting that a metallocarboxypeptidase is responsible for the hydrolysis. To date, there are 27 reviewed metallocarboxypeptidases (EC 3.4.17.) found in humans according to the UniProt [55]. At the same time, only carboxypeptidase B2 (cleaving off C-terminal arginine or lysine residues from biologically active peptides) and PGCP were detected in the blood plasma. NAAG-hydrolyzing activity has been described only for GCPII, its homolog GCPIII, and PGCP. Therefore, only three known enzymes, GCPII, GCPIII, and PGCP can be, in principle, responsible for the observed NAAG-hydrolyzing activity in the plasma samples.

Using the specific substrate of GCPIII, ß-citryl-L-glutamate (BCG) [56], we found out that GCPIII does not contribute to NAAG-hydrolyzing activity. Since the observed BCG-hydrolyzing activity was minimal, we cannot quite exclude the presence of GCPIII in plasma; however, if present, its concentration would be at least 50-fold lower that GCPII (data not shown).

In 1999, Gingras et al. [36] described PGCP, a plasmatic zinc metallopeptidase reportedly possessing the same enzymatic activity as GCPII. PGCP belongs to the MEROPS peptidase family M28 and is a distant homolog of GCPII, sharing 25% amino acid sequence similarity. We prepared two PGCP constructs and expressed them in *Drosophila* S2 cells. Both constructs have an Avi-tag sequence, enabling fast, efficient, and simple purification that makes use of the interaction between the biotinylated Avi-tag and Streptavidin Mutein Matrix [39]. Avi-tag was placed either at the N-terminus of the mature PGCP chain (aviPGCP) or at the C-terminus of the mature PGCP chain, preserving the enzyme's endogenous propeptide part at the N-terminus (ProPGCPavi). PGCP forms enzymatically active dimers, whereas monomers do not possess any enzymatic activity [37]. Removal of the propeptide part is a necessary step for dimer creation, and it is believed to be performed by a protease present in cell medium [37,57]. ProPGCPavi and aviPGCP were purified by affinity chromatography; on SDS-PAGE, we observed a double band for both constructs. The origin of the double band can be explained by cleavage within the sequence of the purified proteins. In the case of aviPGCP, a cleavage similar to that reported within the N-terminal part of purified aviGCPII [39] may have taken place, whereas in the case of ProPGC-Pavi, removal of the propeptide was observed [37].

To confirm that we purified active and properly folded PGCP constructs, we probed them with a cognate substrate of PGCP, the dipeptide SerMet. Because the activity of PGCP had previously been determined in two different buffers, we performed our assay in both of buffers: 100 mM Tris–HCl, 1 mM $ZnCl_2$, pH 7.5 (according to Gingras et al. [36]), and 100 mM sodium acetate, pH 5.5, including 15 mM zinc acetate (according to Zajc et al. [37]). Both PGCP preparations hydrolyzed SerMet; aviPGCP exhibited higher activity than ProPGCPavi, which was in agreement with our assumption than only a fraction of ProPGCPavi might have been activated by removal of the propeptide. The activity of both constructs was higher in the acetate buffer; however, prolonging the incubation time or using larger amounts of enzyme led to total conversion in both buffers. The activity was sensitive to EDTA, a metalloprotease inhibitor, but not sensitive to 2-PMPA, a GCPII-specific inhibitor (Fig. 4A).

Because we used NAAG-hydrolyzing activity for GCPII quantification and because PGCP has been reported to possess this activity as well, we probed the PGCP preparations with a cognate substrate of GCPII, the dipeptide NAAG. The determination was performed in the Tris and acetate buffers described above. We did not detect any NAAG-hydrolyzing activity

80

with either PGCP construct, even when high PGCP concentrations were used (Fig. 4B). When compared with recombinant PGCP, a 500,000-fold lower amount of GCPII exhibited significant NAAG-hydrolyzing activity. This result is in direct contradiction to the results previously published by Gingras et al. [36] who purified PGCP from human plasma and placenta and showed that it cleaved NAAG. This discrepancy might be caused by co-purification of GCPII together with PGCP in Gingras' experiment.

In fact, PGCP is the only glutamate carboxypeptidase found in plasma that has ever been shown to exhibit NAAG-hydrolyzing activity, and the inhibitors we used have been previously shown to be very specific for GCPII/GCPIII. The combination of specific immunochemical detection, specific substrate cleavage, specific inhibitory profile, and detection by LC–MS provides, in our opinion, very strong evidence for our conclusion that GCPII is the proteolytic agent responsible for the NAAG hydrolysis in the blood.

The analysis of the clinical relevation of GCPII in plasma and prostate cancer progression will be the focus of further studies.

CONCLUSIONS

We have conclusively shown that GCPII is present in the blood plasma of people not diagnosed with prostate cancer in concentrations between 1.3 and 17.2 ng/ml. The origin, form, and possible function of GCPII in plasma remain unknown and are under further investigation. The concentration of GCPII in plasma likely cannot profoundly influence targeting of imaging probes or drugs using specific anti-GCPII ligands to prostate cancer cells. PGCP, which belongs to the same peptidase family as GCPII, in our hands possesses SerMet-hydrolyzing activity but not NAAG-hydrolyzing activity, and therefore does not contribute to the NAAG-hydrolyzing activity observed in human plasma.

ACKNOWLEDGMENTS

REFERENCES

1. Siegel R, Ma J, Zou Z, Jemal A. Cancer statistics, 2014. CA Cancer J Clin 2014;64:9–29.
2. Israeli RS, Powell CT, Fair WR, Heston WD. Molecular cloning of a complementary DNA encoding a prostate-specific membrane antigen. Cancer Res 1993;53:227–230.
3. Horoszewicz JS, Kawinski E, Murphy GP. Monoclonal antibodies to a new antigenic marker in epithelial prostatic cells and serum of prostatic cancer patients. Anticancer Res 1987;7:927–935.
4. Robinson MB, Blakely RD, Couto R, Coyle JT. Hydrolysis of the brain dipeptide N-acetyl-L-aspartyl-L-glutamate. Identification and characterization of a novel N-acetylated alpha-linked acidic dipeptidase activity from rat brain. J Biol Chem 1987;262:14498–14506.
5. Sokoloff RL, Norton KC, Gasior CL, Marker KM, Grauer LS. A dual-monoclonal sandwich assay for prostate-specific membrane antigen: Levels in tissues, seminal fluid and urine. Prostate 2000;43:150–157.
6. Rovenska M, Hlouchova K, Sacha P, Mlcochova P, Horak V, Zamecnik J, Barinka C, Konvalinka J. Tissue expression and enzymologic characterization of human prostate specific membrane antigen and its rat and pig orthologs. Prostate 2008;68:171–182.
7. Kinoshita Y, Kuratsukuri K, Landas S, Imaida K, Rovito PM Jr, Wang CY, Haas GP. Expression of prostate-specific membrane antigen in normal and malignant human tissues. World J Surg 2006;30:628–636.
8. Cunha AC, Weigle B, Kiessling A, Bachmann M, Rieber EP. Tissue-specificity of prostate specific antigens: Comparative analysis of transcript levels in prostate and non-prostatic tissues. Cancer Lett 2006;236:229–238.
9. Chandler CJ, Wang TT, Halsted CH. Pteroylpolyglutamate hydrolase from human jejunal brush borders. Purification and characterization. J Biol Chem 1986;261:928–933.
10. Liu H, Rajasekaran AK, Moy P, Xia Y, Kim S, Navarro V, Rahmati R, Bander NH. Constitutive and antibody-induced internalization of prostate-specific membrane antigen. Cancer Res 1998;58:4055–4060.
11. Conway RE, Joiner K, Patterson A, Bourgeois D, Rampp R, Hannah BC, McReynolds S, Elder JM, Gilfilen H, Shapiro LH. Prostate specific membrane antigen produces pro-angiogenic laminin peptides downstream of matrix metalloprotease-2. Angiogenesis 2013;16:847–860.
12. Conway RE, Petrovic N, Li Z, Heston W, Wu D, Shapiro LH. Prostate-specific membrane antigen regulates angiogenesis by modulating integrin signal transduction. Mol Cell Biol 2006;26:5310–5324.
13. Divyya S, Naushad SM, Murthy PV, Reddy Ch R, Kutala VK. GCPII modulates oxidative stress and prostate cancer susceptibility through changes in methylation of RASSF1, BNIP3, GSTP1 and Ec-SOD. Mol Biol Rep 2013;40:5541–5550.
14. Zhang Y, Guo Z, Du T, Chen J, Wang W, Xu K, Lin T, Huang H. Prostate specific membrane antigen (PSMA): A novel modulator

of p38 for proliferation, migration, and survival in prostate cancer cells. Prostate 2013;73:835–841.

15. Lapidus RG, Tiffany CW, Isaacs JT, Slusher BS. Prostate-specific membrane antigen (PSMA) enzyme activity is elevated in prostate cancer cells. Prostate 2000;45:350–354.

16. Kahn D, Williams RD, Seldin DW, Libertino JA, Hirschhorn M, Dreicer R, Weiner GJ, Bushnell D, Gulfo J. Radioimmunoscintigraphy with 111indium labeled CYT-356 for the detection of occult prostate cancer recurrence. J Urol 1994;152:1490–1495.

17. Bander NH, Milowsky MI, Nanus DM, Kostakoglu L, Vallabhajosula S, Goldsmith SJ. Phase I trial of 177lutetium-labeled J591, a monoclonal antibody to prostate-specific membrane antigen, in patients with androgen-independent prostate cancer. J Clin Oncol 2005;23:4591–4601.

18. Liu T, Nedrow-Byers JR, Hopkins MR, Wu LY, Lee J, Reilly PT, Berkman CE. Targeting prostate cancer cells with a multivalent PSMA inhibitor-guided streptavidin conjugate. Bioorg Med Chem Lett 2012;22:3931–3934.

19. Chen Z, Penet MF, Nimmagadda S, Li C, Banerjee SR, Winnard PT Jr, Artemov D, Glunde K, Pomper MG, Bhujwalla ZM. PSMA-targeted theranostic nanoplex for prostate cancer therapy. ACS Nano 2012;6:7752–7762.

20. Taneja SS. ProstaScint(R) scan: Contemporary use in clinical practice. Rev Urol 2004;6 (Suppl 10): S19–S28.

21. Troyer JK, Feng Q, Beckett ML, Wright GL Jr. Biochemical characterization and mapping of the 7 E11-C5. 3 epitope of the prostate-specific membrane antigen. Urol Oncol 1995;1:29–37.

22. Bander NH, Trabulsi EJ, Kostakoglu L, Yao D, Vallabhajosula S, Smith-Jones P, Joyce MA, Milowsky M, Nanus DM, Goldsmith SJ. Targeting metastatic prostate cancer with radiolabeled monoclonal antibody J591 to the extracellular domain of prostate specific membrane antigen. J Urol 2003;170:1717–1721.

23. Frigerio B, Fracasso G, Luison E, Cingarlini S, Mortarino M, Coliva A, Seregni E, Bombardieri E, Zuccolotto G, Rosato A, Colombatti M, Canevari S, Figini M. A single-chain fragment against prostate specific membrane antigen as a tool to build theranostic reagents for prostate cancer. Eur J Cancer 2013;49:2223–2232.

24. Fracasso G, Bellisola G, Cingarlini S, Castelletti D, Prayer-Galetti T, Pagano F, Tridente G, Colombatti M. Anti-tumor effects of toxins targeted to the prostate specific membrane antigen. Prostate 2002;53:9–23.

25. Tagawa ST, Akhtar NH, Nikolopoulou A, Kaur G, Robinson B, Kahn R, Vallabhajosula S, Goldsmith SJ, Nanus DM, Bander NH. Bone marrow recovery and subsequent chemotherapy following radiolabeled anti-prostate-specific membrane antigen monoclonal antibody j591 in men with metastatic castration-resistant prostate cancer. Front Oncol 2013;3:214.

26. Akhtar NH, Pail O, Saran A, Tyrell L, Tagawa ST. Prostate-specific membrane antigen-based therapeutics. Adv Urol 2012;2012:973820.

27. Rochon YP, Horoszewicz JS, Boynton AL, Holmes EH, Barren RJ III, Erickson SJ, Kenny GM, Murphy GP. Western blot assay for prostate-specific membrane antigen in serum of prostate cancer patients. Prostate 1994;25:219–223.

28. Murphy GP, Kenny GM, Ragde H, Wolfert RL, Boynton AL, Holmes EH, Misrock SL, Bartsch G, Klocker H, Pointner J, Reissigl A, McLeod DG, Douglas T, Morgan T, Gilbaugh J. Measurement of serum prostate-specific membrane antigen, a new prognostic marker for prostate cancer. Urology 1998;51:89–97.

29. Murphy GP, Maguire RT, Rogers B, Partin AW, Nelp WB, Troychak MJ, Ragde H, Kenny GM, Barren RJ III, Bowes VA, Gregorakis AK, Holmes EH, Boynton AL. Comparison of serum PSMA, PSA levels with results of Cytogen-356 ProstaScint scanning in prostatic cancer patients. Prostate 1997;33:281–285.

30. Troyer JK, Beckett ML, Wright GL. Detection and characterization of the prostate-specific membrane antigen (Pmsa) in tissue-extracts and body-fluids. Int J Cancer 1995;62:552–558.

31. Beckett ML, Cazares LH, Vlahou A, Schellhammer PF, Wright GL. Prostate-specific membrane antigen levels in sera from healthy men and patients with benign prostate hyperplasia or prostate cancer. Clin Cancer Res 1999;5:4034–4040.

32. Xiao Z, Adam BL, Cazares LH, Clements MA, Davis JW, Schellhammer PF, Dalmasso EA, Wright GL Jr. Quantitation of serum prostate-specific membrane antigen by a novel protein biochip immunoassay discriminates benign from malignant prostate disease. Cancer Res 2001;61:6029–6033.

33. Catalona WJ, Richie JP, Ahmann FR, Hudson MA, Scardino PT, Flanigan RC, deKernion JB, Ratliff TL, Kavoussi LR, Dalkin BL, Waters WB, Macfarlane MT, Southwick PC. Comparison of digital rectal examination and serum prostate specific antigen in the early detection of prostate cancer: Results of a multicenter clinical trial of 6,630 men. J Urol 1994;151:1283–1290.

34. Nadler RB, Humphrey PA, Smith DS, Catalona WJ, Ratliff TL. Effect of inflammation and benign prostatic hyperplasia on elevated serum prostate specific antigen levels. J Urol 1995;154:407–413.

35. Moyer VA. Screening for prostate cancer: U.S. Preventive Services Task Force recommendation statement. Ann Intern Med 2012;157:120–134.

36. Gingras R, Richard C, El-Alfy M, Morales CR, Potier M, Pshezhetsky AV. Purification, cDNA cloning, and expression of a new human blood plasma glutamate carboxypeptidase homologous to N-acetyl-aspartyl-alpha-glutamate carboxypeptidase/prostate-specific membrane antigen. J Biol Chem 1999;274:11742–11750.

37. Zajc T, Suban D, Rajkovic J, Dolenc I. Baculoviral expression and characterization of human recombinant PGCP in the form of an active mature dimer and an inactive precursor protein. Protein Expr Purif 2011;75:119–126.

38. Hlouchova K, Barinka C, Klusak V, Sacha P, Mlcochova P, Majer P, Rulisek L, Konvalinka J. Biochemical characterization of human glutamate carboxypeptidase III. J Neurochem 2007;101:682–696.

39. Tykvart J, Sacha P, Barinka C, Knedlik T, Starkova J, Lubkowski J, Konvalinka J. Efficient and versatile one-step affinity purification of in vivo biotinylated proteins: Expression, characterization and structure analysis of recombinant human glutamate carboxypeptidase II. Protein Expr Purif 2012;82:106–115.

40. Barinka C, Rinnova M, Sacha P, Rojas C, Majer P, Slusher BS, Konvalinka J. Substrate specificity, inhibition and enzymological analysis of recombinant human glutamate carboxypeptidase II. J Neurochem 2002;80:477–487.

41. Sacha P, Zamecnik J, Barinka C, Hlouchova K, Vicha A, Mlcochova P, Hilgert I, Eckschlager T, Konvalinka J. Expression of glutamate carboxypeptidase II in human brain. Neuroscience 2007;144:1361–1372.

42. Beckett D, Kovaleva E, Schatz PJ. A minimal peptide substrate in biotin holoenzyme synthetase-catalyzed biotinylation. Protein Sci 1999;8:921–929.

82

43. Kapust RB, Waugh DS. Controlled intracellular processing of fusion proteins by TEV protease. Protein Expr Purif 2000;19: 312–318.

44. Woodward C, Henderson JW Jr. High-speed amino acid analysis (AAA) on 1.8 μm reversed-phase (RP) columns. Wilmington, DE, USA: Agilent Technologies; 2007.

45. Heidenreich PJB, Bellmunt J, Bolla M, Joniau S, Mason MD, Matveev V, Mottet N, van der Kwast TH, Wiegel T, Zattoni F. editors. Guidelines on Prostate Cancer: European Association of Urology, Arnhem 2012.

46. Dolenc I, Mihelic M. Purification and primary structure determination of human lysosomal dipeptidase. Biol Chem 2003;384: 317–320.

47. Foss CA, Mease RC, Cho SY, Kim HJ, Pomper MG. GCPII imaging and cancer. Curr Med Chem 2012;19:1346–1359.

48. Chang SS. Overview of prostate-specific membrane antigen. Rev Urol 2004;6 (Suppl 10): S13–S18.

49. Wu X, Ding B, Gao J, Wang H, Fan W, Wang X, Zhang W, Ye L, Zhang M, Ding X, Liu J, Zhu Q, Gao S. Second-generation aptamer-conjugated PSMA-targeted delivery system for prostate cancer therapy. Int J Nanomed 2011;6:1747–1756.

50. Rahn KA, Watkins CC, Alt J, Rais R, Stathis M, Grishkan I, Crainiceau CM, Pomper MG, Rojas C, Pletnikov MV, Calabresi PA, Brandt J, Barker PB, Slusher BS, Kaplin AI. Inhibition of glutamate carboxypeptidase II (GCPII) activity as a treatment for cognitive impairment in multiple sclerosis. Proc Natl Acad Sci USA 2012;109:20101–20106.

51. Denmeade SR, Mhaka AM, Rosen DM, Brennen WN, Dalrymple S, Dach I, Olesen C, Gurel B, Demarzo AM, Wilding G, Carducci MA, Dionne CA, Moller JV, Nissen P, Christensen SB, Isaacs JT. Engineering a prostate-specific membrane antigen-activated tumor endothelial cell prodrug for cancer therapy. Sci Transl Med 2012;4:140ra186.

52. Schmittgen TD, Teske S, Vessella RL, True LD, Zakrajsek BA. Expression of prostate specific membrane antigen and three alternatively spliced variants of PSMA in prostate cancer patients. Int J Cancer 2003;107:323–329.

53. Cao KY, Mao XP, Wang DH, Xu L, Yuan GQ, Dai SQ, Zheng BJ, Qiu SP. High expression of PSM-E correlated with tumor grade in prostate cancer: A new alternatively spliced variant of prostate-specific membrane antigen. Prostate 2007;67:1791–1800.

54. Su SL, Huang IP, Fair WR, Powell CT, Heston WD. Alternatively spliced variants of prostate-specific membrane antigen RNA: Ratio of expression as a potential measurement of progression. Cancer Res 1995;55:1441–1443.

55. http://www.uniprot.org/uniprot/?query=ec%3A3.4.17.-+reviewed%3Ayes+AND+organism%3A%22Human+[9606]%22&sort=score; searched January 31, 2014.

56. Collard F, Vertommen D, Constantinescu S, Buts I, Van Schaftingen E. Molecular identification of beta-citrylglutamate hydrolase as glutamate carboxypeptidase 3. J Biol Chem 2011; 286:38220–38230.

57. Bromme D, Nallaseth FS, Turk B. Production and activation of recombinant papain-like cysteine proteases. Methods 2004;32: 199–206.

83

7.2. Paper II

Tomáš Knedlík, Barbora Vorlová, Václav Navrátil, Jan Tykvart, František Sedlák, Šimon Vaculín, Miloslav Franěk, Pavel Šácha and Jan Konvalinka

Mouse glutamate carboxypeptidase II (GCPII) has a similar enzyme activity and inhibition profile but a different tissue distribution to human GCPII.

Mouse glutamate carboxypeptidase II (GCPII) has a similar enzyme activity and inhibition profile but a different tissue distribution to human GCPII

Tomáš Knedlík[1,2], Barbora Vorlová[1,3], Václav Navrátil[1,2], Jan Tykvart[1,2,†], František Sedlák[1,3,4], Šimon Vaculín[5], Miloslav Franěk[5], Pavel Šácha[1] and Jan Konvalinka[1,2]

1 Institute of Organic Chemistry and Biochemistry of the Czech Academy of Sciences, Prague, Czech Republic
2 Department of Biochemistry, Faculty of Science, Charles University, Prague, Czech Republic
3 First Faculty of Medicine, Charles University, Prague, Czech Republic
4 Department of Genetics and Microbiology, Faculty of Science, Charles University, Prague, Czech Republic
5 Department of Normal, Pathological and Clinical Physiology, Third Faculty of Medicine, Charles University, Prague, Czech Republic

Glutamate carboxypeptidase II (GCPII), also known as prostate-specific membrane antigen (PSMA) or folate hydrolase, is a metallopeptidase expressed predominantly in the human brain and prostate. GCPII expression is considerably increased in prostate carcinoma, and the enzyme also participates in glutamate excitotoxicity in the brain. Therefore, GCPII represents an important diagnostic marker of prostate cancer progression and a putative target for the treatment of both prostate cancer and neuronal disorders associated with glutamate excitotoxicity. For the development of novel therapeutics, mouse models are widely used. However, although mouse GCPII activity has been characterized, a detailed comparison of the enzymatic activity and tissue distribution of the mouse and human GCPII orthologs remains lacking. In this study, we prepared extracellular mouse GCPII and compared it with human GCPII. We found that mouse GCPII possesses lower catalytic efficiency but similar substrate specificity compared with the human protein. Using a panel of GCPII inhibitors, we discovered that inhibition constants are generally similar for mouse and human GCPII. Furthermore, we observed highest expression of GCPII protein in the mouse kidney, brain, and salivary glands. Importantly, we did not detect GCPII in the mouse prostate. Our data suggest that the differences in enzymatic activity and inhibition profile are rather small; therefore, mouse GCPII can approximate human GCPII in drug development and testing. On the other hand, significant differences in GCPII tissue expression must be taken into account when developing novel GCPII-based anticancer and therapeutic methods, including targeted anticancer drug delivery systems, and when using mice as a model organism.

Glutamate carboxypeptidase II (GCPII; EC 3.4.17.21) is a membrane metalloprotease that has been studied intensively over the past 20 years in three different scientific fields: neuroscience, prostate oncology, and dietology. In humans, GCPII is expressed predominantly in the brain [1,2], prostate [3,4], small intestine

[5], and kidney [4,6]. Because GCPII plays different physiological roles in these tissues, three alternative names for the enzyme have historically been used: *N*-acetylated alpha-linked acidic dipeptidase (NAALA-Dase) [7], prostate-specific membrane antigen (PSMA) [8], and folate hydrolase [5]. The close GCPII homolog GCPIII [9,10], recently identified as β-citryl-glutamate hydrolase [11], is also expressed in human tissues.

In the human central nervous system, GCPII hydrolyzes the most abundant peptide neurotransmitter, *N*-acetyl-L-aspartyl-L-glutamate (NAAG), into *N*-acetyl-L-aspartate and glutamate [7]. Inhibition of this proteolytic activity with selective GCPII inhibitors has been shown to be neuroprotective in experiments with mouse models [12]; NAAG activation of metabotropic glutamate type 3 receptors exerts neuroprotective effects toward glutamate-mediated excitotoxicity caused by elevated levels of glutamate released during stroke, traumatic brain injury, and other pathological conditions [13–15]. In addition to the brain, GCPII is expressed on the human jejunal brush border [5,16], where it cleaves the terminal glutamates from poly-γ-glutamylated folates, enabling their transport across the intestinal mucosa (folate absorption) [17]. On the other hand, the function of GCPII in the human prostate is unknown. GCPII is overexpressed in prostate cancer [3,18]; therefore, it has been suggested as a promising target for prostate cancer diagnosis and treatment using targeted strategies [19–21].

An appropriate animal model is necessary for the development and testing of novel therapeutics. Mice, rats, and pigs are among the most promising candidates to become such a model for GCPII research. Several years ago, our laboratory conducted a study comparing human GCPII with its porcine and rat orthologs [22]. The orthologs showed similarity in their enzymatic properties, but considerable differences in terms of their tissue distribution [22]. However, mouse GCPII was not included in the study, even though mice now are the most widely used preclinical models for GCPII-targeted research (stroke [12], traumatic brain injury [23,24], amyotrophic lateral sclerosis [25], inflammatory, and neuropathic pain [26,27], reviewed in Refs [13,28]). Therefore, a comparative analysis of mouse GCPII characterization is needed.

Mouse GCPII shares 91% amino acid similarity with human GCPII and preserves the internalization signal MXXXL, despite low similarity in the intracellular domain [29]. Mouse GCPII also possesses both NAAG-hydrolyzing and folate hydrolase activities [29]. In contrast to the expression pattern of human GCPII, mouse GCPII is expressed in largest amounts in the kidney and, surprisingly, is absent in the mouse

prostate [29]. Results from studies with GCPII-knockout mice have been contradictory: some reports have described normal development to adulthood [9,30] and others have noted early embryonic death [31,32].

In the current study, we prepared and characterized recombinant mouse GCPII and compared it with its human counterpart. We put a strong focus on distribution of GCPII in mouse tissues, as this information is highly relevant for the development of novel GCPII-based anticancer and neuroprotective therapies using mouse models.

Results

### Efficient one-step purification method yields purified recombinant mouse GCPII (Avi-mGCPII)

As recombinant extracellular human GCPII was shown to correctly represent the endogenous full-length GCPII [33,34], we prepared the recombinant extracellular part of mouse GCPII (Avi-mGCPII) using a *Drosophila* S2 expression system, according to the protocol previously established in our laboratory [34]. Avi-mGCPII has a TEV cleavable Avi-tag sequence attached to the N terminus of the mouse GCPII extracellular domain (amino acids 45–752), enabling fast one-step purification (Fig. 1A).

Avi-mGCPII was purified from the conditioned medium of cells stably transfected with Avi-mGCPII by affinity chromatography based on the biotin–streptavidin interaction [34], yielding 3 mg of pure protein from 1 L conditioned medium (Fig. 1B).

Mouse GCPII has lower catalytic efficiency than human GCPII

To characterize the enzyme activity of Avi-mGCPII, we determined kinetic parameters (K_M and k_{cat}) for cleavage of both substrates: *N*-acetyl-L-aspartyl-L-glutamate (NAAG) and pteroyl-di-L-glutamate (Table 1). The data revealed that the catalytic efficiency of Avi-mGCPII is lower than that of its human counterpart. The enzymes had similar turnover numbers but differed in their K_M values. The differences were more pronounced for pteroyl-di-L-glutamate than for NAAG. Surprisingly, both enzymes had higher catalytic efficiencies for cleavage of pteroyl-di-L-glutamate than for NAAG (Table 1).

Furthermore, to analyze the inhibition profile of Avi-mGCPII, we determined K_i values for several commonly used GCPII inhibitors (using pteroyl-di-L-glutamate as a substrate). The set of GCPII inhibitors included 2-(phosphonomethyl)pentanedioic acid

86
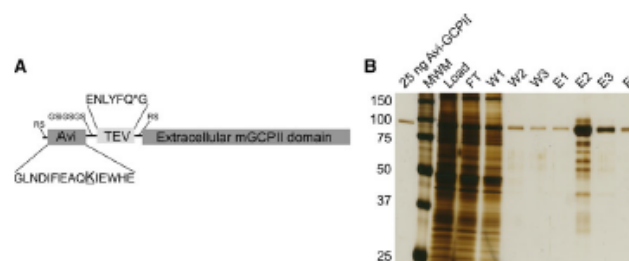
Fig. 1. Schematic structure of Avi-mGCPII and affinity purification. (A) Schematic structure of Avi-mGCPII containing an Avi sequence (the biotinylated lysine residue is enlarged and underlined) and TEV protease cleavage sequence (the cleavage site is marked with an asterisk). (B) Silver-stained SDS/PAGE gel showing affinity purification of Avi-mGCPII expressed in *Drosophila* S2 cells. MWM, molecular weight marker; load, concentrated S2 cell medium; FT, flow-through; W1–W3, wash fractions; E1–E4, elution fractions. Ten microliter samples was loaded onto the gel, except for the E2 fraction (1 µL was loaded).

Table 1. Kinetic parameters of recombinant mouse and human GCPII (Avi-mGCPII and Avi-hGCPII, respectively) for their substrates. Kinetic parameters (K_M and k_{cat}) of *N*-acetyl-ʟ-aspartyl-ʟ-glutamate (NAAG) and pteroyl-di-ʟ-glutamate cleavage were determined using radioenzymatic [34] and HPLC assays [39], respectively. The values shown are mean ± standard deviation of duplicate measurements.

Enzymes	NAAG			Pteroyl-di-ʟ-glutamate		
	K_M [nM]	k_{cat} [s^{-1}]	k_{cat}/K_M [× 10^7 s^{-1} M]	K_M [nM]	k_{cat} [s^{-1}]	k_{cat}/K_M [× 10^7 s^{-1} M]
Avi-mGCPII	1900 ± 100	1.44 ± 0.02	0.077 ± 0.001	290 ± 20	3.63 ± 0.09	1.26 ± 0.08
Avi-hGCPII	550 ± 60	1.45 ± 0.04	0.265 ± 0.007	39 ± 2	5.09 ± 0.09	13.2 ± 0.8

(2-PMPA) [35], (S)-2-(3-((S)-1-carboxy-3-methylbutyl)ureido)pentanedioic acid (ZJ-43) [36], (S)-2-(3-((S)-1-carboxy-(4-iodobenzamido)pentyl)ureido)pentanedioic acid (DCIBzL) [37], quisqualate, DKFZ-PSMA-11 [38], and beta-citryl-ʟ-glutamate (Table 2). We also tested three compounds recently prepared in our laboratory: JB-352 and JB-277 (originally reported as compounds **3** and **22a** [39]) and JS-686 (originally compound **7** [40]).

Mouse and human GCPII exhibit similar substrate specificities

To obtain information about the substrate specificity of Avi-mGCPII, we screened 19 different dipeptide libraries of the general formula *N*-Ac-A-X [where A represents a given single N-terminal amino acid and X represents a mixture of 19 proteinogenic amino acids (all except for cysteine)]. The *N*-acetylated dipeptide libraries were incubated with the enzymes, and the cleaved amino acids were analyzed by HPLC [41]. As a negative control, the potent and selective GCPII inhibitor 2-PMPA was used to block the specific enzyme activity.

Overall, we found no significant differences in hydrolysis of dipeptide substrates between mouse and

human GCPII, as illustrated by heat maps showing mouse and human GCPII processing of individual *N*-acetylated dipeptides (Fig. 2). The enzymes exhibited a clear preference for glutamate in the C-terminal position (i.e., glutamate carboxypeptidase activity); mouse GCPII possesses higher selectivity toward the C-terminal glutamate.

GCPII is highly expressed in mouse kidney, brain, and major salivary glands

To analyze GCPII distribution in mouse tissues, we collected tissues samples from six mice (three females and three males) and analyzed them by western blot using the anti-GCPII antibody GCP-04 [2,42].

Mouse GCPII was expressed predominantly in the mouse kidney and brain (Fig. 3), which is in agreement with previous data [9]. Interestingly, we observed high and variable expression in the mouse major salivary glands. The different apparent molecular weights are likely caused by different glycosylation of GCPII in the tissues.

We also determined the NAAG-hydrolyzing activity in the tissue lysate samples using tritium-labeled NAAG as a substrate and compared these results with

Table 2. Inhibition of recombinant mouse and human GCPII (Avi-mGCPII and Avi-hGCPII, respectively) by a panel of GCPII inhibitors. Inhibition constants (K_i values) were determined using an HPLC-based assay using pteroyl-di-L-glutamate as a substrate. The values shown are mean ± standard deviation of duplicate measurements.

Compound	K_i (Avi-mGCPII) (nM)	K_i (Avi-hGCPII) (nM)
Quisqualate	580 ± 60	520 ± 80
2-PMPA	0.56 ± 0.05	0.26 ± 0.03
ZJ-43	5.9 ± 0.9	0.58 ± 0.07
JB-352	0.66 ± 0.06	0.17 ± 0.04
β-citryl-L-glutamate	24 000 ± 3000	16 000 ± 5000
DCIBzL	0.028 ± 0.003	0.017 ± 0.002
JB-277	0.68 ± 0.07	0.05 ± 0.02
DKFZ-PSMA-11	0.10 ± 0.01	0.018 ± 0.002
JS-686	0.049 ± 0.005	0.021 ± 0.004

the data obtained by western blot analysis. Recombinant mouse GCPII was used as a standard, and the observed levels of NAAG-hydrolyzing activity were converted to amounts of GCPII, which were then normalized to the total protein concentrations in the homogenates (Fig. 4).

88
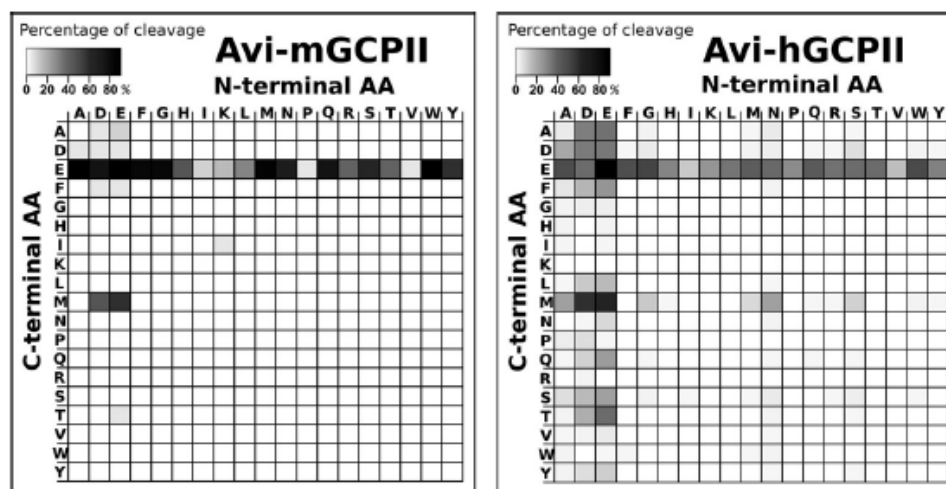
Fig. 2. Heat maps representing the substrate specificities of mouse and human GCPII. Recombinant mouse and human GCPII (Avi-mGCPII and Avi-hGCPII, respectively) were incubated with 19 dipeptide libraries of the general formula *N*-Ac-A-X-OH [where A represents a given single N-terminal amino acid and X represents a mixture of 19 proteinogenic amino acids (all except for cysteine)]. The samples were incubated for 1.5 h at 37 °C, and the cleaved C-terminal amino acids were quantified using HPLC. As negative controls, experiments either with the GCPII-specific inhibitor 2-PMPA or without Avi-mGCPII/Avi-hGCPII were performed. The grayscale key represents the percentage of conversion of the particular amino acid in the reaction mixture.

The results confirmed high expression of GCPII in the kidney, brain, and major salivary glands. We did not detect GCPII in the mouse prostate (Fig. 4).

To further examine the location of GCPII in the highly expressing tissues, we performed immunohistochemistry using the anti-GCPII antibody GCP-04 [2,42]. We found relatively high expression in the white matter in the brain, on luminal side of proximal tubules in the kidney and in the abluminal cells in the major salivary glands (mainly in the sublingual gland) (Fig. 5).

mRNA expression profile differentiates GCPII and GCPIII expression levels in mouse tissues

The GCP-04 antibody cross-reacts with GCPIII, which also cleaves NAAG [11,43]. Therefore, we decided to further analyze the tissue distribution of both homologs by quantitative RNA determination (qPCR). For these analyses, we used either commercially available panels of mouse tissue cDNA libraries (Fig. 6A) or cDNA libraries prepared from mouse tissues (female 1 and male 1; Fig. 6B,C).

The results from commercial cDNA libraries represent the average tissue distribution of both transcripts in the mouse population. Each library was pooled from several hundred mice and normalized by the vendor to several different housekeeping genes (beta-actin, G3PDH, phospholipase A2, and ribosomal protein S29). The highest expression of mouse GCPII mRNA was in the kidney, brain, and testis, while mouse GCPIII mRNA was predominantly expressed in the testis, heart, lung, and skeletal muscle (Fig. 6A).

To gain insight into expression of both transcripts in individual mice, we also quantified mRNA transcripts in cDNA libraries prepared from mouse tissues dissected from one female and one male mouse. The results were normalized to the starting amount of total RNA and are in good agreement with findings from the pooled libraries (Fig. 6B,C).

Discussion

GCPII is a potential pharmaceutical target for a number of pathological conditions caused by glutamate excitotoxicity in the central nervous system, including stroke and traumatic brain injury. Moreover, GCPII has been intensively studied as a target for diagnosis and treatment of prostate cancer, as it is overexpressed in the malignant prostate. In last two decades, a large

89
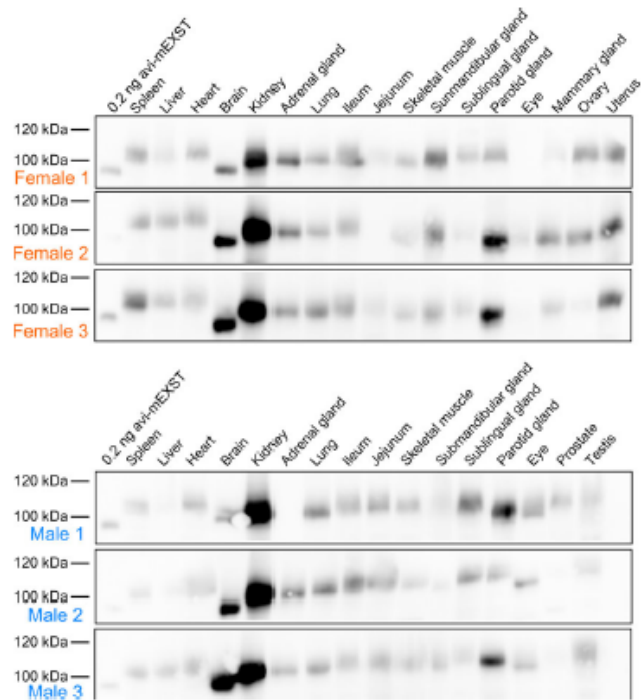
Fig. 3. Western blot analysis of GCPII expression in a panel of mouse tissues. Mouse tissue samples (from three males and three females) were homogenized, and lysates were resolved by SDS/PAGE (50 µg of total protein per lane). Mouse GCPII was visualized using the anti-GCPII primary antibody GCP-04 [2] and HRP-conjugated goat anti-mouse secondary antibody.
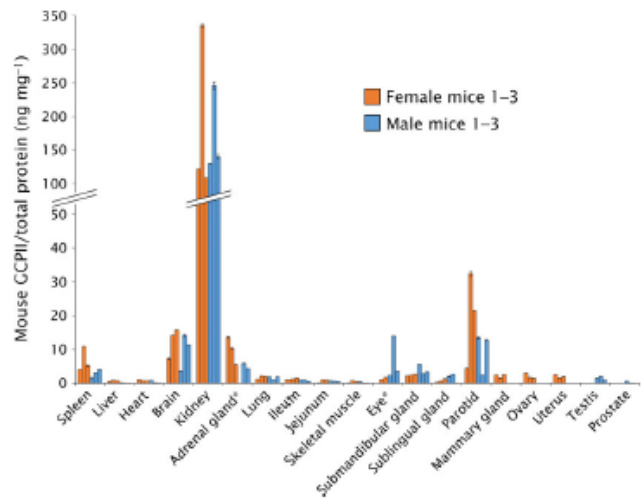
Fig. 4. GCPII expression in mouse tissues determined by radioenzymatic assay. The amount of GCPII in mouse tissues was determined by radioenzymatic assay using [³H]NAAG as a substrate and recombinant mouse GCPII (Avi-mGCPII) as a standard. Each tissue sample was measured in duplicate using 1–50 µg total protein in the reaction; the amount of mouse GCPII was normalized to total protein concentration (ng GCPII per mg total protein). The assay was performed with the same tissue samples used in the western blot analysis. *Not determined (adrenal gland: sample M1; eye: sample F1).

90
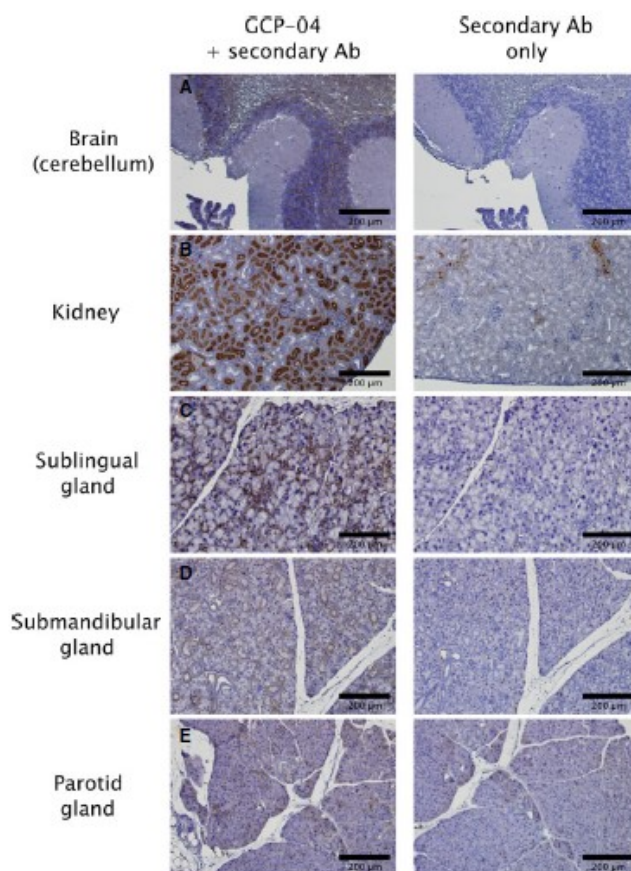
Fig. 5. Immunohistochemical staining of chosen mouse tissue sections. Formalin-fixed, paraffin-embedded mouse tissue sections were incubated with anti-GCPII antibody GCP-04 (at 10 µg·mL⁻¹ concentration) to visualize and localize mouse GCPII expression [42]. (A) Brain (cerebellum): positive choroid plexus, stratum granulare, white matter. (B) Kidney: positive luminal side of proximal tubules, Bowman capsule; little crossreactivity of secondary anti-mouse antibody with capillaries and blood vessels could be seen in the negative control. (C) Sublingual gland: positive staining of abluminal cells (probably myoepitelial cells). (D) Submandibular gland: faint staining of intercallated ducts and some non-glandular abluminal cells. (E) Parotid gland: faint staining of some non-glandular abluminal cells.

number of papers have been published describing novel GCPII inhibitors acting as neuroprotective drugs [28,44] and GCPII inhibitor-based tools for imaging and/or treating prostate cancer [19,20,45–47]. Most of these compounds and methods were evaluated using mouse models. However, there has been no direct comparison of mouse and human GCPII, which would provide important information to assess the usefulness of such mouse models. Therefore, we set out to perform a systematic and detailed study to compare the enzymatic properties of mouse and human GCPII, as well as tissue distributions on both the mRNA and protein levels.

We expressed the recombinant extracellular part of mouse GCPII with an N-terminal Avi-tag

(Avi-mGCPII), which enables fast and efficient one-step purification [34]. Even though GCPII is a trans-membrane enzyme, its extracellular domain is the catalytically active portion and correctly represents endogenous full-length GCPII [33]. To compare the enzymatic properties of mouse and human GCPII, we analyzed the cleavage of their substrates: *N*-acetyl-L-aspartyl-L-glutamate (NAAG), which is cleaved by GCPII in the brain, and pteroyl-di-L-glutamate, which is a model substrate for poly-gamma-glutamylated folates hydrolyzed by GCPII in the small intestine. Because mouse and human GCPII have high sequence similarity (86% identity and 97% similarity in the extracellular part; Fig. 7), we did not expect to find any significant differences in their enzymatic

91
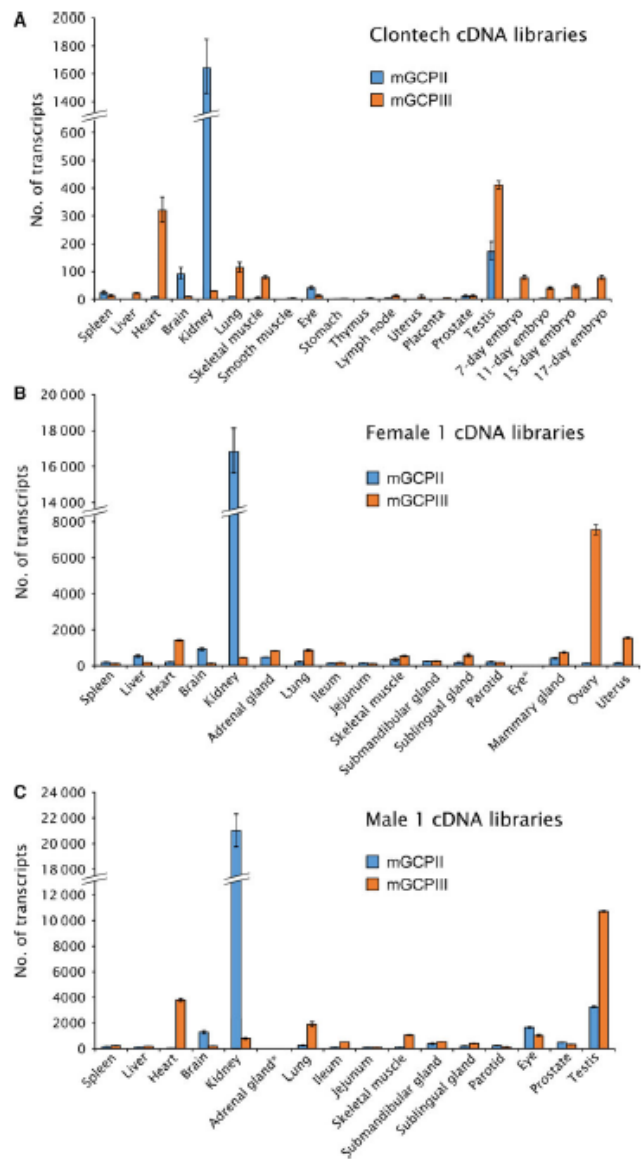
Fig. 6. Quantification of mouse GCPII and GCPIII (mGCPII and mGCPIII, respectively) transcripts using qPCR. (A) Quantification of mGCPII and mGCPIII transcripts using qPCR in commercial mouse tissue cDNA libraries from Clontech. The 'number of transcripts' corresponds to the amount of transcripts in 1.0 μL of 10-fold diluted cDNA libraries (for experimental details, see Experimental procedures). Error bars show standard deviations from triplicate measurements. (B, C) Quantification of mGCPII and mGCPIII transcripts using qPCR in cDNA libraries prepared from mouse tissues dissected from one female (B) and one male mouse (C). The 'number of transcripts' corresponds to the amount of transcripts per 10 ng of total RNA as a starting material for cDNA synthesis (for experimental details, see Experimental procedures). Error bars show standard deviations from triplicate measurements. *Not determined.

properties. In fact, we found that while the enzymes are quite similar in NAAG-hydrolyzing activity, there is an order-of-magnitude difference in their catalytic efficiencies for cleavage of pteroyl-di-L-glutamate. This difference lies in the K_M values of mouse and human GCPII (290 vs. 39 nM for pteroyl-di-L-glutamate and

92

Human GCPII (1)   MWNLLHETDSAVATARRPRWLCAGALVLAG-GFFLLGFLFGWFIKSSNEAT-
Mouse GCPII (1)   MWNALQDRDSAEVLGHRQRWLRVGTLVLALTGTFLIGFLFGWFIKPSNEATG

Human GCPII (51) NITPKHNMKAFLDELKAENIKKFLYNFTQIPHLAGTEQNFQLAKQIQSQWKE
Mouse GCPII (53) NVSHSGMKKEFLHELKAENIKKFLYNFTRTPHLAGTQNNFELAKQIHDQWKE

Human GCPII (103) FGLDSVELAHYDVLLSYPNKTHPNYISIINEDGNEIFNTSLFEPPPPGYENV
Mouse GCPII (105) FGLDLVELSHYDVLLSYPNKTHPNYISIINEDGNEIFKTSLSEQPPPGYENI

Human GCPII (155) SDIVPPFSAFSPQGMPEGDLVYVNYARTEDFFKLERDMKINCSGKIVIARYG
Mouse GCPII (157) SDVVPPYSAFSPQGTPEGDLVYVNYARTEDFFKLEREMKISCSGKIVIARYG

Human GCPII (207) KVFRGNKVKNAQLAGAKGVILYSDPADYFAPGVKSYPDGWNLPGGGVQRGNI
Mouse GCPII (209) KVFRGNMVKNAQLAGAKGMILYSDPADYFVPAVKSYPDGWNLPGGGVQRGNV

Human GCPII (259) LNLNGAGDPLTPGYPANEYAYRRGIAEAVGLPSIPVHPIGYYDAQKLLEKMG
Mouse GCPII (261) LNLNGAGDPLTPGYPANEHAYRHELTNAVGLPSIPVHPIGYDDAQKLLEHMG

Human GCPII (311) GSAPPDSSWRGSLKVPYNVGPGFTGNFSTQKVKMHIHSTNEVTRIYNVIGTL
Mouse GCPII (313) GPAPPDSSWKGGLKVPYNVGPGFAGNFSTQKVKMHIHSYTKVTRIYNVIGTL

Human GCPII (363) RGAVEPDRYVILGGHRDSWVFGGIDPQSGAAVVHEIVRSFGTLKKEGWRPRR
Mouse GCPII (365) KGALEPDRYVILGGHRDAWVFGGIDPQSGAAVVHEIVRSFGTLKKKGRRPRR

Human GCPII (415) TILFASWDAEEFGLLGSTEWAEENSRLLQERGVAYINADSSIEGNYTLRVDC
Mouse GCPII (417) TILFASWDAEEFGLLGSTEWAEEHSRLLQERGVAYINADSSIEGNYTLRVDC

Human GCPII (467) TPLMYSLVHNLTKELKSPDEGFEGKSLYESWTKKSPSPEFSGMPRISKLGSG
Mouse GCPII (469) TPLMYSLVYNLTKELQSPDEGFEGKSLYDSWKEKSPSPEFIGMPRISKLGSG

Human GCPII (519) NDFEVFFQRLGIASGRARYTKNWETNKFSGYPLYHSVYETYELVEKFYDPMF
Mouse GCPII (521) NDFEVFFQRLGIASGRARYTKNWKTNKVSSYPLYHSVYETYELVKFYDPTF

Human GCPII (571) KYHLTVAQVRGGMVFELANSIVLPFDCRDYAVVLRKYADKIYSISMKHPQEM
Mouse GCPII (573) KYHLTVAQVRGAMVFELANSIVLPFDCQSYAVALKKYADTIYNISMKHPQEM

Human GCPII (623) KTYSVSFDSLFSAVKNFTEIASKFSERLQDFDKSNPIVLRMMNDQLMFLERA
Mouse GCPII (625) KAYMISFDSLFSAVNNFTDVASKFNQRLQELDKSNPILLRIMNDQLMYLERA

Human GCPII (675) FIDPLGLPDRPFYRHVIYAPSSHNKYAGESFPGIYDALFDIESKVDPSKAWG
Mouse GCPII (677) FIDPLGLPGRPFYRHIIYAPSSHNKYAGESFPGIYDALFDISSKVNASKAWN

Human GCPII (727) EVKRQIYVAAFTVQAAAETLSEVA
Mouse GCPII (729) EVKRQISIATFTVQAAAETLREVA

Fig. 7. Sequence alignment of the mouse and human GCPII proteins. Identical amino acid residues are highlighted in yellow, similar residues in green, and different residues in white. A blue frame marks the internalization signal MXXXL [54], and a black frame corresponds to predicted GCPII transmembrane domain (predicted by TMHMM Server v. 2.0). Black circles denote potential N-glycosylation sites ('N-X-S/T'). Green spheres: residues defining the S1' pocket [49]; red spheres: residues forming the S1 pocket [48]; purple sphere: proton shuttle catalytic base [55]; blue spheres: zinc ligands [56,57].

93

1900 vs. 550 nM for NAAG). Their turnover numbers are quite similar (3.6 vs. 5.1 s^{-1} and 1.4 vs. 1.5 s^{-1}, respectively) (see Table 1). Slightly surprisingly, our data revealed that the catalytic efficiency of NAAG cleavage by mouse and human GCPII is significantly lower than that of pteroyl-di-L-glutamate cleavage (20-fold and 50-fold, respectively) (see Table 1).

Additionally, we analyzed the inhibition profile of Avi-mGCPII using several GCPII inhibitors commonly used in research, including 2-PMPA, ZJ-43, DCIBzL, DKFZ-PSMA-11, and quisqualate. We also tested several other inhibitors that were prepared in our laboratory. Generally, we did not observe considerable differences in the K$_i$ values obtained for mouse and human GCPII. However, inhibitors ZJ-43 and JB-277 were exceptions; the K$_i$ values for Avi-mGCPII were 10-fold higher (Table 2). Both compounds belong to the urea-based group of GCPII inhibitors, together with DCIBzL. Surprisingly, the K$_i$ value of DCIBzL was identical for both enzymes. As seen in Fig. 7, mouse and human GCPII are highly similar and key amino acid residues participating in substrate binding and hydrolysis are identical [48–50]. Thus, in the absence of an experimentally determined structure of mouse GCPII, it is difficult to explain the observed differences in inhibitor binding and catalytic efficiency.

Next, we assessed the substrate specificity of Avi-mGCPII. We screened dipeptide libraries covering almost all *N*-acetylated dipeptide substrates, not including cysteine-containing dipeptides. Unsurprisingly, mouse GCPII exhibited a strong preference for glutamate in the P1′ position, cleaving almost any dipeptide with a C-terminal glutamate (i.e., glutamate carboxypeptidase activity). It also cleaves dipeptides with methionine in the P1′ position and an acidic amino acid (aspartate or glutamate) in the P1 position. Dipeptides containing any other C-terminal amino acid were not hydrolyzed by mouse GCPII. The substrate specificity of mouse GCPII thus seems to be even more pronounced than that of the human enzyme (Fig. 2).

In addition to the enzymatic properties of mouse GCPII, its tissue distribution is a relevant aspect both to understand the physiological function of the enzyme and to assess the use of mouse models for targeted drug delivery and GCPII inhibition experiments. Therefore, we set out to elucidate GCPII expression in mouse tissues. To see individual differences, we collected tissue samples from six mice (three females and three males).

To assess GCPII expression on the protein level, we prepared mouse tissue lysates and detected mouse GCPII by western blot using the anti-GCPII antibody GCP-04, which was raised against human GCPII

[2,42]. Because GCP-04 recognizes a linear epitope in the GCPII primary structure (amino acids 100–104: WKEFG [22]), which is conserved in the mouse GCPII sequence, the antibody can be used for selective and sensitive detection of mouse GCPII as well. We confirmed very high expression of GCPII in the mouse kidney and high expression in the mouse brain, which is in agreement with high GCPII expression in the corresponding human tissues [22]. Furthermore, we observed high expression of GCPII in the mouse major salivary glands. Relatively high variability among individual samples of major salivary glands is probably caused by close association of salivary glands that are macroscopically quite similar. This makes the proper dissection of topographically complicated ventral cervical region particularly cumbersome and might lead to cross-contamination. Therefore, we localized GCPII expression by immunohistochemistry using anti-GCPII antibody GCP-04. We observed GCPII expression in all three salivary glands (sublingual, submandibular, and parotid); however, GCPII is expressed predominantly in the sublingual gland, while the expression in the submandibular and parotid glands is lower (Fig. 5).

Mouse prostate contains negligible levels of GCPII, which is consistent with previous findings [9] and in contrast with human prostate, which expresses large amounts of GCPII [6,22,51]. Additionally, as human and mouse prostates differ considerably in their morphology, we dissected a mouse prostate into its individual parts (anterior, dorsal, and lateral prostate) and searched for potential GCPII expression in each part separately. Nevertheless, we did not detect GCPII expression in any of the tested parts of mouse prostate. Our data suggest that GCPII might also be absent in the mouse jejunum, a tissue where human GCPII cleaves off glutamates from glutamylated folates [17]. Rat jejunum and ileum were shown not to contain GCPII, in contrast to the corresponding human tissues, which express large amounts of GCPII [22]. Folates in rat intestine are hydrolyzed by γ-glutamyl hydrolase, not GCPII [52], and the situation in mice may be thus similar.

Furthermore, we verified GCPII tissue distribution obtained by western blot analysis by quantification of NAAG-hydrolyzing activity in mouse tissues. The activity-based GCPII expression profile correlated well with the western blot results, confirming strong GCPII expression in the mouse kidney, brain, and salivary glands and no expression in mouse prostate and jejunum.

GCPIII is a close GCPII homolog found both in humans and in mouse. The GCP-04 antibody also

94

recognizes GCPIII but is roughly 10-fold less sensitive toward GCPIII than toward GCPII [42]. Moreover, GCPIII also hydrolyzes NAAG, although with a lower catalytic efficiency [10,11,43]. Therefore, GCPII distribution in mouse tissues obtained by western blot analysis with GCP-04 and activity assay based on NAAG hydrolysis could be distorted by a high amount of GCPIII and low amount of GCPII in a particular tissue. Because there is no specific antibody against GCPIII, we explored GCPII/GCPIII expression in mouse tissues on the mRNA level to differentiate between the two homologs. We quantified GCPII and GCPIII transcripts in both commercially available mouse tissue cDNA libraries and cDNA libraries we prepared from isolated mouse tissues (Fig. 6). Taking these qPCR data into account, GCPIII appears to be the source of the NAAG-hydrolyzing activity in the mouse ovary, uterus, and heart. GCPIII was most strongly expressed in the testis but was accompanied by rather high quantities of GCPII.

To conclude, we prepared and characterized recombinant mouse GCPII and compared it with human GCPII. We found that the differences in enzymatic activity, inhibition profile, and substrate specificity between mouse and human GCPII are rather small; therefore, mouse GCPII can serve as a suitable substitute for human GCPII in enzymological studies.

Due to the observed lack of GCPII expression in the mouse prostate, mouse might not seem to be an ideal model for the development of prostate cancer diagnostic/therapeutic agents. However, most such studies employ human tumor xenografts in mouse models. For this purpose, mice are generally suitable, because the distribution of GCPII in other tissues is quite similar to that in humans. Therefore, mouse GCPII appears to be a good model for the development of GCPII-targeted drugs for treatment of prostate cancer and neuronal disorders.

Experimental procedures

Cloning of mouse GCPII (Avi-mGCPII)

The pIRES/mGCPII plasmid encoding full-length mouse GCPII (amino acids 1-752) was a kind gift from Warren Heston (Cleveland Clinic, USA).

Because the sequence contained two conflicts compared to the annotated mouse GCPII sequence, we performed site-directed mutagenesis to remove them (G240A and E287N). The primers 5'-gctgactactttgttcctG<u>CG</u>gtgaagtcctatcc-3' and 5'-ggataggacttcac<u>CG</u>Caggaacaaagtagtcagc-3' were used to remove the sequence conflict at position 240,

and the primers 5'-catgagttgaca<u>AAC</u>gctgttggccttc-3' and 5'-gaaggccaacagc<u>GTT</u>tgtcaactcatg-3' to remove the sequence conflict at position 287 (changed deoxyribonucleotides are underlined, changed codons capitalized). The mutagenesis was carried out according to the manufacturer's protocol (QuikChange™ Site-Directed Mutagenesis; Stratagene, San Diego, CA, USA).

Then, the sequence corresponding to the extracellular part of mouse GCPII (amino acids 45-752) was amplified by PCR using primers 5'-a<u>aaagatct</u>aaaccttccaatgaagctactgg-3' and 5'-a<u>aactcgagt</u>taagctacttccctcagagtc-3' (restriction sites introduced into the sequence are underlined; the primers introduced a *Bgl*II site at the 5' end and an *Xho*I site at the 3' end). The resulting DNA fragment was cleaved with *Bgl*II and *Xho*I and ligated into pMT/BiP/AviTEV/rhGCPII plasmid [34] cleaved with the same endonucleases. The correct sequence of the resulting plasmid pMT/BiP/Avi-mGCPII was verified by DNA sequencing.

Transfection of *Drosophila* S2 cells and expression of Avi-mGCPII

Drosophila S2 cells expressing BirA biotin-protein ligase localized in the endoplasmic reticulum (described in Ref. [34]) were used to prepare stable Avi-mGCPII transfectants. The cells were transfected using Calcium Phosphate Transfection Kit (Invitrogen, Waltham, MA, USA) with 9 μg of pMT/BiP/Avi-mGCPII together with 0.5 μg of pCoBlast (Invitrogen), as previously described [10]. The transfected cells were cultivated in the presence of both blasticidin (5 μg·mL^{-1}, Invitrogen) and hygromycin B (300 μg·mL^{-1}; Invitrogen).

To express Avi-mGCPII, approximately 2×10^6 stably transfected cells was transferred into a 35-mm Petri dish supplemented with 2 mL SF900II medium (Invitrogen). The following day, protein expression was induced by adding CuSO$_4$ (Sigma-Aldrich, St. Louis, MO, USA) to a final concentration of 1 mM. After three days, cells were harvested by centrifugation, and the medium was analyzed by western blot.

The large-scale expression of Avi-mGCPII was performed as previously described [33]. The final volume of cell suspension was 1000 mL.

Purification of Avi-mGCPII

Purification of Avi-mGCPII was performed as previously described [34]. Briefly, cell medium (1000 mL) containing secreted biotinylated Avi-mGCPII was centrifuged at 3400 *g* for 45 min. Then, it was concentrated 10-fold using a LabScale TFF System (Merck Millipore, Billerica, MA, USA) with a Pellicon® XL 50 Cassette, Biomax 100. The concentrated medium was centrifuged again at 3400 *g* for 20 min and equilibrated with 300 mM Tris/HCl, 450 mM NaCl, pH 7.2 in a 2 : 1 ratio. The equilibrated

95

concentrated Avi-mGCPII medium was then mixed with 1 mL Streptavidin Mutein Matrix (Roche, Basel, Switzerland) and incubated with gentle shaking at 6 °C for 15 h. Afterward, the resin was washed with 50 column volumes of 100 mM Tris/HCl, 150 mM NaCl, pH 7.2. Bound biotinylated proteins were eluted with 5 mL of 100 mM Tris/HCl, 150 mM NaCl, 2 mM D-biotin, pH 7.2, in five consecutive elution fractions (after the first elution fraction, the resin was incubated with elution buffer for 1 h). After regeneration of the resin, the flow-through fraction was again mixed with the resin, and the purification procedure was repeated.

Determination of kinetic parameters by radioenzymatic assay

Kinetic parameters (K_M and k_{cat}) of *N*-acetyl-L-aspartyl-L-glutamate (NAAG) cleavage by Avi-mGCPII were determined as previously described [34], with a minor modification: The reactions were performed in a 96-well plate, and appropriate amounts of Avi-mGCPII were mixed with 25 mM Bis-Tris propane, 150 mM NaCl, 0.001% octaethylene glycol monododecyl ether (Affymetrix, Santa Clara, CA, USA), pH 7.4.

Determination of kinetic and inhibition constants by HPLC

Kinetic parameters (K_M and k_{cat}) of pteroyl-di-L-glutamate cleavage by Avi-mGCPII, as well as K_i values for all inhibitors, were determined as previously described [39]. Briefly, in a 96-well plate, Avi-mGCPII was mixed with 25 mM Bis-Tris propane, 150 mM NaCl, 0.001% octaethylene glycol monododecyl ether (Affymetrix), pH 7.4 (and tested inhibitor, if used), into a final volume of 90 μL. Reactions were started by adding 10 μL of 4 μM pteroyl-di-L-glutamate and incubated at 37 °C for 20 min. The reactions were stopped with 20 μL of 25 μM 2-PMPA and subsequently analyzed on an Agilent 1200 Series system using an Acquity UPLC HSS T3 1.8 μm column (2.1 × 100 mm; Waters, Milford, MA, USA).

Animals and tissue isolation

Six C57BL/GJ mice (three males (M) and three females (F)) were sacrificed by cervical dislocation with agreement of the local ethical commission. The ages of the mice were as follows: M1: 5 months; M2: 8 months; M3: 12 months; F1: 8 months; F2 and F3: 12 months. Samples of tissues (for preparation of tissue lysates) were immediately transferred into microtubes and frozen at −80 °C. Samples of tissues (for qPCR quantification) were immediately transferred into RNAlater, impregnated with it for 2 days at 4 °C, and then stored at −80 °C.

Tissue lysate sample preparation

A small piece of tissue (approx. 30 mg) was transferred into 250 μL of 50 mM Tris/HCl, 100 mM NaCl, pH 7.4, in a 2-mL microtube. Tissue samples were homogenized using TissueLyser II (30 Hz, 3 min). The homogenates were then diluted with 250 μL of the lysis buffer. Octaethylene glycol monododecyl ether (Affymetrix) was added to reach 1% final concentration, and the homogenate was sonicated in a water bath for 5 min at 0 °C. Finally, the samples were centrifuged at 600 g for 15 min, and the resulting supernatant was stored at −80 °C until further use. The lysate protein concentration was determined using Bradford 1 × Dye Reagent (Bio-Rad, Hercules, CA, USA).

Radioenzymatic determination of NAAG-hydrolyzing activity in mouse tissues

The determination of NAAG-hydrolyzing activity in mouse tissues was performed as previously described [53]. A sample of tissue lysate was mixed with 20 mM Tris/HCl, 150 mM NaCl, 0.1% Tween 20, pH 7.4, to a final volume of 90 μL. Reactions were started by adding 10 μL of 1 μM NAAG (containing 50 nM tritium-labeled NAAG), and incubated at 37 °C for 15 h. The reactions were stopped with 100 μL of ice-cold 200 mM KH_2PO_4, 2 mM 2-mercaptoethanol, pH 7.4. The released glutamate was separated from the unreacted substrate using ion-exchange AG1-X resin (Bio-Rad). The radioactivity of the sample was quantified by liquid scintillation using the Rotiszint ECO Plus scintillation cocktail (Roth) in a Tri-Carb Liquid Scintillation Counter (Perkin-Elmer, Waltham, MA, USA). The samples were measured in duplicate.

SDS/PAGE and western blotting

Protein samples were resolved by reducing SDS/PAGE. Proteins were electroblotted onto a nitrocellulose membrane (wet blotting: 100 V/1 h). After blotting, the membrane was blocked with 0.55% (w/v) casein solution in PBS (Casein Buffer 20X-4X Concentrate, SDT, Baesweiler, Germany) at room temperature for 1 h. To visualize GCPII, the blots were probed with the antibody GCP-04 (described in [2]) for 12 h at 4 °C (200 ng·mL^{-1}; diluted in 0.55% casein solution), washed three times with PBS containing 0.05% Tween 20 (PBST buffer), and incubated with goat anti-mouse antibody conjugated with horseradish peroxidase (Thermo Scientific, Waltham, MA, USA; diluted in 0.55% casein solution, 1 : 25 000). The blots were then washed three times with PBST to remove unbound antibodies and developed with SuperSignal West Femto Chemiluminescent Substrate (Thermo Scientific).

96

Chemiluminescence was captured with a ChemiDoc-It™ 600 Imaging System (UVP, Upland, CA, USA).

Immunohistochemistry

Immunohistochemistry was performed according to the protocol described previously using anti-GCPII antibody GCP-04 [2] with minor modifications [42]. Briefly, after standard histological processing (fixation, dehydration, embedding into paraffin, cutting, paraffin removal, rehydration), heat antigen retrieval was performed using 10 mM sodium citrate, 0.1% Tween 20, pH 6.0 buffer and heating to 110 °C for 15 min in an autoclave. Afterward, samples were incubated in 1.5% hydrogen peroxide solution for 20 min to reduce endogenous peroxidase activity and in 10% fetal bovine serum in PBS to block unspecific interactions. The slides were then stained by primary anti-GCPII antibody GCP-04 (10 μg·mL^{-1} in 4 °C, overnight), followed by extensive washing (five times with PBS containing 0.1% Tween 20) and incubation with secondary antibody Histofine® Simple Stain™ MAX PO (MULTI) (Nichirei Bioscience Inc., Tokyo, Japan) diluted 1 : 2 with 10% fetal bovine serum in PBS at room temperature for 1 h. After further extensive washing (five times with PBS containing 0.1% Tween 20), GCPII was visualized using DAB/Plus kit (Diagnostic BioSystems, Pleasanton, CA, USA, 60 s). The slides were counterstained with Harris' hematoxylin and mounted in polyvinyl alcohol-based media.

Carboxypeptidase activity assay

Carboxypeptidase activity (i.e., substrate specificity) of mouse GCPII was determined using N-Ac-A-X peptide libraries according to a previously published method [41]. Briefly, 1.2 μg Avi-mGCPII was diluted into 25 mM Bis-Tris propane, 150 mM NaCl, 0.001% octaethylene glycol monododecyl ether (Affymetrix), pH 7.4, and incubated in the presence of 25 μM dipeptide for 1.5 h at 37 °C. As negative controls, reactions without the enzyme and in the presence of 1 mM 2-PMPA, a highly selective GCPII inhibitor, were performed. The reaction mixture was then analyzed using HPLC, as previously described [41].

Total RNA isolation and reverse transcription

First, tissue samples were transferred from RNA later solution (Invitrogen, #AM7021) to RLT buffer (part of the RNEasy Mini Kit, Qiagen, Hilden, Germany, #74106) supplied with β-mercaptoethanol and homogenized with 5-mm steel beads (Qiagen; #69989) using TissueLyser II (#85300; Qiagen). Total RNA was isolated using RNeasy Mini Kit according to the manufacturer's instructions. The concentration and purity of isolated RNA were determined spectrophotometrically using a Nanodrop ND-1000 spectrophotometer. The integrity of each RNA sample was analyzed using the Agilent RNA 6000 Nano kit run on an Agilent 2100 Bioanalyzer. Only samples without significant degradation were used for subsequent steps.

RNA was then reverse-transcribed using M-MLV (#28025013; Invitrogen) according to the manufacturer's instructions. Each 20 μL reaction contained up to 2 μg total RNA, 2.5 μM oligo(dT)$_{20}$ primers (#18418020; Invitrogen), 50 ng random hexamers (100 ng if more than 1 μg RNA was transcribed), 40 units of RNAseOUT, 200 units of M-MLV reverse transcriptase, and other components as specified by the manufacturer.

Quantitative PCR (qPCR) analysis

All qPCRs were carried out in triplicate in FrameStar 480/96 multiwell plates (#4ti-0951; 4titude, Wotton, UK) sealed with adhesive optical foil (#4729692001; Roche) using a LightCycler 480 II instrument (Roche) in a total volume of 10 μL. Each reaction consisted of LightCycler 480 Probe Master (Roche) diluted according to the manufacturer's instructions, forward and reverse primers (1 μM final concentration each), fluorescent probe (see description of individual assays for final concentration), and 1 μL of sample or template DNA (positive and nontemplate controls as well as interplate calibrators were included on each plate). Initial denaturation for 3 min at 95 °C was followed by 45 cycles of 10 s at 95 °C, 30 s at 66 °C, and 30 s at 72 °C. The threshold cycle numbers (C_q) were then determined from fluorescence intensities acquired during the qPCR runs by the second-derivative maximum method using LightCycler 480 software (Roche). The presence and size of PCR products were analyzed by agarose gel electrophoresis.

The amount of mouse GCPII (encoded by the gene Folh1) was quantified by an assay set of forward and reverse primers (sequences 5′-gattgccagatatgggaaagtg-3′ and 5′-cctgccagttgagcattttt-3′) and fluorescent hydrolysis probe #6 from the Roche Universal Probe Library (LNA octamer sequence 5′-cagaggaa-3′; final concentration 100 nM). This set was designed to amplify nucleotides 714–773 in mouse GCPII transcript NM_016770 to yield an amplified product of 60 bps, which spans the region of exons 5 and 6 and corresponds to amino acids 202–223 in the longest open reading frame (ORF). This assay should not amplify genomic sequence because it spans a 1029-bp intron.

The amount of mouse GCPIII transcript (encoded by the gene Naalad2) was quantified by an assay set of forward and reverse primers (sequences 5′-aatgatgcagagagactattacgc-3′ and 5′-ccagctttgtctggtggag-3′) and fluorescent hydrolysis probe #52 from the Roche Universal Probe Library (LNA octamer sequence 5′-gggaggag-3′; final concentration 50 nM). This set was designed to amplify nucleotides 922–981 in mouse GCPIII transcript NM_028279 to yield an amplified product of 60 bps, which spans the region of exons 7 and 8 and corresponds to

97

amino acids 289–309 in the longest ORF. This assay should not amplify genomic sequence because it spans a 880-bp intron.

As a standard for absolute quantification, serial 10-fold dilutions covering concentrations from 10^8 to 10^2 copies per reaction of either pcDNA4 plasmid with subcloned coding sequence of full-length mouse GCPII (longest ORF from NM_016770 coding amino acids 1–752) or pMT/BiP plasmid with subcloned coding sequence of extracellular part of mouse GCPIII (part of longest ORF from NM_028279 coding amino acids 36–740) were amplified with the corresponding assay set. The initial concentration of plasmid DNA (purified by QIAprep Spin Miniprep Kit, #27106; Qiagen) prior to dilution was determined spectrophotometrically at 260 nm (Nanodrop ND-1000; Thermo Scientific).

To enable precise absolute comparison between the determined amounts of both transcripts, obtained calibration curves were further normalized against each other by quantification of a common region of both plasmids. The region containing the ampicillin resistance gene was quantified by a set of primers with sequences 5′-gcagaagtggtcctg-caact-3′ and 5′-agcttcccggcaacaatta-3′ and fluorescent hydrolysis probe #58 from the Roche Universal Probe Library (final concentration 50 nM). In this way, two calibration curves were obtained for each plasmid, one for the amplification of target transcript and one for the common sequence. Finally, the slope and intercept values of both curves were transformed for each plasmid so that the transformed slope and intercept values of the curves for the common sequence were equal between the two plasmids and corresponded to the average value between the two plasmids.

The amount of both transcripts was determined in the prepared tissue cDNA libraries. In each qPCR, an amount of cDNA corresponding to the starting amount of total RNA of 5–10 ng was used, and the amount of GCPII and GCPIII transcripts were normalized to the total amount of RNA. Both transcripts were also quantified in 1.0 μL of 10-fold diluted commercial tissue cDNA libraries (Mouse MTC Panels I and III supplied by Clontech, Mountain View, CA, USA, #636745 and 636757), which had been normalized to several control genes by the vendor (beta-actin, G3PDH, phospholipase A2, and ribosomal protein S29).

Statistical analysis

All values are presented as the mean ± standard deviation.

Acknowledgements

Author contributions

The manuscript was written through contributions of all authors. All authors have given approval to the final version of the manuscript. JK and PS conceived the project and analyzed data, TK, BV, JT, VN, PS and JK wrote the manuscript, TK, BV, VN, JT, FS, SV and MF designed, performed and interpreted the experiments.

References

1 Berger UV, Carter RE, Mckee M and Coyle JT (1995) N-acetylated alpha-linked acidic dipeptidase is expressed by non-myelinating Schwann-cells in the peripheral nervous-system. *J Neurocytol* **24**, 99–109.

2 Sacha P, Zamecnik J, Barinka C, Hlouchova K, Vicha A, Mlcochova P, Hilgert I, Eckschlager T and Konvalinka J (2007) Expression of glutamate carboxypeptidase II in human brain. *Neuroscience* **144**, 1361–1372.

3 Bostwick DG, Pacelli A, Blute M, Roche P and Murphy GP (1998) Prostate specific membrane antigen expression in prostatic intraepithelial neoplasia and adenocarcinoma: a study of 184 cases. *Cancer* **82**, 2256–2261.

4 Silver DA, Pellicer I, Fair WR, Heston WD and Cordon-Cardo C (1997) Prostate-specific membrane antigen expression in normal and malignant human tissues. *Clin Cancer Res* **3**, 81–85.

5 Pinto JT, Suffoletto BP, Berzin TM, Qiao CH, Lin SL, Tong WP, May F, Mukherjee B and Heston WDW (1996) Prostate-specific membrane antigen: a novel folate hydrolase in human prostatic carcinoma cells. *Clin Cancer Res* **2**, 1445–1451.

6 Kinoshita Y, Kuratsukuri K, Landas S, Imaida K, Rovito PM Jr, Wang CY and Haas GP (2006) Expression of prostate-specific membrane antigen in normal and malignant human tissues. *World J Surg* **30**, 628–636.

7 Robinson MB, Blakely RD, Couto R and Coyle JT (1987) Hydrolysis of the brain dipeptide N-acetyl-L-aspartyl-L-glutamate. Identification and characterization of a novel N-acetylated alpha-linked acidic dipeptidase activity from rat brain. *J Biol Chem* **262**, 14498–14506.

98

8 Horoszewicz JS, Kawinski E and Murphy GP (1987) Monoclonal-antibodies to a new antigenic marker in epithelial prostatic cells and serum of prostatic-cancer patients. *Anticancer Res* **7**, 927–936.

9 Bacich DJ, Ramadan E, O'Keefe DS, Bukhari N, Wegorzewska I, Ojeifo O, Olszewski R, Wrenn CC, Bzdega T, Wroblewska B *et al.* (2002) Deletion of the glutamate carboxypeptidase II gene in mice reveals a second enzyme activity that hydrolyzes N-acetylaspartylglutamate. *J Neurochem* **83**, 20–29.

10 Hlouchova K, Barinka C, Klusak V, Sacha P, Mlcochova P, Majer P, Rulisek L and Konvalinka J (2007) Biochemical characterization of human glutamate carboxypeptidase III. *J Neurochem* **101**, 682–696.

11 Collard F, Vertommen D, Constantinescu S, Buts L and Van Schaftingen E (2011) Molecular identification of beta-citrylglutamate hydrolase as glutamate carboxypeptidase 3. *J Biol Chem* **286**, 38220–38230.

12 Slusher BS, Vornov JJ, Thomas AG, Hurn PD, Harukuni I, Bhardwaj A, Traystman RJ, Robinson MB, Britton P, Lu XCM *et al.* (1999) Selective inhibition of NAALADase, which converts NAAG to glutamate, reduces ischemic brain injury. *Nat Med* **5**, 1396–1402.

13 Neale JH, Olszewski RT, Gehl LM, Wroblewska B and Bzdega T (2005) The neurotransmitter N-acetylaspartylglutamate in models of pain, ALS, diabetic neuropathy, CNS injury and schizophrenia. *Trends Pharmacol Sci* **26**, 477–484.

14 Wroblewska B, Wroblewski JT, Pshenichkin S, Surin A, Sullivan SE and Neale JH (1997) N-acetylaspartylglutamate selectively activates mGluR3 receptors in transfected cells. *J Neurochem* **69**, 174–181.

15 Bruno V, Wroblewska B, Wroblewski JT, Fiore L and Nicoletti F (1998) Neuroprotective activity of N-acetylaspartylglutamate in cultured cortical cells. *Neuroscience* **85**, 751–757.

16 Halsted CH, Ling EH, Luthi-Carter R, Villanueva JA, Gardner JM and Coyle JT (1998) Folylpoly-gamma-glutamate carboxypeptidase from pig jejunum – molecular characterization and relation to glutamate carboxypeptidase II. *J Biol Chem* **273**, 20417–20424.

17 Chandler CJ, Wang TT and Halsted CH (1986) Pteroylpolyglutamate hydrolase from human jejunal brush borders. Purification and characterization. *J Biol Chem* **261**, 928–933.

18 Mhawech-Fauceglia P, Zhang S, Terracciano L, Sauter G, Chadhuri A, Herrmann FR and Penetrante R (2007) Prostate-specific membrane antigen (PSMA) protein expression in normal and neoplastic tissues and its sensitivity and specificity in prostate adenocarcinoma: an immunohistochemical study using multiple tumour tissue microarray technique. *Histopathology* **50**, 472–483.

19 Chen Z, Penet MF, Nimmagadda S, Li C, Banerjee SR, Winnard PT Jr, Artemov D, Glunde K, Pomper MG and Bhujwalla ZM (2012) PSMA-targeted theranostic nanoplex for prostate cancer therapy. *ACS Nano* **6**, 7752–7762.

20 Heck MM, Retz M, D'Alessandria C, Rauscher I, Scheidhauer K, Maurer T, Storz E, Janssen F, Schottelius M, Wester HJ *et al.* (2016) Systemic radioligand therapy with (177)Lu labeled prostate specific membrane antigen ligand for imaging and therapy in patients with metastatic castration resistant prostate cancer. *J Urol* **196**, 382–391.

21 Hrkach J, Von Hoff D, Ali MM, Andrianova E, Auer J, Campbell T, De Witt D, Figa M, Figueiredo M, Horhota A *et al.* (2012) Preclinical development and clinical translation of a PSMA-targeted docetaxel nanoparticle with a differentiated pharmacological profile. *Sci Transl Med* **4**, 128ra39.

22 Rovenska M, Hlouchova K, Sacha P, Mlochova P, Horak V, Zamecnik J, Barinka C and Konvalinka J (2008) Tissue expression and enzymologic characterization of human prostate specific membrane antigen and its rat and pig orthologs. *Prostate* **68**, 171–182.

23 Zhong C, Zhao X, Van KC, Bzdega T, Smyth A, Zhou J, Kozikowski AP, Jiang J, O'Connor WT, Berman RF *et al.* (2006) NAAG peptidase inhibitor increases dialysate NAAG and reduces glutamate, aspartate and GABA levels in the dorsal hippocampus following fluid percussion injury in the rat. *J Neurochem* **97**, 1015–1025.

24 Zhong CL, Zhao XR, Sarva J, Kozikowski A, Neale JH and Lyeth BG (2005) NAAG peptidase inhibitor reduces acute neuronal degeneration and astrocyte damage following lateral fluid percussion TBI in rats. *J Neurotraum* **22**, 266–276.

25 Ghadge GD, Slusher BS, Bodner A, Canto MD, Wozniak K, Thomas AG, Rojas C, Tsukamoto T, Majer P, Miller RJ *et al.* (2003) Glutamate carboxypeptidase II inhibition protects motor neurons from death in familial amyotrophic lateral sclerosis models. *Proc Natl Acad Sci USA* **100**, 9554–9559.

26 Chen SR, Wozniak KM, Slusher BS and Pan HL (2002) Effect of 2-(phosphono-methyl)-pentanedioic acid on allodynia and afferent ectopic discharges in a rat model of neuropathic pain. *J Pharmacol Exp Ther* **300**, 662–667.

27 Nagel J, Belozertseva I, Greco S, Kashkin V, Malyshkin A, Jirgensons A, Shekunova E, Eilbacher B, Bespalov A and Danysz W (2006) Effects of NAAG peptidase inhibitor 2-PMPA in model chronic pain – relation to brain concentration. *Neuropharmacology* **51**, 1163–1171.

28 Zhou J, Neale JH, Pomper MG and Kozikowski AP (2005) NAAG peptidase inhibitors and their potential

99

for diagnosis and therapy. *Nat Rev Drug Discov* **4**, 1015–1026.

29 Bacich DJ, Pinto JT, Tong WP and Heston WD (2001) Cloning, expression, genomic localization, and enzymatic activities of the mouse homolog of prostate-specific membrane antigen/NAALADase/folate hydrolase. *Mamm Genome* **12**, 117–123.

30 Gao Y, Xu SY, Cui ZW, Zhang MK, Lin YY, Cai L, Wang ZG, Luo XG, Zheng Y, Wang Y *et al.* (2015) Mice lacking glutamate carboxypeptidase II develop normally, but are less susceptible to traumatic brain injury. *J Neurochem* **134**, 340–353.

31 Tsai G, Dunham KS, Drager U, Grier A, Anderson C, Collura J and Coyle JT (2003) Early embryonic death of glutamate carboxypeptidase II (NAALADase) homozygous mutants. *Synapse* **50**, 285–292.

32 Han LQ, Picker JD, Schaevitz LR, Tsai GC, Feng JM, Jiang ZC, Chu HC, Basu AC, Berger-Sweeney J and Coyle JT (2009) Phenotypic characterization of mice heterozygous for a null mutation of glutamate carboxypeptidase II. *Synapse* **63**, 625–635.

33 Barinka C, Rinnova M, Sacha P, Rojas C, Majer P, Slusher BS and Konvalinka J (2002) Substrate specificity, inhibition and enzymological analysis of recombinant human glutamate carboxypeptidase II. *J Neurochem* **80**, 477–487.

34 Tykvart J, Sacha P, Barinka C, Knedlik T, Starkova J, Lubkowski J and Konvalinka J (2012) Efficient and versatile one-step affinity purification of in vivo biotinylated proteins: expression, characterization and structure analysis of recombinant human glutamate carboxypeptidase II. *Protein Expr Purif* **82**, 106–115.

35 Jackson PF, Cole DC, Slusher BS, Stetz SL, Ross LE, Donzanti BA and Trainor DA (1996) Design, synthesis, and biological activity of a potent inhibitor of the neuropeptidase N-acetylated alpha-linked acidic dipeptidase. *J Med Chem* **39**, 619–622.

36 Kozikowski AP, Zhang J, Nan FJ, Petukhov PA, Grajkowska E, Wroblewski JT, Yamamoto T, Bzdega T, Wroblewska B and Neale JH (2004) Synthesis of urea-based inhibitors as active site probes of glutamate carboxypeptidase II: efficacy as analgesic agents. *J Med Chem* **47**, 1729–1738.

37 Chen Y, Foss CA, Byun Y, Nimmagadda S, Pullambahatla M, Fox JJ, Castanares M, Lupold SE, Babich JW, Mease RC *et al.* (2008) Radiohalogenated prostate-specific membrane antigen (PSMA)-based ureas as imaging agents for prostate cancer. *J Med Chem* **51**, 7933–7943.

38 Eder M, Schafer M, Bauder-Wust U, Hull WE, Wangler C, Mier W, Haberkorn U and Eisenhut M (2012) Ga-68-complex lipophilicity and the targeting property of a urea-based PSMA inhibitor for PET imaging. *Bioconjug Chem* **23**, 688–697.

39 Tykvart J, Schimer J, Barinkova J, Pachl P, Postova-Slavetinska L, Majer P, Konvalinka J and Sacha P (2014) Rational design of urea-based glutamate carboxypeptidase II (GCPII) inhibitors as versatile tools for specific drug targeting and delivery. *Bioorg Med Chem* **22**, 4099–4108.

40 Tykvart J, Schimer J, Jancarik A, Barinkova J, Navratil V, Starkova J, Sramkova K, Konvalinka J, Majer P and Sacha P (2015) Design of highly potent urea-based, exosite-binding inhibitors selective for glutamate carboxypeptidase II. *J Med Chem* **58**, 4357–4363.

41 Tykvart J, Barinka C, Svoboda M, Navratil V, Soucek R, Hubalek M, Hradilek M, Sacha P, Lubkowski J and Konvalinka J (2015) Structural and biochemical characterization of a novel aminopeptidase from human intestine. *J Biol Chem* **290**, 11321–11336.

42 Tykvart J, Navratil V, Sedlak F, Corey E, Colombatti M, Fracasso G, Koukolik F, Barinka C, Sacha P and Konvalinka J (2014) Comparative analysis of monoclonal antibodies against prostate-specific membrane antigen (PSMA). *Prostate* **74**, 1674–1690.

43 Navratil M, Tykvart J, Schimer J, Pachl P, Navratil V, Rokob TA, Hlouchova K, Rulisek L and Konvalinka J (2016) Comparison of human glutamate carboxypeptidases II and III reveals their divergent substrate specificities. *FEBS J* **283**, 2528–2545.

44 Majer P, Jancarik A, Krecmerova M, Tichy T, Tenora L, Wozniak K, Wu Y, Pommier E, Ferraris D, Rais R *et al.* (2016) Discovery of orally available prodrugs of the glutamate carboxypeptidase II (GCPII) inhibitor 2-phosphonomethylpentanedioic acid (2-PMPA). *J Med Chem* **59**, 2810–2819.

45 Chen Y, Dhara S, Banerjee SR, Byun Y, Pullambhatla M, Mease RC and Pomper MG (2009) A low molecular weight PSMA-based fluorescent imaging agent for cancer. *Biochem Biophys Res Commun* **390**, 624–629.

46 Gorin MA, Pomper MG and Rowe SP (2016) PSMA-targeted imaging of prostate cancer: the best is yet to come. *BJU Int* **117**, 715–716.

47 Yang X, Mease RC, Pullambhatla M, Lisok A, Chen Y, Foss CA, Wang Y, Shallal H, Edelman H, Hoye AT *et al.* (2016) [(18)F]Fluorobenzoyllysinepentanedioic acid carbamates: new scaffolds for positron emission tomography (PET) imaging of prostate-specific membrane antigen (PSMA). *J Med Chem* **59**, 206–218.

48 Barinka C, Hlouchova K, Rovenska M, Majer P, Dauter M, Hin N, Ko YS, Tsukamoto T, Slusher BS, Konvalinka J *et al.* (2008) Structural basis of interactions between human glutamate carboxypeptidase II and its substrate analogs. *J Mol Biol* **376**, 1438–1450.

49 Barinka C, Rovenska M, Mlcochova P, Hlouchova K, Plechanovova A, Majer P, Tsukamoto T, Slusher BS, Konvalinka J and Lubkowski J (2007) Structural

100

insight into the pharmacophore pocket of human glutamate carboxypeptidase II. *J Med Chem* **50**, 3267–3273.

50 Mlcochova P, Plechanovova A, Barinka C, Mahadevan D, Saldanha JW, Rulisek L and Konvalinka J (2007) Mapping of the active site of glutamate carboxypeptidase II by site-directed mutagenesis. *FEBS J* **274**, 4731–4741.

51 O'Keefe DS, Bacich DJ and Heston WD (2004) Comparative analysis of prostate-specific membrane antigen (PSMA) versus a prostate-specific membrane antigen-like gene. *Prostate* **58**, 200–210.

52 Shafizadeh TB and Halsted CH (2007) Gamma-glutamyl hydrolase, not glutamate carboxypeptidase II, hydrolyzes dietary folate in rat small intestine. *J Nutr* **137**, 1149–1153.

53 Knedlik T, Navratil V, Vik V, Pacik D, Sacha P and Konvalinka J (2014) Detection and quantitation of glutamate carboxypeptidase II in human blood. *Prostate* **74**, 768–780.

54 Rajasekaran SA, Anilkumar G, Oshima E, Bowie JU, Liu H, Heston W, Bander NH and Rajasekaran AK (2003) A novel cytoplasmic tail MXXXL motif mediates the internalization of prostate-specific membrane antigen. *Mol Biol Cell* **14**, 4835–4845.

55 Klusak V, Barinka C, Plechanovova A, Mlcochova P, Konvalinka J, Rulisek L and Lubkowski J (2009) Reaction mechanism of glutamate carboxypeptidase II revealed by mutagenesis, X-ray crystallography, and computational methods. *Biochemistry* **48**, 4126–4138.

56 Mesters JR, Barinka C, Li WX, Tsukamoto T, Majer P, Slusher BS, Konvalinka J and Hilgenfeld R (2006) Structure of glutamate carboxypeptidase II, a drug target in neuronal damage and prostate cancer. *EMBO J* **25**, 1375–1384.

57 Speno HS, Luthi-Carter R, Macias WL, Valentine SL, Joshi ART and Coyle JT (1999) Site-directed mutagenesis of predicted active site residues in glutamate carboxypeptidase II. *Mol Pharmacol* **55**, 179–185.

101

7.3. Paper III

Pavel Šácha, Tomáš Knedlík, Jiří Schimer, Jan Tykvart, Jan Parolek, Václav Navrátil, Petra Dvořáková, František Sedlák, Karel Ulbrich, Jiří Strohalm, Pavel Majer, Vladimír Šubr and Jan Konvalinka

iBodies: Modular Synthetic Antibody Mimetics Based on Hydrophilic Polymers Decorated with Functional Moieties.

Angew Chem Int Ed Engl 2016, **55**(7):2356-2360.

iBodies: Modular Synthetic Antibody Mimetics Based on Hydrophilic Polymers Decorated with Functional Moieties

Pavel Šácha⁺, Tomáš Knedlík⁺, Jiří Schimer, Jan Tykvart, Jan Parolek, Václav Navrátil,
Petra Dvořáková, František Sedlák, Karel Ulbrich, Jiří Strohalm, Pavel Majer, Vladimír Šubr,*
and Jan Konvalinka*

Abstract: Antibodies are indispensable tools for biomedicine and anticancer therapy. Nevertheless, their use is compromised by high production costs, limited stability, and difficulty of chemical modification. The design and preparation of synthetic polymer conjugates capable of replacing antibodies in biomedical applications such as ELISA, flow cytometry, immunocytochemistry, and immunoprecipitation is reported. The conjugates, named "iBodies", consist of an HPMA copolymer decorated with low-molecular-weight compounds that function as targeting ligands, affinity anchors, and imaging probes. We prepared specific conjugates targeting several proteins with known ligands and used these iBodies for enzyme inhibition, protein isolation, immobilization, quantification, and live-cell imaging. Our data indicate that this highly modular and versatile polymer system can be used to produce inexpensive and stable antibody substitutes directed toward virtually any protein of interest with a known ligand.

The discovery of antibodies specifically targeting biologically relevant molecules revolutionized the life sciences. Nevertheless, the use of antibodies has several disadvantages, such as limited stability, difficulty of chemical modification, and difficulty targeting proteins in mouse models. To address these limitations, researchers have developed alternative molecular recognition tools capable of replacing antibodies in biomedical research applications (antibody mimetics). These include affibodies,[1] designed ankyrin repeat proteins (DARPins),[2] and aptamers.[3] Recently, chemically synthesized small molecules that fulfill some functions of antibodies have been described.[4] Polymers capable of molecular recognition of other molecules were described several decades ago. These molecularly imprinted polymers (MIPs) are based on structure complementarity with the target molecules and are used as molecular biosensors and binders.[5]

We set out to develop novel antibody mimetics based on N-(2-hydroxypropyl)methacrylamide (HPMA) copolymer conjugates decorated with three different low-molecular-weight ligands. We chose water-soluble and biocompatible HPMA copolymers since they have been used for the development of drug delivery vectors, imaging agents, and polymer drugs.[6] The HPMA copolymers are multivalent synthetic macromolecules that carry a number of reactive groups that enable covalent attachment of various ligands such as fluorescent probes, therapeutics, proteins, and oligonucleotides.[7]

Specific recognition, immobilization, and imaging of a protein of interest require a specific targeting ligand (e.g., an inhibitor), an affinity anchor, and an imaging probe attached to the polymer backbone (Figure 1a). As an affinity tag, we chose biotin because it can be readily used for high-affinity immobilization on a variety of commercially available resins (Figure 1b). As an imaging probe, we chose the fluorophore ATTO488 (Figure 1c). The choice of targeting ligand depends on the protein of interest; we developed and tested these antibody mimetics with glutamate carboxypeptidase II, HIV-1 protease, pepsin, and His-tagged proteins (Figure 1d–g). To reflect functional similarity to antibodies and the use of inhibitors as targeting ligands, we propose the name iBodies for these polymer conjugates. All prepared iBodies were characterized in terms of chemical identity and the content of individual ligands, and their characteristics are summarized in Table 1 and Table S2 in the Supporting Information. We assume statistical distribution of the attached moieties, since each ligand terminates with the same sterically unhindered reactive moiety ($-CH_2CH_2NH_2$). The synthesis and characteristics of the conjugates are described in detail in the Supporting Information.

For developing the technique, we chose human glutamate carboxypeptidase II (GCPII; also known as prostate-specific membrane antigen or PSMA). GCPII is a transmembrane metallopeptidase that is strongly expressed in the brain and

[*] Dr. P. Šácha,[+] T. Knedlík,[+] Dr. J. Schimer, Dr. J. Tykvart, J. Parolek,
V. Navrátil, P. Dvořáková, Dr. F. Sedlák, Dr. P. Majer, Dr. J. Konvalinka
Institute of Organic Chemistry and Biochemistry
Academy of Science of the Czech Republic
Flemingovo n. 2, 16610 Prague 6 (Czech Republic)
E-mail: konval@uochb.cas.cz

Prof. K. Ulbrich, Dr. J. Strohalm, Dr. V. Šubr
Institute of Macromolecular Chemistry
Academy of Science of the Czech Republic
Heyrovského n. 2, 16206 Prague 6 (Czech Republic)
E-mail: subr@imc.cas.cz

Dr. P. Šácha,[+] T. Knedlík,[+] Dr. J. Schimer, Dr. J. Tykvart, J. Parolek,
V. Navrátil, Dr. J. Konvalinka
Department of Biochemistry, Faculty of Science, Charles University
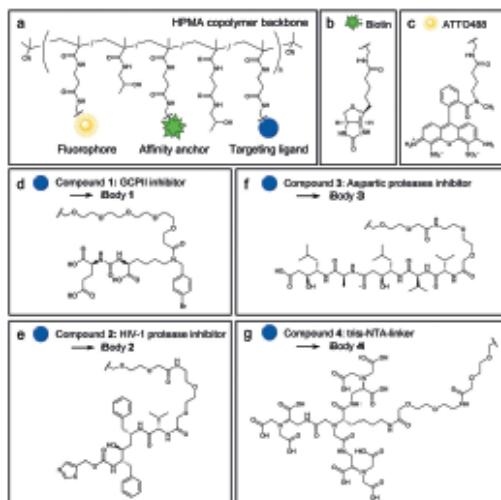Hlavova 8, 12843 Prague 2 (Czech Republic)

Dr. F. Sedlák
First Faculty of Medicine, Charles University
Kateřinská 32, 12108 Prague 2 (Czech Republic)

[+] These authors contributed equally to this work

Supporting information for this article is available on the WWW
under http://dx.doi.org/10.1002/anie.201508642.

Figure 1. Structures of the iBodies and their functional modules. a) HPMA copolymer decorated with functional molecules. b) The affinity anchor biotin. c) ATTO488 fluorophore. d) GCPII inhibitor. e) HIV-1 protease inhibitor. f) A class-specific inhibitor of aspartic proteases. g) A nitrilotriacetic acid (NTA)-based ligand for binding the His-tag.

Table 1: The composition and basic characteristics of the iBodies.

Conjugate (M_n)	Target	No. of inhibitor moieties	No. of ATTO488 units	No. of biotin units	K_i [nM]
iBody 1 (148 800)[a]	GCPII	19	7	51	0.0043 ± 0.0005
iBody 2 (40 600)[b]	HIV-1 protease	6	–	7	7.9 ± 0.5
iBody 3 (42 100)[b]	Aspartic proteases	7	–	9	18.9 ± 0.2[b]
iBody 4 (135 800)[a]	His-tag sequence	12	7	46	3.5 ± 0.1[c]
iBody 5 (108 100)[a]	–	–	6	41	–
iBody 6 (37 800)[b]	–	–	–	8	–

[a] M_n = number-average molecular weight. For full molecular characteristics of the conjugates, see Table S2–S4 and Figure S8 in Supporting Information. [b] K_i value was determined for wild-type HIV-1 protease. [c] For iBody 4, a dissociation constant K_D is shown instead of an inhibition constant K_i.

prostate; its expression is markedly increased in prostate carcinoma.[8]

The polymer conjugate targeting GCPII (iBody 1, Figure S1 in the Supporting Information) contains a tight-binding GCPII inhibitor as a targeting ligand. To avoid steric hindrance between GCPII and the polymer molecules, the previously described inhibitor (called compound **22 a**,[9] Table S1) was modified with a PEG_3 linker to yield compound **1** (Figure 1 d). As a negative control, we prepared the

corresponding conjugate lacking the GCPII inhibitor (iBody 5; Figure S2).

The utility of iBody **1** for the inhibition, binding, and visualization of GCPII was tested with a variety of common biochemical methods in which antibodies are normally used: immunoprecipitation and affinity pull-downs, flow cytometry, immunocytochemistry, and ELISA.

First, we tested whether iBody **1** inhibits the enzymatic activity of GCPII and determined K_i values for compound **1** and iBody **1** (Figure 2 a). Interestingly, attachment of several molecules of compound **1** to the HPMA copolymer led to a significant drop in the K_i value [K_i(compound 1) = 2.0 nM vs. K_i(iBody 1) = 4.3 pM]. This nearly three-order-of-magnitude decrease in K_i can be explained by the synergic effect of several inhibitor molecules on the polymer scaffold and increased local inhibitor concentration (19 inhibitor molecules per polymer chain).

The binding of iBody **1** to GCPII was further evaluated by surface plasmon resonance (SPR), which revealed an extremely high association rate and a low dissociation rate (Figure 2 b). The dissociation constant ($K_D < 20$ pM) is comparable to that of the tightest-binding anti-GCPII antibodies available.

To analyze the utility of iBody **1** for visualizing GCPII-expressing cells, we incubated LNCaP cells (a cell line that endogenously expresses GCPII) and PC3 cells (which do not express GCPII) with iBody **1**. As controls, we used iBody **5** (which lacks a GCPII inhibitor) and a fluorescently labeled anti-GCPII monoclonal antibody 2G7[10] (mAb 2G7-ATTO488). iBody **1** and the anti-GCPII mAb bound specifically to LNCaP cells and not to PC3 cells, while iBody **5** did not bind to either LNCaP or PC3 cells. iBody **1** and the mAb were taken up into the cells through internalization of membrane-embedded GCPII as expected.[11] Additionally, binding of iBody **1** to LNCaP cells was blocked by 2-(phosphonomethyl)pentanedioic acid (2-PMPA), a specific GCPII inhibitor (Figure 2 c).

To analyze the potential use of iBodies in flow cytometry, LNCaP and PC3 cells were first incubated with iBody **1**, iBody **5**, or 2G7-ATTO488[10] and then analyzed by flow cytometry. The results indicate that both iBody **1** and the anti-GCPII mAb specifically recognize GCPII-expressing cells (LNCaP) and enable their separation from GCPII-negative cells (PC3). Moreover, iBody **1** and iBody **5** exhibited very low non-specific binding to PC3 cells, which was approximately 5-fold lower than that of mAb 2G7-ATTO488 (Figure 2 d).

Furthermore, we used iBody **1** to isolate GCPII from cell lysates. iBodies **1** and **5** were immobilized on Streptavidin Sepharose resin, and GCPII was pulled down from LNCaP cell lysate (Figure 2 e). An anti-GCPII mAb (J591[12]) bound to Protein G Sepharose was used as a positive control. As shown by subsequent western blot analysis, the amount of GCPII immunoprecipitated when using iBody **1** was comparable to that obtained with mAb J591. These findings suggest that iBodies could also be useful for the isolation of target proteins from complex biological materials such as tissue lysates or blood samples.

104
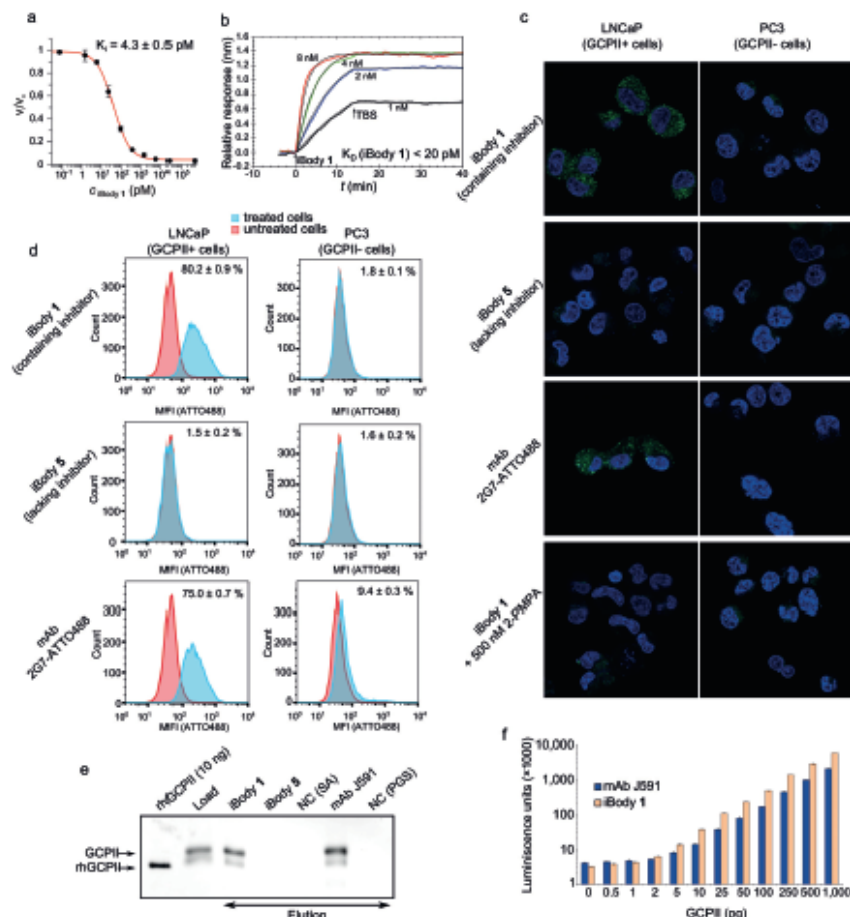
Figure 2. Application of iBody 1, which targets glutamate carboxypeptidase II (GCPII). a) The inhibition potency of iBody 1 in terms of GCPII hydrolytic activity. b) SPR analysis of iBody 1 binding to immobilized GCPII ($K_D < 20$ pM). c) Confocal microscopy of cells positive (LNCaP) and negative (PC3) for GCPII expression. Cells were stained with iBody 1; to compare iBody staining with antibody staining, the anti-GCPII monoclonal antibody (mAb) 2G7[10] labeled with ATTO488 (2G7-ATTO488) was used. Binding of iBody 1 to LNCaP cells can be blocked by using 2-PMPA, a specific GCPII inhibitor. d) Flow cytometry analysis of LNCaP and PC3 cells incubated with iBody 1, iBody 5 (which lacks the targeting module), or 2G7-ATTO488. e) Western blot analysis of affinity isolation of GCPII from LNCaP cell lysate using iBody 1 or the anti-GCPII mAb J591. iBody 5, blank Streptavidin Agarose (NC (SA)), and blank Protein G Sepharose (NC (PGS)) were used as negative controls. rhGCPII is a recombinant extracellular GCPII. Load = LNCaP cell lysate. f) Sandwich ELISA with the anti-GCPII capture mAb 2G7 and either the biotinylated anti-GCPII mAb J591 or iBody 1 used as the detecting agent.

Finally, we used iBodies for the quantitative detection of GCPII. We employed a sandwich ELISA in which the detecting anti-GCPII mAb was replaced with iBody 1. The detection limit was as low as 0.5 pg GCPII; furthermore, the signal was linear over a nearly three-order-of-magnitude concentration range (Figure 2 f).

To demonstrate versatility of iBodies, we also developed iBodies targeting the aspartic proteases HIV-1 and pepsin. HIV-1 protease plays a crucial role in viral replication[13] and a number of specific inhibitors are available. As aspartic

proteases, both HIV-1 protease and pepsin are also efficiently inhibited by the peptidic inhibitor pepstatin A.[14]

The polymer conjugate targeted towards HIV-1 protease (iBody 2; Figure S3) contains compound 2, a specific HIV-1 protease inhibitor derived from the commercially available inhibitor ritonavir (Figure 1e), as a targeting ligand. The analogous iBody 3 (Figure S4) contains compound 3 (Figure 1 f), a derivative of the class-specific aspartic protease inhibitor pepstatin A, as a targeting ligand. As a negative control, we prepared the corresponding conjugate lacking an

105

inhibitor (iBody **6**; Figure S5). We successfully used iBody **2** and iBody **3** to pull down HIV-1 protease from an LNCaP cell lysate spiked with HIV-1 protease (Figure S7a).

Besides HIV-1 protease, another aspartic protease, pepsin, was also successfully pulled down from LNCaP lysate (spiked with pepsin) by using iBody **3** (Figure S7b), thus showing the general applicability of this iBody. In both experiments, iBody **6** (which contains only biotin and no inhibitor) was used as a negative control. This iBody was unable to pull down either HIV-1 protease or pepsin from an LNCaP cell lysate (Figure S7a,b).

Finally, the use of iBodies is not limited to enzymes. Theoretically, iBodies can be designed to target any molecule of interest for which a ligand is known. To demonstrate this general principle, we set out to target proteins containing a polyhistidine tag (His-tag), the most common affinity tag used for protein purification and visualization. Because the His-tag is bound by nickel-loaded nitrilotriacetic acid (NTA) derivatives, we prepared tris-NTA connected to a linker[15] (compound **4**, Figure 1g) and subsequently iBody **4** (Figure S6). iBody **4** was decorated with the fluorophore ATTO488 for visualization and biotin for both visualization and immobilization. As a negative control, iBody **5**, which bears only the fluorophore ATTO488 and biotin, was used.

We compared the sensitivity and specificity of iBody **4** with that of commercially available peroxidase-conjugated anti-polyhistidine antibody by western blot. iBody **4** exhibited slightly increased sensitivity and equal specificity in comparison to the commercial antibody (Figure 3a, b). When using iBody **4**, we detected as little as 100 pg of the His-tagged DNA damage protein 1 (Ddi1-His). Additionally, we specifically pulled down the protein from an *E. coli* lysate (Figure 3c). To quantify the binding, we analyzed the interaction between iBody **4** and Ddi1-His by SPR, which indicated $K_D = 3.5$ nM (Figure 3d).

Our approach has two major advantages. First, the system is remarkably modular: any compound, functional group, or tag for any specific purpose can be added to form the final polymer conjugate. For the targeting of a specific protein with an iBody, simple replacement of the targeting moiety (the inhibitor) is sufficient to yield a new specific polymer conjugate. To some extent, this resembles the concept of molecularly imprinted polymers (MIPs). MIPs rely on lock-and-key interaction with the target, which makes them more suitable for the extraction of target compounds/proteins, even though the targeting of proteins on the cell surface has been reported.[16] Second, the system is truly versatile: a single iBody can be used for several methods, as we have shown for GCPII. One potential limitation of the system is the need for a ligand that specifically binds to the target protein. Moreover, for attachment to the polymer backbone, the ligand must be modified with a linker that does not significantly compromise its binding affinity. Nonetheless, if a potent ligand is known and the attachment of the linker does not lead to a dramatic loss of potency, the preparation of a specific iBody is rather straightforward.

In summary, we have developed inexpensive, stable, and modular synthetic conjugates called iBodies for use as antibody mimetics. The presented data demonstrate that the
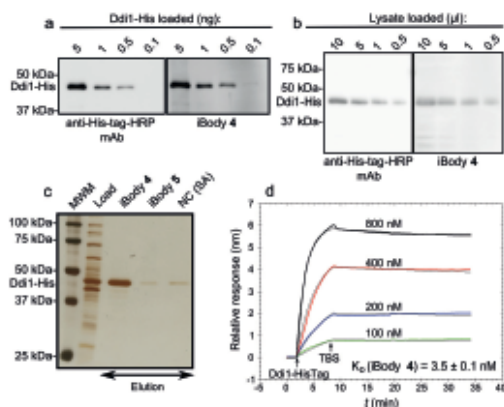
Figure 3. Application of iBody 4, which targets His-tagged proteins. a) Comparison of iBody 4 and anti-polyhistidine antibody sensitivity for the visualization of purified Ddi1-His by western blot. b) Comparison of iBody 4 and the anti-polyhistidine antibody for the visualization of Ddi1-His in a cell lysate by western blot. c) Affinity isolation of Ddi1-His by using iBody 4. iBody 5 (which does not possess the tris-NTA ligand), and blank resin (NC) were used as negative controls. MWM = molecular weight marker. d) Binding of Ddi1-His to immobilized iBody 4 as analyzed by SPR.

prepared iBodies targeting various proteins of interest are efficient substitutes for the corresponding antibodies in standard immunochemical methods. Overall, iBodies offer an inexpensive, non-animal-based alternative for antibodies in biochemical methods involving the isolation and visualization of proteins, cells, and tissues.

[1] K. Nord, E. Gunneriusson, J. Ringdahl, S. Stahl, M. Uhlen, P. A. Nygren, *Nat. Biotechnol.* **1997**, *15*, 772.

[2] H. K. Binz, M. T. Stumpp, P. Forrer, P. Amstutz, A. Pluckthun, *J. Mol. Biol.* **2003**, *332*, 489.

[3] A. D. Ellington, J. W. Szostak, *Nature* **1990**, *346*, 818.

[4] P. J. McEnaney, K. J. Fitzgerald, A. X. Zhang, E. F. Douglass, Jr., W. Shan, A. Balog, M. D. Kolesnikova, D. A. Spiegel, *J. Am. Chem. Soc.* **2014**, *136*, 18034.

106

[5] a) Y. Hoshino, H. Koide, T. Urakami, H. Kanazawa, T. Kodama, N. Oku, K. J. Shea, *J. Am. Chem. Soc.* **2010**, *132*, 6644; b) G. Wulff, *Angew. Chem. Int. Ed. Engl.* **1995**, *34*, 1812; *Angew. Chem.* **1995**, *107*, 1958.

[6] a) R. Haag, F. Kratz, *Angew. Chem. Int. Ed.* **2006**, *45*, 1198; *Angew. Chem.* **2006**, *118*, 1218; b) J. Kopeček, P. Kopečková, *Adv. Drug Delivery Rev.* **2010**, *62*, 122.

[7] V. Šubr, L. Kostka, J. Strohalm, T. Etrych, K. Ulbrich, *Macromolecules* **2013**, *46*, 2100.

[8] a) R. G. Lapidus, C. W. Tiffany, J. T. Isaacs, B. S. Slusher, *Prostate* **2000**, *45*, 350; b) M. B. Robinson, R. D. Blakely, R. Couto, J. T. Coyle, *J. Biol. Chem.* **1987**, *262*, 14498.

[9] J. Tykvart, J. Schimer, J. Barinkova, P. Pachl, L. Postova-Slavetinska, P. Majer, J. Konvalinka, P. Sacha, *Bioorg. Med. Chem.* **2014**, *22*, 4099.

[10] T. Knedlik, V. Navratil, V. Vik, D. Pacik, P. Sacha, J. Konvalinka, *Prostate* **2014**, *74*, 768.

[11] H. Liu, A. K. Rajasekaran, P. Moy, Y. Xia, S. Kim, V. Navarro, R. Rahmati, N. H. Bander, *Cancer Res.* **1998**, *58*, 4055.

[12] H. Liu, P. Moy, S. Kim, Y. Xia, A. Rajasekaran, V. Navarro, B. Knudsen, N. H. Bander, *Cancer Res.* **1997**, *57*, 3629.

[13] H. G. Krausslich, R. H. Ingraham, M. T. Skoog, E. Wimmer, P. V. Pallai, C. A. Carter, *Proc. Natl. Acad. Sci. USA* **1989**, *86*, 807.

[14] J. Eder, U. Hommel, F. Cumin, B. Martoglio, B. Gerhartz, *Curr. Pharm. Des.* **2007**, *13*, 271.

[15] Z. Huang, P. Hwang, D. S. Watson, L. Cao, F. C. Szoka, Jr., *Bioconjugate Chem.* **2009**, *20*, 1667.

[16] a) Y. Ma, G. Q. Pan, Y. Zhang, X. Z. Guo, H. Q. Zhang, *Angew. Chem. Int. Ed.* **2013**, *52*, 1511; *Angew. Chem.* **2013**, *125*, 1551; b) S. Shinde, Z. El-Schich, A. Malakpour, W. Wan, N. Dizeyi, R. Mohammadi, K. Rurack, A. Gjorloff Wingren, B. Sellergren, *J. Am. Chem. Soc.* **2015**, *137*, 13908.

Supporting Information

iBodies: Modular Synthetic Antibody Mimetics Based on Hydrophilic Polymers Decorated with Functional Moieties

Pavel Šácha⁺, Tomáš Knedlík⁺, Jiří Schimer, Jan Tykvart, Jan Parolek, Václav Navrátil, Petra Dvořáková, František Sedlák, Karel Ulbrich, Jiří Strohalm, Pavel Majer, Vladimír Šubr,* and Jan Konvalinka*
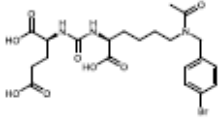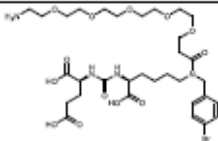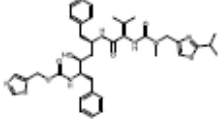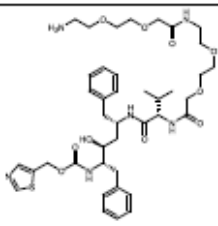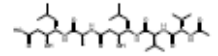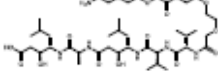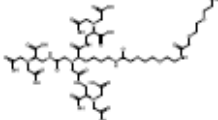
anie_201508642_sm_miscellaneous_information.pdf

Titles of Supporting Information

Supplementary Table S1

Summary of low-molecular-weight compounds.

Name	M_r	Formula	Targeting	K_i [pM]	Modification
compound 22a[1]	530		GCPII	45 ± 5.7[1]	-
compound 1	780		GCPII	$2,030 \pm 430$	PEG linker
ritonavir	721		HIV-1 protease	15 ± 2[2]	-
compound 2	815		HIV-1 protease	12 ± 1	PEG linker
acetyl-pepstatin	644		aspartic proteases	$116,000 \pm 5,000$[2]*	-
compound 3	892		aspartic proteases	$623,000 \pm 1,710$*	PEG linker
compound 4	1,159		His-tag sequence	ND	PEG linker

* K_i values were determined for wild-type HIV-1 protease.

2

110

Supplementary Table S2

The composition and full characteristics of the prepared iBodies

Conjugate	M_n (precursor)	Đ (precursor)	M_w (precursor)	M_n (conjugate)	Đ (conjugate)	M_w (conjugate)	Inhibitor (wt%)	ATTO488 (wt%)	Biotin (wt%)
iBody 1	79,000	1.20	94,600	148,800	1.37	203,900	9.8 %	3.9 %	9.8 %
iBody 2	24,800	1.08	26,700	40,600	1.65	67,000	11.7 %	-	4.7 %
iBody 3	24,800	1.08	26,700	42,100	1.32	55,500	15.3 %	-	5.9 %
iBody 4	73,800	1.23	90,600	135,800	1.88	255,000	11.3 %	4.2 %	9.7 %
iBody 5	79,000	1.20	94,600	108,100	1.63	176,200	-	5.1 %	10.8 %
iBody 6	24,800	1.08	26,700	37,800	1.53	57,800	-	-	6.4 %

* M_w: weight-average molecular weight; M_n: number-average molecular weight; Đ: dispersity

3

Supplementary Table S3

Composition of iBodies determined by analytical methods

#		iBody 1	iBody 2	iBody 3	iBody 4	iBody 5	iBody 6
1	ATTO488 (wt%)	3.9	-	-	4.2	5.1	-
2	Biotin (wt%)	9.8	4.7	5.9	9.7	10.8	6.4
3	Targeting ligand (wt%)	9.8	11.7	15.3	11.3	-	-
4	No. of ATTO488 units	7	-	-	7	6	-
5	No. of biotin units	51	7	9	46	41	8
6	No. of targeting ligand units	19	6	7	12	-	-
7	Normalized ATTO488 content	1.0	-	-	1.0	1.0	-
8	Normalized biotin content	7.5	1.1	1.2	6.9	6.4	1.0
9	Normalized targeting ligand content	2.8	1.0	1.0	1.8	-	-

To find out whether the aminolytic reaction follows the statistical course, we calculated the composition of the iBodies by analytical methods and compared this to the theoretical composition of the iBodies calculated from the reaction stoichiometry. The values (in red) of the corresponding parameters correlate well, thus proving that the reaction proceeds statistically. The composition of iBodies, as determined by analytical methods (described in the Supporting Information, p. 29). Lines 1-3 represent mass fraction (wt%) of the individual moieties (ATTO488, biotin, targeting ligand). Lines 4-6 represent the number of units (ATTO488, biotin, targeting ligand) per conjugate. Lines 7-9 represent the ratios between the moieties. Ratios were normalized to the lowest-incorporated moiety.

Supplementary Table S4

Theoretical composition of iBodies calculated from the reaction stoichiometry

| #		iBody 1	iBody 2	iBody 3	iBody 4	iBody 5	iBody 6
1	m (ATTO488; mg)	2.5	-	-	2.5	2.5	-
2	m (biotin; mg)	5.0	6.0	6.0	5.0	5.0	5.0
3	m (targeting ligand; mg)	6.2	13.0	10.0	6.0	-	-
4	n (ATTO488; μmol)	2.9	-	-	2.9	2.9	-
5	n (biotin; μmol)	17.5	20.9	20.9	17.5	17.5	17.5
6	n (targeting ligand; μmol)	8.0	16.0	11.2	4.7	-	-
7	$n_{norm.}$ (ATTO488; μmol)	1.0	-	-	1.0	1.0	-
8	$n_{norm.}$ (biotin; μmol)	6.0	1.3	1.9	6.0	6.0	1.0
9	$n_{norm.}$ (targeting ligand; μmol)	2.7	1.0	1.0	1.6	-	-

The theoretical composition of iBodies, as calculated from the reaction stoichiometry (described in the Supporting Information, p. 28-33). Lines 1-3 represent the masses of the individual moieties (ATTO488, biotin, targeting ligand) expected to be incorporated into the iBodies. Lines 4-6 represent the moles of each moiety expected to be incorporated into the iBodies. Lines 7-9 represent the ratios between the molar amounts, normalized to the lowest-incorporated moeity.
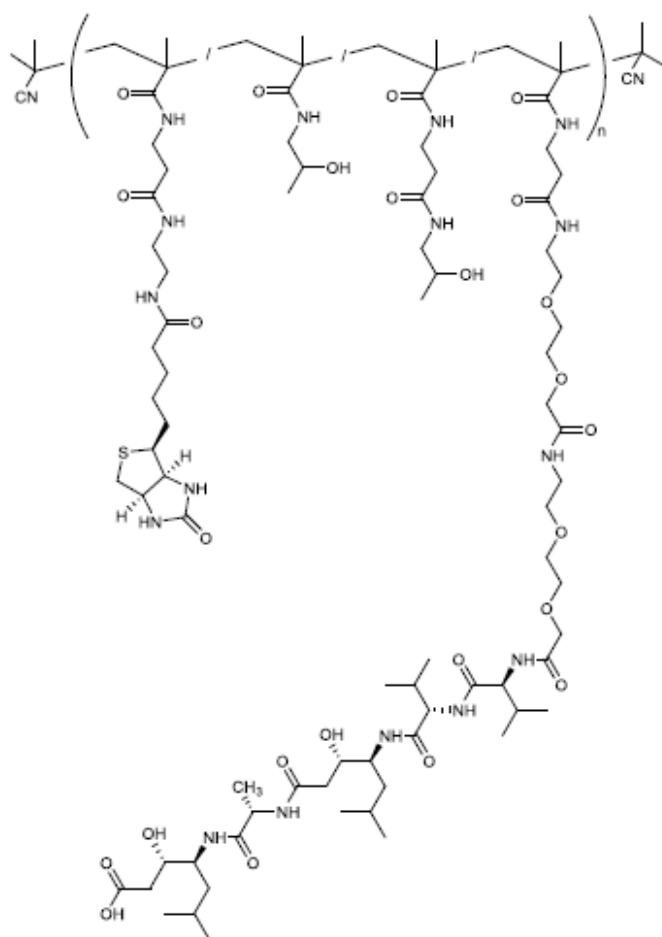
4

Supplementary Figure S1
Structure of iBody 1 targeting GCPII.
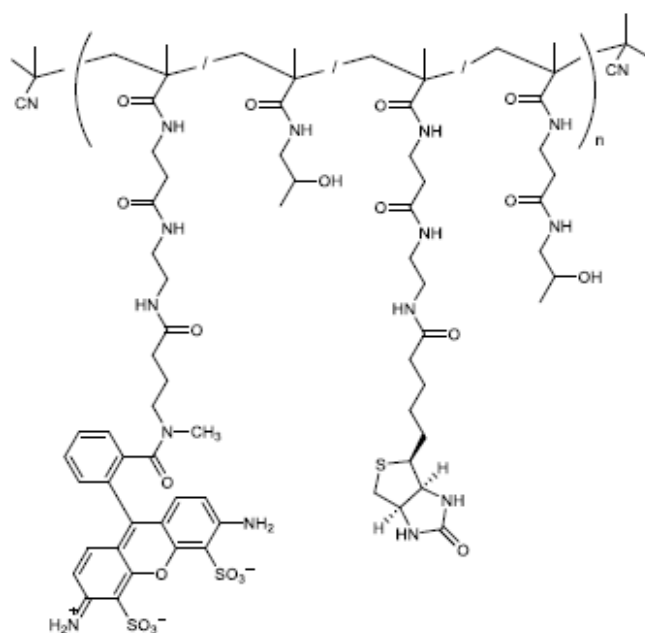
Supplementary Figure S2
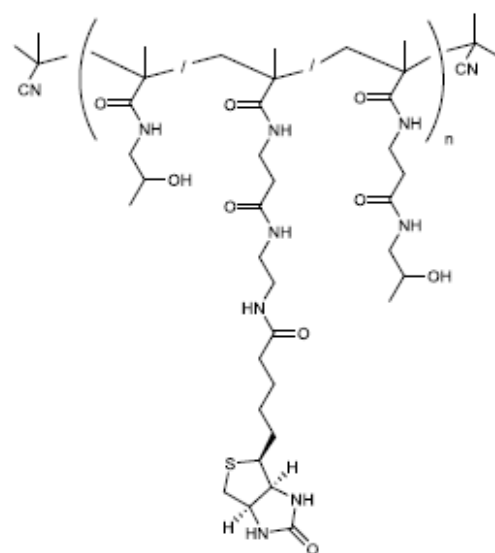Structure of iBody 5 used as a negative control.

6
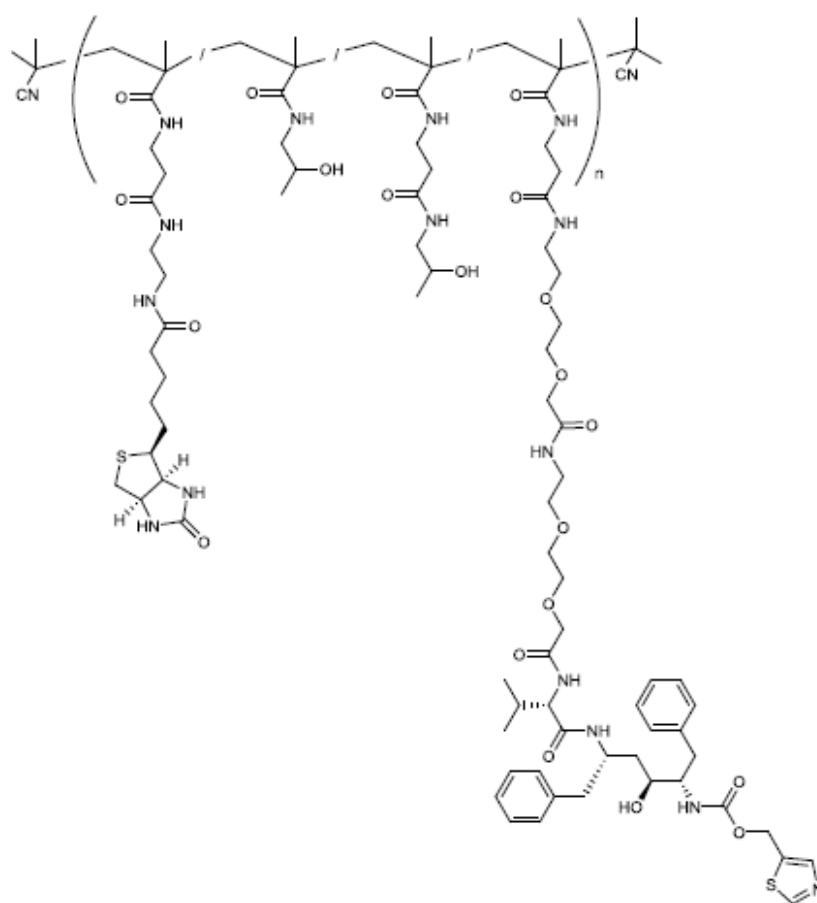
Supplementary Figure S3
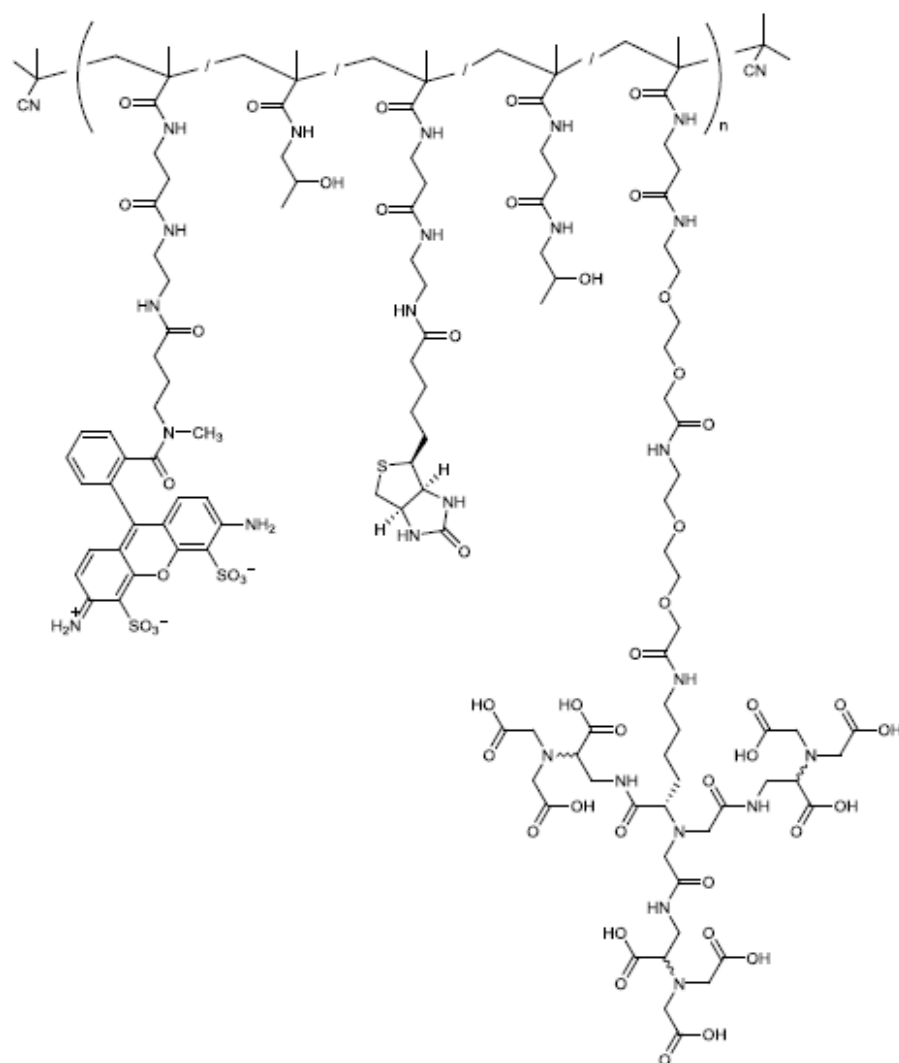Structure of iBody **2** targeting HIV-1 protease.

7

Supplementary Figure S4
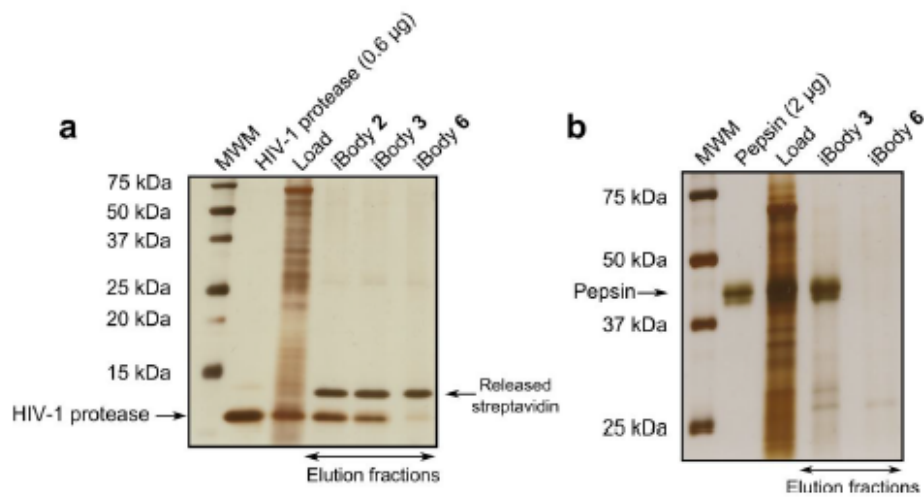Structure of iBody 3 targeting aspartic proteases.

Supplementary Figure S5

Structure of iBody 6 used as a negative control.

9

Supplementary Figure S6
Structure of iBody 4 targeting His-tagged proteins.

10

Supplementary Figure S7

iBodies targeting HIV-1 protease and aspartic proteases (pepsin). a) Affinity isolation of HIV-1 protease from the HIV-1 protease-spiked LNCaP cell lysate using iBody **2** and iBody **3**; iBody **6** lacking the targeting ligand was used as a negative control. b) Affinity isolation of pepsin from the pepsin-spiked cell lysate using iBody **3**; as a negative control, iBody **6** was used.

Supplementary methods
HPLC-based GCPII inhibition assay

The inhibitory effects of all inhibitors and iBodies targeting GCPII were tested using an HPLC-based assay with recombinant extracellular GCPII, as described previously[1]. The data were processed and IC_{50} values were obtained using GraFit v.5.0.11 (Erithacus Software Ltd.).

From the kinetic parameters of pteroyl-di-L-glutamate cleavage and by assuming a competitive mode of inhibition, the K_i value was calculated using the Cheng-Prusoff equation[3]. Measurements were performed in duplicate; the Ki values are presented as the mean ± standard deviation.

Pull-down/immunoprecipitation of GCPII from LNCaP lysate

LNCaP cells endogenously expressing GCPII were lysed by sonication in 50 mM Tris-HCl, pH 7.4, 150 mM NaCl, 1 % Tween 20. The resulting cell lysate was diluted in 20 mM Tris-HCl, pH 7.4, 150 mM NaCl, 0.1 % Tween 20 (TBST) to a final protein concentration of 2 mg/ml.

First, 200 μl of 30 nM iBody 1 and 5 in TBST were bound onto 30 μl Streptavidin Agarose Ultra Performance (Solulink) for 30 min at room temperature. After washing with TBST (3×1,000 μl), the resin was mixed with 200 μl of the LNCaP lysate and incubated for 1 h at room temperature. The resin was then washed with TBST (5×1,000 μl). Finally, proteins were eluted from Streptavidin Agarose by adding 30 μl of reducing SDS sample buffer and heating to 98 °C for 10 min.

To compare iBodies with antibodies, an analogous immunoprecipitation experiment with the monoclonal antibody J591[4] was performed. First, 200 μl of 30 nM J591 was bound to 30 μl Protein G Sepharose (GE Healthcare), washed with TBST, and mixed with LNCaP lysate. After incubation, the resin was washed with TBST, and proteins were eluted with reducing SDS sample buffer and heating.

Isolated GCPII was visualized on Western blot using mAb GCP-04, followed by goat anti-mouse secondary antibody conjugated with horseradish peroxidase. 10 μl of the sample was loaded into each lane.

12

Quantitative detection of GCPII using ELISA

When iBody 1 was used in place of the detecting antibody, a 96-well Maxisorb plate (Nunc) was coated with the GCPII-specific mouse antibody 2G7[5] in borate buffer (500 ng/well; 1 h at RT). The surface was blocked with 1.1 % (w/v) casein solution in TBS (Casein Buffer 20X-4X Concentrate, SDT). Afterwards, recombinant extracellular GCPII in TBST was added (ranging from 0.5 pg – 1 ng/well) and, after washing with TBST (3×200 μl), 500 pM iBody 1 or biotinylated anti-GCPII mAb J591 in TBST was added to bind GCPII. After washing out the unbound conjugate (3×200 μl TBST), NeutrAvidin conjugated with horseradish peroxidase was added (50 ng/well; Thermo Scientific), followed by a final TBST wash (5×200 μl) and measurement of 4-iodophenol-enhanced luminol chemiluminescence on a Tecan Infinite M1000 PRO spectrophotometric reader. Measurement of each sample was performed in triplicate; values are presented as the mean ± standard deviation.

Confocal microscopy of fluorescently labeled cells

LNCaP and PC3 cells were grown in 4-Chamber 35 mm Glass Bottom Dishes (In Vitro Scientific). LNCaP cells (which endogenously express GCPII) were grown in RPMI-1640 medium (Sigma-Aldrich) with addition of FBS (final concentration of 10 %), while PC3 cells (which do not express GCPII) were grown in DMEM-High Glucose medium (GE Healthcare) with addition of L-glutamine (final concentration of 4 mM) and FBS (final concentration of 10 %).

After two days, iBody solution was added to the media to a final concentration of 10 nM. If desirable, 2-(phosphonomethyl)pentanedioic acid (2-PMPA) was added to a final concentration of 500 nM. As a control, fluorescently labeled anti-GCPII monoclonal antibody 2G7[5] (2G7-ATTO488) was added to a final concentration of 100 nM. The cells were incubated in the presence of iBodies for 2 h at 37 °C. Then, the media were removed, a 0.5 μg/ml solution of Hoechst Stain Solution H34580 (Sigma) in PBS was added, and cells were incubated for 10 min at 37 °C to stain cell nuclei. Finally, the cells were washed twice with 500 μl PBS.

Confocal images (pinhole 1 Airy unit) of cells in each chamber were taken with a Zeiss LSM 780 confocal microscope (Carl Zeiss Microscopy) using an oil-immersion objective (Plan-Apochromat 63x/1.40 Oil DIC M27). The fluorescent images were collected at room temperature using 4.5 % of the 405 nm diode laser (max. power 30 mW) for excitation with emission collected from 410 to 585 nm (voltage on detector: 850 V) for Hoechst 34580 and 4.0 % of the 488 nm argon-ion laser (max. power 25 mW) for excitation

13

with emission collected from 517 to 534 nm (voltage on detector: 870 V) for ATTO488. All images were taken using the same settings. The microscope was operated and the images were processed with ZEN 2011 software (Carl Zeiss Microscopy).

Quantification of iBody binding to GCPII by surface plasmon resonance (SPR)

All SPR measurements were performed at 25 °C according to a previously described protocol[1, 6]. In a typical experiment, a 7:3 mixture of HS-$(CH_2)_{11}$-PEG_4-OH and HS-$(CH_2)_{11}$-PEG_6-O-CH_2-COOH alkanethiols (Prochimia) at a final concentration of 0.2 mM was incubated with an SPR chip (provided by the Institute of Photonics and Electronics, Prague) for 1 h at 37 °C. The chip was then washed with UV ethanol and deionized water and dried with a flow of nitrogen gas. Finally, the chip was mounted to the prism on the SPR sensor.

Activation of carboxylic terminal groups on the sensor surface was performed *in situ* by injecting a 1:1 mixture of 11.51 mg/ml *N*-hydroxysuccinimide (NHS) and 76.68 mg/mL 1-ethyl-3-(3-dimethylaminopropyl)-carbodiimide hydrochloride (EDC) in deionized water (Biacore) for 5 min at a flow rate of 20 µl/min. The next part of the experiment was performed at a flow rate of 30 µl/min. Then, a mixture of the antibody D2B[7], which recognizes native GCPII (20 ng/µl), and BSA (20 ng/µl) in 10 mM sodium acetate, pH 5.0, was loaded for 8 min. Next, a high ionic strength solution (PBS with 0.5 M NaCl) was used to wash out noncovalently bound molecules, followed by addition of 1 M ethanolamine (Sigma-Aldrich) for deactivation of residual activated carboxylic groups.

An 8 ng/µl solution of recombinant extracellular GCPII in TBS (Avi-GCPII[8]) was used for Avi-GCPII immobilization onto the D2B/BSA layer on the golden chip to saturate all binding sites. Finally, at a flow rate of 60 µl/min, 4 different concentrations (1, 2, 4, and 8 nM) of iBody 1 in TBS were applied for approximately 10 min (association), followed by injection of TBS alone (dissociation).

Kinetic curves of binding were exported and subsequently fitted using the One-To-One interaction model in TraceDrawer v.1.5 (Ridgeview Instruments AB) to obtain k_{on} and k_{off} parameters.

SDS-PAGE and Western blotting

Protein samples were resolved by SDS-PAGE, and gels were electroblotted onto a nitrocellulose or PVDF membrane (wet blotting: 100 V/1 h). Membranes were blocked with 1.1 % (w/v) casein solution in PBS (Casein Buffer 20X-4X Concentrate, SDT) at room temperature for 1 h. Afterwards, the blots were incubated with the primary antibody GCP-

14

04[9] at 4 °C for 12 h (200 ng/ml; diluted in 0.55 % casein solution), washed three times with PBS containing 0.05 % Tween 20 (PBST), and incubated with goat anti-mouse secondary antibody conjugated with horseradish peroxidase (Thermo Scientific; diluted 1:25,000 in 0.55 % casein solution). For polyhistidine sequence (His-tag) detection, either anti-polyhistidine-peroxidase antibody (Sigma Aldrich, #A7058-1VL) (1:2,000 dilution in PBST) or iBody 4 (5 nM in PBST, loaded with nickel ions) followed by NeutrAvidin-HRP conjugate (dilution 1:2,000 in PBST) was used.

Finally, the blots were washed three times with PBST to remove free antibodies, and SuperSignal West Dura/Femto Chemiluminescent Substrate (Thermo Scientific) was applied. Chemiluminiscence was captured with a ChemiDoc-It™ 600 Imaging System (UVP).

Preparation of a fluorescently labeled anti-GCPII monoclonal antibody 2G7 (2G7-ATTO488)

An antibody against human native GCPII (2G7[5]) was labeled with a fluorophore ATTO488 using ATTO488 NHS ester (Sigma Aldrich, #41698). First, 77 µl of a 2.5 mg/ml solution of the antibody 2G7 in PBS was mixed with 8.6 µl of 100 mM bicarbonate buffer, pH 8.3. ATTO488 NHS ester was dissolved in dry DMSO at 10 mg/ml. Afterwards, 1 µl of the ATTO488 NHS ester solution was mixed with the antibody solution and incubated for 1 h at room temperature. Finally, the fluorophore-antibody conjugate (2G7-ATTO488) was separated from the free fluorophore by gel permeation chromatography using Sephadex G-25 column. Fractions containing 2G7-ATTO488 were pooled and concentrated using Amicon Ultra 30 kDa centrifugal filter (Millipore).

Flow cytometry

PC3 and LNCaP cell lines were grown on a 100 mm dish to 90 % confluence in DMEM and RPMI medium, respectively; both supplemented with 10 % FBS and 4 mM L-glutamine. The medium was removed, and cells were rinsed with PBS and subsequently incubated in 1.5 ml trypsin/EDTA solution for 3 min to release adherent cells from the dish surface. Cells were resuspended and transferred into 8 ml of DMEM or RPMI medium, centrifuged at 250×g for 2 min, and washed with 5 ml PBS. Then, 500 µl of 10 % fetal bovine serum in PBS was added to block the cell surface. The final concentration of the cell suspension was 4×10^6 cells/ml.

Afterwards, 50 µl of cell suspension (containing 2×10^5 cells) was placed into wells of a polypropylene 96-well plate (round bottom) and incubated with 10 nM solutions of iBodies

15

and 400 nM 2G7-ATTO488 for 1 h at 37 °C. Cells were washed twice with 200 µl of 10 % fetal bovine serum in PBS. Finally, the cell suspension was diluted with 200 µl of 10 % fetal bovine serum in PBS, and a single cell suspension was analyzed with a BD LSR Fortessa™ cell analyzer (Becton, Dickinson and Company).

The gates on the side scatter and forward scatter were set to ensure measurement of viable cells, and 10,000 events were measured for each well. All experiments (all staining agents and both cell lines) were performed in triplicates. Analysis was performed using BD FACSDiva™ Software. A histogram showing a representative measurement for each sample is presented. The number in the top corner of each histogram represents the percentage of the treated cell population having a higher MFI signal than the highest 1 % of the untreated cell population. The number was calculated for each measurement and is shown as the mean ± standard deviation.

Inhibition of HIV-1 protease activity with inhibitors and iBodies

The inhibition analyses were performed by spectrophotometric assay using the chromogenic peptide substrate KARVNle*NphEANle-NH$_2$ as previously described[10].

The 1 ml reaction mixture contained 100 mM sodium acetate, 300 mM NaCl, pH 4.7, 6.8 pmol of HIV-1 protease[10] and inhibitor in concentrations ranging between 2 and 130 nM. Substrate was added to a final concentration of 16 µM. Afterwards, the hydrolysis of substrate was followed as a decrease in absorbance at 305 nm using a UNICAM UV500 UV–VIS spectrophotometer (Thermo, Cambridge, MA). The data were analyzed using the equation for competitive inhibition according to Williams and Morrison[11]. The mechanism of inhibition was determined by analysis of Lineweaver-Burk plots.

Pull-down of HIV-1 protease from spiked LNCaP lysate

LNCaP cells grown on two 100 mm Petri dishes were lysed by sonication (3×5 min, in water bath) in 2 ml of 50 mM Tris-HCl, 150 mM NaCl, 1 % Tween 20, pH 7.4.

First, 200 nM iBody **2** or **3** in 20 mM Tris-HCl, 150 mM NaCl, 0.1 % Tween 20, pH 7.4, was bound to 30 µl Streptavidin Agarose Ultra Performance (Solulink) at room temperature for 1 h. iBody **6**, which lacks the targeting ligand, was used as a negative control. To block unoccupied biotin binding sites, the resin was incubated with 1 ml of 2 mM biotin, 20 mM Tris-HCl, 150 mM NaCl, pH 7.4. Then, the resin was washed three times with 1 ml of 100 mM sodium acetate, 300 mM NaCl, 0.1 % Tween 20, pH 4.7. The washed resin was mixed with 200 µl of LNCaP cell lysate spiked with HIV-1 protease[10] (12 ng/µl, total protein

16

124

concentration 1 mg/ml) in 100 mM sodium acetate, 300 mM NaCl, 0.1 % Tween 20, pH 4.7, and incubated for 30 min at room temperature. The resin was washed four times with 1 ml of 100 mM sodium acetate, 300 mM NaCl, 0.1 % Tween 20, pH 4.7. Finally, bound HIV-1 protease was eluted from Streptavidin Agarose by adding 30 µl reducing SDS sample buffer and heating to 98 °C for 10 min. Ten microliters of the samples was loaded onto the gel.

Pull-down of pepsin from spiked LNCaP lysate

The experiment was performed analogously to the above described pull-down of HIV-1 protease.

200 nM iBody 3 was bound to 30 µl Streptavidin Agarose (Solulink) at room temperature for 1 h; iBody 6 lacking the targeting ligand was used as a negative control. Biotin binding sites were blocked with biotin and after washing with the acetate buffer, the resin was mixed with LNCaP cell lysate spiked with pepsin (100 ng/µl, Worthington Biochemical Corporation; total protein concentration 1.5 mg/ml) in 100 mM sodium acetate, 300 mM NaCl, 0.1 % Tween 20, pH 4.7, and incubated for 5 min at room temperature. The resin was washed with the acetate buffer and bound pepsin was eluted from Streptavidin Agarose by adding 30 µl reducing SDS sample buffer and heating to 98 °C for 10 min. 5 µl of the samples was loaded onto the gel.

Expression and purification of His-tagged DNA damage protein 1

DNA coding for full-length DNA-damage protein 1 (Ddi1) of *Leishmania major* was synthesized by GenScript and subcloned into pET16b vector for N-terminal hexahistidine tagged fusion protein production (Ddi1-HisTag). Ddi1-HisTag was expressed in *E. coli* BL21(DE3)RIL host cells, subsequently resuspended in 50 mM Tris-HCl, 50 mM NaCl, 1 mM EDTA, pH 8.0 and lysed by three passages through EmulsiFlex-C3 high pressure homogenizer (Avestin, Canada) at 1200 bar. Purification was performed using nickel affinity chromatography using Ni-NTA Superflow resin (Qiagen) with isocratic elution with 250 mM imidazole. Afterwards, pooled elution fractions were dialyzed overnight against 50 mM HEPES, pH 7.4, 150 mM NaCl, 10 % glycerol. The dialyzed sample was applied onto a size-exclusion chromatography column HiLoad 16/60 Superdex 200 (GE Healthcare). Individual fractions were analyzed by SDS-PAGE and fractions containing Ddi1-HisTag were pooled, aliquoted and storred at -80 °C until further use.

17

Quantification of iBody binding to Ddi1-HisTag by surface plasmon resonance (SPR)

The experiment was performed analogously to quantitation of iBody 1 binding to GCPII.

Activation of carboxylic terminal groups on the sensor surface was performed *in situ* by injecting a 1:1 mixture of 11.51 mg/ml *N*-hydroxysuccinimide (NHS) and 76.68 mg/mL 1-ethyl-3-(3-dimethylaminopropyl)-carbodiimide hydrochloride (EDC) in deionized water (Biacore) for 5 min at a flow rate of 20 µl/min. The next part of the experiment was performed at a flow rate of 30 µl/min. Then, a 20 ng/µl solution of NeutrAvidin (Thermo Scientific) in 10 mM sodium acetate, pH 5.0, was loaded for 8 min. Next, a high ionic strength solution (PBS with 0.5 M NaCl) was used to wash out noncovalently bound molecules, followed by addition of 1 M ethanolamine (Sigma-Aldrich) for deactivation of residual activated carboxylic groups. Afterwards, 1 µM solution of iBody 4 in TBS was used for iBody 4 immobilization onto the NeutrAvidin layer; the bound iBody 4 was subsequently charged with nickel ions using 100 mM NiCl$_2$. Finally, four different concentrations of Ddi1-HisTag (100, 200, 400 and 800 nM) in 50 mM HEPES, 150 mM NaCl, pH 7.4 were applied for approximately 10 min (association), followed by injection of the HEPES buffer alone (dissociation).

Kinetic curves of binding were exported and subsequently fitted using the One-To-One interaction model in TraceDrawer v.1.5 (Ridgeview Instruments AB) to obtain k_{on} and k_{off} parameters.

Pull-down of Ddi1-HisTag from an *E. coli* lysate

200 nM iBody 4 in 20 mM Tris-HCl, 150 mM NaCl, 2 mM NiCl$_2$, 0.1 % Tween 20, pH 7.4 was bound to 30 µl Streptavidin Agarose (Solulink) at room temperature for 1 h. iBody 5 lacking the targeting ligand and blank Streptavidin Agarose were used as negative controls. To block biotin binding sites, the resin was then incubated with 1 ml of 2 mM biotin, 100 mM Tris-HCl, 150 mM NaCl, pH 7.2. Afterwards, the resin was washed three times with 1 ml of 20 mM Tris-HCl, 150 mM NaCl, 0.1 % Tween 20, pH 7.4 (TBST). The resin was then mixed with 1 ml of Ddi1-HisTag *E. coli* lysate (diluted in TBST to final protein concetration of 325 ng/µl), and incubated at room temperature for 1 h. The resin was washed five times with 1 ml of 25 mM imidazol in TBST. Bound proteins were eluted from Streptavidin Agarose by adding 30 µl 1 M imidazol in 20 mM Tris-HCl, 150 mM NaCl, pH 7.4), and incubated for 15 min at 37 °C.

18

Inductively coupled plasma atomic emission spectroscopy (ICP-OES)

The ICP-OES measurements were performed with the SPECTRO ARCOS optical emission spectrometer (SPECTRO Analytical Instruments, Kleve, Germany) with radial plasma observation. The SPECTRO ARCOS features a Paschen-Runge spectrometer mount; the wavelength range between 130 and 770 nm can be analyzed simultaneously. An air-cooled ICP-generator, based on a free-running 27.12 MHz system, is installed. For sample introduction, a Modified-Lichte nebulizer with a cyclonic spray chamber was used.

For calibration, commercially available Br and S standard solutions (Analytika) were used. 0.5 % (v/v) Triton X-100 and 2 % HNO_3 solution were used for organic matrix matching strategy and improvement of LOD. Before analysis, the analyzed polymer conjugate solutions were diluted with 0.5 % Triton X-100 solution, as well as all calibration standard solutions. All used chemicals were suprapur quality. All calibrations and sample solutions were prepared or controlled by weighing on an analytical balance. Calibration solutions with concentration 0.2, 1.0, 2.0, 5.0, and 10.0 mg/kg and blank solution Br and S were prepared. For organic matrix background structure compensation the Spectro-SmartBg function was used.

Each sample aliquot (200 – 400 μl) was weighted on analytical balance and then diluted with 0.5 % Triton X-100 and 2 % HNO_3 solution to 5 ml (weight controlled), mixed and then analyzed via the described method. Then the concentrations of original samples were calculated.

Calibration parameters:

| Element line	LOD (mg/kg)	Corr. Coefficient
Br 148.845	0.018	0.9996
Br 153.174	0.060	0.9994
Br 154.065	0.024	0.9996
S 142.731	0.121	0.9998
S 180.731	0.004	0.9998
S 182.034	0.003	0.9999

19

Synthesis of low-molecular-weight compounds

All chemicals were purchased from Sigma-Aldrich, unless stated otherwise. All inhibitors tested in the biological assays were purified using preparative scale HPLC Waters Delta 600 (flow rate 7 ml/min, gradient shown for each compound - including RT), with column Waters SunFire C18 OBD Prep Column, 5 μm, 19×150 mm. The purity of compounds was tested on analytical Jasco PU-1580 HPLC (flow rate 1 ml/min, invariable gradient 2-100 % ACN in 30 minutes, R_T shown for each compound) with column Watrex C18 Analytical Column, 5 μm, 250×5 mm. The final inhibitors were all at least of 99 % purity. Structure was further confirmed by HRMS at LTQ Orbitrap XL (Thermo Fisher Scientific) and by NMR (Bruker Avance I™ 500 MHz equipped with Cryoprobe). All interaction constants are in Hertz units.

Synthesis of compound 1

Compound 1 was synthesized according to the scheme depicted below:

a) NaBH₃CN, MeOH + 1%AcOH
b) 1)TBTU, DIEA, DMF; 2)TFA

20
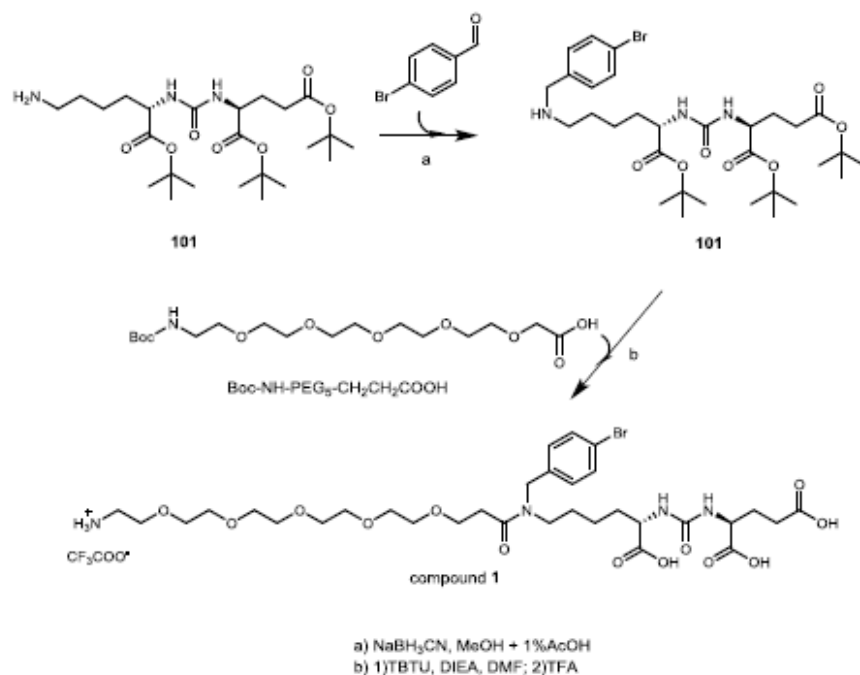
Compound 102:

Di-tert-butyl 2-(3-(6-((4-bromobenzyl)amino)-1-(tert-butoxy)-1-oxohexan-2-yl)ureido)pentanedioate, compound 102: 300 mg (0.615 mmol, 1.0 eq) of di-tert-butyl 2-(3-(6-amino-1-(tert-butoxy)-1-oxohexan-2-yl)ureido)pentanedioate (compound 101, prepared as described in Murelli *et al.*[12]) and 120 mg (0.646 mmol, 1.05 eq) of 4-bromobenzaldehyde was dissolved in 5 ml of methanol in a round-bottom flask. 50 µl of glacial acetic acid was added and, upon fast stirring, 120 mg (1.85 mmol, 3.0 eq) of sodium cyanoborohydride was added in one portion. After 12 hours, the reaction mixture was quenched by addition of 10 ml of water. The reaction mixture was further diluted after 10 minutes by 50 ml of water and was extracted 3 times by EtOAc (3×25 ml). The organic phase was dried and evaporated and crude product was purified by chromatography on silica (mobile phase: EtOAc + 1 % of saturated ammonia in water, TLC rf = 0.55). 395 mg of pure product was isolated (yield = 48 %). Analytical HPLC (grad 2-100 %, 30 min) R_T = 23.4 min. HRMS (ESI+): calculated for $C_{31}H_{51}O_7N_3Br$ $[M]^+$ 656.29049. Found 656.29062. ^{1}H NMR (500 MHz, DMSO-d6): 7.47 (m, 2H, *m*-Ph), 7.27 (m, 2H, *o*-Ph), 6.29 (d, 1H, J = 8.5, HN-Glu-2), 6.24 (d, 1H, J = 8.4, HN-Lys-2), 4.02 (btd, 1H, J^1 = 8.6, J^2 = 5.1, Glu-2), 3.96 (td, 1H, J^1 = 8.1, J^2 = 5.4, Lys-2), 3.62 (s, 2H, **CH₂-Ph**), 2.41 (t, 2H, J = 7.1, Lys-6), 2.25 (ddd,1 H, J^1 = 16.6, J^2 = 8.8, J^3 = 6.8, Glu-4b), 2.18 (ddd, 1H, J^1 = 16.6, J^2 = 8.8, J^3 = 6.1, Glu-4a), 1.86 (m, 1H, **Glu-3b**), 1.66 (m, 1H, Glu-3a), 1.57 (m, 1H, Lys-3b), 1.49 (m, 1H, Lys-3a), 1.40 (m, 2H, Lys-5), 1.38 (bs, 27 H, *t*Bu), 1.29 (m, 2H, Lys-4). ^{13}C NMR (125.7 MHz, DMSO-d6): 172.50 (**Lys-1**), 172.11 (Glu-1), 171.63 (Glu-5), 157.31 (NH-CO-NH), 140.83 (*i*-Ph), 131.07 (*m*-Ph), 130.26 (*o*-Ph), 119.52 (*p*-Ph), 80.76 (**CH(CH₃)₃**), 80.45 (**CH(CH₃)₃**), 79.95 (**CH(CH₃)₃**), 53.18 (Lys-2), 52.38 (**CH₂-Ph**), 52.36 (Glu-2), 48.49 (Lys-6), 32.17 (Lys-3), 31.07 (Glu-4), 29.24 (**Lys-5**), 27.93 (**CH(CH₃)₃**), 27.84 (**CH(CH₃)₃**), 27.82 (**CH(CH₃)₃**), 27.77 (**GLu-3**), 23.03 (Lys-4).
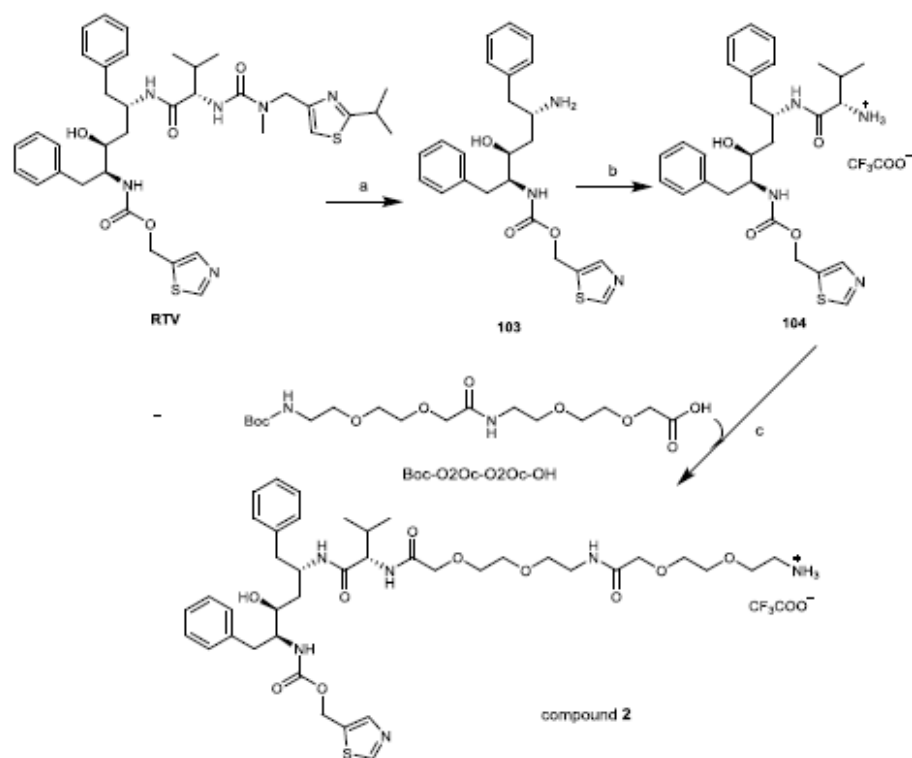
Compound 1:

(24S,28S)-19-(4-bromobenzyl)-24,28,30-tricarboxy-18,26-dioxo-3,6,9,12,15-pentaoxa-19,25,27-triazatriacontan-1-aminium 2,2,2-trifluoroacetate, compound 1: 137 mg (0.34 mmol, 1.1 eq) of Boc-NH-PEG₅-CH₂CH₂COOH (PurePEG, #432705) was dissolved in 1 ml of DMF along with 1222 mg (0.38 mmol, 1.25 eq) of TBTU. 132 µl (0.76 mmol, 2.5 eq) of DIEA were added in one portion and the reaction mixture was left stirring for 10 minutes. 200 mg (0.30 mmol, 1.0 eq) of compound 102 dissolved in 1 ml of DMF were added in one portion and the reaction mixture was monitored by TLC analysis, until all compound 102

disappeared (approx. 4 h). The DMF was then rotary evaporated, the crude mixture was dissolved in 20 ml of EtOAc and was extracted twice with concentrated bicarbonate, twice with 10 % KHSO₄ and once with brine. The organic layer was dried and rotary evaporated to complete dryness. 1 ml of TFA was then added to the oily crude product and was left sonicated for 15 minutes. TFA was removed by flow of nitrogen and the product was purified by preparative HPLC (gradient: 15-50 % ACN, R_T = 33 min). 83.4 mg isolated (overall yield = 30 %). R_T at analytical HPLC (grad 2-100 %, 30 min) 17.1 min. HRMS (ESI-): calculated for $C_{32}H_{50}O_{13}N_4Br$ [M]⁻ 777.25632. Found 777.25681.

Synthesis of compound 2

Compound **2**, based on a commercially available HIV protease inhibitor drug ritonavir (RTV), was synthesized according to the below depicted scheme:

a) 1) Dioxan/HCl, 65 °C, 20 h 2) K₂CO₃
b) 1) Boc-Val-OH, TBTU, DIEA, DMF, 2) TFA
c) 1) TBTU, DIEA, DMF, 2) TFA

22

Isolation of ritonavir (RTV) from commercially available capsules: RTV is suspended in capsules in an oily mixture of rather non–polar compounds. 50 tablets (100 mg RTV each) were cut open and the oily substance was squeezed out into a round-bottom shaped 2 l flask. 200 ml of hexan was added along with 500 ml of diethyl ether. The resulting suspension was triturated and sonicated for 3 hours until all oil turned into a white precipitate. This precipitate was filtred and again triturated/sonicated in pure diethyl ether, after which the pure RTV was filtred. 3.6 g of RTV was obtained (isolation yield 72 %). The purity of RTV was determined by HPLC and was well above 99 % (analytical HPLC R_T = 23.7 min).

Compound 103

Partial hydrolysis of ritonavir (RTV), thiazol-5-ylmethyl ((2S,3S,5S)-5-amino-3-hydroxy-1,6-diphenylhexan-2-yl)carbamate, compound 103: 1.00 g of RTV was dissolved in 50 ml of dioxan in a bottom-round flask. 50 ml of concentrated hydrochloric acid was added and the resulting mixture was stirred at 65 °C for 20 hours (note that different temperature and/or time lead to different cleavage products). After 20 hours the mixture was let cool down to RT. The reaction mixture was neutralized by addition of K_2CO_3 until the resulting mixture showed basic pH. The solvents were concentrated using rotary evaporater to roughly 50 ml and diluted by 150 ml of water and washed 3 times by 100 ml of EtOAc. The water phase was discarded and organic phase was dried and evaporated. 885 mg of crude product was obtained and was used in the next step without further purification (purity roughly 70 % - HPLC determination). For spectral determination, 50 mg was purified using preparative HPLC (gradient: 20-50 % ACN in 40 minutes. R_T = 15 min). Analytical HPLC R_T = 17.3 min. HRMS (ESI+): calculated for $C_{23}H_{28}O_3N_3S$ [M]$^+$ 426.18459. Found 426.18454. NMR measured for trifluoroacetate salt. ^{1}H NMR (500 MHz, DMSO-d6): 9.06 (d, 1H, ^4J = 0.8, N-**CH**-S), 7.84 (q, 1H, ^4J = 0.8, S-C-**CH**-N), 7.81 (bs, 3H, **NH₃⁺**), 7.32-7.15 (m, 10H, **Ph-**), 7.20 (bs, 1H, **NH**), 5.50 (bs, 1H, **OH**), 5.15 (dd, 1H, J_{gem} = 13.2, ^4J = 0.8, O-**CH₂**), 5.11 (dd, 1H, J_{gem} = 13.2, ^4J = 0.8, COO-**CH₂**), 3.69 (m, 1H, HO-**CH**), 3.67 (m, 1H, HO-CH-**CH**-NH), 3.50 (bm, 1H, NH₃⁺-**CH**), 2.87 (dd, 1H, J_{gem} = 14.0, ^3J = 6.4, NH₃⁺-CH-**CH₂**-Ph), 2.80 (dd, 1H, J_{gem} = 14.0, ^3J = 7.3, NH₃⁺-CH-**CH₂**-Ph), 2.79 (dd, 1H, J_{gem} = 13.7, ^3J = 3.7, NH-CH-**CH₂**-Ph), 2.79 (dd, 1H, J_{gem} = 13.7, ^3J = 10.5, NH-CH-**CH₂**-Ph), 1.58 (bs, 2H, OH-CH-**CH₂**-CH). ^{13}C NMR (125.7 MHz, DMSO-d6): 155.39 (O-**C**-N), 155.77 (N-**CH**-S), 143.23 (S-**C**-CH-N), 139.52 (**Ph**), 136.37 (**Ph**), 134.14 (S-C-**CH**-N), 129.61 (**Ph**), 129.18 (**Ph**), 128.81 (**Ph**), 128.23 (**Ph**), 127.07 (**Ph**), 126.12 (**Ph**), 69.81 (HO-**CH**), 57.49 (COO-**CH₂**), 56.94 (HO-CH-

23

CH-NH), 50.87 (NH₃⁺-CH), 38.71 (NH₃⁺-CH-CH₂-Ph), 35.69 (NH-CH-CH₂-Ph), 34.66 (CH-CH₂-CH).
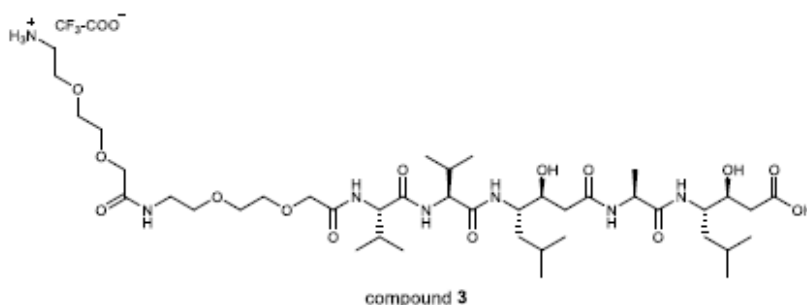
Compound 104

Thiazol-5-ylmethyl ((2S,3S,5S)-5-((S)-2-amino-3-methylbutanamido)-3-hydroxy-1,6-diphenylhexan-2-yl)carbamate, compound **104**: 526 mg (1.64 mmol, 1.0 eq) of TBTU was added to 356 mg (1.64 mmol, 1.0 eq) Boc-Val dissolved in 1.5 ml of DMF along with 690 µl of DIEA (3.94 mmol, 2.4 eq). The crude hydrolysate of RTV (700 mg, 1.64 mmol, 1.0 eq), dissolved in 1 ml of DMF, was added after 5 minutes of stirring in one portion. The reaction was left overnight and DMF was rotary evaporated. The reaction mixture was dissolved in 50 ml of EtOAc and washed two times by saturated NaHCO₃, two times with 10 % KHSO₄ and once with brine. The organic mixture was dried, evaporated and the product was purified using Flash chromatography (TLC analysis: EtOAc, R_f = 0.65). Product was further dissolved in 5 ml of hot EtOAc and 5 ml of diethyl ether was added. The resulting gel was filtrated and dried to give very pure (>99 %, HPLC) 250 mg of product (yield = 25 %). The product was then treated with TFA (approx. 1 ml) for 15 minutes, alternately sonicated and stirred. The remaining TFA was then removed by flow of nitrogen. The oily product was dissolved in water/ACN and was lyophilisated. Analytical HPLC R_T = 17.4 min. HRMS (ESI+): calculated for C₂₈H₃₇O₄N₄S [M]⁺ 525.25300. Found 525.25292. ¹H NMR (500 MHz, DMSO-d6): 9.06 (d, 1H, ⁴J = 0.8, N-CH-S), 8.24 (d, 1H J = 8.2, -NH-CO), 8.00 (bd, 3H, J = 5.2, -NH₃⁺), 7.85 (q, 1H, ⁴J = 0.8, S-C-CH-N), 7.28-7.13 (m, 10H, Ph-), 6.94 (d, J = 9.4, 1H, NH-CO-O), 5.12 (d, 2H, ⁴J = 0.8, O-CH₂), 4.16 (m, 1H, CH-NH-CO), 3.78 (m, 1H, CH-NH₃⁺, partial overlap with water residual peak), 3.58 (td, 1H, J = 6.8, J = 2.0, CH-OH), 3.48 (m, 1H, Ph-CH2-CH-NH), 2.72-2.67 (m, 4H, 2xCH-CH₂-Ph), 2.00 (m, 1H, CH-(CH₃)₂), 1.50 (m, 1H, OH-CH-CH₂), 1.43 (m, 1H, OH-CH-CH₂), 0.89 (d, 3H, J = 6.8 -CH3), 0.84 (d, 3H, J = 6.8 -CH3). ¹³C NMR (125.7 MHz, DMSO-d6): 167.33 (CO Val), 158.33(q, $J_{C,F}$ = 34.4, CF₃COO-), 155.79 (O-C-N), 155.71 (N-CH-S), 143.23 (S-C-CH-N), 139.50 (Ph), 138.55 (Ph), 134.23 (S-C-CH-N), 129.56 (Ph), 129.17 (Ph), 128.30 (Ph), 128.25 (Ph), 126.26 (Ph), 126.09 (Ph), 116.44 (q, $J_{C,F}$ = 294.8, CF₃-COO⁻) 68.90 (HO-CH), 57.56 (CO-CH-NH3), 57.44 (COO-CH₂), 55.74 (HO-CH-CH-NH), 47.98 (CONH-CH), 39.75 (NH-CH-CH₂-Ph), 37.77 (-CH₂-CH-CH-), 37.33 (Ph-CH₂-CH-NH), 30.04 (CH(CH₃)₂), 17.26 and 18.69 (2xCH₃).

Compound 2

(5S,6S,8S,11S)-5,8-dibenzyl-6-hydroxy-11-isopropyl-3,10,13,22-tetraoxo-1-(thiazol-5-yl)-2,15,18,24,27-pentaoxa-4,9,12,21-tetraazanonacosan-29-aminium 2,2,2-trifluoroacetate, compound 2: 64 mg (157 µmol, 1.0 eq) of Boc-O2Oc-O2Oc-OH (Iris-Biotech, #BAA1485) was dissolved in 1 ml of DMF along with 51 mg (157 µmol, 1.0 eq) of TBTU and 95 µl (558 µmol, 3.5 eq) of DIEA and the whole reaction mixture was stirred for 15 minutes. 100 mg (157 µmol, 1.0 eq) of compound 104 (dissolved in 0.5 ml of DMF) was added into the mixture in one portion. After 3 hours all volatiles were evaporated, the crude product was dissolved in 25 ml of EtOAc and was washed two times with saturated NaHCO$_3$, two times with 10 % KHSO$_4$ and once with brine. The organic layer was dried and evaporated. The Boc-protecting group was then removed by stirring in 1 ml of TFA for 15 minutes. The product was purified using preparative HPLC (gradient: 15-50 % ACN in 40 minutes. R_T = 31 min). Analytical HPLC R_T = 17.7 min. HRMS (ESI+): calculated for C$_{40}$H$_{59}$O$_{10}$N$_6$S [M]$^+$ 815.40079. Found 815.40096. ^{1}H NMR (500 MHz, DMSO-d6): 9.05 (d, 1H, J = 0.8, N-**CH-S**), 7.96 (d, 1H, J = 8.7, **NH-CO-Val**), 7.85 (q, 1H, J = 0.8, **S-C-CH-N**), 7.81 (vbs, 3H, -**NH$_3$$^+$**), 7.79 (bt, 1H, J = 5.8, Linker **NH-CO**), 7.31 (d, 1H, J = **NH-Val-2**), 7.24-7.08 (m, 10H, 2x**Ph**), 6.92 (d, 1H, J = 9.4, **NH-COO-CH$_2$-thiazol**), 5.16 (dd, 1H, J_{gem} = 13.2, ^4J = 0.8, **NH-COO-CH$_2$-thiazol**), 5.12 (dd, 1H, J_{gem} = 13.2, ^4J = 0.8, **NH-COO-CH$_2$-thiazol**), 4.13 (m, 1H,**CH-NH-CO-Val**), 4.13 (dd, 1H, ^2J = 9.3, ^3J = 6.8, **Val-2**), 3.92-3.89 (m, 4H, linker 2x**NH-CO-CH$_2$-**), 3.82 (m, 1H, **CH-NH-COO-CH$_2$-thiazol**), 3.62-3.51 (m, 12H, linker, **OH-CH**), 3.46 (bt, 2H, **O-CH$_2$-CH$_2$-NH-CO-CH$_2$-**), 3.29 (bt, 2H, **O-CH$_2$-CH$_2$-NH-CO-CH$_2$** -), 2.98 (m, 2H, **CH$_2$-NH$_3$$^+$**), 2.71-2.65 (m, 2H Ph-**CH$_2$**-CH-NH-Thiazol, 1H Ph-**CH$_2$**-NH-Val), 2.58 (dd, 1H, J_{gem} = 13.6, ^3J = 8.4, Ph-**CH$_2$-NH-Val**), 1.84 (o, 1H, J = 6.8, **Val-3**), 1.46 (m, 2H, **OH-CH-CH$_2$-**), 0.76 (d, 3H, J = 6.8, **Val-4**), 0.74 (d, 3H, J = 6.8, **Val-4**). ^{13}C NMR (125.7 MHz, DMSO-d6): 170.04 (**Val-1**), 169.56 (**NH-CO-Linker**), 168.90 (**Val-NH-CO-**), 158.31 (q, J = 34.4, **CF$_3$COO$^-$**), 155.82 (**COO-CH2-thiazol**, **S-CH-N**), 143.24 (**S-C-CH-N**), 139.60 (*i*-**Ph**), 138.92 (*i*-**Ph**), 134.30 (**S-C-CH-N**), 129.47 (*o*-**Ph**), 129.25 (*o*-**Ph**), 128.20 (*m*-**Ph**), 128.08 (*m*-**Ph**), 126.04 (*p*-**Ph**), 126.03 (*p*-**Ph**), 116.46 (q, J = 293.5, **CF$_3$COO$^-$**), 70.44 (linker), 70.17 (linker), 70.03 (linker), 69.83 (linker), 69.66 (linker), 69.48 (linker), 69.22 (linker), 69.11 (**CH-OH**), 66.85 (linker), 57.40 (**O-CH$_2$-thiazol**), 57.07 (**Val-2**), 55.64 (**CH-COO-CH$_2$-thiazol**), 47.45 (**CH-NH-Val**), 39.90 (**CH$_2$-CH-NH-Val**), 38.74 (**CH$_2$-NH$_3$$^+$**), 38.44 (**OH-CH-CH$_2$**), 38.23 (**CH$_2$-NH-COO-CH$_2$**), 37.41 (**OCO-NH-CH$_2$-Ph**), 31.19 (**Val-3**), 19.48 (**Val-4**), 18.10 (**Val-4**).

25

Synthesis of compound 3

Compound 3 is based on the aspartic proteases inhibitor pepstatin A.

compound **3**

(19S,22S,25S,26S,30S,33S)-33-((S)-2-carboxy-1-hydroxyethyl)-26-hydroxy-25-isobutyl-19,22-diisopropyl-30,35-dimethyl-8,17,20,23,28,31-hexaoxo-3,6,12,15-tetraoxa-9,18,21,24,29,32-hexaazahexatriacontan-1-aminium, compound **3**: The pepstatin inhibitor was synthesized by standard amino-Fmoc synthesis on solid phase, using 2-chlortrityl chloride resin (Iris-Biotech). The first amino acid (Fmoc-Sta-OH) was attached to the solid phase according to the manufacturer's instructions: the resin was left to react with Fmoc-Sta-OH (0.6 eq to resin substitution) in presence of 4 equivalents of DIEA for 2 hours in DCM. The remaining reactive residues were quenched with mixture of DCM/MeOH/DIEA (17:2:1) for 15 minutes. All other amino acids and the linker Boc-O2Oc-O2Oc-OH (Iris-Biotech, #BAA1485) were added using HOBt/DIC method. The peptide was then cleaved from the solid phase using 95 % TFA and the crude product was purified using preparative HPLC (gradient: 10-50 % ACN in 40 minutes. $R_T = 26$ min). Analytical HPLC $R_T = 16.5$ min. HRMS (ESI-): calculated for $C_{41}H_{76}O_{14}N_7$ [M]⁻ 890.54557. Found 590.54413.

Synthesis of compound 4

Compound 4 was synthesized according to the scheme depicted below:

105

Boc-O2Oc-O2Oc-OH
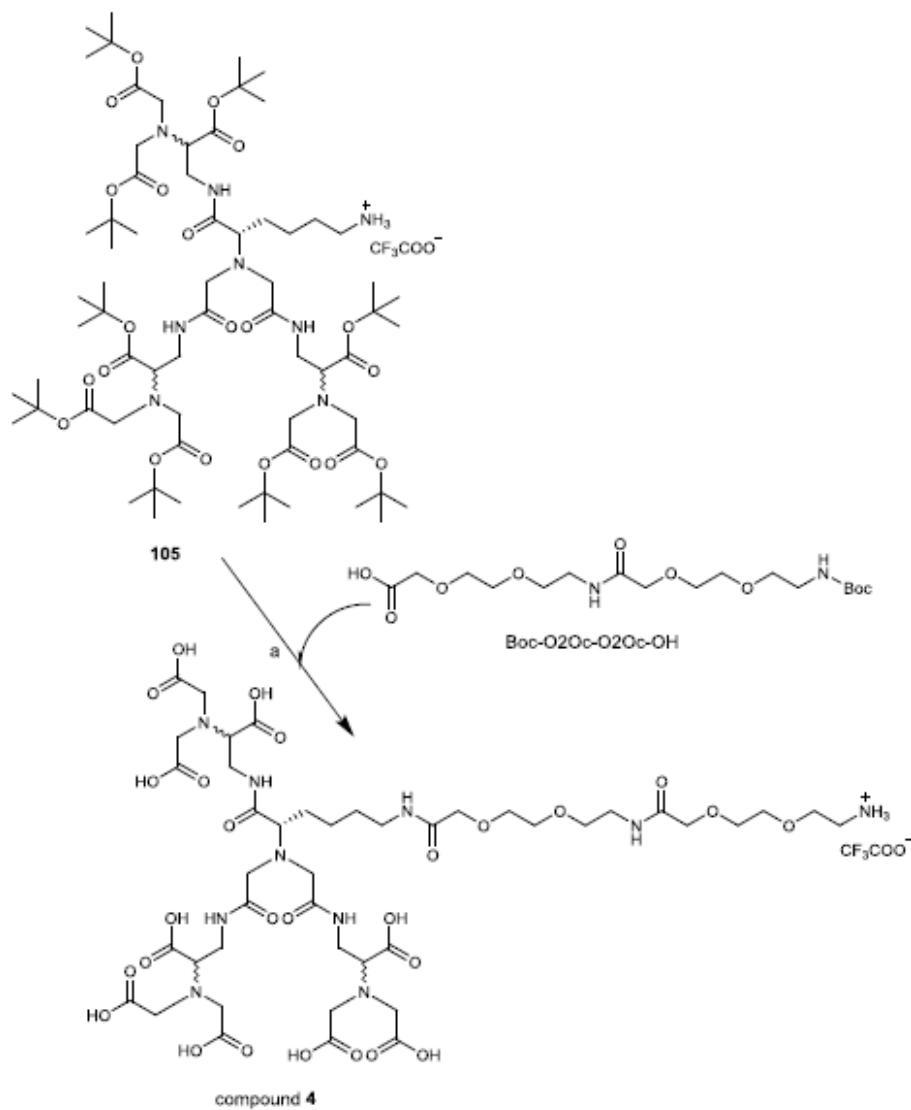
compound **4**

a) 1) Boc-NH-PEG$_5$-COOH, DCC, DMF; 2) TFA

Compound 105

NH$_2$-tris-NTA(o-tBu)$_9$, compound **105**: The synthesis was performed as described previously[13] with an only minor variation in one step (for the reaction between 3 monomers

27

of NTA and lysine tricarboxylic acid derivative TSTU was used as an activation reagent, instead of NHS/DCC, because it gave much better yields).

Compound 4

Compound 105 (52 mg, 38 μmol, 1.0 eq, purified by HPLC before this step) was dissolved in 1 ml of DMF and 15 mg (38 μmol, 1.0 eq) of the linker Boc-O2Oc-O2Oc-OH (Iris-Biotech, #BAA1485) was added in one portion. To this reaction mixture was added 16 mg (76 μmol, 2.0 eq) of DCC and the reaction was left for 24 hours stirring at room temperature. The solvents were evaporated and the crude mixture was treated with 1 ml of pure TFA, and the reaction mixture was alternately stirred and sonicated for 3 hours. The TFA was removed by flow of nitrogen and the final product was purified by preparative scale HPLC (gradient: 2-30 % ACN in 50 minutes, $R_T = 35$ min). 14 mg isolated (overall yield = 32 %) R_T at analytical HPLC (grad 2-100 %, in 30 min) 12.0 min. HRMS (ESI+): calculated for $C_{43}H_{71}O_{27}N_{10}$ [M]$^+$1159.44846. Found 1159.44849.

Synthesis of monomers, polymer precursors and polymer conjugates

Synthesis of HPMA copolymer conjugates (iBodies)

Generally, the HPMA copolymer conjugates (iBodies 1–6) were prepared by reaction of the polymer precursor poly(HPMA-co-Ma-ß-Ala-TT) with the affinity anchor N-(2-aminoethyl)biotinamide hydrobromide (biotin-NH$_2$) or with a combination of fluorophore (ATTO488-amine), affinity anchor (biotin-NH$_2$), and targeting ligand (compounds 1–4). To achieve statistical representation of all three ligands in the conjugate, the aminolysis of the statistical TT groups-containing polymer precursor[14] with the -CH$_2$CH$_2$NH$_2$ group-bearing compounds was performed simultaneously in one step. Yield of the aminolytic reaction was approximately 60–70 % for all three compounds. The compounds were dissolved in DMSO, and N,N-diisopropylethylamine (DIPEA) was added. The reaction mixture was stirred at room temperature, and the unreacted thiazolidine-2-thione groups were quenched with 1-aminopropan-2-ol. Polymer conjugates were isolated by precipitation into an acetone:diethyl ether mixture (3:1), filtered off, washed with acetone and diethyl ether, and dried *in vacuo*. Finally, the conjugates were purified on a Sephadex LH-20 chromatography column with methanol as the mobile phase, precipitated into diethyl ether, filtered off, and dried *in vacuo*.

28

The synthesis of all iBodies, polymer precursors and monomers is described in more detail below.

Determination of the composition (i.e. the number of each moiety) of the iBodies

Content of ATTO-488 was determined using spectrophotometry ($\varepsilon_{502nm} = 90,000$ l.mol^{-1}.cm^{-1}, water). For polymer conjugates containing only biotin and/or targeting group, content of biotin was determined spectrophotometrically using HABA/avidin reagent according to manufacturer's instruction (Sigma-Aldrich). For polymer conjugates containing both biotin and ATTO488, content of biotin was determined using inductively coupled plasma atomic emission spectroscopy (ICP-OES; sulphur detection), since HABA/avidin method was not applicable due to ATTO488 absorption at 500 nm. Content of targeting groups (compounds 1-4) was determined in the sample hydrolyzate (6N-HCl, 115 °C, 16 h) using HPLC-based *o*-phtaldialdehyde pre-column derivatization method on the Chromolith C18 column with a fluorescence detector (Ex. 229 nm, Em. 450 nm). As standards, the corresponding low-molecular-weight inhibitors were hydrolyzed and derivatized in the same way.

Determination of molecular weight of polymer conjugates

The weight-average molecular weights (M_w), number average molecular weights (M_n), and dispersities ($Đ$) of the polymer precursor and conjugates were determined using HPLC Shimadzu system equipped with a UV detector, an Optilab®rEX differential refractometer and multi-angle light scattering DAWN® 8™ (Wyatt Technology, USA) detector and size-exclusion chromatography TSKgel G4000SW column. The M_w, M_n and $Đ$ were calculated using the Astra V software. The refractive index increment dn/dc = 0.167 ml/g was used for calculation. For these experiments, a 20 % 300 mM acetate:80 % methanol (v/v) buffer was used. The flow rate was 0.5 mL/min. The data are summarized in Table S2.

Synthesis of monomers

N-(2-Hydroxypropyl)methacrylamide (HPMA) was synthesized by reaction of methacryloyl chloride with 1-aminopropan-2-ol in dichloromethane in the presence of sodium carbonate[15].

3-(3-Methacrylamidopropanoyl)thiazolidine-2-thione (Ma-ß-Ala-TT) was prepared by reaction of 3-methacrylamidopropanoic acid and 4,5-dihydrothiazole-2-thiol (H-TT) (4.37 g, 37 mmol) in the presence of 1-ethyl-3-(3-dimethylaminopropyl)-carbodiimide hydrochloride

29

(EDC). Briefly, Ma-ß-Ala-OH (4.0 g, 28 mmol), H-TT (3.5 g, 29 mmol), and a catalytic amount of 4-dimethylaminopyridine (DMAP) were dissolved in dichloromethane (50 ml), and EDC (6.9 g, 36 mmol) was added. The reaction was carried out at room temperature for 2 h. The reaction mixture was then extracted with distilled water (3×20 ml), 2 wt% aqueous NaHCO$_3$ (20 ml), and distilled water (20 ml). The organic layer was dried with Na$_2$SO$_4$, dichloromethane was evaporated, and Ma-ß-Ala-TT was crystallized from ethyl acetate. The crystals were filtered off, washed with diethyl ether, and dried *in vacuo*. Yield: 4.6 g (64 %).

Synthesis of iBody 1

Monomers *N*-(2-hydroxypropyl)methacrylamide (HPMA) and 3-(3-methacrylamido-propanoyl)thiazolidine-2-thione (Ma-ß-Ala-TT) were synthesized as described earlier[14]. Polymer precursor poly(HPMA-co-Ma-ß-Ala-TT) was prepared by reversible addition-fragmentation chain transfer (RAFT) copolymerization[15-16]. 0.659 g of mixture of HPMA (85 %mol, 500 mg), Ma-ß-Ala-TT (15 %mol, 159 mg dissolved in 0.8 ml dimethyl sulfoxide), 1.22 mg 2-cyano-2-propyl benzodithioate and 0.45 mg 2,2'-azobis(2-methylpropionitrile) was dissolved in 3.8 ml tert-butanol and the solution was introduced into polymerization ampule. The mixture was bubbled with argon for 10 min and ampule was sealed. Polymerization was carried out at 70 °C for 16 h. Polymer precursor was isolated by precipitation into mixture of acetone:diethyl ether (3:1), filtered off, washed with acetone and diethyl ether and dried in vacuum. Terminating dithiobenzoate group was removed as described by Perrier[17]. The polymer precursor poly(HPMA-co-Ma-β-Ala-TT) with molecular weight M_n = 79,000 g/mol, M_w = 94,600 g/mol, dispersity Đ = 1.20 and content of reactive thiazolidine-2-thione groups 13.4 mol% was obtained.

Polymer precursor poly(HPMA-*co*-Ma-β-Ala-TT) (45 mg; M_n = 79,000 g/mol, M_w = 94,600 g/mol, Đ = 1.20; 13.4 mol% TT), compound 1 (6.2 mg) and *N*-(2-aminoethyl)biotinamid hydrobromid (biotin-NH$_2$) (5 mg) were dissolved in 0.2 ml DMSO. ATTO-488-NH$_2$ (2.5 mg) was dissolved in 0.1 ml DMSO and added to the solution. Then 2.5 μl of *N,N*-diisopropylethylamine (DIPEA) was added. Reaction was carried out for 4 h at room temperature and then 5 μl of 1-aminopropan-2-ol was added and the reaction was stirred for 10 min. Polymer conjugate poly(HPMA-*co*-Ma-β-Ala-Compound1-*co*-Ma-β-Ala-ATTO488-*co*-Ma-β-Ala-NH-biotin) was isolated by precipitation into mixture of acetone:diethyl ether (3:1), filtered off, washed with acetone and diethyl ether and dried in vacuum. Polymer conjugate was purified on chromatography column Sephadex LH-20 in

30

methanol, precipitated into diethyl ether, filtered off and dried in vacuum. Yield of the iBody 1 ($M_n = 148,800$ g/mol, $M_w = 203,900$ g/mol, $Đ = 1.37$) was 33 mg, content of compound 1 was 9.8 wt%, content of biotin was 9.8 wt% and content of ATTO-488 was 3.9 %.

Synthesis of iBody 2

Polymer precursor poly(HPMA-co-Ma-ß-Ala-TT) was prepared by RAFT copolymerization as described in the Synthesis of iBody 1 by using following composition of polymerization mixture: HPMA (90 %mol; 500 mg), Ma-ß-Ala-TT (10 %mol, 100 mg), 4.29 mg 2-cyano-2-propyl benzodithioate and 1.59 mg 2,2′-azobis(2-methylpropionitrile. The polymer precursor with molecular weight $M_n = 24,800$ g/mol, $M_w = 26,700$ g/mol, dispersity $Đ = 1.08$ and content of reactive thiazolidine-2-thione groups 10.4 mol% was obtained.

Polymer precursor (74 mg; $M_n = 24,800$ g/mol, $M_w = 26,700$ g/mol, $Đ = 1.08$; 10.4 mol% TT) and biotin-NH$_2$ (6 mg) were dissolved in 0.4 ml DMSO and the solution was stirred for 20 min. Then 13 mg of compound 2 and 12.2 µl of N,N-diisopropylethylamine (DIPEA) was added. Reaction was carried out for 4 h at room temperature and then 5 µl of 1-aminopropan-2-ol was added and the reaction was stirred for 10 min. Polymer conjugate poly(HPMA-co-Ma-ß-Ala- Compound2-co-Ma-ß-Ala-NH-biotin) was isolated by precipitation into mixture of acetone:diethyl ether (3:1), filtered off, washed with acetone and diethyl ether and dried in vacuum. Polymer conjugate was purified on chromatography column Sephadex LH-20 in methanol, precipitated into diethyl ether, filtered off and dried in vacuum. Yield of the iBody 2 ($M_n = 40,600$ g/mol, $M_w = 67,000$ g/mol, $Đ = 1.65$) was 62 mg, content of compound 2 was 11.7 wt% and content of biotin was 4.7 wt%.

Synthesis of iBody 3

Polymer precursor (55 mg, $M_n = 24,800$ g/mol, $M_w = 26,700$ g/mol, $Đ = 1.08$; 10.4 mol% TT) and biotin-NH$_2$ (6 mg) were dissolved in 0.32 ml DMSO and the solution was stirred for 20 min. Then 10 mg of compound 3and 8.7 µl of N,N-diisopropylethylamine (DIPEA) was added. Reaction was carried out for 4 h at room temperature and then 5 µl of 1-aminopropan-2-ol was added and the reaction was stirred for 10 min. Polymer conjugate poly(HPMA-co-Ma-β-Ala- Compound3-co-Ma-β-Ala-NH-biotin) was isolated by precipitation into mixture of acetone:diethyl ether (3:1), filtered off, washed with acetone and diethyl ether and dried in vacuum. Polymer conjugate was purified on chromatography column Sephadex LH-20 in methanol, precipitated into diethyl ether, filtered off and dried in vacuum. Yield of the

31

iBody 3 ($M_n = 42,100$ g/mol, $M_w = 55,500$ g/mol, $Đ = 1.32$) was 35 mg, content of compound 3 was 15.3 wt% and content of biotin was 5.9 wt%.

Synthesis of iBody 4

Polymer precursor poly(HPMA-co-Ma-ß-Ala-TT) was prepared by RAFT copolymerization as described in the Synthesis of iBody 1 by using following composition of polymerization mixture: in 7.3 ml of tert-butanol, following compounds were dissolved: 1,000 mg of HPMA (85 %mol), 318 mg Ma-ß-Ala-TT (15 %mol, dissolved in 1.9 ml DMSO), 2.42 mg 2-cyano-2-propyl benzodithioate and 0.90 mg 2,2'-azobis(2-methylpropionitrile. The polymer precursor with molecular weight $M_n = 73,800$ g/mol, $M_w = 90,600$ g/mol, dispersity $Đ = 1.23$ and content of reactive thiazolidine-2-thione groups 14.6 mol% was obtained.

Polymer precursor poly(HPMA-*co*-Ma-β-Ala-TT) (40 mg, $M_n = 73,800$ g/mol, $M_w = 90,600$ g/mol, $Đ = 1.23$; 14.6 mol% TT), compound 4 (6.0 mg) and *N*-(2-aminoethyl)biotinamid hydrobromid (biotin-NH₂) (5 mg) were dissolved in 0.2 ml DMSO. ATTO-488-NH₂ (2.5 mg) was dissolved in 0.1 ml DMSO and added to the solution. Then 8.0 µl of *N,N*-diisopropylethylamine (DIPEA) was added. Reaction was carried out for 4 h at room temperature and then 5 µl of 1-aminopropan-2-ol was added and the reaction was stirred for 10 min. Polymer conjugate poly(HPMA-*co*-Ma-β-Ala-Compound4-*co*-Ma-β-Ala-ATTO488-*co*-Ma-β-Ala-NH-biotin) was isolated by precipitation into mixture of acetone:diethyl ether (3:1), filtered off, washed with acetone and diethyl ether and dried in vacuum. Polymer conjugate was purified on chromatography column Sephadex LH-20 in methanol, precipitated into diethyl ether, filtered off and dried in vacuum. Yield of iBody 4 ($M_n = 135,800$ g/mol, $M_w = 255,000$ g/mol, $Đ = 1.88$) was 22 mg; content of compound 4 was 11.3 %, content of ATTO-488 was 4.2 % and content of biotin was 9.7 wt%.

Synthesis of iBody 5

Polymer precursor poly(HPMA-*co*-Ma-β-Ala-TT) (45 mg, $M_n = 79,000$ g/mol, $M_w = 94,600$ g/mol, $Đ = 1.20$; 13.4 mol% TT) and *N*-(2-aminoethyl)biotinamid hydrobromid (biotin-NH₂) (5 mg) were dissolved in 0.2 ml DMSO. ATTO-488-NH₂ (2.5 mg) was dissolved in 0.1 ml DMSO and added to the solution. Then 2.5 µl of *N,N*-diisopropylethylamine (DIPEA) was added. Reaction was carried out for 4 h at room temperature and then 5 µl of 1-aminopropan-2-ol was added and the reaction was stirred for 10 min. Polymer conjugate poly(HPMA-*co*-Ma-β-Ala-ATTO488-*co*-Ma-β-Ala-NH-biotin)

32

was isolated by precipitation into mixture of acetone:diethyl ether (3:1), filtered off, washed with acetone and diethyl ether and dried in vacuum. Polymer conjugate was purified on chromatography column Sephadex LH-20 in methanol, precipitated into diethyl ether, filtered off and dried in vacuum. Yield of the iBody 5 (M_n = 108,100 g/mol, M_w = 176,200 g/mol, Đ = 1.63) was 32 mg, content of biotin was 10.8 wt% and content of ATTO-488 was 5.1 %.

Synthesis of iBody 6

Polymer precursor poly(HPMA-*co*-Ma-β-Ala-TT) (40 mg, M_n = 24,800 g/mol, M_w = 26,700 g/mol, Đ = 1.08; 10.4 mol% TT) and *N*-(2-aminoethyl)biotinamid hydrobromid (biotin-NH$_2$) (5 mg) were dissolved in 0.25 ml DMSO. Then 3.0 µl of *N,N*-diisopropylethylamine (DIPEA) was added. Reaction was carried out for 4 h at room temperature and then 5 µl of 1-aminopropan-2-ol was added and the reaction was stirred for 10 min. Polymer conjugate poly(HPMA-*co*-Ma-β-Ala-NH-biotin) was isolated by precipitation into mixture of acetone:diethyl ether (3:1), filtered off, washed with acetone and diethyl ether and dried in vacuum. Polymer conjugate was purified on chromatography column Sephadex LH-20 in methanol, precipitated into diethyl ether, filtered off and dried in vacuum. Yield of the iBody 6 (M_n = 37,800 g/mol, M_w = 57,800 g/mol, Đ = 1.53) was 28 mg, content of biotin was 6.4 wt%.

33
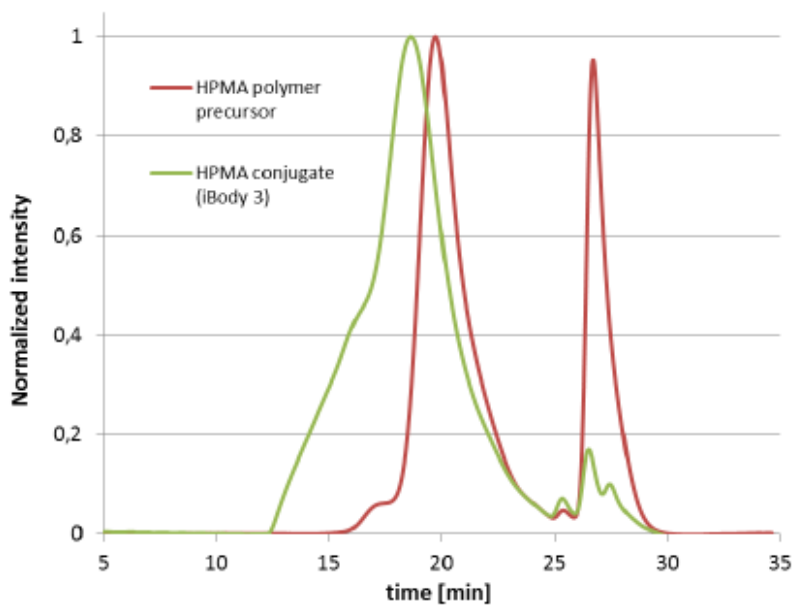
Supplementary Figure S8

Example of a GPC chromatogram of the HPMA polymer precursor (red) and the resulting ligand-decorated HPMA copolymer conjugate (iBody 3, green) from differential refractometer. The HPMA polymers (both precursors and conjugates) are eluted between 12 and 25 min; the peak in time between 25 and 30 min represents the buffer. The shift of the peak maximum of the HPMA copolymer conjugate corresponds to its increased molecular weight and dispersity. The small shoulder at 17 min on GPC record of polymer precursor is caused by the side reaction during RAFT polymerization (termination reaction of two polymer radicals forming dead polymer).[18]

34

List of references

[1]   J. Tykvart, J. Schimer, J. Barinkova, P. Pachl, L. Postova-Slavetinska, P. Majer, J. Konvalinka, P. Sacha, *Bioorg Med Chem* **2014**, *22*, 4099.

[2]   J. Fanfrlik, A. K. Bronowska, J. Rezac, O. Prenosil, J. Konvalinka, P. Hobza, *J Phys Chem B* **2010**, *114*, 12666.

[3]   Y. Cheng, W. H. Prusoff, *Biochemical Pharmacology* **1973**, *22*, 3099.

[4]   H. Liu, P. Moy, S. Kim, Y. Xia, A. Rajasekaran, V. Navarro, B. Knudsen, N. H. Bander, *Cancer Research* **1997**, *57*, 3629.

[5]   T. Knedlik, V. Navratil, V. Vik, D. Pacik, P. Sacha, J. Konvalinka, *Prostate* **2014**, *74*, 768.

[6]   K. Hegnerova, M. Bockova, H. Vaisocherova, Z. Kristofikova, J. Ricny, D. Ripova, J. Homola, *Sensors and Actuators B-Chemical* **2009**, *139*, 69.

[7]   B. Frigerio, G. Fracasso, E. Luison, S. Cingarlini, M. Mortarino, A. Coliva, E. Seregni, E. Bombardieri, G. Zuccolotto, A. Rosato, M. Colombatti, S. Canevari, M. Figini, *European Journal of Cancer* **2013**, *49*, 2223.

[8]   J. Tykvart, P. Sacha, C. Barinka, T. Knedlik, J. Starkova, J. Lubkowski, J. Konvalinka, *Protein Expr Purif* **2012**, *82*, 106.

[9]   P. Sacha, J. Zamecnik, C. Barinka, K. Hlouchova, A. Vicha, P. Mlcochova, I. Hilgert, T. Eckschlager, J. Konvalinka, *Neuroscience* **2007**, *144*, 1361.

[10]   M. Kozisek, J. Bray, P. Rezacova, K. Saskova, J. Brynda, J. Pokorna, F. Mammano, L. Rulisek, J. Konvalinka, *J Mol Biol* **2007**, *374*, 1005.

[11]   J. W. Williams, J. F. Morrison, *Methods Enzymol* **1979**, *63*, 437.

[12]   R. P. Murelli, A. X. Zhang, J. Michel, W. L. Jorgensen, D. A. Spiegel, *Journal of the American Chemical Society* **2009**, *131*, 17090.

[13]   Z. Huang, P. Hwang, D. S. Watson, L. Cao, F. C. Szoka, Jr., *Bioconjug Chem* **2009**, *20*, 1667.

[14]   a)V. Subr, K. Ulbrich, *Reactive & Functional Polymers* **2006**, *66*, 1525; b)K. Ulbrich, V. Subr, J. Strohalm, D. Plocova, M. Jelinkova, B. Rihova, *Journal of Controlled Release* **2000**, *64*, 63.

[15]   P. Chytil, T. Etrych, J. Kriz, V. Subr, K. Ulbrich, *Eur J Pharm Sci* **2010**, *41*, 473.

[16]   V. Subr, L. Sivak, E. Koziolova, A. Braunova, M. Pechar, J. Strohalm, M. Kabesova, B. Rihova, K. Ulbrich, M. Kovar, *Biomacromolecules* **2014**, *15*, 3030.

[17]   S. Perrier, P. Takolpuckdee, C. A. Mars, *Macromolecules* **2005**, *38*, 2033.

[18]   G. Moad, *Macromolecular Chemistry and Physics* **2014**, *215*, 9.

35

143

My contribution to the publications included in the thesis

Paper I: Knedlík et al., *Prostate* 2014, **74**(7):768-780

I conducted all the experiments presented. I prepared two constructs of human plasma glutamate carboxypeptidase, expressed them in insect cells, purified and tested them for their enzyme activity. I also demonstrated the presence of glutamate carboxypeptidase II (GCPII) in the human blood plasma. Finally, I determined GCPII concentration in the blood plasma of volunteers not diagnosed with prostate cancer. I also wrote a draft of the manuscript.

Paper II: Knedlík et al., *FEBS Open Bio* 2017, **7**(9):1362-1378.

I expressed and purified recombinant mouse glutamate carboxypeptidase II (GCPII). I performed the majority of the experiments, including analysis of GCPII enzyme activity, inhibition profile and distribution of the GCPII protein in mouse tissues. I also wrote a draft of the manuscript.

Paper III: Šácha & Knedlík et al., *Angew Chem Int Ed Engl* 2016, **55**(7):2356-2360.

I was responsible for the biochemical part of the project. I conducted the majority of the experiments that evaluated applicability and functionality of the prepared conjugates in biochemical methods. I tested all conjugates in a number of applications ranging from enzyme inhibition assay and surface plasmon resonance to cell culture experiments using flow cytometry and confocal microscopy. Besides, I also supervised undergraduate students, who significantly contributed to the paper. I also wrote a draft of the manuscript.

....

Tomáš Knedlík

I hereby confirm

....

Jan Konvalinka, PhD

Jméno a příjmení (s adresou)	Číslo OP	Datum vypůjčení	Poznámka